Biomarkers for arthritis:
Regulation of extracellular transglutaminase activity by non-conventional export

Thesis submitted in fulfillment of the requirements of the degree of Doctor of Philosophy

2013

Magdalena Adamczyk, M.Sc.

School of Dentistry,
Cardiff University

Form: PGR_Submission_2012_01

NOTICE OF SUBMISSION OF THESIS FORM: POSTGRADUATE RESEARCH

APPENDIX 1:
Specimen layout for Thesis Summary and Declaration/Statements page to be included in a Thesis

DECLARATION

This work has not been submitted in substance for any other degree or award at this or any other university or place of learning, nor is being submitted concurrently in candidature for any degree or other award.

Signed ..... (candidate) Date 30/09/2013

STATEMENT 1

This thesis is being submitted in partial fulfillment of the requirements for the degree of PhD (insert MCh, MD, MPhil, PhD etc, as appropriate)

Signed ..... (candidate) Date 30/09/2013

STATEMENT 2

This thesis is the result of my own independent work/investigation, except where otherwise stated. Other sources are acknowledged by explicit references. The views expressed are my own.

Signed ..... (candidate) Date 30/09/2013

STATEMENT 3

I hereby give consent for my thesis, if accepted, to be available for photocopying and for inter-library loan, and for the title and summary to be made available to outside organisations.

Signed ..... (candidate) Date 30/09/2013

STATEMENT 4: PREVIOUSLY APPROVED BAR ON ACCESS

I hereby give consent for my thesis, if accepted, to be available for photocopying and for inter-library loans **after expiry of a bar on access previously approved by the Academic Standards & Quality Committee.**

Signed ..... (candidate) Date 30/09/2013

Cardiff University Electronic Theses and Dissertations Publication Form

This form is to be completed by those choosing to make the full text of their work electronically available.

Details of the Work

I hereby deposit the following item in the digital repository (ORCA) maintained by Cardiff University, and/or in any other repository authorized for use by Cardiff University:

Author Name: Magdalena Adamczyk

Title: Biomarkers for arthritis: Regulation of extracellular transglutaminase activity by non-conventional export

Supervisor/School: Professor Daniel Aeschlimann (DENTL), Dr Vera Knäuper (DENTL)

Research grant (if any): support from Arthritis Research UK (grant no. 18461) and Cardiff University (PhD studentship)

Qualification/Degree obtained: PhD

This item is a product of my own research endeavours and is covered by the agreement below in which the item is referred to as "the Work".

Non-exclusive Rights

Rights granted to the digital repository through this agreement are entirely non-exclusive. I am free to publish the Work in its present version or future versions elsewhere.

I agree that Cardiff University may electronically store, copy or translate the Work to any approved medium or format for the purpose of future preservation and accessibility. Cardiff University is not under any obligation to reproduce or display the Work in the same formats or resolutions in which it was originally deposited.

Cardiff University Digital Repository

I understand that work deposited in the digital repository will be accessible to a wide variety of people and institutions, including automated agents and search engines via the World Wide Web.

I understand that once the Work is deposited, the item and its metadata may be incorporated into public access catalogues or services, national databases of electronic theses and dissertations such as the British Library's EThOS or any service provided by the National Library of Wales.

I understand that the Work may be made available via the National Library of Wales Online Electronic Theses Service under the declared terms and conditions of use (link or append). I agree that as part of this service the National Library of Wales may electronically store, copy or convert the Work to any approved medium or format for the purpose of future preservation and accessibility. The National Library of Wales is not under any obligation to

reproduce or display the Work in the same formats or resolutions in which it was originally deposited.

The Student's attention is particularly drawn to the following clauses.

I agree as follows:

1. That I am the author or have the authority of the author/s to make this agreement and do hereby give Cardiff University the right to make available the Work in the way described above.

2. That the electronic copy of the Work deposited in the digital repository and covered by this agreement, is the final corrected version of the Work, subject to point 4 below.

3. That I have exercised reasonable care to ensure that the Work is original and, to the best of my knowledge, does not breach any laws including those relating to defamation, libel, copyright, data protection or any other intellectual property rights.

4. That I have, in instances where the intellectual property of other authors or copyright holders is included in the Work, gained explicit permission where appropriate for the inclusion of that material in the Work, and in the electronic form of the Work as accessed through an open access digital repository, or that I have identified and removed that material for which adequate permission has not been obtained.

5. That Cardiff University does not hold any obligation to take legal action on behalf of the Depositor, or other rights holders, in the event of a breach of intellectual property rights, or any other right, in the material deposited.

6. That I will indemnify and keep indemnified Cardiff University and the National Library of Wales from and against any loss, liability, claim or damage, including without limitation any related legal fees and court costs (on a full indemnity basis), related to any breach by myself of any term of this agreement.

Signature ..... **Date 12.12.2013**

Acknowledgments

I would like to thank my supervisors for their support and own effort that enabled me to submit this Thesis. I would like to thank Professor Daniel Aeschlimann for inspiration, long scientific discussions and always finding a time to answer my questions. This shaped me as a scientist and helped me to ask important questions. I also want to thank Dr Vera Knäuper for giving me a helping hand when I needed it and for her useful ideas. I would also like to thank Dr Sharon Dewitt for support in confocal imaging and for her encouragement during the PhD.

I would also like to acknowledge my funding bodies: Arthritis Research UK Biomechanics and Bioengineering Centre and School of Dentistry. I want to thank them for giving me the opportunity to develop as a scientist and be a part of the interdisciplinary community at Cardiff University.

I would like to thank my parents and grandparents for all their love, understanding and wisdom that they have given me. I also want to thank my sister, which support and positive attitude have helped me to achieve my goals. Finally, I would like to thank Łukasz for giving me love and strength, without which I would not be able to follow my dreams. Doing PhD was an amazing experience but many times challenging therefore I want to thank Łukasz for being here with me. Again I want to thank all those incredible people for making sure that I stay positively motivated during this time. I dedicate this work to you.

Summary of Thesis

Transglutaminase 2 (TG2) is an enzyme with a predominant role in cell stress response and tissue repair. Dramatically increased production of this enzyme is associated with early changes in arthritis, and the activity of the protein has been shown to directly contribute to both inflammatory and degenerative arthritis, although through distinct molecular mechanisms. Aberrant TG2 activity during joint disease might lead to protein modifications that are not normally present in extracellular matrix components. Those novel epitopes can possibly serve as a qualitative biomarker besides their potential role in disease pathogenesis. TG2 is released from cells via a non-conventional route, and this mechanism controls its extracellular activity. This pathway is likely to be shared with other proteins undergoing alternative secretion, many of which are potent biological signaling molecules.

The aim of this project is to investigate whether non-classical secretion of TG2 is mediated by activation of the ligand-gated ion channel 7 (P2X7R) in analogy to interleukin-1β processing and release. Specifically, we are exploring whether ATP, a P2X7R agonist, which might be released from damaged cells at the sites of injury, triggers active release of TG2 from cells.

To test this hypothesis we first employed macrophage and breast cancer cell models, where P2X7R is endogenously expressed, to look for involvement of ATP signaling in TG2 externalization through microvesicle shedding. By establishing HEK293 cells stably expressing P2X7R we show for the first time that introduction of functional P2X7R alone is sufficient to reconstitute rapid non-conventional TG2 export in a cell model. P2X7R activation induced time-dependent release of TG2 but not other cytoplasmic proteins, and this response was blocked by a selective P2X7R inhibitor. TG2 release was dependent on Ca^{2+} influx triggered by P2X7R activation and might be related to P2X7R-dependent membrane pore formation. These results provide a mechanistic explanation for a link between active TG2 release and inflammatory responses.

Table of Contents

CHAPTER 1 INTRODUCTION 1
1.1 Common forms of arthritis 1
1.2 Cells and mediators involved in pathology of OA and RA 2
1.3 Biological markers for arthritis 5
1.4 Post-translational protein modifications 6
1.5 Family of transglutaminases 7
1.6 Enzymatic reaction mediated by transglutaminases 9
1.7 Biological function of TG-mediated reactions 12
1.8 TG2 – the candidate molecule catalyzing post-translational protein modifications 14
1.8.1 TG2 protein expression 14
1.8.2 TG2 protein structure and regulation of enzymatic activity 14
1.8.3 Intracellular functions of TG2 17
1.8.4 Extracellular TG2 and its interaction partners in the ECM and on the cell surface 18
1.8.5 Studies using TG2 knock-out mice 21
1.9 Involvement of TG2 in pathological processes 21
1.9.1 TG2 and development of autoimmunity 22
1.9.2 Protein modifications mediated by TG2 in arthritis 24
1.9.3 TG2 expression and activation during chondrocyte differentiation/maturation 25
1.9.4 TG2 expression in osteoarthritis 26
1.9.5 Potential link between chondrocyte maturation, inflammatory mediators and TG2 28
1.10 Non-conventional release of TG2 29
1.11 Release of proteins via the conventional pathway 29
1.12 Emerging mechanism of non-conventional protein secretion 31
1.12.1 Non classical protein transport bypassing the Golgi compartment 32
1.12.2 Release of proteins lacking the signal peptide 33
1.13 Extracellular ATP – a trigger of non-classical protein secretion 35
1.14 ATP as an inflammatory mediator 36
1.15 Extracellular ATP and its receptors 36
1.15.1 P2X receptors 37
1.15.2 P2X receptor architecture 38
1.15.3 P2X receptor subunit structure and their arrangement in the closed channel state 39
1.15.4 ATP binding and P2X channel opening 39
1.15.5 Ion channel of P2X receptors 42
1.16 P2X7 receptor (P2X7R) 42
1.16.1 P2X7R as a membrane channel 43
1.16.2 P2X7R-dependent "pore formation" 45
1.16.3 C-terminus of P2X7R 46
1.16.4 Cytoskeleton re-arrangements upon P2X7R activation 46
1.17 The "Inflammasome" assembly upon P2X7R activation 47
1.18 Mechanism of interleukin-1b secretion – a prototypic non-conventionally secreted protein 49
1.19 Link between P2X7R and arthritis 50
1.20 THE AIMS OF THE PROJECT 52

CHAPTER 2 MATERIALS AND METHODS 53

GENERAL MATERIALS AND METHODS 53

2.1 CELL CULTURE 53
2.1.1 CELLS PASSAGING 53
2.1.2 CELL COUNTING 54
2.3 SAMPLE PROCESSING FOR WESTERN BLOTTING 54
2.3.1 PROTEIN EXTRACTION 54
2.3.2 PROTEIN CONCENTRATION DETERMINATION 54
2.3.3 SDS POLYACRYLAMIDE GEL ELECTROPHORESIS 54
2.3.4 WESTERN BLOTTING 55
2.4. STATISTICAL ANALYSIS 57

MATERIALS AND METHODS IN CHAPTER 3 58

2.5 TG2 STORAGE AND DETERMINATION OF PROTEIN CONCENTRATION USING THE SPECTROPHOTOMETER 58
2.6 EXCITATION AND EMISSION SPECTRA DETERMINATION OF ABZ-APQQEA AND ABZ-APE(Γ-CAD-DNP)QEA 58
2.7 REAL-TIME FLUORESCENCE ASSAY FOR MONITORING OF TRANSGLUTAMINASE ACTIVITY BY DETERMINING ISOPEPTIDASE ACTIVITY 59
2.8 TG2 ISOPEPTIDASE ACTIVITY ASSAY USING LIVE CELLS 59

MATERIALS AND METHODS IN CHAPTER 4 60

2.9 THP-1 DIFFERENTIATION WITH IL-6, TPA AND ATRA 60
2.10 THP-1 CELL CULTURE ON DIFFERENT SUBSTRATES 61
2.11 THP-1 CELL DIFFERENTIATION WITH ATRA IN PARALLEL WITH LPS PRIMING 61
2.12 THP-1 CELL DIFFERENTIATION WITH ATRA FOLLOWED BY LPS PRIMING 61
2.13 ENZYME-LINKED IMMUNOSORBENT ASSAY (ELISA) FOR IL-1B 62
2.14 STIMULATION OF MDA-MB-231 CELLS TO DETECT TG2 IN THE MEDIA 63
2.15 INTRACELLULAR CALCIUM MEASUREMENTS IN MDA-MB-231 CELLS 63
2.16 IMMUNOLOCALIZATION OF TG2 IN MDA-MB-231 CELLS 64

MATERIALS AND METHODS IN CHAPTER 5 65

2.17 CLONING THE P2X7R CODING SEQUENCE INTO PCDNA 5/FRT/V5-HIS EXPRESSION VECTOR 65
2.17.1 AMPLIFYING P2X7R CODING SEQUENCE BY PCR 65
2.17.2 CONSTRUCTION OF P2X7R EXPRESSION VECTOR 67
2.18 TRANSFECTION OF HEK293 CELLS WITH P2X7R AND P2X7R-V5-HIS CONSTRUCTS AND SELECTION OF STABLY TRANSFECTED COLONIES 68
2.19 CHARACTERIZATION OF HEK293 CELLS STABLY EXPRESSING P2X7R 70
2.19.1 IMMUNOLABELLING OF P2X7R IN STABLY TRANSFECTED HEK293 CELLS 70
2.19.2 SHEDDING OF AMPHIREGULIN-AP UPON P2X7R ACTIVATION 71
2.19.2.1 TRANSFECTION OF HEK293 CELL LINES OVEREXPRESSING P2X7R WITH AMPHIREGULIN-AP 71
2.19.2.2 CO-TRANSFECTION OF HEK293 CELLS WITH P2X7R AND AMPHIREGULIN-AP 72
2.19.3 CALCIUM MEASUREMENTS IN AGONIST TREATED HEK293 CELLS USING CONFOCAL MICROSCOPY 72
2.19.3.1 DYNAMIC Ca^{2+} IMAGING 73
2.19.3.2 CALCIUM MEASUREMENTS IN AGONIST TREATED HEK293 CELLS USING THE PLATE READER 73

MATERIALS AND METHODS IN CHAPTER 6 74

2.20 DETECTION OF TG2 IN CELL FREE SUPERNATANT USING WESTERN BLOTTING. 74
2.21 TRANSFECTION OF HEK293 P2X7R CELLS WITH TG2-GFP AND GFP-TG2 CONSTRUCTS. 75

2.22 Annexin V labeling of the exposed phosphatidyloserine. 76
2.23 Densitometry analysis 77

MATERIALS AND METHODS IN CHAPTER 7 77
2.24 Detection of TG2 in cell free supernatant in the presence of inhibitors and at various Ca^{2+} concentrations using Western blotting. 77
2.25 Monitoring P2X7R-dependent pore formation by YO-PRO-1 uptake. 77

CHAPTER 3 REAL-TIME FLUORESCENCE ASSAY FOR MONITORING OF TRANSGLUTAMINASE ACTIVITY BY DETERMINING ISOPEPTIDASE ACTIVITY 79

3.1 INTRODUCTION 79
The aims of the chapter: 80

3.2 RESULTS 82

3.2.1 ISOPEPTIDE SUBSTRATE CLEAVAGE MEDIATED BY TG2 (ASSAY PRINCIPLE) 82
3.2.2 Fluorescence spectra of the Abz-APE(γ-cad-Dnp)QEA substrate 85
3.2.3 Optimization of the isopeptidase assay using an automated "high throughput" plate reader 87
3.2.4 Isopeptidase activity of recombinant TG2 89
3.2.5 TG2 activation by Ca^{2+} 91
3.2.6 Buffer composition for the isopeptidase measurements 91
3.2.7 Analysis of product of TG2-mediated isopeptidase cleavage 94
3.2.8 Standard reaction conditions 96
3.2.9 The isopeptidase assay sensitivity 96
3.2.10 TG2 activity in the presence of nucleotides 99
3.2.11 TG2 activity in live cells 101

3.3 DISCUSSION 106

CHAPTER 4 TG2 UPREGULATION AND RELEASE IN DIFFERENT CELL TYPES 111

4.1. INTRODUCTION 111
The aims of the chapter: 113

4.2 RESULTS 114
4.2.1 TG2 upregulation during THP-1 monocyte differentiation into macrophage-like cells 114
4.2.2 Establishing the assay for analysis of ATP-induced IL-1β release from LPS-primed THP-1 cells 117
4.2.2.1 Optimization of THP-1 cell differentiation with ATRA 117
4.2.2.2 ATRA-mediated THP-1 cell differentiation simultaneous with LPS priming 117
4.2.2.3 THP-1 cell differentiation with ATRA followed by LPS priming 120
4.2.3 Constitutive TG2 release into the medium by serum starved MDA-MB-231 breast cancer cells 123
4.2.3.1 TG2 expression by MDA-MB-231 cells and its localization upon ATP and BzATP treatment 123
4.2.3.2 Enhanced secretion of TG2 in MDA-MB-231 cells stimulated with ATP 126
4.2.3.3 Changes in intracellular calcium induced by ATP and BzATP stimulation. 129
4.2.3.4 Attempt to inhibit TG2 secretion with P2X7R and P2X4R inhibitor 131

4.3 DISCUSSION 134

CHAPTER 5 ESTABLISHING CELL MODEL EXPRESSING FUNCTIONAL P2X7R 140

5.1 INTRODUCTION 140
THE AIMS FOR THE CHAPTER: 141
5.2 RESULTS 142
5.2.1 CLONING OF THE P2X7R CODING SEQUENCE INTO MAMMALIAN CELL EXPRESSION VECTOR 142
5.2.2 STABLE TRANSFECTION OF HEK293 CELLS WITH P2X7R AND P2X7R-V5-HIS EXPRESSION CONSTRUCTS 144
5.2.3 ACCESSING FUNCTIONALITY OF TRANSGENE IN HEK293 CELLS 147
5.2.3.1 P2X7R IMMUNOLOCALIZATION 147
5.2.3.2 ADAM ACTIVATION BY P2X7R 150
5.2.3.3 CHANGES IN INTRACELLULAR CALCIUM 153
5.2.3.4 BZATP DOSE RESPONSE MEASURED BY CHANGES IN INTRACELLULAR Ca^{2+} 159
5.3 DISCUSSION 162
CHAPTER 6 TG2 EXTERNALIZATION UPON P2X7R ACTIVATION 165
6.1 INTRODUCTION 165
THE AIMS OF THE CHAPTER: 167
6.2 RESULTS 168
6.2.1 TIME-DEPENDENT RELEASE OF TG2 INTO THE MEDIUM UPON P2X7R ACTIVATION 168
6.2.2 INHIBITION OF TG2 RELEASE WITH P2X7R INHIBITOR 171
6.2.3 EFFECT OF BZATP TREATMENT ON CELL VIABILITY 173
6.2.4 P2X7R-MEDIATED SECRETION OF TG2 FROM HEK293 CELLS IS NOT LINKED TO LOSS OF CELL MEMBRANE INTEGRITY 175
6.2.5 TG2 LOCALIZATION UPON P2X7R-STIMULATION 177
6.2.6 EXPOSURE OF PHOSPHATIDYLOSERINE EVOKED BY BZATP STIMULATION 184
6.3 DISCUSSION 186
CHAPTER 7 THE ROLE OF CA^{2+} SIGNALING IN TG2 SECRETION 190
7.1 INTRODUCTION 190
THE AIMS FOR THE CHAPTER: 192
7.2 RESULTS 193
7.2.1 POSSIBLE MECHANISMS OF P2X7R-EVOKED SIGNALING MEDIATING TG2 EXTERNALIZATION 193
7.2.2 REGULATION OF TG2 EXTERNALIZATION BY EXTRACELLULAR Ca^{2+} 195
7.2.4 TG2 RELEASE AFTER BLOCKING THE P2X7R ION CHANNEL 200
7.2.5 ANALYZING THE ROLE OF Ca^{2+} IN REGULATION OF P2X7R PORE FORMATION 200
7.3 DISCUSSION 205
CHAPTER 8 GENERAL DISCUSSION 210
8.1 PROPOSED MECHANISM: RAPID TG2 RELEASE IS TRIGGERED BY DANGER SIGNALS IN OSTEOARTHRITIS 211
8.2 CURRENT UNDERSTANDING OF CONSTITUTIVE TG2 RELEASE 213
8.2.1 TG2 RELEASE VIA RECYCLING ENDOSOMES 213
8.2.2 TG2 ENDOCYTOSIS FROM THE CELL SURFACE 214
8.2.3 TG2 SHED FORM CELLS IN MICROVESICLES AND MICROPARTICLES 215
8.3 MODULATORS OF TG2 AVAILABILITY ON THE CELL SURFACE/ECM 215
8.3.1 TG2 RELEASE REGULATED BY NITRIC OXIDE 215
8.4 FINAL CONCLUSIONS 216
REFERENCES 218

APPENDIX 1 ..... **243**
APPENDIX 2 ..... **245**
APPENDIX 3 ..... **248**
APPENDIX 4 ..... **265**

List of abbreviations

AA – amino acid

ADAMs – a disintegrin and metalloprotease proteins

AM – acetomethylester

ATP – adenosine-5'-triphosphate

ATRA – *all-trans* retinoic acid

Arf1 – ADP ribosylation factor 1

BzATP – 3'-O-(4-benzoyl)benzoyl adenosine 5'-triphosphate

C – cysteine

Ca^{2+} – calcium ions

CEB – cell extraction buffer

CD – coeliac disease

CMV – cytomegalovirus

COP – coat protein complex

CPPD – calcium pyrophosphate dihydrate

D – aspartic acid

DMEM – Dulbecco's Modified Eagle Medium

DMSO – dimethyl sulfoxide

DTT – dithiothreitol

ECM – extracellular matrix

EDTA – ethylenediaminetetraacetic acid

EGF – epidermal growth factor

ELISA – enzyme-linked immunosorbent assay

FXIIIa – factor XIIIa

FBS – fetal bovine serum

FGF2 – fibroblast growth factor 2

FN – fibronectin

GDP – guanosine-5’-diphosphate

G proteins – guanine nucleotide-binding proteins

GPR56 – G-protein-coupled receptor 56

GTP – guanosine-5’-triphosphate

GTPγS – guanosine-5’-(γ-thio)triphosphate

H – histidine

HBGB-1 – high-mobility group box chromosomal protein 1

HEPES – 4-(2-hydroxyethyl)-1-piperazineethanesulfonic acid

HLA-DQ – human leukocyte antigen, DQ subregion

HRP – horseradish peroxidase

HSPGs – heparan sulfate proteoglycans

IκBα - nuclear factor of kappa light polypeptide gene enhancer in B-cells inhibitor α

IL-1 – interleukin-1

IL-6 – interleukin-1

INFγ – interferon γ

K^+ – potassium cations

LAMP – lysosome-associated membrane proteins

LB medium – Luria-Bertani medium

LPS – lipopolysaccharide

LRP 1 – lipoprotein receptor-related protein 1

MHC – major histocompatibility complex

MMPs – matrix metalloproteinases

MVB – multivesicular bodies

MVs – microvesicles

MPs – microparticles

MW – molecular weight

Na^+ – sodium cations

NEM – N-ethylmaleimide

NFκB – nuclear factor kappa-light-chain-enhancer of activated B cells

NK cells – natural killer cells

NLR – Nod-like receptor

NSF – *N*-ethylmaleimide-sensitive factor

OA – osteoarthritis

ON – overnight

OptiMEM – modified Eagle's Minimum Essential Medium

P2X4R – ligand gated ion channel 4

P2X7R – ligand gated ion channel 7

PAD – peptidyl arginine deiminase

PBS – phosphate buffered saline

PCR – polymerase chain reaction

PEN - penicillin

PMSF – phenylmethanesulfonyl fluoride

Pi – inorganic phosphate

PSS – physiological salt solution buffer

RA – rheumatoid arthritis

ER – endoplasmic reticulum

RT – room temperature

SDS – sodium dodecyl sulfate

SNAREs – soluble N-ethylmaleimide-sensitive fusion (NSF) protein accessory receptors

STREP – streptomycin

TAE – Tris-Acetate EDTA buffer

TBS – Tris-buffered saline

TBST – Tris-buffered saline with Tween-20

TG – transglutaminase

TG2 – transglutaminase 2

TGFβ – transforming growth factor β

TIMP – tissue inhibitor of metalloproteinase

TNFα – tumour necrosis factor α

TPA – 12-O-tetradecanoylphorbol-13-acetate

W – tryptophane

Chapter 1 Introduction

1.1 Common forms of arthritis

Osteoarthritis (OA) is the most common form of joint disease in humans. According to data provided by Arthritis Research UK approximately eight million people in the United Kingdom have painful OA of the knee joint and more than one million adults consult their general practitioner each year with OA[1]. OA is strongly age related disorder and during ageing the prevalence to develop OA rapidly rises. Another important risk factor is joint injury or medical intervention such as joint surgery, which may lead to OA in later life. Other factors such as joint mal-alignment, obesity and gender also have a big impact on the outcome of the disease. OA is currently classified as a degenerative disease and the changes within the joint are manifested by cartilage loss associated with an increase in subchondral bone density and bone formation (Tab. 1.1).

On the other hand rheumatoid arthritis is a chronic autoimmune inflammatory disease that affects not only one joint, but can drive systemic inflammation (Tab. 1.1) (Pratt et al. 2009). Around 400,000 adults in United Kingdom suffer from RA[2]. The major risk factor is thought to be genetic predisposition, as mutations in allels of major histocompatibility complex (MHC) class II or human leukocyte antigen (HLA) DR subregion increases risk of developing RA up to 1.5-fold (Klippel 2007). A higher prevalence is seen in women than men with a factor of 3:1. As for all inflammatory diseases, an unhealthy lifestyle, bacterial or viral infections through lifetime can irreversibly lead to the autoimmune response that starts in the joint.

[1] Information source: http://www.arthritisresearchuk.org/arthritis-information/data-and-statistics/osteoarthritis.aspx
[2] Information source: http://www.arthritisresearchuk.org/arthritis-information/data-and-statistics/rheumatoid-arthritis.aspx

Table. 1.1 Comparison of the main features in OA and RA.

Osteoarthritis (OA)	Rheumatoid arthritis (RA)
Age-related degenerative disease	Chronic autoimmune disease
Gradual loss of cartilage and bone drive synovial inflammation	Inflammation drives destruction of cartilage and bone
Slow progression	Moderate to rapid progression
Primary target organ – cartilage	Primary target organ – synovial membrane
Focal dysregulation within joint	Systemic inflammation

Information in the table taken from Klippel 2007.

1.2 Cells and mediators involved in pathology of OA and RA

Although the pathology of OA and RA is different, the overall outcome for the patient can be similar (Loeser et al. 2012; Ademowo et al. 2013). Traumatic injury, aberrant joint loading or autoimmune reaction can lead to loss of articular cartilage, increase formation of the blood vessels and infiltration of immune cells into synovial fluid (Ademowo et al. 2013). Patients, which are affected by OA or RA, often feel tenderness, stiffness or pain within the joint. Different cell types are primary involved in the pathology of joint degeneration in OA (Goldring and Goldring 2007) and RA (Pratt et al. 2009) progression.

RA is an autoimmune disease that is mostly driven by activated blood cells infiltrating the joint space (Ademowo et al. 2013). Monocytes are being attracted to the joint, where they differentiate into macrophages. They secrete proinflammatory cytokines such as interleukin-1β (IL-1β) that further recruits T cells, B cells and dendritic cells into the joint. However, synovial fibroblasts are also playing an important role as they release proinflammatory cytokines: tumor necrosis factor alpha (TNF-α) and interleukin-6 (IL-6), which drive destructive responses in cartilage and chondrocytes. At the site of inflammation, synovial fibroblasts secrete chemokines (such as IL-8) and matrix metalloproteinases (MMPs), which contribute to cartilage and bone destruction. Beside elevated levels of cytokines and infiltrating cells, new blood vessels forming in the synovial walls, invade the joint space, which makes the joint wall thicker and swollen (Klippel 2007). Pannus tissue is forming at

the site, where bone, cartilage and synovium meet. Pannus formation further induces underlying bone erosion and joint degradation. RA is very heterogeneous disease and it is not clear, what drives the inflammation that leads to the disease. Beside genetic predispositions, alcohol abuse, smoking, bacterial and viral infections are considered as risk factors (Pratt et al. 2009).

OA is no longer considered as mainly a degenerative disorder as it is associated with both local (synovial) inflammation and potentially also low-level systemic inflammation (de Lange-Brokaar et al. 2012; van der Kraan 2012) (Fig. 1.1) Degradation of cartilage can cause synovitis and lead to changes in subchondral bone (Goldring and Goldring 2010). The chondrocytes respond to mechanical forces that deplete proteoglycan content, damage the collagen network and promote matrix degradation. As the main risk factor for OA is age, this disease develops due to changes in joint mechanics that ultimately cause cartilage surface thinning, cartilage extracellular matrix (ECM) reorganization, and loss of its elastic properties (Goldring 2000). The building blocks of articular cartilage are collagen, mainly type II, proteoglycans predominantly aggrecan and various glycoproteins, which upon OA progression change their composition. Chondrocytes in articular cartilage normally stay in the resting state but during OA progression undergo hypertrophy. Chondrocytes in OA cartilage are able to produce various inflammatory mediators, such as IL-1β and IL-1β converting enzyme (caspase-1) (de Lange-Brokaar et al. 2012). This is accompanied with elevated expression of MMPs (1,3 and 13) (Goldring and Goldring 2010), aggrecanases (ADAMTS-4 and ADAMTS-5). Also proinflammatory cytokines can be present such as IL-6 or TNF-α coming from infiltrating cells or synovium. Increased levels of tissue markers for inflammation such as advanced glycation endproducts (AGE) and high-mobility group box chromosomal protein 1 (HMGB-1) were found in the synovium of spontaneous OA mouse model, which positively correlated with increased serum levels of proinflammatory cytokine IL-1β (Kyostio-Moore et al. 2011). Moreover, accumulation of components of the complement system (C3a and C5b-9) in synovial fluid collected from early OA patients, has previously been identified, using proteomic techniques and enzyme-linked immunosorbent assays (ELISA) (Wang et al. 2012). Fragments of degraded cartilage, which act on synovial fibroblasts to release inflammatory mediators, might initiate the presence of inflammation during

OA. Alternatively, synovium itself could play a role as source of infiltrating macrophages, which drive cartilage destruction (Berenbaum 2012). It is therefore important to investigate how chondrocytes respond to inflammatory mediators and danger signals present in the synovial fluid, in order to be able to understand the molecular mechanisms driving OA progression and to define potential targets for therapeutic intervention.

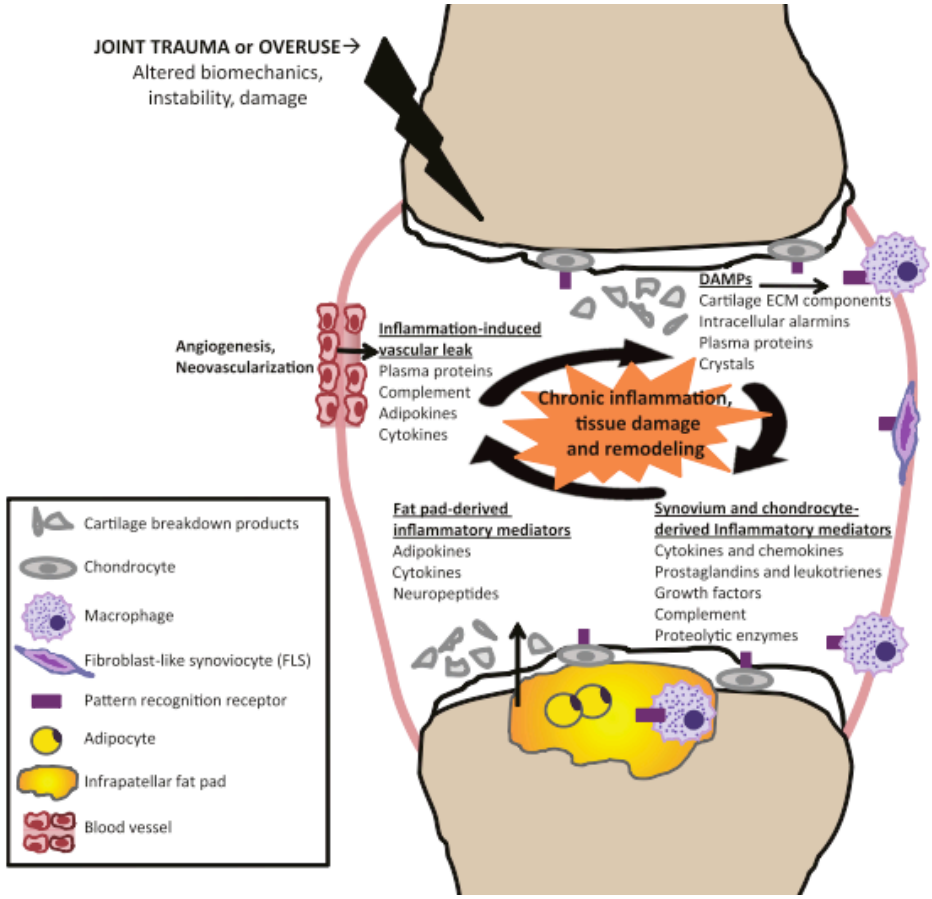

Fig. 1.1 Joint destruction in OA and the main mediators involved. Excessive mechanical stress on quiescent chondrocytes leads to their differentiation and production of cytokines, chemokines and MMPs that drive cartilage degradation. Tissue disruption leads to production of damage-associated molecular patterns (DAMPs), fragments of degraded ECM and alarmin proteins that feeds back on residual macrophages, synovial fibroblasts and chondrocytes to secrete inflammatory molecules. This promotes further cartilage destruction, expression of proteolytic enzymes and an innate immune response. Reproduced from Sokolove and Lepus 2013.

1.3 Biological markers for arthritis

The diagnosis of OA is confirmed by x-ray or MRI, yet these scans detect gross structural changes, which occur late in disease, and there are currently no reliable diagnostic or prognostic biochemical markers for early diagnosis (Rousseau and Delmas 2007; Ademowo et al. 2013). Hence, there is an urgent need to identify biological markers for early diagnosis and/or patient stratification for therapy (Ademowo et al. 2013). The fast growing field of biological markers needs novel approaches to identify diagnostics indicators with higher specificity and/or sensitivity for distinct disease processes (Rousseau and Delmas 2007). Genetic, proteomic and metabolomic studies are in progress to improve the prediction and outcome of RA (Smolen et al. 2008) and OA (Goldring and Goldring 2007). For OA, it is likely that a combination of several biological markers in addition to imaging techniques will be needed to diagnose the stadium of joint disease (Goldring and Goldring 2007). As OA is a degenerative disorder affecting mainly joint tissues, molecules of bone, cartilage and synovial tissue turnover have been tested as potential biomarkers (Berenbaum 2013). Products of metabolism such as MMPs, TIMPs and products of cartilage breakdown have been thought to be good candidates for detecting pathological changes within joint (Sokolove and Lepus 2013). However, changes in protein turnover seem to have a low specificity to detect OA, as changes in protein turnover can occur for many reasons and this is particular problem in an aged population (Berenbaum 2013)). In the context of RA, mainly autoantibodies or cytokines were tested (Smolen et al. 2008). Many of them failed to be good candidates for biomarkers, as body fluids from patients showed highly variable levels of these molecules independently of disease status. As RA is a highly heterogeneous joint disease, which maybe influenced by a range of different gene products there are many variations in the pathogenesis of the disorder.

Recent evidence suggests that diagnostic assays based on the detection of proteins or peptides with posttranslational modifications may have a higher specificity than assays detecting changes in protein levels (Doyle and Mamula 2002). Therefore these assays could potentially be a highly predictive to detect abnormalities in RA and OA cartilage. The biochemical modifications within the proteins might play an important role during initiation of the disease, compromise

protein function and potentially leading to the development of autoimmunity (Doyle and Mamula 2005).

1.4 Post-translational protein modifications

Protein synthesis is based on the 20 amino acids, which are the building blocks for newly synthesized proteins. However, these 20 amino acids can be further posttranslationally modified in various ways giving a total of 140 distinctive amino acids present in proteins (Doyle and Mamula 2002). The term "posttranslational modification" is generally used to describe any type of covalent modification that can be added to the synthesized protein/polypeptide in the intracellular or extracellular environment. This term can be used to describe the modification of a currently present amino acid that subsequently changes its nature through introduction of structural bridges within the protein. The covalent modifications either occur spontaneously or are enzymatically added to the proteins. There are up to 27 different types of protein covalent modifications and the most abundant include: N-linked glycosylation, phosphorylation, methylation, ubiquitylation, acetylation, citrullination, palmitoylation, sulfation and O-linked glycosylation (Khoury et al. 2011). Posttranslational modifications are important for the structure and function of proteins, as they can change protein conformation, and they are believed to modulate protein stability by acting as allosteric effectors (Xin and Radivojac 2012).

During the inflammatory responses the nature of posttranslational modifications such as glycosylation, citrullination, glycation or deamidation is altered (Doyle and Mamula 2002). Infection or trauma also induces many posttranslational modifications, which are mediated by enzymes that can be released at the site of inflammation. Thus, not only protein modifications should be analyzed but also localization and catalytic activity of enzymes involved in regulation these modifications can provide initial clues of disease progression. Early OA disease-specific modified peptides are likely to provide a sensitive biochemical indicator, if such peptides can be identified in the future, as exemplified by the association of citrullinated peptides with RA (Nijenhuis et al. 2004). Anti-citrullinated protein/peptide antibodies are a powerful biomarker for diagnosing RA (Szodoray et al. 2010). It was shown that anti-citrullinated peptide antibodies that can be detected

in the sera of patients with RA are the best disease indicator currently available and that they have strong prognostic significance (van Venrooij et al. 2006). Those antibodies can be found in RA patient samples with the established test called cyclic citrullinated peptide assay, which has a sensitivity reaching up to 80%. One of the enzymes that is responsible for mediating posttranslational modifications during inflammation is transglutaminase 2 – a member of the transglutaminase family of proteins. Transglutaminase 2 is upregulated in the stress response (Siegel et al. 2008) and represents a self-antigen during coeliac disease (Sollid 2002). Transglutaminase 2 has a potential role in OA and is the candidate molecule studied in this project.

1.5 Family of transglutaminases

Transglutaminases (TGs) are a family of proteins that mediate post-translational protein modifications that are essential in diverse biological processes such as blood coagulation, extracellular matrix stabilization or skin barrier formation (Iismaa et al. 2009). In man, there are nine members of the transglutaminase family described: TG1, TG2, TG3, TG4, TG5, TG6, TG7, Factor XIIIa (FXIIIa) and Band 4.2 protein. They are closely related to cysteine proteases and together they are classified into the superfamily of papain-like enzymes (Lorand and Graham 2003). The expression of the different transglutaminases varies between tissues, therefore the original nomenclature of the family members was derived form the tissue, where the presence and activity of a specific transglutaminase was first detected (Grenard et al. 2001) (Tab.1.2). Eight transglutaminases, TG1-7 and FXIIIa, are enzymatically active. Band 4.2 protein is the only member that lacks enzymatic activity and acts as a scaffolding protein in erythrocytes. Four family members are present as zymogens and proteolytic cleavage generates the fully active enzyme. This was reported for TG1 (Steinert et al. 1996), TG3 (Ahvazi et al. 2003), TG5 (Pietroni et al. 2008) and FXIIIa (Muszbek et al. 1996). All family members have a similar protein structure that consist of a N-terminal β-sandwich, α/β catalytic core domain that harbors the cysteine-histidine-aspartic acid active site residues together with tryptophan residues stabilizing the active site as well as two C-terminal β-barrels (Pinkas et al. 2007). TG1 and FXIIIa contain an additional pro-peptide before the N-terminal β-sandwich that is cleaved for enzyme activation (Iismaa et al. 2009).

Table. 1.2 Tissue expression, function and involvement in disease pathology of different members of transglutaminase family.

Protein	Other name	Main distribution	Biological function	Link with disease
TG1	TG_K, keratinocyte TG	Keratinocytes, other tissues at low level	Cornified-envelope formation	Lammellar ichthyosis
TG2	TG_C, tissue TG	Ubiquitous expression	Cell adhesion and motility, matrix assembly, signal transduction, cell survival, apoptosis, cell differentiation and many others	Coeliac disease, and many others suspected including Alzheimer's disease, Parkinson's disease, Huntington's disease, osteoarthritis, breast and ovarian cancer
TG3	TG_E, epidermal TG	Epithelium, brain, hair follicle	Cell-envelope formation	Dermatitis herpetiformis
TG4	TG_P, prostate TG	Prostate, salivary gland	Semen coagulation	Unknown
TG5	TGx	Uterus, keratinocytes, osteoblasts, ovaries, mammary gland	Cornified cell envelope formation	Peeling skin syndrome
TG6	TG_Y	Testis, lungs, cerebral cortex, olfactory lobe, cerebellum, spinal cord, stratified epithelia	Unknown	gluten ataxia, cerebellar ataxia
TG7	TG_Z	Testis, lung, and many other tissues	Unknown	Unknown
FXIIIa	Fibrin-stabilizing factor	Platelets, monocytes, macrophages, chondrocytes, dendritic cells	Blood clot formation, wound healing, bone development, embryo implantation during pregnancy	FXIIIa deficiency (= bleeding disorder)
Band 4.2	B4.2	Erythrocytes, bone marrow, spleen	Scaffolding protein in membrane of erythrocytes	Unknown

Table adapted from (Lorand and Graham 2003) and (Mehta and Eckert 2005).

1.6 Enzymatic reaction mediated by transglutaminases

TGs are capable of catalyzing Ca^{2+}-dependent acyl-transferase reactions, which can give rise to various posttranslational protein modifications (Aeschlimann and Thomazy 2000). The substrates of TGs are mainly the γ-carboxamide group of the side chain of the targeted glutamine (Q) residue normally localized within a flexible region of the protein (Mehta and Eckert 2005). Q accessibility seems to be more important than the sequence, which surrounds the Q residue although there is sequence specificity. On the other hand, TGs do not react with free amino acid Q. A unique crosslinking reaction is the most characteristic reaction catalysed by TGs and results in the formation of covalent N^{ε}(γ-glutamyl)lysyl isopeptide bonds between proteins or within polypeptides (Lorand and Graham 2003). However, depending on the nature of the substrates available, TGs catalyze other reactions that can be grouped into: 1) transamidation – these reactions lead to protein crosslinking or amine incorporation; 2) esterification; 3) hydrolysis – involved in deamidation and isopeptide cleavage (Iismaa et al. 2009). The reaction starts, when the protein- or polypeptide-bound "acceptor" Q reacts with cysteine localized in the TGs active site (Fig. 1.2). At first, the thiol group of cysteine (C) together with histidine (H) and tryptophan (W) residues form an oxyanion intermediate with the γ-carboxyamide group of the Q in the substrate. Then the substrate transiently acylates the thiol group in the active site to form the acylenzyme intermediate with the Q-containing substrate. This step is rate-limiting and results in the ammonium or amine release and formation of a covalently bound transient γ-glutamylthioester (Lorand and Graham 2003). The reaction can further proceed into transamidation, esterification or hydrolysis and depends on the nucleophile that provides the electron pair and all reactions ultimately lead to thioester bond cleavage in the enzyme active site and enzyme regeneration (Mehta and Eckert 2005) (Fig. 1.3). The transamidation begins with the nucleophilic attack of the amino group of the second "donor" substrate (Iismaa et al. 2009) (Fig. 1.2). The W residue stabilizes the oxyanion intermediate that is formed with the active site C through hydrogen bonding. If the second substrate is the ε-amino group of deprotonated lysine localized on another protein, the reaction results in protein crosslinking leading to γ-glutamyl-ε-lysine isopeptide bond formation between two proteins. Another possibility of transamidation is the amine or polyamine incorporation into the acceptor Q on the donor protein. The

esterification occurs when the second available substrate is an alcohol. However, in the absence of a second donor substrate, a H_2O molecule can drive the reaction resulting in hydrolysis. This leads to deamidation of the protein-bound glutamine residue, i.e. replacement of the $–NH_2$ group into –OH, which converts glutamine into glutamate. The hydrolysis can also occur in the presence of already crosslinked polypeptide, whereby the isopeptide bond is cleaved by TGs. This effectively constitutes the reverse reaction of the second step in the transamidation/esterification reaction. The reactions of transamidation compete between each other and with esterification and they are reversible (Lorand and Graham 2003). However, both reactions leading to hydrolysis proceed only into one direction.

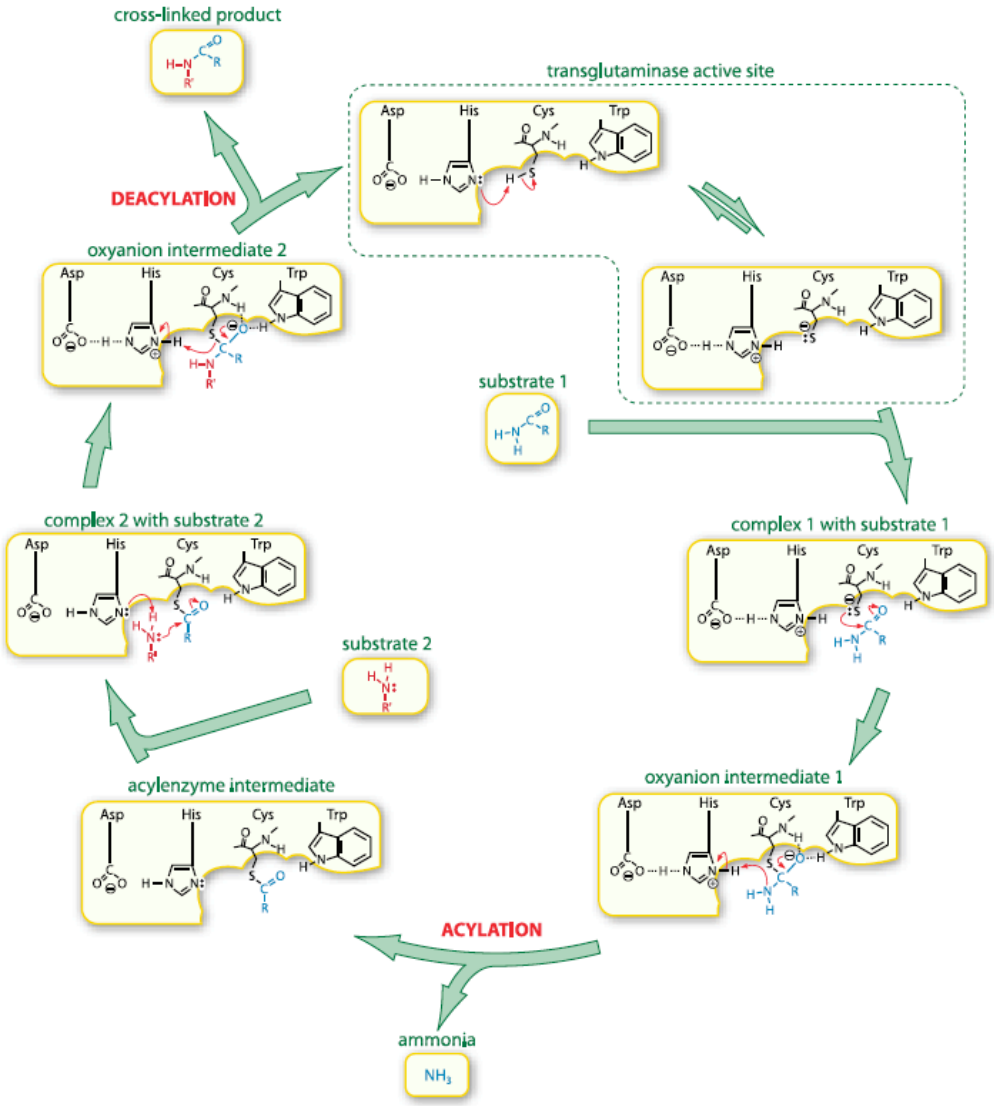

Fig. 1.2 Mechanism of reactions catalyzed by transglutaminases. The active site of TGs relies on catalytic triad cysteine, histidine and aspartic acid residues, and the W involved in the transition state stabilization. The reaction begins when the γ-carboxamide group in the side chain of Q residue in the first substrate transiently acylates the thiol group in the TG2 active site. This leads to the formation of the oxyanion intermediate that is stabilized by the hydrogen bonds on both C and W. Formation of the thioester acylenzyme intermediate results in release of ammonium. In the presence of the second substrate (e.g. an amine), the electron pair of the of the amino group enhances the formation of the second oxyanion intermediate stabilized by hydrogen bonding with C and W residues. This results in the crosslinking of both substrates and release of the product that is followed by enzyme regeneration. Reproduced from Iismaa et al 2009.

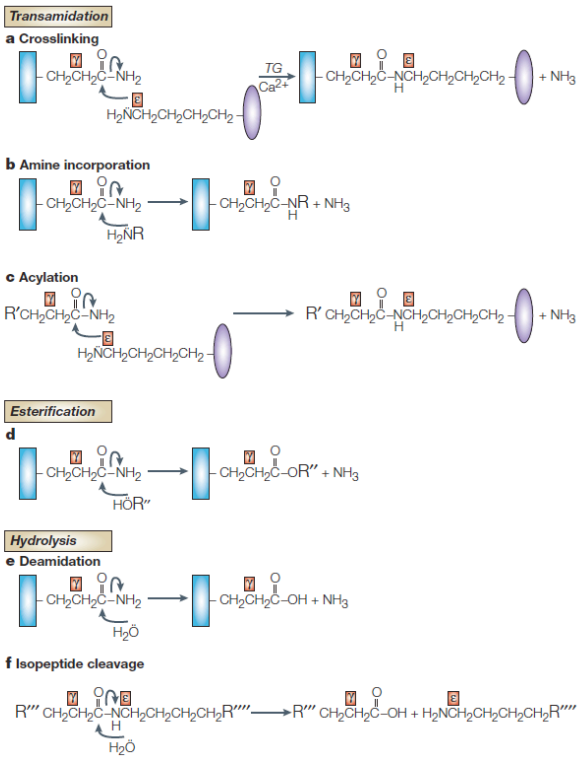

Fig. 1.3 Types of reactions catalyzed by transglutaminases. The Ca^{2+}-dependent acyl-transfer reactions mediated by TGs can be classified into transamidation (a, b, c), esterification (d) or hydrolysis (e, f) depending on the second nucleophile donor. Q acceptor residue (blue rectangle); lysine donor residue (purple ellipse); R (side chain of primary amine); R' (peptide with reactive Q); R'' (ceramide); R''' and R'''' (the side chains of branched isopeptides). Reproduced from Lorand and Graham 2003.

1.7 Biological function of TG-mediated reactions

The reactions catalyzed by transglutaminases have many important biological roles (Aeschlimann and Thomazy 2000). The deamidation reaction that preferably occurs in an acidic environment leads to the change of uncharged glutamine into negatively charged glutamate, which can dramatically affect protein behaviour. This is exemplified by the role of deamidation of peptides in the context of coeliac disease (Sollid 2002). Cross-linking of two proteins leading to covalent complexes is important for mediating tissue stability. TGs' extracellular activity contributes to ECM stabilization by selectively crosslinking proteins (Aeschlimann and Paulsson 1991; Raghunath et al. 1996; Raghunath et al. 1999). The formation of covalent N^{ε}(γ-glutamyl)lysyl isopeptide bonds between or within polypeptides, enhances the strength of the tissue and makes it more resistant to proteolytical or chemical

degradation (Aeschlimann and Thomazy 2000). This feature is also important in the process of wound healing, the stress responses and programmed cell death (Raghunath et al. 1996; Iismaa et al. 2009). For example, stabilization of the intracellular content by crosslinking during formation of apoptotic bodies is an important function of TG2. Stabilization of protein assemblies is also of importance during blood-clot formation and is mediated by FXIIIa (Komáromi et al. 2011). The FXIII protein present in plasma is a tetramer that consists of two FXIIIa subunits (with transglutaminase activity) and two FXIIIb subunits (belongs to distinct protein family and act as inhibitory proteins). In the last phase of the blood coagulation cascade, FXIII becomes cleaved by thrombin in the presence of Ca^{2+}. The disassembly of the FXIIIb subunits from FXIIIa leads to transglutaminase activation and formation of the γ-glutamyl-ε-lysine bridges that stabilize the fibrin clot. This is important for avoiding delayed bleeding and the process of wound healing as it makes the elastic fibrin matrix resistant to lytic enzymes that can be used for the wound closure and infiltration of the repair cells (Iismaa et al. 2009). Thus, both FXIIIa and TG2 are important molecules in tissue repair, with specific roles in clot formation and angiogenesis. Additionally, the presence of TGs is important in differentiation of keratinocytes and their crosslinking activity is required for cornification of the epidermal cells (Mehta and Eckert 2005). The expression of TGs varies between the skin layers. TG2 is mostly expressed in the dermis and epidermal cell adjacent to the basement membrane (Rhgjamonth 1996). Both TG1 and TG5 can be detected in the upper layers of epidermis whereas TG3 is present in the outer part of granular layer and in the part corresponding to stratum corneum (John et al. 2012). It seems that TG2 is involved in stabilizing the junction between the dermal and epidermal layers (Candi et al. 2002). On the other hand TG1, TG3 and TG5 introduce cross-links within the cornified envelope. In this case, not only protein cross-linking through transamidation but also anchorages of the protein scaffold to the underlying lipid membrane through esterification is of importance (Nemes et al. 1999).

1.8 TG2 – the candidate molecule catalyzing posttranslational protein modifications

1.8.1 TG2 protein expression

One member of the TG family – transglutaminase 2 (TG2) is a ~80 kDa protein widely distributed throughout the body and in many instances expressed at much higher level than any of the other enzymes of the family (Thomázy and Davies 1999; Lorand and Graham 2003; Nurminskaya and Belkin 2012). As TG2 is the most abundantly expressed member of the transglutaminase family, it is also one of the most studied and as a consequence has been postulated to have many intra- and extracellular functions (Pinkas et al. 2007). Endothelial cells, smooth muscle cells and fibroblasts show constitutive expression of TG2 (Iismaa et al. 2009). Moreover, macrophages, hepatocytes and chondrocytes express TG2 at variable levels during cell differentiation with the highest levels at terminal differentiation (Aeschlimann and Thomazy 2000). Most of the protein localizes in the cytosol (80%) but it can also be found associated with the cell membrane (10-15%) and nuclear membrane (5%) (Lorand and Graham 2003). The *TGM2* gene that encodes TG2 contains 13 exons and 12 introns and is localized on chromosome 20q11-12. Of the nine described TGs in man, TG2 evolved from the same branch as TG3 and TG6 (Grenard et al. 2001). TG3 and TG6 likely arose form a cluster of genes that was formed through tandem gene duplication of an ancestral tissue type protogene. The elements regulating gene expression differ between isoenzymes (Aeschlimann and Thomazy 2000). The *TGM2* gene contains response elements for retinoic acid (ATRA) (Nagy et al. 1996), interleukine-6 (IL-6) (Suto et al. 1993), transforming growth factor β (TGF-β) (Ritter and Davies 1998) and nuclear factor kappa-light-chain-enhancer of activated B cells (NF-κB) signaling pathways (Mehta and Han 2011a).

1.8.2 TG2 protein structure and regulation of enzymatic activity

Similarly to other members of the TG family, TG2 consists of four domains (Mehta and Eckert 2005). The first being the β-sandwich on the N-terminus. The catalytic core domain contains six β-strands and four α-helices. The active site cysteine (C277) is situated in a pocket formed by three α-helices. Two tryptophan residues

(W241 and W332), which stabilize the substrate in the active site are flanking the pocket. Two other residues of the catalytic triad: histidine (H335) and aspartic acid (D358) are localized on the neighboring β-sheets. The core domain is connected to β-barrel 1 by a flexible loop. β-barrel 1 is created by six β-strands and one β-turn. Most distal domain forming the C-terminus is β-barrel 2, which is composed of seven β-strands that are localized antiparallel to each other. TG2 is a protein with enzymatic activity that is allosterically regulated by guanine nucleotides (GTP/GDP) and Ca^{2+} ions (Achyuthan and Greenberg 1987; Begg et al. 2006). Guanosine-5'-triphosphate (GTP) serves as a potent allosteric inhibitor of TG2 that suppresses Ca^{2+}-activated crosslinking activity. Thus, in the cytosol TG2 remains in a GTP-bound "closed" conformation, which lacks transamidation activity (Fig. 1.4). TG2 possesses GTPase activity and hydrolyses GTP to GDP (Nakaoka et al. 1994). GTP-binding decreases the accessibility of the TG2 substrate binding pocket by masking the active site (Di Venere et al. 2000). The GTP-bound conformation of TG2 can be changed by > 200 μM of Ca^{2+}, facilitating transition into the "open" conformation and inducing catalytic activity (Pinkas et al. 2007). Activation of TG2 requires binding of at least two Ca^{2+} ions and is associated with a large conformational change, whereby the two C-terminal β-barrels rotate almost 180˚ into the plane (120 Å from closed to open) of the core/β-sandwich domain of the enzyme. This rotation opens the active site and allows substrate access. Current understanding suggests that TG2 is rapidly converted into the activated form upon its release from cell in the presence of high extracellular Ca^{2+} concentrations. However, some reports suggest that secreted TG2 remains in a GTP/GDP-associated closed conformation after externalization and beyond and that this depends on the microenvironment encountered (Johnson and Terkeltaub 2005).

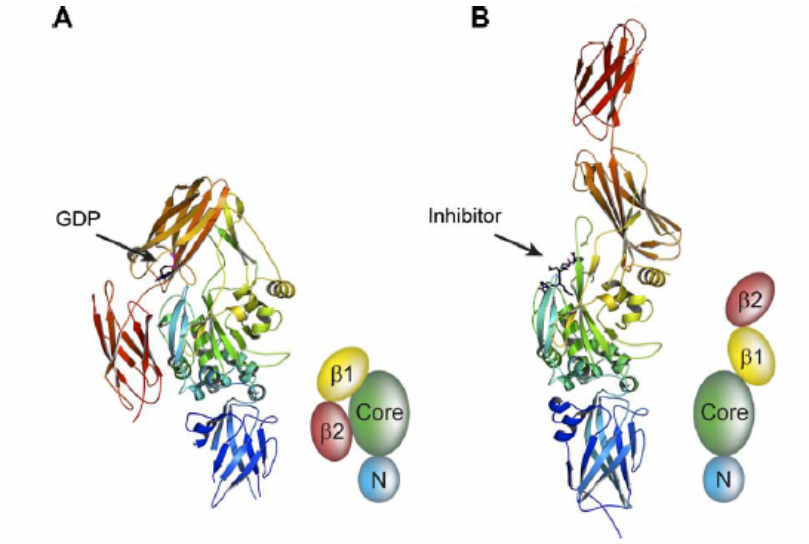

Fig. 1.4 Schematic representation of the closed and open confirmation of TG2. A. closed conformation of TG2 with GDP bound; **B.** open confirmation after addition of a specific inhibitor, Ac-P(DON)LPF-NH_2, trapping the transamidation intermediate; Blue – N-terminal β-sandwich, green – catalytic core domain, yellow and red – β-barrels. Reproduced from Pinkas et al. 2007.

Before the TG2 crystal structure was solved in both the "closed" (GDP-bound) and "open" (inhibitor-stabilized) state by Liu and colleagues (Liu et al. 2002) and Pinkas and colleagues (Pinkas et al. 2007), respectively. It was predicted that TG2 catalyzed crosslinking of two proteins with bulky residues would lead to drastic changes in TG2 conformation (Liu et al. 2002; Mehta and Eckert 2005). Thus, it was postulated that expansion of the TG2 structure is necessary for a internal "channel" to be formed, where both substrates could interact with the enzyme's catalytic residues (Mehta and Eckert 2005). Although the GTP/GDP "closed" form seems to truly represent the TG2 inactive state, it is still debatable whether the inhibitor-bounded "open" structure is actually representing the activated TG2 or just one of the transition states (Király et al. 2011). TG2 can act as an ATPase as well and the crystal structure with adenosine-5'-triphosphate (ATP) bound has been solved (Han et al. 2010). This confirmed that ATP can bind to the same pocket as GTP, but showed that different residues coordinate the ATP molecule through hydrogen bonds and ionic interactions. However the affinity for ATP is several orders of magnitude lower compared to GTP (Achyuthan and Greenberg 1987; Schaertl et al. 2010).

The Ca^{2+} activated TG2 crystal structure is still missing and therefore, the presence of 3-6 Ca^{2+} binding sites proposed in the literature, based on calorimetric analysis and computational studies remains a matter of debate (Bergamini et al. 2010; Király et al. 2013). The crystal structure of the closely related TG3 was solved in the presence of Ca^{2+}, and the data set confirmed the existence of three Ca^{2+} binding sites (Ahvazi et al. 2002). The first of the Ca^{2+} binding sites seems to be constantly occupied and crucial for activity. Occupation of the second Ca^{2+} binding site induces small structural changes, but the ultimate conformational change and full enzyme activation is mediated by binding of Ca^{2+} ion into the third site. This allows for exposure of the two tryptophane residues and enables them to stabilize the active site and approach of the substrate.

A recent study revealed the presence of an internal disulfide bond that situated between cysteine residues (C370-C371 and C230-C370) stabilizes the open conformation (Stamnaes et al. 2010). This modification occurs through oxidation in the extracellular environment and is regulated by redox conditions. The shift between those disulfide bonds is suggested to be a mechanism for regulation of the TG2 enzymatic activity, whereby oxidation reversibly inactivates the enzyme. Thus, the level of active TG2 present in the extracellular milieu can be influenced by the local oxidation state and modulated by the presence of Ca^{2+} as well as substrate.

An interesting and unusual feature of TG2 is the large conformational change for activation. TG2's structural change to the "open" conformation could potentially expose self-epitopes normally not present within the tissue that drive immunological responses (Pinkas et al. 2007). In gluten sensitivity, the production of autoantibodies against TG2 is detected (Sollid 2002).

1.8.3 Intracellular functions of TG2

Inside the cell, where the concentrations of free GTP are fluctuating from 50 to 300 μM (Király et al. 2011), TG2 efficiently binds and can hydrolyze GTP to GDP, and like other G proteins, participates in signaling pathways. Thus, inside the cell TG2 acts as a high-molecular-weight G-protein involved in G-protein coupled receptor signaling, e.g. linking with α_{1B} adrenergic receptor or oxytocin receptor for PLCδ signal transduction (Nakaoka et al. 1994). GTP binding probably also protects TG2 from intracellular cleavage by calpain (Zhang et al. 1998). It is debatable whether

intracellular TG2 can catalyse reactions of transamidation (Nurminskaya and Belkin 2012). Some reports suggest that intracellular TG2-catalysed transamidation reactions lead to modification of the small RhoA GTPases and that this promotes its binding to ROCK-2 protein kinase and its phosphorylation (Singh et al. 2001). The later acts on the cytoskletetal protein vimentin and induces cell adhesion. Also, the interaction of TG2 with the microtubule network and more specifically, β-tubulin was reported (Song et al. 2013). TG2 can be imported into the nucleus by nuclear transporter protein, importin-α3, and has been reported to modify histones (Peng et al. 1999). There is also strong evidence that indicates that TG2 mediates cell-matrix interactions that affect spreading and migration (Stephens et al. 2004). In fact it was shown that TG2 alters cell spreading on a number of ECM substrates such as fibronectin, collagen type I and laminin variants. This may involve both intracellular as well as extracellular activities of TG2. However, it has been shown TG2 plays a role in activation of PKC-α signaling and phosphorylation of FAK kinase that enables focal adhesion formation.

1.8.4 Extracellular TG2 and its interaction partners in the ECM and on the cell surface

TG2 interacts with many ECM and transmembrane proteins and this is known to affect cell adhesion, motility and spreading as well as signaling and cell differentiation (Stephens et al. 2004; Johnson and Terkeltaub 2005; Zemskov et al. 2006). In many instances, those interactions have roles that are independent of TG2 transamidation activity. TG2 was shown to interact with fibronectin (Gaudry et al. 1999), integrins (Akimov and Belkin 2001; Zemskov et al. 2006), syndecan-4 (Scarpellini et al. 2009); GPR56 (G-protein coupled receptor 56) (Xu et al. 2006), low density lipoprotein receptor-related protein 1 (LRP1) (Zemskov et al. 2007), MMP-2 (Stephens et al. 2004), platelet-derived growth factor receptor (PDGFR) (Zemskov et al. 2009) to name a few (Fig. 1.5). Hydrolysis of extracellular ATP by TG2 was postulated to be major function of cell-surface TG2 in osteoblasts and the hydrolysis product inorganic pyrophosphate is likely involved in promoting mineralization (Nakano et al. 2007).

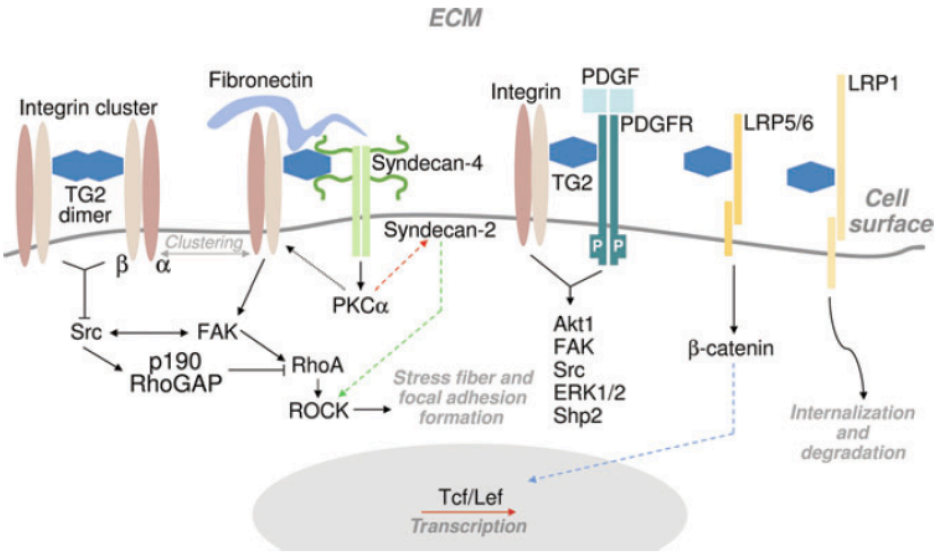

Fig. 1.5 The main binding partners of TG2 present on the cell-surface and in the ECM and the effect of these potential interactions on downstream signaling. Reproduced from Belkin 2011.

Fibronectin (FN) is a major component of the extracellular matrix (Mecham 2011). It is a glycoprotein of high molecular weight that is abundantly synthesized by fibroblast and many other cell types. It forms an organized ECM. An alternative splice variant of FN is available as soluble form in plasma as well. FN is a key substrate for cell surface receptors, integrins, and this complex mediates cell adhesion, spreading as well as migration. Overexpression of TG2 in fibroblasts causes significant increases in crosslinking of FN (Verderio et al. 1998). However, TG2 activity is not crucial for FN polymerization into fibrils but enables binding of soluble FN and thereby initiate its incorporation into ECM (Akimov and Belkin 2001). TG2 binds to FN and this interaction does not require catalytic activity (Gaudry et al. 1999). The interaction is mediated by a short sequence localized in the N-terminal β-sandwich domain. TG2 binds FN at the $I_6II_{1,2}I_{7\text{-}9}$ modules that are localized in the gelatin-binding region of FN. This interaction does not restrict the interaction of FN with integrins. In fibroblasts, TG2 is co-expressed on the cell surface with α5β1 integrin (Akimov and Belkin 2001). In monocytes differentiated into macrophages cell-surface TG2 was proposed to be in a complex with integrins containing the β1, β3 and β5 subunits (Akimov and Belkin 2001). TG2 and β2 integrin interaction possibly occurs in recycling endosomes as both proteins could be co-immunoprecipitated from perinuclear vesicles isolate from NIH3T3 fibroblasts

(Zemskov et al. 2011). The recruitment of TG2 into recycling endosomes may involve interaction of TG2 with phosphatidylinositol (3)-phosphate (PI(3)P), phosphatidylinositol (4)-phosphate (PI(4)P) and phosphatidylinositol (5)-phosphate (PI(5)P) through unique sequence (^{590}KIRILGEPKQRKK^{602}) (Zemskov et al. 2011).

TG2 can be actively internalized from the cell surface and degraded intracellularly. It was shown that both PDGF and soluble FN induced TG2 endocytosis and lysosomal degradation (Zemskov et al. 2009). TG2 internalization may require interaction with low density lipoprotein receptor-related protein (LRP1) for endocytosis, at least in some cell types (Zemskov et al. 2006).

Syndecan-4 belongs to the family of heparan sulphate proteoglycans and is a transmembrane proteoglycan (Mecham 2011). The TG2 interaction with syndecan-4 leads to protein kinase C α activation (Telci et al. 2008). Kinase activation transactivates inside-out signaling through β1 integrin. TG2 was shown to associate with heparan sulphate chains of syndecan-4 and binding was not affected by changes in the TG2 conformation and do not affect TG2/FN interactions (Scarpellini et al. 2009). TG2 and syndecan-4 were co-localizing at the focal adhesions underlying the cell membrane of mouse fibroblasts. Wang and colleagues (2012) showed that TG2 is interacting with heparan sulphate through a binding site (^{202}KFLKNAGRDCSRRSSPVYVGR^{222}). Binding of TG2 to syndecan-4 in the absence of interaction with FN could restore activation of protein kinase C α signaling, ERK1/2 phosphorylation and rescue ability of cells to spread. As MMPs are involved in the shedding of heparan sulphate from the cell surface, they proposed a model in which TG2-bound is to syndecan-4 in its "closed" form and is shed from the cell surface by MMPs and that this cleavage might induce TG2 "opening" and its activation. Another group has proposed that heparan sulphate is binding to TG2 in its "closed" form as they identified clusters of positively charged residues (^{262}RRWK^{265} and ^{598}KQKRK^{602}) that is adopting a linear binding pocket when TG2 is in its compact conformation (Lortat-Jacob et al. 2012). Therefore it was suggested, that TG2 activation through Ca^{2+} leads to a reduced affinity for heparan sulphate and therefore TG2 "release" from this complex.

1.8.5 Studies using TG2 knock-out mice

TG2 knock-out mice have been developed using homologous recombination to delete exon 6, that encodes catalytic the core domain (Laurenzi and Melino 2001). Surprisingly, TG2 deficient mice had no developmental abnormalities, no obvious changes within the organs and were reproducing normally. There was some residual TG activity detectable in liver and thymus extracts, probably due to TG1 compensating for TG2 deficiency. The authors of that study showed that TG2 expression is not necessary for the process of apoptosis as in both thymocytes and fibroblasts derived from knock-out animals apoptosis was occurring normally. However, the fibroblasts from TG2 deficient mice were less adherent, when transferred into cell culture. Another line of TG2 knock-out mice was established using the Cre/loxP site-specific system (Nanda et al. 2001). Here exons 6-8 were deleted, leading to the loss of the whole TG2 catalytic core. These mice lacking TG2 were viable and normal in size as well as weight. However, in this study the thymus from $tgm2^{-/-}$ mice showed a significant increases in number of apoptotic cells induced by dexamethasone treatment indicating that crosslinking of cellular content by TG2 might be required for apoptotic cell clearance. As before, the fibroblasts isolated from TG2 knock-out mice were less adherent in cell culture than fibroblasts from wild-type mice. The lack of obvious abnormalities in TG2 deficient mice may be explained by the activity of other TGs (FXIIIa in particular) that partially compensate the absence of TG2 (Mehta and Eckert 2005). Many studies have been conducted using these mice and collectively, these show that deficiencies become apparent once the mice are subjected to different types of stress (Oh et al. 2011). The inflammatory response in particular is substantially different than in normal mice (Yoo et al. 2013).

1.9 Involvement of TG2 in pathological processes

The importance of studying the TGs pleiotropic functions emerged from the realization that this enzyme has a big impact on inflammatory, autoimmune as well as degenerative diseases (Iismaa et al. 2009). The involvement of TG2 has been well documented for different stages of a number of different diseases, where are upregulated or aberrant activity of the enzyme has been reported. Most evidence

exists for coeliac disease, Alzheimer's disease, Parkinson's disease, Huntington's disease, osteoarthritis, cancer and fibrotic processes in different organs. The common link may be a function of T2 in inflammation and wound healing. While many of the non-catalytic actions of TG2 are important in the interaction with other molecules, however the Ca^{2+} dependent enzymatic activity is the function that enables TG2 to introduce novel post-translational protein modifications. Posttranslational protein modifications introduced by TG2 create neo epitopes within a target antigen, which could then be recognized by immune cells as foreign molecules (Sollid 2002). Therefore, TG2 is an interesting candidate molecule potentially driving reactions during inflammatory processes and associate fibrosis in a number of diseases including osteoarthritis.

1.9.1 TG2 and development of autoimmunity

Coeliac disease (CD) is a chronic autoimmune disorder caused by the ingestion of gluten, which is a major component of wheat, rye and barley (Sollid 2002). Gluten derived peptides that are resistant to further proteolytic cleavage by proteases due to its high proline content. In certain individuals those proteolysis resistant peptides that are observed can drive an aberrant immune response. The disease is manifested by the inflammation of the gut's mucosa, ultimately leading to flattening and destruction of the intestinal villi and the presence of antibodies against gluten as well as the main auto-antigen TG2. Coeliac disease is present in certain individuals of genetic predisposition (HLA class II haplotype DQ2 or DQ8).

The disease develops, when undigested fragments of gluten cross the lamina propria of the small bowel, where they become substrates for TG2 (Sollid and Jabri 2013). Gluten is composed of gliadin and glutenin polypeptides that contain many prolines and glutamines in their structure. Therefore they are excellent targets for the TG2-dependent deamidation reaction, leading to conversion of glutamines to glutamic acid (Fig. 1.6A). Once the deamidated fragments are internalized by antigen presenting cells (APC), which residue in the gut, they can be presented to T-cells on the HLA DQ2 or DQ8 molecules on the surface of APC. T-cell population ($CD4^{+}$) is responding to deamidated gluten fragments or covalent complexes of gluten peptides and TG2. This leads to the autoimmune reaction driven by those reactive T-cells. This is followed by activation of autoreactive B-cells, their differentiation into

plasma cells and production of antibodies against deamidated gluten or the TG2-gluten complex. The stable complexes represent the TG2-substrate thioester intermediate state this complex has a long half life allowing detection as an antigen (Hadjivassiliou et al. 2010). The antibodies to TG2 belong to the immunoglobulin A, G and M isotypes (IgA, IgG and IgM) (Sollid and Jabri 2013). The antibodies for TG2 are mainly against the Ca^{2+} activated form of the enzyme (Iversen et al. 2013). Understanding of the pathology of coeliac disease helped to develop the novel benchmark tests to screen for CD that are widely used in clinics (Caja et al. 2011). The tests detect circulating IgA class antibodies against TG2 or antibodies to deamidated gliadin peptides. These tests were shown to have the highest sensitivity and specificity. This allows diagnosing up to 98% of untreated CD patients. These tests are currently the most powerful tools for CD diagnosis and have in some instances replaced the small intestinal biopsy that is highly invasive.

There are some analogies to the situation in rheumatoid arthritis, where auto-antibodies against citrullinated proteins are formed. The activated T-cells ($CD45^{+}$) infiltrate synovium in patients of specific genetic background (Molberg and Sollid 2006). The anti-citrullinated antibodies are formed due to activity of peptidyl arginine deiminase (PAD). This enzyme replaces the aldimine (=NH) group on the protein-bound arginine with a ketone group (=O) to form citrulline in Ca^{2+} dependent manner (Fig. 1.6B). One of the examples are autoantibodies found in RA patients specific for citrullinated fillagrin (an epidermal protein) (Nijenhuis et al. 2004). Autoantibodies against other citrullinated proteins (such as fibrin and vimentin) have been also detected in the synovium of rheumatoid arthritis patients (Szodoray et al. 2010). It is possible that TG2 involvement in the process of autoimmunity development will be only restricted to CD but it is also possible that it occurs in other inflammatory conditions as well (Molberg and Sollid 2006; Sollid and Jabri 2013).

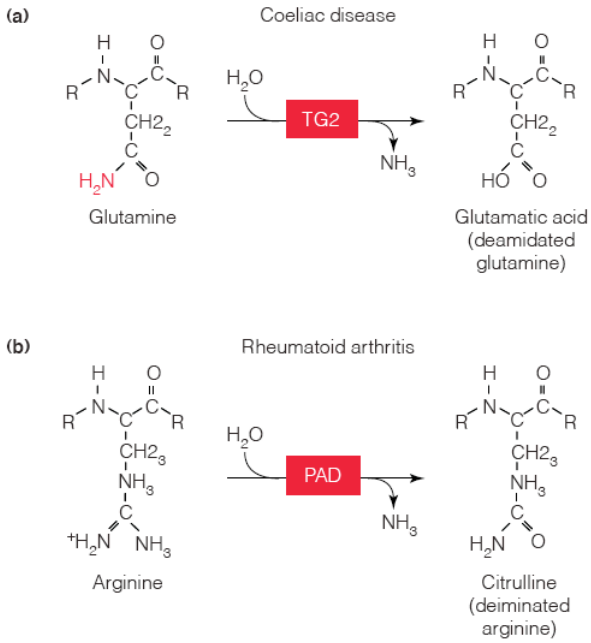

Fig. 1.6 Main enzymes involved in the development of autoimmunity during coeliac disease and rheumatoid arthritis. A) TG2-dependent deamidation in the presence of H_2O transforms glutamine into glutamic acid by removal of amide. **B)** Deimination reaction catalyzed by PAD enzyme that converts arginine residue into citrulline. Reproduced from Molberg and Sollid 2006.

1.9.2 Protein modifications mediated by TG2 in arthritis

Once released from the cells, TG2 becomes catalytically active in the extracellular space and catalyzes reactions that might promote or contribute to pathology of RA and OA. During RA induction in a rat model, TG2 was shown to be secreted from the synoviocytes at the sites of collagen type II degradation and to become enzymatically active (Lauzier et al. 2012). Recent studies report that TG2 activity can enhance joint destruction in a rheumatoid arthritis mouse model (Dzhambazov et al. 2009). In this model for collagen-induced arthritis, TG2 was found to be responsible for modifying an immunodominant fragment of type II collagen (CII260-270). TG2 crosslinking and/or deamidation of this epitope mediates a T-cell response to the fragment. Moreover, TG2 was shown to transamidate S100A11 calgranulin, which is a small protein involved in Ca^{2+} homeostasis and cytoskeletal rearrangement (Cecil and Terkeltaub 2008). Once the S100A11 is released by the cells it acts like an inflammatory cytokine and promotes chondrocyte differentiation/maturation. Mechanistically, TG2 that localizes in the conditioned medium of the mouse articular chondrocytes became enzymatically active when the

cells were treated with IL-1β. TG2-mediated crosslinking of the S100A11 molecule by forming γ-glutamyl-ε-lysine isopeptide bridges into a functional homodimer, which binds more efficiently to the cell surface receptor for advanced glycation end products (RAGE). This enhances outside-in signaling, the activation of p38 MAPK kinase and NFκB signaling pathways, and ultimately induced chondrocyte hypertrophy.

1.9.3 TG2 expression and activation during chondrocyte differentiation/maturation

Both, TG2 and cell-associated FXIIIa are present in bone and growth plate cartilage (Aeschlimann et al. 1996; Nurminskaya and Kaartinen 2006). The immunohistochemical staining for TG2 and FXIIIa showed its expression in the growth plate of human long bones. Both enzymes are expressed in normal articular cartilage, mainly in the superficial zone, deep zone as well as in the central part of menisci where maturation occurs (Johnson et al. 2001). Cellular FXIII is a a dimer of two FXIIIa subunits, present not only in platelets or monocytes but also in chondrocytes of the growth plate (Muszbek et al. 1996). Cartilage contains many substrates for TG2 (fibronectin, collagen II, III, V and XI, osteopontin, osteonectin, fibrilin) (Aeschlimann et al. 1996) as well as for FXIIIa (Muszbek et al. 2011). However, it was shown that besides some common substrates, where often different sites are targeted, the enzymes have a preference for distinct molecules (Watanabe et al. 2013).

During embryonic development, chondrocytes of the growth plate undergoes terminal differentiation into the hypertrophic cells (Johnson et al. 2003). At a specific stage in chondrocyte differentiation, TG2 is upregulated and catalytically active in the ECM. Interestingly, the TG2 externalization precedes tissue mineralization (Aeschlimann et al. 1995). It is unknown which stimulus is responsible for triggering the sudden TG2 externalization. The released TG2 becomes enzymatically active, and this is an important stage in chondrocyte maturation and endochondral ossification. TG2-mediated crosslinking of the chondrocyte extracellular matrix is thought to contribute to formation of the scaffold for matrix calcification. During chondrogenesis, TG2 is regulating, through an autocrine pathway, the transition into the pre-hypertrophic stage and thereby to inhibit deposition of cartilaginous ECM.

Down regulation of TG2 expression increases synthesis of extracellular matrix rich in GAGs and promotes expression of early chondrogenic markers (Nurminsky et al. 2011). Therefore, TG2 plays an active part in chondrocyte differentiation.

1.9.4 TG2 expression in osteoarthritis

At the site of injury, chondrocytes become hypertrophic and able to mineralize the local tissue (Nurminskaya and Kaartinen 2006). Therefore, hypertrophic chondrocytes are found in close proximity of hydroxyapatite and calcium pyrophosphate dihydrate crystal deposits. The development of chondrocyte hypertrophy close to the surface of the cartilage that ultimately leads to its destruction as well as superficial bone formation and remodelling of the subchondral bone plate are present in osteoarthritis (Goldring 2000). A characteristic feature of osteoarthritic articular cartilage is the presence of high levels enzymatically active TG2 that promotes chondrocyte hypertrophy (Tarantino et al. 2011). Thus, it is postulated that TG2 serves as a marker of cartilage remodelling in OA progression. Immunohistochemical staining reveals, that elevated expression of TG2 is induced in within clusters of hypertrophic chondrocytes in OA-affected human articular cartilage (Fig. 1.7), which is correlated with increased TG2 levels. A similar pattern of stronger TG2 staining is observed in mice after inducing knee instability, leading to upregulated TG2 expression.

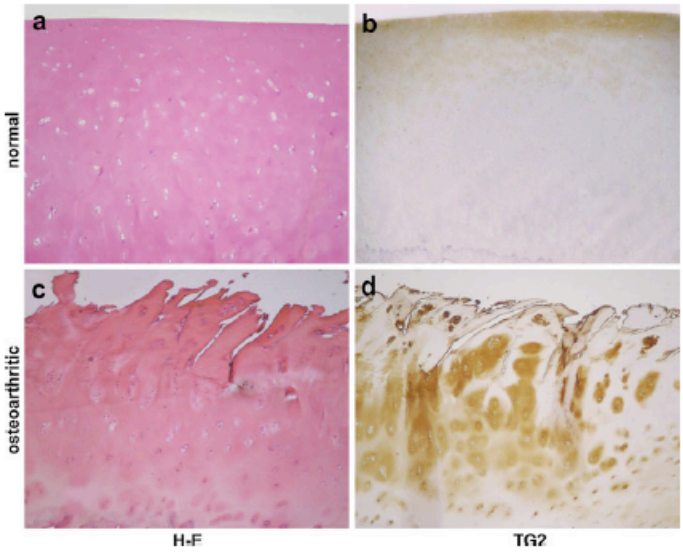

Fig. 1.7 TG2 expression in normal and osteoarthritic articular cartilage. The specimens of human femur head were stained with Hematoxylin-Eosin staining to visualize cells and detect extracellular matrix (a and c) and anti-TG2 antibodies to investigate its expression pattern (b and d). Reproduced from Tarantino et al 2011.

As both TG2 and FXIIIa can be found in the growth plate of the long bones, Tarantino and colleagues (2009) looked more closely, whether there are any skeletal differences between the knees of wild-type and TG2 deficient mice. Although there were no overt differences between wild-type and knock-out animals, they found a five fold higher expression of FXIIIa in cartilage. Hypertrophic chondrocytes from TG2 knock-out mice express FXIIIa, which is probably compensating for the absence of TG2. Also TGF-β1 expression, which has an anabolic role in cartilage and controls osteoblast differentiation, was increased when compared to the wild-type. TG2 has been proposed to have a role in TGF-β1 activation (Telci et al. 2009) and hence, increased expression of TGF-β1 could be the result of feedback regulation and reduced active TGF-β1 levels in these mice.

Induction of OA in the TG2 knock-out mice using surgery to cause joint instability revealed that in the absence of TG2, the severity of OA is reduced as indicated by grading the histological sections of the mice and there is more osteophyte formation (Orlandi et al. 2009). This may relate to differences in the inflammatory response between wild-type and TG2 $^{-/-}$ mice.

Evaluation of TG2 as a biomarker was also reported and carried out using the Hartley guinea pig model (Huebner et al. 2009). Guinea pigs at 4, 7 and 12 month of age were analyzed as the OA develops spontaneously in this model over this time frame. In the early stages of OA, TG2 was mainly expressed in the superficial and middle zone of the cartilage. At later stages, TG2 staining was more disperse within the tissue and accumulated at the centre margin of the superficial layer. Enhanced expression of TG2 and formation of N^{ε}(γ-glutamyl)lysyl isopeptide bonds was detected. TG2 upregulation was linked with MMP-13 and collagen type X expression in cartilage. TG2 levels measured in the synovial fluid from OA knees by ELISA correlated with the histological score of severity. Taken together, this indicates that TG2 is not only upregulated in OA cartilage but efficiently released into synovial fluid. Interestingly, a similar correlation was not found for FXIIIa.

1.9.5 Potential link between chondrocyte maturation, inflammatory mediators and TG2

It has been proposed that the mechanism of upregulation of TG2 activity during stimulation with proinflammatory IL-1β is driven by nitric oxide (NO) (Johnson et al. 2001). Peroxynitrite donors significantly enhanced TG2 activity in meniscal cells derived from OA patients. CXCL1 and CXCLl8 chemokines were also stimulating TG2 activity (Merz et al. 2003). An organ culture of knee articular cartilage from healthy donors treated with TGFβ and IL-1β for 48h had increased TG2 expression (Johnson et al. 2001).

TG2 is involved in the mechanism of tissue calcification promoted by cell differentiation and proinflammatory stimulation (Johnson et al. 2003). ATRA, which is a metabolite derived from vitamin A, directly upregulates TG2 expression and induces chondrocyte hypertrophy (Aeschlimann and Thomazy 2000). It has been shown that induction of TG2 promotes the expression of hypertrophic markers such as collagen type X, alkaline phosphatase (AP) or metalloproteinase-13 (MMP-13) suggesting of a direct link (Johnson et al. 2003). Moreover, treatment with both ATRA and IL-1β increases TG2 transamidation activity in articular chondrocytes isolated from murine and bovine knee explants, but not in those isolated form TG2-knock-out mice (Johnson et al. 2003). However, the same treatment failed to induce residual transamidation activity from FXIIIa that is overexpressed in TG2 deficient animals as previously outlined (Huebner et al. 2009). Upregulation of TG2 expression increased the levels of inorganic pyrophosphate and nucleotide pyrophosphatase phosphodiesterase that drive cartilage mineralization (Johnson et al. 2003).

Additionally, Johnson and colleagues (2005) proposed an interesting hypothesis suggesting that pathological changes in OA may at least in part be due to the presence of an inactive form of TG2 and not driven by its transamidation activity (Johnson and Terkeltaub 2005). They showed that cartilage hypertrophy and mineralization is mediated by the presence of the Mg-GTP bound form of TG2. They used the GTP binding mutant (TG2 K173L) in combination with the human chondrocytic cell line (CH-8) to show that addition of this mutant fails to induce matrix calcification and collagen type X upregulation. Moreover, they observed that

the GTP binding mutant was unable to be externalized from the cells in contrast to wild-type TG2 or C277S active site mutant.

1.10 Non-conventional release of TG2

Literature evidence indicates that TG2 is released by cells in specific context and that the products of its activity can promote chondrocyte hypertrophy (Tarantino et al. 2011) and drive autoimmunity (Sollid 2002). Chondrocytes, osteoblasts, fibroblasts, macrophages and epithelial cells can actively externalize TG2, but the mechanism of TG2 externalization remains elusive (Lorand and Graham 2003). Current understanding of TG2 secretion is based on its well-documented interaction with ECM or cell membrane proteins. It is believed that when secreted, TG2 binds immediately to ECM proteins and interact with number of substrates such as fibronectin, collagen, syndecan, vitronectin, osteopontin or binds tightly to the cell surface (Belkin 2011). These interactions are thought to stabilize the ECM assemblies. However, it is not known whether TG2 becomes permanently associated with them.

The structural features of TG2 suggest that it is secreted in a non-conventional manner (Aeschlimann and Paulsson 1994; Nurminskaya and Belkin 2012). The endoplasmic reticulum (ER)/Golgi-independent release pathway is predicted as TG2 lacks carbohydrate modifications despite the presence of potential N-glycosylation sites. TG2 lacks an amino-terminal signal sequence directing it to the ER and lacks disulfide bonds despite the presence of many cysteine residues (with exception of the disulfide bonds which regulate TG2 extracellular activity). Proteins that are not generated through the classical ER/Golgi secretory pathway share similar features such as the lack of a leader sequence and lack of specific posttranslational modifications (Nickel and Rabouille 2009). But many of them have a modified amino acid at the N-teminus (Aeschlimann and Paulsson 1994).

1.11 Release of proteins via the conventional pathway

Most secretory proteins synthesized in eukaryotic cells enter into the lumen of the rough endoplasmic reticulum and follow the ER/Golgi secretory pathway (Bruce et al. 2002). Those two compartments are part of a complex cellular machinery that controls protein folding, oligomerization, glycosylation and disulfide bond formation

prior to delivery of proteins to the cell surface (Trombetta and Parodi 2003). The synthesis of the proteins starts on the surface of ER but only for proteins that contain the ER signal sequence (Bruce et al. 2002) (Fig. 1.8). This is a short amino acid sequence, localized on the N-terminus of newly synthesized proteins. It is usually composed of hydrophobic amino acids (e.g. LLLVGILFWA) and this sequence is recognized by the signal recognition particle (SRP), expressed on the surface of ER membrane. Ribosomes with newly synthesized polypeptide attached are captured by SRP, which facilitates the translocation of the polypeptide chain into the ER lumen. After active translocation of the whole polypeptide, the signal sequence is cleaved off from the protein and proteolytically degraded inside the ER. The lumen of the ER is the location where the N-linked oligosaccharides are attached to asparagines. N-linked glycosylation sites in proteins contain specific sequences: N-X-S or N-X-T (whereby X is any amino acid but not proline) that allow for the sugar attachment. The carbohydrate synthesis and remodeling is continued in the Golgi apparatus after exit of newly synthesized proteins from the ER and their translocation into Golgi in COPII-coated membrane vesicles. The COPII coat is composed of small GTPases (Sar1, Sec23-24 and Sec13-31) that interact with cargo receptors and concentrate proteins inside budding vesicles. After reaching the Golgi complex, proteins are further modified, folded and sorted in *cis*, *trans* and *medial* cisterns of the Golgi. Here further O-linked oligosaccharides might be added to S/T residues localized on proteins. Transport of proteins through the Golgi compartments in the direction of the cell surface and back to the ER is mediated by COPI vesicles, which contain ADP ribosylation factor 1 GTPase (Arf1). Arf1 is a protein that regulates the COPI coat association. The fusion events between membranes are dependent on transmembrane proteins called SNAREs (soluble N-ethylmaleimide-sensitive fusion (NSF) protein accessory receptors). The SNAREs complex localized on vesicles (v-SNAREs) interact directly with target SNAREs (t-SNAREs) and when they are in minimal proximity with each other fusion occurs (Zhao et al 2008). This process is mediated by *N*-ethylmaleimide-sensitive factor (NSF) ATPase, which is necessary for intracellular membrane fusion and SNAREs recycling. Also transport of COPI-coated vesicles is dependent on transmembrane protein, syntaxin-5 that belongs to the t-SNAREs family (Nickel and Rabouille 2009) (Fig. 1.8).

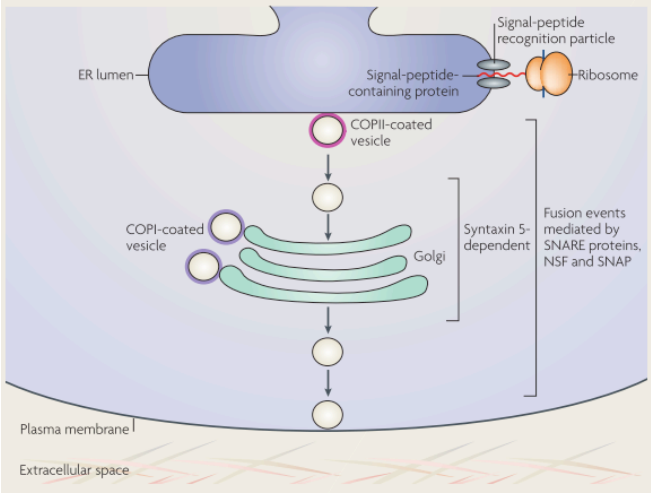

Fig. 1.8 ER/Golgi-dependent pathway of protein secretion for proteins with an leader sequence. Reproduced from Nickel and Rabouille 2009.

1.12 Emerging mechanism of non-conventional protein secretion

Protein synthesis and transport through the ER/Golgi system is a highly controlled and effective process, which allows release of proteins with full biological activity (Bruce et al. 2002). It seems that non-conventional secretion is also a regulated event that applies to a smaller number of proteins (Nickel and Seedorf 2008). The reasons why some of the the proteins undergo non-classical export can vary and some hypotheses were proposed to explain the existance of classical and non-classical patways. Binding of substrates to their receptors that potentially might occur inside the ER or Golgi can potentially lead to aggregation and misfolding, therefore it is preferable that their synthesis and release is separated. This is important for signaling molecules such as TG2 as binding to the receptors can potentially induce autocrine signaling (Nickel and Seedorf 2008). Also some of the proteins that are sensitive to redox potential might be misfolded or inactivated in the oxidative environment of ER and Golgi. Therefore, the synthesis in the cytoplasm seems to be a safe option and it ensures proper protein folding and omits the need for re-folding during synthesis as evident in classical secretory pathway. The known mechanisms of non-conventional protein secretion can be grouped into two different types: 1) non-classical delivery of membrane proteins, which contain the leader sequence but are being supply to the cell surface via Golgi-independent pathway or 2) the release of cytoplasmic proteins that are lacking the signal peptide (Nickel and Rabouille 2009). Rabouille and

colleagues (2012) grouped them further into vesicular and non-vesicular non-conventional release. The non-classical vesicular delivery of proteins to the outside of the cell can occur via secretion of proteins through vesicles bypassing the Golgi compartment or autophagy-mediated release (Deretic et al. 2012). The non-vesicular type of release involves direct translocation of proteins through the cell membrane or secretion of proteins or peptides with lipid modifications through ABC membrane transporters.

1.12.1 Non classical protein transport bypassing the Golgi compartment

COPII positive vesicles emerge from the ER and are involved in the subsequent transport of proteins to the Golgi, whereas COPI positive vesicles are mediating the movement through Golgi and from Golgi back to the ER (Nickel and Rabouille 2009). However, some proteins bypass the Golgi compartments and are directly transported from the ER to the cell surface in COPII vesicles. This was reported for cystic fibrosis transmembrane conductance regulator (CFTR) (Wang et al. 2004) as well as for CD45 membrane receptor (Baldwin and Ostergaard 2002). CD45 receptor contains a glycosylation pattern characteristic for the ER (numerous N-glycan that are of high mannose type) and was shown to localize in the cell membrane of T lymphoma cells even in the absence of further branched oligosaccharides that should be added in Golgi compartments (Baldwin and Ostergaard 2002). Meanwhile, in CFTR trafficking to the membrane occurs in the absence of syntaxin-5, Sar1 GTPase or Arf1, which are all markers mostly associated with COPI vesicles (Rabouille et al. 2012). However, CFTR delivery requires syntaxin 13 t-SNARE, which is involved in the formation of late endosomes, which suggests a different vesicular transport route. In some instances, the process of bypassing Golgi cisterns occurs in a COPII-independent manner suggesting that membrane molecules are transported directly from ER to the cell surface via a distinct vesicular transport (Nickel and Seedorf 2008). This is the case for the yeast heat-shock protein 150 (Hsp150), where secretion occurs in the absence of functional (Sec24p) protein of the COPII coat complex (Fatal et al. 2004). Other examples include Kv4 voltage-gated K^+ channel in neurons that are delivered to the membrane through a non-COPII mediated pathway (Hasdemir et al. 2005). It was postulated that Golgi-independent secretion of proteins

can occur simultaneously to classical release and that this might be induced only during specific situations and/or in certain cell types (Nickel and Seedorf 2008).

1.12.2 Release of proteins lacking the signal peptide

Non-conventional export of cytoplasmic and nuclear proteins that lack an ER-signal peptide is being extensively studied as proteins secreted in this matter such as cytokines, growth factors and signaling molecules play an important role during inflammatory processes, cell differentiation, proliferation or oxidative stress (Nickel and Seedorf 2008). Even though the mechanism of their release can be different, all proteins share a few distinct features: lack of a classical signal peptide and lack of posttranslational modifications that occur during ER/Golgi protein maturation. Also, all of them were shown to be resistant to Brefeldin A treatment of cells – a drug that blocks Arf1 recruitment to Golgi and consequently vesicular transport trough ER/Golgi compartments. The possible mechanisms of non-classical export involving translocation across the membrane can be both vesicular and non-vesicular for leaderless secretory proteins (Rabouille et al. 2012) (Fig. 1.9).

Examples of proteins that lack a signal peptide and function mainly outside the cell are members of interleukin family: IL-1α, IL-1β, IL-18 and IL-33 (Dinarello 2009), fibroblast growth factor 2 (FGF2) (Seelenmeyer et al. 2005), galectin-1 (Zhu and Ochieng 2001), galectin-3 (Keller et al. 2008), high-mobility group box 1 protein (HMGB-1) (Gardella et al. 2002) or thioredoxin (Rubartelli et al. 1992). Soluble proteins secreted in an non-conventional way can have different biological functions intracellulary and extracellularly (Dinarello 2009). Interestingly, in many occasions non-conventional release is triggered by an external signal such as heat shock for IL-1α (Tarantini et al. 2001), oxidative stress in T lymphocytes for thioredoxin (Kondo et al. 2004) lysophosphatidylcholine treatment for HMGB-1 (Gardella et al. 2002) or bacterial lipopolysaccharide (LPS) treatment followed by ATP stimulation in monocytes/macrophages in case of IL-1β (Qu et al. 2007).

FGF2 is an example of a protein released by the non-vesicular route described as self-sustained membrane translocation (Nickel and Rabouille 2009). FGF2 is an important growth factor required in development, and for tissue repair and angiogenesis (Nickel 2011). A possible mechanism of FGF2 release involves its recruitment by the phosphoinositide phosphatidyl-inositol-4,5-bisphosphate

(PtdIns(4,5)P_2) onto the inner side of the cell membrane, followed by extracellular trapping by heparan sulphate proteoglycans (HSPGs) (Zehe et al. 2006). Interestingly FGF2 remains folded during the process of membrane translocation (Torrado et al. 2009). FGF2 seems to directly insert into the lipidic membrane pore upon PtdIns(4,5)P_2 oligomerization (Steringer et al. 2012).

Thioredoxin, which is involved in maintaining the redox balance inside the cell, shows cytokine/chemokine activities when released (Nishinaka et al. 2001) and plays a role during inflammation (Bianchi and Agresti 2005). Eleveated levels of thioredoxin can be also found in RA (Xu et al. 2008). Once released, thioredoxin can activate transient receptor potential channels (TRPC) at the cell surface by breaking cyteine bridges on extracellular loops of TRPC and causing its activation.

Autophagy based release is a novel emerging mechanism for export of IL-1β and HMGB-1 (Deretic et al. 2012). An example of a protein that is released after rapid environmental change is high-mobility group box 1 protein (HMGB-1). It has been shown that in the nucleus HMGB-1 regulates gene expression (Bonaldi et al. 2003). However, in monocytic cells, LPS stimulation leads to extensive transport of HMGB-1 from the nucleus to the lysosomes. Furthermore, the secretion of HMGB-1 is potentiated by lysophosphatidylcholine released from monocytes at sites of inflammation (Gardella et al. 2002). Lysophosphatidylcholine is the metabolite formed due to the activity of phospholipase PLA_2, and which is present at the later stages of inflammation. In the presence of inflammatory mediators and cytokines it is secreted into extracellular space and acts as chemotactic cytokine (Degryse and de Virgilio 2003).

The most intensively studied leaderless protein over the last years is the proinflammatory cytokine IL-1β. It can be rapidly released from monocytes and macrophages upon LPS stimulation and extracellular ATP treatment, possibly through vesicular trafficking (Mackenzie et al. 2001). However, little is known about intracellular sorting of IL-β that preceeds its release.

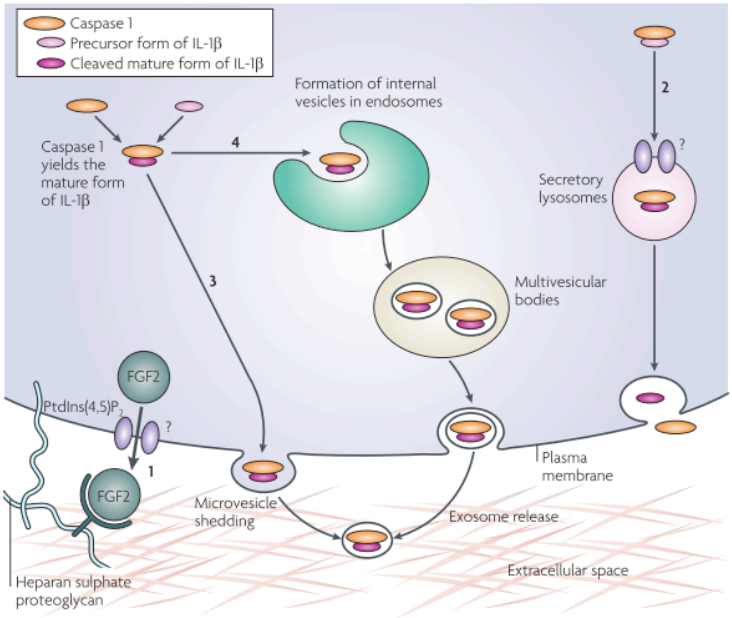

Fig. 1.9 ER/Golgi-independent pathway of protein secretion for proteins lacking a leader sequence. 1. Non-vesicular mechanism (direct translocation of FGF2) 2. Lysosome-dependent pathway, 3. Microvesicle-dependent secretion, 4. Multivesicular bodies (exoxomes). Reproduced from Nickel and Rabouille 2009.

1.13 Extracellular ATP – a trigger of non-classical protein secretion

ATP (adenosine 5'-triphosphate) is the most widely used carrier of free energy within the cells and a fast-acting intercellular messenger (Bruce et al. 2002). Still, ATP remains an intracellular molecule harboring extracellular functions. It is debatable how ATP reaches the extracellular space, however a few mechanisms of its release have been proposed. Cell injury and death is not the only cause of ATP leakage (Jorgensen et al. 1997) because ATP can be released through nonlytic pathways, like fluid shear stress (Li et al. 2005) or mechanotransduction (Garcia and Knight 2010). Moreover, in neuronal cells ATP is released in secretory vesicles (Burnstock 2008) or through channels formed by connexins or pannexins (Di Virgilio 2005). Cell manipulation causing mechanical stress such as cell stretching triggers ATP release (Solini et al. 1999). For a long time, ATP was not considered a signaling molecule. However, since the discovery that ATP can permeabilize cells (Cockcroft and Gomperts 1979) and is released by neuronal cells (Burnstock 1972), it has become one of the most important transmitters allowing for local cell-cell communication.

1.14 ATP as an inflammatory mediator

It has been demonstrated that moderate release of ATP during chronic infection can play an anti-inflammatory role by activating dendritic cells and macrophages to secrete anti-inflammatory cytokines such as IL-10 and IL-1 receptor antagonist thereby inhibiting dendritic cell initiated Th1 responses (F Di Virgilio et al. 2009). The concentration of cytosolic ATP is 10^6-fold higher than in the extracellular milieu and ATP is present in a negatively charged form (ATP^{4-}), which makes it a good candidate for alarming surrounding tissues about danger and trigger early events of inflammation (Di Virgilio et al. 2001). In addition, ATP released from activated monocytes or platelets can act through autocrine/paracrine pathways that amplify the danger signal (la Sala et al. 2003). A high dose of extracellular ATP (milimolar concentrations) initiates the immune response and stimulates antigen presenting cells to release pro-inflammatory cytokines such as IL-1β, IL-18, IL-6 or tumor necrosis factor α (Di Virgilio 1995; Falzoni et al. 1995; Ferrari et al. 2006). High ATP concentrations or prolonged stimulation can eventually lead to cell death, which occurs due to the massive upset of ion homeostasis, probably by colloido-osmotic lysis (Ferrari et al. 1997; Andrei et al. 2004). Initially, it was suspected that the extracellular increase of proinflammatory cytokines such IL-1β is simply due to the cytotoxic effect of ATP, but it has since become evident that cytokine maturation and release is mediated by a series of complex intracellular events (Jorgensen et al. 1997).

1.15 Extracellular ATP and its receptors

It was shown that released ATP is quickly converted by ecto-enzymes to ADP, AMP and adenosine in order to terminate its action (la Sala et al. 2001) (Fig. 1.10). Those cell surface ecto-ATPases are called ectonucleotidases (Zimmerman 2000). Purinergic receptors are membrane proteins that respond to the extracellular nucleotides and form three classes of proteins. These are P1 (adenosine receptors), P2Y (G-protein-coupled receptors) and P2X (ligand-gated ion channels) (Surprenant and North 2009; Baroja-Mazo and Pelegrín 2012). Two subfamilies of them are transmembrane proteins, that respond to extracellular ATP: metabotropic P2Y and ionotropic P2X receptors (Di Virgilio 2007). Extracellular ATP acts via a signal

amplification system, to generate other inflammatory mediators and spread the alarm signal in the local milieu (Abbracchio and Burnstock 1994). The release of cytoplasmic ATP that occurs upon cell injury can lead to 5-10 mM local ATP concentrations in surrounding tissue (Di Virgilio et al. 2001). This high concentration of ATP is known to activate one member of the P2X family – P2X7R, which stimulates the release of non-conventionally secreted IL-1β.

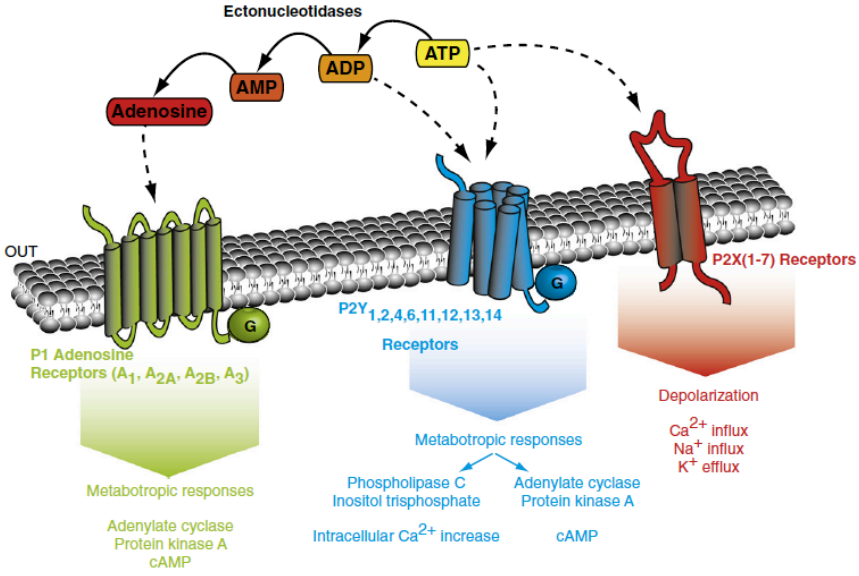

Fig. 1.10 Extracellular ATP activates ligand-gated ion channels (P2X) and G-protein coupled receptors (P2Y) on the cell surface. Ectonucleotidases quickly hydrolyse ATP into ADP, AMP and adenosine. Adenosine acts as an agonist for P1 receptors. Activation of P2X receptors leads to Na^+ and Ca^{2+} influx and K^+ efflux, which induces cell membrane depolarization. Activation of P2Y induces metabotropic responses, PLC activation, IP_3 production and release of Ca^{2+} from intracellular stores. P1 activation also evokes metabotropic responses by stimulating or inhibiting cAMP production. Reproduced from Baroja-Mazo et al (2012).

1.15.1 P2X receptors

Up to now seven P2X receptors have been described (P2X1-7) and were shown to be widely expressed within different tissues in vertebrates (Khakh and North 2006; Kaczmarek-Hájek et al. 2012). Homologue receptors have been described in invertebrate organisms, such as in flatworm (*Schistostoma mansoni*), unicellular amoeba (*Dictyostelium discoideum*) or green algae (*Ostreococcus tauri*) (Kaczmarek-Hájek et al. 2012). However, there are no reports about P2X signaling in prokaryotic organisms (Fountain and Burnstock 2009). P2X are also not present in model organisms such as *Drosophila melanogaster*, *Caenorhabditis elegans* and

yeast. Therefore P2X evolution remains unclear. The P2X receptor expressed in *D. discoideum* was found to be localized on vacuoles and is thought to be responsible for osmoregulation. Therefore, it is likely that plasma membrane P2X found in vertebrates might have evolved from an intracellular channel.

1.15.2 P2X receptor architecture

P2X receptors are trimeric, nonselective cation channels that have a unique molecular structure when compared to other classes of ligand-gated receptors (Young 2010). The topology of the P2X is very similar to the acid-sensing receptors (ASICs), with which they might share a common ancestor. However, the lack of clear homology on the sequence level or 3D structure eliminates a close relation. All P2X receptors share a similar structural organization with both C- and N-terminus localized on the intracellular side of the membrane, two hydrophobic transmembrane domains (TM1 and TM2) and an extensively glycosylated extracellular domain with conserved disulfide bridges (North 2002; Browne et al. 2010). The transmembrane arrangement of the P2X receptor in its ATP-free resting state was confirmed in the zebrafish P2X4 receptor crystal structure, which has been solved at 3.1Å resolution (Kawate et al. 2009). The crystallization of the receptor was possible after introducing three point mutations and by excluding the N- and C-terminal intracellular domains (ΔzfP2X4-B). The crystal structure confirmed the trimmeric nature of P2X receptors and showed that assembly of three subunits, each of them spanning the plasma membrane twice, forms the functional receptor. The large extracellular chalice-like shaped domain composed mainly of β-strands is reaching up to 7 nm above the cell membrane plane whereas the transmembrane region is formed by six α-helices that are situated angled and antiparallel to each other and are approx. 2.8 nm in length (see Fig. 1.10 for a model of P2X2 based on this structure). On the extracellular portion, 3 non-canonical ATP binding sites where described. The extracellular domain mediates ATP, competitive antagonist and metal ion interactions whereas the transmembrane part takes an active part in channel opening (Browne et al. 2010).

1.15.3 P2X receptor subunit structure and their arrangement in the closed channel state

In the resting state, the zfP2X4 structure was compared to the shape of a "dolphin" with the head, upper and lower body, both flippers and dorsal fin (Fig. 1.10B) (Kawate et al. 2009). The three β-sheets of the upper body are in contact with each other, while there are few contacts between the lower body domains of the subunits. The β-sheets of the body region are strictly conserved, suggesting that similar interactions are common to other P2X family members. The residues of the left flipper are less conserved; therefore they could be mediating receptor specific desensitization after ATP removal. The channel surface is formed out of the three TM2 α-helices and these are surrounded by three peripheral TM1 helices. In the resting state, both α-helical TM domains of each subunit are in tight contact, which prevents ion entry.

1.15.4 ATP binding and P2X channel opening

Members of the P2X ligand-gated ion channels act in the membrane as cell surface channels (North 2002). However, P2X7R has the additional function of mediating the formation of a membrane "pore", which likely represents a more dilated state ATP binding allows the Na^+, Ca^{2+}, K^+ and Cl^- diffusion through the channel and the transport of the ions differs between P2X family members (Kawate et al. 2011). The ATP-bound crystal structure of the truncated ΔzfP2X4-C receptor resolved at 2.8 Å resolution showed for the first time how the receptor is changing its confirmation upon nucleotide binding (Hattori and Gouaux 2012) (Fig. 1.10A). Truncation of the receptor and removal of the intracellular domains was not ideal to fully understand the conformational changes. However, it allowed capturing the receptor in an open, but not fully dilated state, where ATP is bound to all available pockets (Jiang et al. 2013). The structure confirmed the presence of the three non-canonical ATP-binding sites on the extracellular part of the receptor that were predicted (Ferrari et al. 2006; Kawate et al. 2009) (Fig. 1.11A). The ATP-binding pockets ("jaws") are composed of positively charge amino acid residues localized approx. 4 nm from the cell membrane. ATP binding involves coordination of a few strictly conserved residues localized on head domain, body domain, right flipper and dorsal fin (Hattori and

Gouaux 2012). In the resting state, the receptors have empty “jaws” localized between head domain and dorsal fin. These adapt ATP via hydrophobic interactions. ATP is also recognized by the hydrophilic/charged residues of the upper and lower body domains, which form hydrogen bonds and salt bridges with the phosphate groups and adenine base of ATP. Upon binding to the P2X receptor subunit, ATP is becoming U-shaped by folding the α-, β- and γ-phosphates. Binding of ATP to the empty pocket tightens the “jaws”, which shifts the head from the dorsal fin and flexes the lower body by approx. 0.8 nm in direction to the upper body. In fact the upper body of the receptor remains braced and less affected by the movement upon ATP binding. Widening of the extracellular vestibule is followed by movement of TMs domains. This movement creates a wider space in the canter of the 3 subunits. This type of movement is called “iris-like” motion, where TM domains of each subunit shift relative to the extracellular domain to open the cation channel. TM1 and TM2 turn anticlockwise (approx. 1 and 5.5 nm, respectively) to the cell membrane orientation and leave a space for ion flow of 1 nm in its widest place. It is likely that the antagonist bind to the same “jaws” as ATP (Jiang et al. 2013). However, more residues are involved in its coordination and binding of inhibitors prevents jaw closure that is necessary for ion conduction.

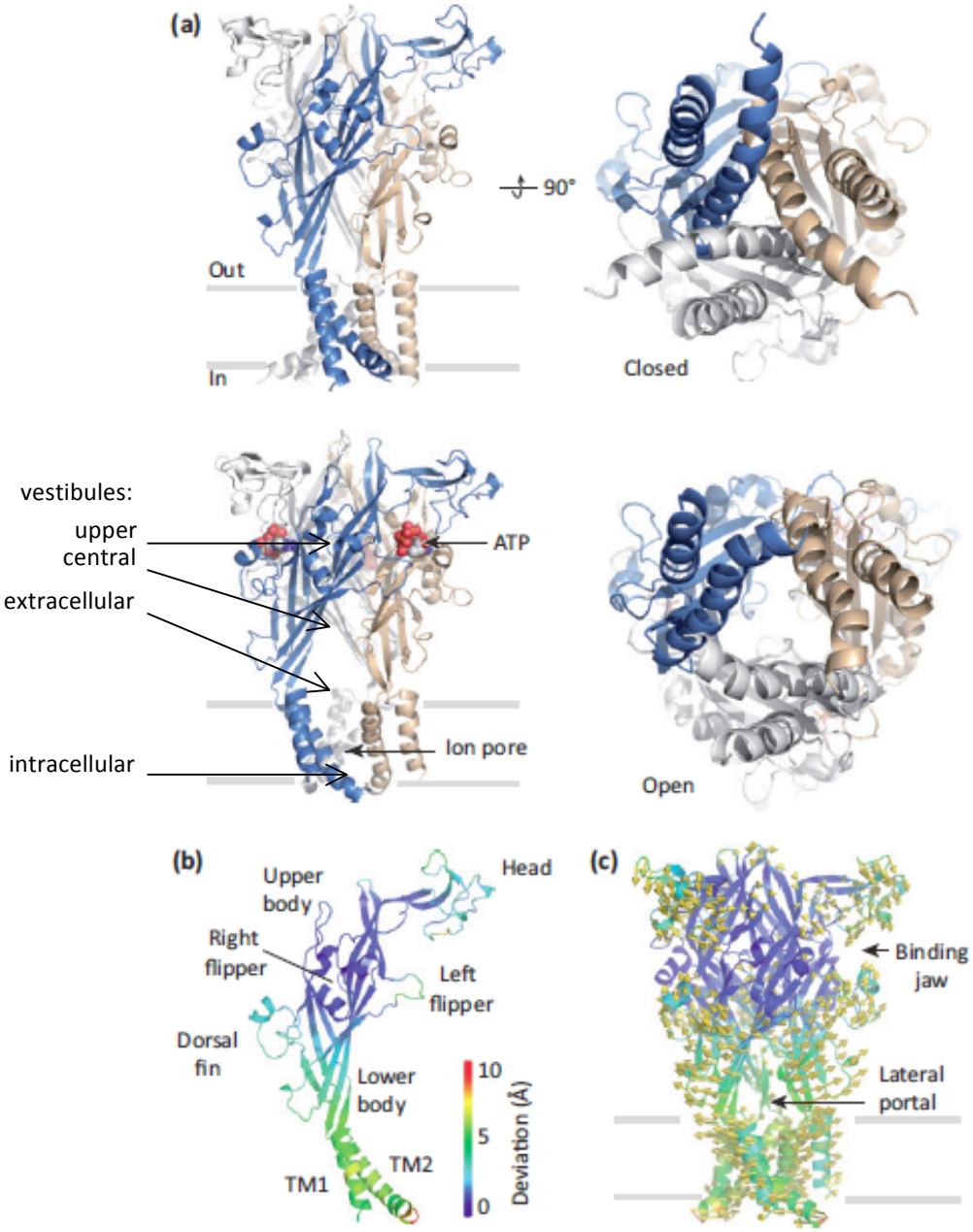

Fig. 1.11 Model of the rat P2X2 trimeric channel based on the ΔzfP2X4 crystal structure. A) Model of rP2X2 receptor showing the change from closed to open conformation and movement in receptor vestibules. The lateral (left) and down (right) view of subunits (each shown in different colors) and the ATP (red spheres) are visualized. B) Representation of the one subunit of the trimeric P2X receptor with its "dolphin-like" structure. C) Trimeric receptor with the lateral portal for ion permeation and ATP binding "jaw". Grey lines represent the layers of cell membrane. The receptor is shown in the expected arrangement relative to the membrane plane. Reproduced from Jiang et al 2013, with modifications.

1.15.5 Ion channel of P2X receptors

Activation of P2X requires subunit motion that allows the channel expansion to create a gap for cations translocation (Kawate et al. 2011). There were two models proposed for the cation flow through the channel. 1) The central pathway that is formed between three-fold axis of subunits or 2) the lateral portal pathway localized in the region that connects the lower body with the TM helices (Fig. 1.11C). Based on the P2X4 crystal structure, computational studies revealed that the 0.8 nm wide lateral portals are preferable as there are less electrostatic barriers for ions to pass through the presumptive channel than in the central opening. Even in the closed receptor state the lateral windows are wide enough to facilitate ion entry through that route. The surface of lateral portal is composed of many cysteine residues and harbours a negative electrostatic potential necessary for Na^+ and Ca^{2+} cation selection. It was also proposed that the acidic residues in the central vestibule and regions localized just above the lateral portal could participate in concentrating the cations before they enter the transmembrane gate, pass the channel and leave through the intracellular vestibule (Kawate et al. 2009; Hattori and Gouaux 2012). Similarly, on the other side of the membrane, the negatively charged glutamate residues could attract K^+ ions before they diffuse through the channel. For some P2X receptors the cations may still penetrate the central vestibule region but this is thought to serve a modulatory mechanism rather than an ion flow pathway (Kawate et al. 2011). Studies with gadolinium ions (Gd^{3+}) showed that the receptor can be allosterically regulated by ions (Kawate et al. 2009). Furthermore, Jiang et al (2013) suggested that Ca^{2+} or other ions that pass through the channel can bind to TM domains and further facilitate conformational changes that stabilize the channel. The driving force for ion transport are the pre-established concentration gradients across the membrane (North 2002).

1.16 P2X7 receptor (P2X7R)

The P2X7R is an important molecule to study in the context of non-conventional protein secretion as it was shown to respond to high concentrations of extracellular ATP and trigger release of the proinflammatory cytokine IL-1β (Perregaux et al.

1992; Ferrari et al. 1997). The P2X7R sequence was originally cloned form rat brain was described in 1996 (Surprenant et al. 1996). The P2X7R is an ion gated channel similar to P2X4R. P2X4 and P2X7 are closely related and probably, were product of gene duplication (Kaczmarek-Hájek et al. 2012). P2RX7 gene encodes a full-length protein of approx. 77 kDa (Ferrari et al. 2006). The mRNA for P2X7R was found to be strongly expressed in liver, thymus, heart, skeletal muscles and pancreas and at lower lovers, was also detected in prostate, spleen and brain (Rassendren et al. 1997). Functional P2X7R is mainly present in murine and human monocytes, peritonel macrophages, leukocytes, B and T lymphocytes or dendritic cells (Di Virgilio et al. 2001). P2X7R was also found to be expressed in neutrophils and is involved in the organism defence mechanism (Suh et al. 2001). Also cells of the nervous system like microglia, oligodendrocytes, astrocytes and Schwann cells express P2X7R (Coddou et al. 2011). Functional P2X7R activation can be evoked by high concentrations of ATP (1-4 mM) and much lower doses of its potent analogue BzATP (5-20 μM) (Jarvis and Khakh 2009; Coddou et al. 2011). Unlike P2X4R, P2X7R has a relatively large intracellular C-terminal domain, which is likely responsible for some unusual features (Costa-Junior et al. 2011). This will be discussed later.

1.16.1 P2X7R as a membrane channel

P2X7R channel formation is normally accompanied with fast Na^+ and Ca^{2+} influx and K^+ efflux along the chemical gradient, which induces cell membrane depolarization (Khakh and North 2006). P2X7R is adopting a trimmeric stoichiometry in the cell membrane, thus it is likely that changes in conformation upon ATP binding are going to be similar to those described for zfP2X4. Progressive increases in pore size can cause dramatic changes in membrane permeability and in cation concentration inside the cell. The recently proposed model of P2X receptor activation with its dynamic changes from the closed to the open channel configuration might potentially involve a few intermediary stages (Jiang et al. 2013). ATP gating that induces a shift in the subunits arrangement of subunits that leads to ion transport can be referred to the 2 conductivity types: O_1 and O_2 (Fig. 1.12). Sustained stimulation with ATP causes either a shift from open (O_1) to the desensitized state (D), which is mainly observed for P2X1 and P2X3 receptor, or is follows further slow dilation described by O_2 state, which is mainly seen for P2X2,

P2X4, and P2X7. It is thought that the O_1 conducting state allows for small cations to be passed through the channel. Progression to the O_2 state, however, is necessary for entry of the bigger organic cations, such as N-methyl-D-glucamine (NMDG) or fluorescent dyes like YO-PRO-1 and ethidium bromide. The O_2 state can be referred to as a "pore dilation" receptor shape. The structural arrangement forming the channel for this state has, however, not been determined yet. It is still under debate if those larger molecules permeate P2X itself or whether other hemichannels are involved in this process (Jarvis and Khakh 2009; Jiang et al. 2013). Recently Khadra and colleagues (2013) proposed a revised model of P2X7R channel function that also includes a transitional desensitization step under certain conditions. They showed that stimulation of native rat P2X7R with agonist enables different responses depending on agonist concentration. Sustained stimulation of P2X7R with low amounts of potent agonist BzATP (3.2 μM) results in monophasic current and channel opening that is followed by receptor desensitization and its internalization from the membrane. However, when BzATP reaches saturating concentrations (320 μM) the receptor activation is followed by its further dilation. The authors suggested that this might be the effect of three ATP/BzATP molecules binding to the receptor and be required for full receptor sensitization and its dilation into the "pore" state (Fig. 1.12). However, this would suggest that the ΔzfP2X4R structure with ATP reflects the "pore" state. As there are important differences between P2X7R and P2X4R in terms of receptor electrophysiology, the resolution of the receptor structure with the C-terminal domain is necessary. It was suggested that the state when two ATP molecules are bound to the receptor might represent the physiological responses mediated by P2X7R whereas the state with three ATP binding sites occupied and fully dilated might ultimately lead to cell death (Jiang et al. 2013).

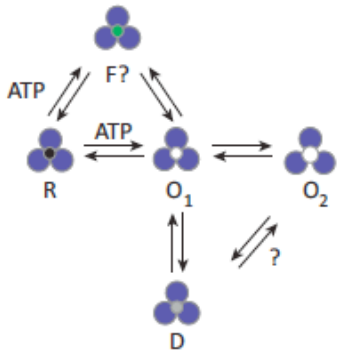

Fig. 1.12 Allosteric regulation of P2X channel opening by ATP. Receptor is composed of the three subunits that surround the pore. ATP-binding induces a shift from the closed, resting state (R) to the open, conducting state (O_1 and O_2). The channel can be closed and move to desensitized state (D) or further dilate by shifting to the O_2 state. The primed state (F) when ATP is bound but the channel remains closed has been proposed for P2X2. Reproduced from Jiang et al 2013, with modifications.

1.16.2 P2X7R-dependent "pore formation"

There are many recent studies trying to understand the phenomenon of a dilated P2X7R membrane channel, as inferred from dye uptake through the "pore". P2X7R as well as closely related P2X2 and P2X4 receptors have the ability to form a membrane pore in neuronal cells upon prolonged stimulation with ATP (Khakh et al. 1999; Chaumont and Khakh 2008; Sun et al. 2013). However, there are differences in "pore" formation between these receptors and only P2X7R activation leads to membrane "blebbing", cytoskeletal changes, cell death or lysis (North 2002). It was suggested that the sustained stimulation with ATP causes spontaneous aggregation of receptor subunits (of 6 or more) and leads to the formation of a large nonselective pore within the membrane (Di Virgilio et al. 2001). However, it is possible that other membrane hemichannels are involved in the formation of the membrane "pore"(Baroja-Mazo et al. 2012), activated by downstream signaling. P2X7R is widely expressed on monocytes/macrophages and microglia indicating a role in the release of proinflammatory mediators and inflammasome activation in macrophages. It is likely that P2X7R acts primarily as a membrane channel but the phenomenon of "pore" formation requires further investigation. Some recent evidence suggests that different activities of P2X7R may be involved in controlling inflammatory mediators and pain sensitivity (Khakh and North 2006; Sorge et al. 2012).

1.16.3 C-terminus of P2X7R

The feature that distinguishes P2X7R from the other P2X family members is the long C-terminal tail, which has been implicated in its function (Costa-Junior et al. 2011; Sun et al. 2013). It has been proposed that the intracellular C-terminus is the key element that upon changes in membrane potential, can induce specific downstream signaling and is required for "pore formation" (Surprenant et al. 1996). Deletion of the C-terminus prevented dye uptake but did not change P2X7R channel function.

The large C-terminus could possibly be involved in "pore formation" through interaction with some other proteins. It was reported that the C-terminus of P2X7R has a conserved LPS binding motif, that might modulate the inflammatory response in macrophages (Denlinger et al. 2001). It was suggested that this conserved binding domain binds LPS and inhibits downstream signaling events in macrophages, such as ERK1/2 phosphorylation and IκBα degradation. Moreover, the C-terminus is important for P2X7R activation and proper cell surface localization. Recently a R578Q point mutation in the C-terminus was shown to have reduced ability to form a pore (Wickert et al. 2013). Likewise, signaling through ERK1/2 phosphorylation was shown to be impaired. This mutation abolished receptor oligomerization and affected proper delivery to the cell surface due to altered N-glycosylation of receptor monomers. Therefore oligosaccharide modification of P2X7R is necessary for the trimmer assembly and membrane trafficking.

Ion flow through open rat P2X7R is modulated by Ca^{2+} (Roger et al 2008). The presence of calmodulin enhanced and prolonged Ca^{2+} entry. Calmodulin can interact with the C-terminus of rat P2X7R through a unique binding motif. Calmodulin and P2X7R association is constitutive and occurs in the absence of ATP stimulation but is enhanced upon agonist addition. However, the same was not true for the human P2X7R (Roger et al. 2010). Human P2X7R hat a reduced ion transport capacity compared to rat P2X7R, which might be due to a lack of its interaction with calmodulin affecting channel function and linking it with downstream events.

1.16.4 Cytoskeleton re-arrangements upon P2X7R activation

Cell morphological changes upon agonist treatment are remarkable in cells expressing P2X7R such as extensive formation of membrane protrusions on the cell

surface (Solle et al. 2001). The physiological agonist is believed to be ATP. However, in humans, it is still unclear if P2X7R is regulated by agents other than ATP (Ferrari et al. 2006). Little is known about the downstream signaling molecules that are activated upon P2X7R stimulation. However, P2X7R activation leads to significant cytoskeleton re-arrangement (Mackenzie et al. 2005). The polymerized F-actin fibril network is disrupted and G-actin, which can freely move in the cytosol is translocated into newly formed membrane protrusions. Likewise, vinculin is also shifted into cell protrusions and accumulates at the edge of the cell membrane. Moreover, α-tubulin is detected at the periphery of newly formed membrane "blebs". A number of inhibitors that disturb the cytoskeletal rearrangement were tested but only inhibitor of ROCK-1 kinase increased cell blebbing and changed the timing of events, suggesting its involvement (Morelli et al. 2003).

1.17 The "Inflammasome" assembly upon P2X7R activation

The term "Inflammasome" was established to describe a multiprotein complex that is involved in the regulation of the innate immune response associated with activation of inflammatory caspases (Martinon et al. 2009). The inflammasome relies strongly on intracellular sensors, such as NOD-like receptors (NLRs), which can recognize both microbial or nonmicrobial danger signals. ATP activated P2X7R induces rapid efflux of K^+ from the cell, which stimulates inflammasome assembly driven by caspase-1 autoprocessing and leading to final maturation of IL-1β (Dinarello 2004). As the activation of the inflammasome in cells of hematopoetic origin has been directly linked to proteolytic cleavage of pro-IL-1β by caspase-1, the inflammasome is likely to be a crucial element in autoimmunity and rheumatic diseases (Martinon et al. 2009).

The inflammasome requires the assembly of a cytosolic protein scaffold that consist of the sensor (NLR protein), adaptor (ASC protein) and effector protein such as a specific caspase that activates proinflammatory cytokines (Sidiropoulos et al. 2008). The mechanism of ligand selective NLR activation remains unknown but specific stimuli can promote assembly of different types of inflammasomes: NALP1, NALP3, IPAF or NAIP (Martinon et al. 2002). NALP1, NALP3 and IPAF are expressed in human tissues (Martinon et al. 2009). All of them have been found to effectively recruit caspase-1 (Sidiropoulos et al. 2008; Dinarello 2009; Martinon et

al. 2009). The leucine-rich repeats (LRR) in NLRs are proposed to sense pathogen-associated patterns and drive oligomerisation of its NACHT domains (Martinon et al. 2009). Activation of the NALP3 inflammasome after NLRs-dependent ligand sensing occurs through the NLRs effector domains. The pyrin domain (PYD) and caspase recruitment domain (CARD) become activated through close homotypic complex formation. The protein assembly leads to engagement of PYD or CARD-containing molecules such as pro-caspase-1 into the complex. The oligomerisation of inflammasome initiates the processing of pro-caspase-1. Active caspase-1 processes the pro-IL-1β, which is released from the cells as a mature IL-1β (Khakh and North 2006) (Fig. 1.13).

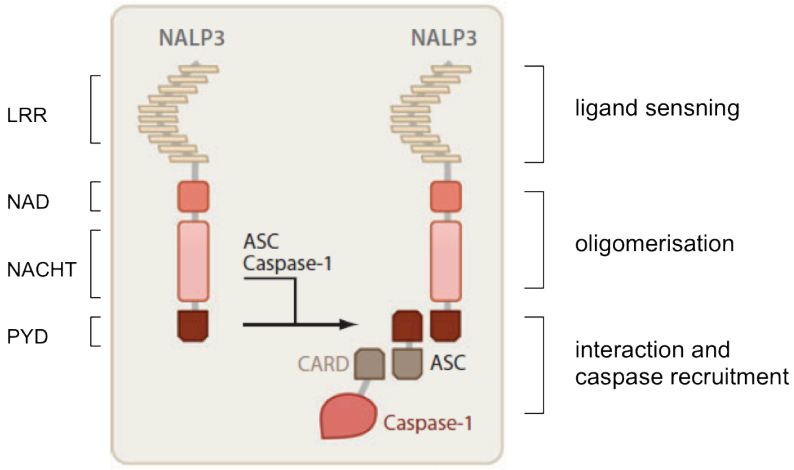

Fig. 1.13 Structural organization of the NALP3 inflammasome. The NOD-like receptors (NLRs) are consisting of three important domains: C-terminal leucine-rich repeat (LRR), multihistocompatability complex transcriptor (NACHT), NAD and N-terminal pyrin domain (PYD). PYD-PYD and caspase recruitment domain CARD-CARD interactions are needed for caspase-1 recruitment by the NALP3 inflammasome. Reproduced from Martinon et al. 2009, with modifications.

The process of inflammasome formation and the recruitment steps require further study (Dubyak 2012). However, the link between ATP mediated P2X7R activation and inflammasome assembly indicates that the inflammasome is regulated largely by this pathway. Opening of the cation selective channel after ATP binding and effective IL-1 β release may be connected by P2X7R activating a novel downstream protein, which links the two pathways. However, the most plausible scenario is that cell membrane permeabilisation and P2X7R formation leads to

cytosolic K^+ depletion. This promotes activation of NALP3 by stabilizing the inflammasome protein complex (Perregaux and Gabel 1994) (Fig. 1.14)

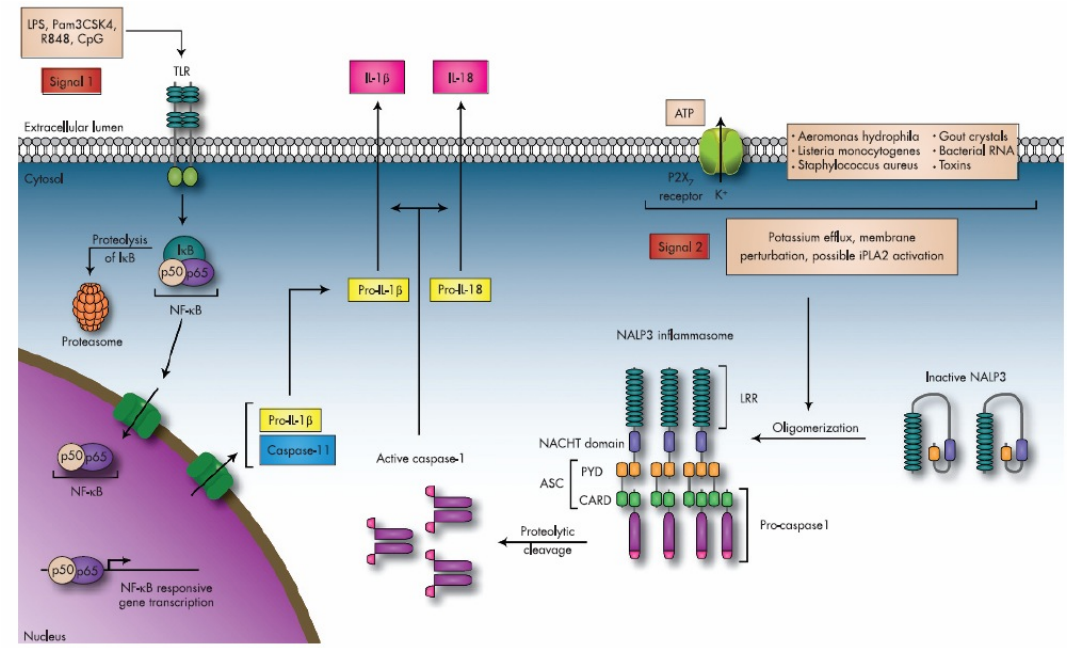

Fig. 1.14 Complexity of the IL-1β and IL-18 synthesis and secretion in response to exogenous signals. There are two signals required for IL-1β maturation and release. In immune cells, activation of Toll-like receptors (TLR) by LPS priming drives NF-κB downstream signaling and thereby pro- IL-1β, pro-caspase 1 and pro-caspase 11 production. The second signal triggered by ATP activation of P2X7R and induces rapid efflux of K^+ from the cell, which stimulates inflammasome assembly. Inflammasome complex formation initiates the processing of pro-caspase 1 that after being cleaved into caspase-1 can process pro- IL-1β into mature IL-1β. Reproduced from Sidiropoulos et al. 2008.

1.18 Mechanism of interleukin-1β secretion – a prototypic non-conventionally secreted protein

There are many hypotheses on how IL-1β could be trafficked into the extracellular space. In human blood monocytes, LPS stimulation leads to accumulation of intracellular pro-IL-1β and only 10% of it is released into the extracellular space (C Andrei et al. 2004). The first model suggests that pro-IL-1β and pro-caspase 1 are directed into a specific lysosomal compartment from which proteins are secreted by exocytosis from activated monocytes. This idea is supported by results showing co-

localisation of lysosomal cathepsin D with the inactive precursors of IL-1β and caspase-1 (Bianco et al. 2005). ATP-induced K^+ depletion caused activation of lysosomal specific phospholipases C and A_2, which potentially regulate IL-1β secretion. Lysosomes could represent possible storage vesicles for pro-IL-1β and additionally provide a suitable microenvironment for its processing (Mackenzie et al. 2001; Bianco et al. 2005). However, membrane translocation of pro-IL-1β into the lysosomal compartments remains to be explained.

An alternative pathway of cytokine externalization involves the formation of microvesicles at specific sites of the plasma membrane (Mackenzie et al. 2001; Thomas and Salter 2010). These microvesicles contain pro- and mature IL-1β and are directly shed from the cell surface into the conditioned medium. Microvesicle shedding from LPS-treated THP-1 monocytes occurs within the first 2 min after BzATP stimulation (Mackenzie et al. 2001). Therefore, this mechanism could explain the rapid release of mature bioactive IL-1β. However, it is possible that there is more than one mechanism of release involved, as the microvesicle pathway is not effective after prolonged stimulation with BzATP. It has also been shown that IL-1β can be directly secreted into the medium without microvesicle involvement (Qu et al. 2007).

Another model suggests the possible role for exosomes derived from multivesicular bodies (MVB) as a main pathway for rapid co-release of IL-1β, caspase-1 and inflammasome components from murine macrophages (Théry et al. 2002). Exosomes are small membrane vesicles that are released by most types of cells. They contain a specific subset of proteins that represent cytoplasmic components enclosed within the bi-layer membrane (Qu et al. 2007). The finding that IL-1β can be associated with MHC class II molecules may suggest cytokine incorporation into recycling endosomes and MVBs.

1.19 Link between P2X7R and arthritis

ATP signaling acts as an additional element of innate immunity, as P2X7R is a sensor of early microbial infection or tissue injury (Dubyak 2012). Studies with P2X7R-deficient mice show reduced IL-1β release after LPS-priming and ATP stimulation. Peritoneal macrophages derived from those animals are unable to secrete the mature 17 kDa form of IL-1β (Labasi et al. 2002). Moreover, P2X7r knockout

mice developed less severe collagen induced arthritis. Cartilage destruction was significantly reduced when compared to wild-type mice. Cathepsins that are lysosomal proteins involved in joint destruction can be released form mouse macrophages upon P2X7R activation (Lopez-Castejon et al. 2010). $P2X7R^{-/-}$ macrophages were unable to secrete cathepsins, thus indicating that P2X7R directly contributes to non-inflammatory arthritis (Lopez-Castejon et al. 2010). Interestingly, citrullinated peptides, to which antibodies are formed in patients with RA (Szodoray et al. 2010) were recently shown to be formed after challenging murine mast cells with the P2X7R agonist ATP (Arandjelovic et al. 2012).

The P2X7R is highly polymorphic (Fuller et al. 2009). Analysis of the single nucleotide polymorphisms in RA cohort revealed presence of P2X7R gene mutations that impair receptor function and correlated with the presence of rheumatoid factor in patients carrying those alleles (Al-Shukaili et al. 2011). Recent findings suggest that mutation in P2X7R coding sequence that disables membrane pore formation are related to the reduced chronic pain in OA patients (Sorge et al. 2012). It is therefore interesting whether inhibiting only P2X7R-mediated pore formation but not the channel activity could be a possible therapy to reduce severe pain in those patients.

1.20 The aims of the project

Disease-specific modified peptides are likely to provide a sensitive qualitative indicator of early arthritis. Our candidate molecule that mediates posttranslational modification and produces self-antigens during the cellular stress response is TG2. Little is known about the mechanism that triggers TG2 release, which is critical step in regulating extracellular enzyme activity. The specific aim of this project is therefore to identify the signaling pathway that regulates TG2 externalization.

Within this context, I am setting out to answer the following main questions:

1) Can TG2 be secreted through a non-classical mechanism in the same manner as IL-1β?
2) Does exogenous ATP trigger TG2 release through P2X7R-dependent signaling and does it require pore formation?

Answering those questions would widen our understanding of aberrant release and activation of TG2. These events might drive protein modification initiated by TG2 activity in the matrix or at the cell surface. This knowledge could later be used to identify TG2 modified proteins in articular cartilage. It is likely that specific products accumulate in OA and RA patients due to high levels of TG2 seen in pathology.

Chapter 2 Materials and methods

General materials and methods

2.1 Cell culture

The human embryonic kidney host cell line with an Flp-In site (HEK293 Flp-In) and human epithelial adenocarcinoma cells from mammary gland (MDA-MB-231) were kindly donated by Dr Vera Knäuper. The human monocytic leukemia cells (THP-1) were kindly donated by Dr Xiaoqing Wei. A HEK293 Flp-In cells, HEK293 cells stably expressing wild-type P2X7 receptor (HEK293 P2X7R), HEK293 cells stably expressing P2X7R with V5-His tag (HEK293 P2X7R-V5-His) and MDA-MB-231 cells were grown in Dulbecco's Modified Eagle Medium (DMEM) (Invitrogen) containing 10% heat inactivated fetal bovine serum (FBS) (Invitrogen) and antibiotics (100 μg/ml streptomycin, 100 U/ml penicillin) (Invitrogen). The HEK293 Flp-In cells were grown in the presence of 100 μg/ml Zeocin to maintain the expression of Flp-In site (Invitrogen). The culture medium for HEK293 P2X7R and HEK293 P2X7R-V5-His cells was supplemented with 100 μg/ml Hygromycin B to maintain the expression the transgene (Invitrogen). THP-1 cells were grown in 1640 RPMI medium (Sigma) containing 10% FBS (Gibco), 2 mM L-glutamine (Gibco) and antibiotics (100 μg/ml streptomycin, 100 U/ml penicillin) (Gibco). Cells were maintained at 37 °C in a humidified incubator at 5% level of CO_2.

2.1.1 Cells passaging

Adherent cells were split 1:7 and transferred into fresh 75 cm^2 flask (Starstedt) when they reached 80% confluence. Briefly, cells were detached from the surface with 1 ml trypsin/EDTA solution (0.05%) (Invitrogen) and left for 2-5 min at 37 °C. Trypsin was 'inactivated' by addition of 5 ml of medium containing 10 % FBS and cells were collected by centrifugation for 5 min at 400 x g. Cell pellet was re-suspended in 7 ml of fresh medium and 1 ml was transferred into new 75 cm^2 flask. The non-adherent cells were collected from flask and centrifuged for 5 min at 400 x g. Cell pellet was re-suspended in 7 ml of fresh medium and 1 ml was transferred into new 75 cm^2 flask.

2.1.2 Cell counting

After trypsinization cells were suspended in the medium containing 10% FBS. Desired volume of cell suspension was mixed with Trypan Blue solution (0.4%) (T8154, Sigma) in 1:1 ratio. 10 μl of cell suspension was loaded into Neubauer counting chamber and unstained cells counted according to the manufacturers protocol in order to obtain the cell number per 1 ml of medium.

2.3 Sample processing for Western blotting

2.3.1 Protein extraction

Cells were lysed in Cell Extraction Buffer (CEB) containing 20 mM HEPES, pH 7.4, 150 mM NaCl, 1 mM EGTA, 1% Triton X-100 and 0.25% deoxycholic acid. To the CEB 10% glycerol, 1 mM PMSF and 1 mM NEM were added just before protein extraction. Cells were lysed on ice for 10 min and the obtained extract was cleared by centrifugation at 15, 000 x g for 10 min, 4 °C. The supernatant was collected and frozen at -20 °C for further analysis.

2.3.2 Protein concentration determination

BCA protein assay was performed according to the protocol provided by the manufacturer (Thermo Scientific). In order to calculate protein concentrations, BSA was used as a standard (20 – 2000 μg/ml). 25 μl of each standard and sample as well as appropriate blanks were placed into wells of a 96-well plate and 200 μl of working solution/well was added (working solution: Reagent A with Reagent B at a ratio of 50:1). The plate was sealed and agitated thoroughly for 30 sec, and incubated at 37 °C for 30 min. After equilibrating plate to RT, the absorbance was read at 590 nm using a plate reader. The standard curve for BSA was derived by linear regression and protein concentrations were calculated from the standard curve.

2.3.3 SDS polyacrylamide gel electrophoresis

Protein samples were mixed with an equal volume of 2x sample buffer (25 mM Tris/HCl, pH 6.8, 39 mM EDTA, 4 % w/v SDS, 30 % v/v glycerol, 0.3 % w/v bromophenol blue) containing 2 % β-mercaptoethanol and boiled for 3 min at 98 °C.

A set amount of protein was loaded per lane (10 – 50 μg as indicated). As a molecular weight standard, 30 μg of the Amersham Low Molecular Weight Marker (LMW) (GE Healthcare) was used. Proteins were separated on Novex 4-20% Tris-glycine polyacrylamide gels (Invitrogen) for 2 hours using 125 V constant voltage (~35 mA). The electrophoresis was performed in running buffer (25 mM Tris/HCl, pH 8.8, 192 mM glycine, 0.1 % w/v SDS).

2.3.4 Western blotting

The sponges, blotting paper (Whatman) and nitrocellulose membrane (Schleicher & Schuell) was soaked in the transfer buffer (25 mM Tris/HCl, 192 mM glycine, 20 % v/v methanol). Then the "blotting sandwich" containing sponges, blotting paper, polyacrylamide gel and nitrocellulose membrane was prepared and placed in the transfer chamber. Proteins were transferred onto the nitrocellulose membrane for 2 hours using 125 mA constant current (~25 V) in transfer buffer. After transfer, the nitrocellulose membrane was stained with Ponceau S solution (5 % acetic acid v/v, 0.1 % w/v Ponceau S in H_2O) to visualize transfer efficiency and to mark the protein marker position. After washing with TBS, the membrane was blocked with 5% skimmed milk in TBS for 1 hour to prevent non-specific binding. Primary antibodies (Table 2.1) were diluted in 5% skimmed milk/TBS to the indicated concentration and incubated with the membrane at RT for the indicated time while shaking. The membrane was then washed 3 x 5 min in TBS containing Tween-20 (0.05%) (TBST). Secondary antibodies conjugated to HRP (Table 2.2) were diluted 1:500 in 5% skimmed milk/TBS before addition to the membrane. Following a 1 hour incubation period, the membrane was washed 3 x 5 min with TBST and once with TBS before addition of HRP-substrate. Antibodies binding was visualised using Amersham ECL Plus or Amersham ECL Prime Western Blotting Detection Reagents. The membrane was exposed to Amersham Hyperfilm (GE Healthcare). Film exposure time was adjusted from a few seconds up to 10 min.

Table. 2.1 List of primary antibodies used for immunostaining and Western blotting

Name	Clone	Species	Antigen (amino acids (aa))	Final concentration		Catalog number and manufacturer
				WB	Immunostaining	
Anti-TG2	CUB 7402	Mouse monoclonal	aa 447-478 between catalytic core and β barrel-1	200 ng/ml (1:1000) 1.5h, RT or ON, 4°C	2 µg/ml (1:100)	MS-224-P1, Thermo Scientific
Anti-P2X7R	-	Rabbit polyclonal	aa 331-595 on the C-terminus of human P2X7R	1 µg/ml (1:200) 2h, RT or ON, 4°C	2 µg/ml (1:100)	sc-25698, Santa Cruz
Anti-V5	-	Mouse monoclonal	14 aa sequence: G-L-P-I-P-N-P-L-L-G-L-N-S-T	20 ng/ml (1:5000) 1h, RT	1 µg/ml (1:100)	R96025, Invitrogen
Anti β-tubulin	TUB 2.1	Mouse monoclonal	aa 281-446 on the C-terminus	2.6 µg/ml (1:1000) 1h, RT	-	T4026, Sigma-Aldrich
Anti-actin	-	Rabbit polyclonal	11 aa sequence on the C-terminus: S-G-P-S-I-V-H-R-L-C-F	3.15 µg/ml (1:200) 1h, RT	-	A2066, Sigma-Aldrich
Anti-Flotillin-2	29/Flotillin-2	Mouse	aa 122-379	500 ng/ml (1:500) 1h, RT	-	610383, BD Biosciences
Anti-IκBα		Rabbit polyclonal	peptide on the C-terminus	1 µg/ml (1:200) 2h, RT	-	sc-371, Santa Cruz
Anti-GAPDH	GAPDH-71.1	Mouse monoclonal	not specified	200 ng/ml (1:5000) 1h, RT	-	G8795, Sigma
Anti-IL-1β	CRM56	Mouse	not specified	500 ng/ml (1:1000) ON, 4°C	-	14-7018-81, eBioscience

Table 2.2 List of secondary antibodies used for immunostaining and Western blotting

Conjugate	Species	Final concentration		Cat No and manufacturer
		WB	Immunostaining	
Alexa Fluor 594	Donkey anti-mouse	-	10 μg/ml (1:200)	A21203, Invitrogen
Alexa Fluor 488	Donkey anti-rabbit	-	10 μg/ml (1:200)	A21206, Invitrogen
HRP	Rabbit anti-mouse	2 μg/ml (1:1000)	-	P0260, Dako
HRP	Swine anti-rabbit	2 μg/ml (1:1000)	-	P0399, Dako

2.4. Statistical analysis

Data were analyzed using the GraphPad Prism software version 4.0a. The data presented are the mean ± standard error of the mean (SEM) or mean ± standard deviation (SD) as appropriate. For multiple pairwise comparisons, one-way analysis of variance (ANOVA) using the Tukey pair test was conducted. A p value of ≤ 0.05 was considered as significant.

Materials and methods in Chapter 3

2.5 TG2 storage and determination of protein concentration using the spectrophotometer

Transglutaminase 2 was purified from *E.coli* by our laboratory as previously described (Hadjivassiliou et al. 2008). After purification TG2 was stored at -20°C in a buffer containing 300 mM NaCl, 1 mM EDTA, 20 mM Tris-HCl, pH 7.5. During the time course of the experiments TG2 was defrosted and kept at 4°C. In order to estimate protein concentration the sample was cleared by centrifugation at 14000 x g for 30 min at 4˚C and absorbance was measured with the spectrophotometer (Beckman Coulter, DU 800). Concentration was derived from the OD_{280} reading using the Beer-Lambert law and the extinction coefficient of $\varepsilon = 1352$ cm^2/g. Some experiments were performed using commercially available TG2 (T002, Zedira).

2.6 Excitation and emission spectra determination of Abz-APQQEA and Abz-APE(γ-cad-Dnp)QEA

The excitation and emission spectra of the quenched Abz-APE(γ-cad-Dnp)QEA substrate and unquenched Abz-APQQEA peptide were first determined in the absence of Ca^{2+} and TG2. Solutions of 0.5 μM Abz-APQQEA peptide (Zedira) or 5 μM Abz-APE(γ-cad-Dnp)QEA quenched peptide (A102, Zedira) in Assay Buffer containing 50 mM Tris/HCl, pH 7.4, 50 mM glycine methylester, 100 mM NaCl, 1 mM dithiothreitol (DTT) and lacking Ca^{2+} were measured in a FluoroMax-3 Spectrofluorometer (HORIBA Jobin Yvon) using a 10x2 mm quartz microcell (Hellma Analytics, 104.002F-QS). Slits were set at 1 nm/2 nm for excitation and emission, respectively. The emission spectra were obtained by exciting samples at λ=320 nm and reading emission between 335 – 600 nm. Samples were scanned from 200 – 400 nm and the emission was read at λ=417 in order to determine the excitation spectra. For each sample and appropriate control 5 independent scans were taken and then averaged. The fluorescence of the control (buffer alone) was subtracted form the curves in order to obtain the final spectrum. In order to monitor the formation of the fluorescent reaction product the emission spectra of Abz-APE(γ-

cad-Dnp)QEA were determined in Assay Buffer containing 2 mM Ca^{2+}. The cleavage of 5 µM of Abz-APE(γ-cad-Dnp)QEA substrate was initiated with the addition of 20 µg/ml TG2. The reaction was incubated at 37°C and the emission of the sample was read at different time points using the same settings as above.

2.7 Real-time fluorescence assay for monitoring of transglutaminase activity by determining isopeptidase activity

TG isopeptidase activity was quantified by measuring changes in fluorescence intensity over time, resulting from transglutaminase-mediated cleaveage of Abz-APE(γ-cad-Dnp)QEA (A102; Zedira, Darmstadt, Germany). Reaction kinetics were captured at 37˚C in black optical bottom 96-well plates (165305, Nunc) using a FLUOstar Optima or OMEGA plate reader (BMG LABTECH). The reaction was carried out in 100 µl Assay Buffer containing 50 mM Tris/HCl, pH 7.4, 10 or 55 mM glycine methylester, 100 mM NaCl, 50 µM Abz-APE(γ-cad-Dnp)QEA, 5 mM DTT, and indicated concentration of TG2. The cleavage of quenched substrate Abz-APE(γ-cad-Dnp)QEA was initiated by automated injection of Ca^{2+}. Briefly, after measuring baseline fluorescence for 400 s (10 x 40 s interval), 10 µl $CaCl_2$ (2 - 50 mM) or H_2O as a control was injected. Where indicated 2 mM $MgCl_2$ injection was used as a control. The fluorescence was measured using the 320ex nm excitation filter and the 440 nm emission filter (top optics, gain set to 2450) and using a plate-mode protocol. The change in fluorescence was measured for a 1 h period (90 cycles of 40 s measurement intervals in total). Nucleotides (GTP, GTPγS, GDP, GMP, ATP and BzATP) (all from Sigma) were added at the desired concentration and reaction mixtures were incubated at 37°C for 15 min prior to enzyme activation with $CaCl_2$. To inhibit TG2 activity the TG2 inhibitor Boc-DON-QIVMeEs was used (B003, Zedira). Background fluorescence of reaction in the absence of Ca^{2+} was subtracted form the curves obtained after Ca^{2+}-mediated TG2 enzyme activation. The enzymatic reaction rates were derived by linear regression.

2.8 TG2 isopeptidase activity assay using live cells

Human embryonic kidney cells stably expressing P2X7 receptor (HEK293 P2X7R) and breast cancer cells (MDA-MB-231) were used to optimize the TG2 isopeptidase

assay in live cells. Black optical bottom 96-well plates (165305, Nunc) were coated with 100 µg/ml Poly-L-lysine (mol. weight 150000-300000, P4832, Sigma), washed with PBS and air-dried. HEK293 P2X7R cells or MDA-MB-231 cells were re-suspended in DMEM containing 10 % FBS and lacking antibiotics. Cells were seeded at a density of 6 x 10^4 cells/well and grown overnight. The next day cells were washed with pre-warmed PBS (37°C) following by addition of 80 µl Ca^{2+} -free PSS buffer containing 10 mM HEPES/NaOH, pH 7.4, 147 mM NaCl, 12 mM glucose, 2 mM KCl, 1 mM $MgCl_2$ and supplemented with 50 µM Abz-APE(γ-cad-Dnp)QEA and 55 mM glycine methylester, To some of the wells 10 µg/ml TG2 was added. The isopeptidase cleavage was initiated by automated injection of 2 mM $CaCl_2$ or 2 mM $MgCl_2$ as a control. To assay for TG2 intracellular activity, cells were permeabilized by addition of Triton X-100 at 0.1% v/v to the PSS buffer where indicated.

Materials and methods in Chapter 4

2.9 THP-1 differentiation with IL-6, TPA and ATRA

THP-1 cells were seeded in RPMI medium with 10% FBS. The next day, medium was supplemented with interleukin-6 (IL-6) (0.8 nM in PBS) (human recombinant, Sigma, I1395), 12-O-Tetradecanoyl-phorbol-13-acetate (TPA) (0.5 µg/ml in dimethyl sulfoxide (DMSO)) (Merck Millipore, 524400) or *all-trans* retinoic acid (ATRA) (1 µM in DMSO) (Sigma, R2625). The same volume of PBS or DMSO, respectively, was added as vehicle control. For IL-1β upregulation, half of the wells were simultaneously treated with 0.1 µg/ml bacterial lipopolysaccharide (LPS) from *Salmonella sp*. (kindly donated by Dr Xiaoqing Wei) or LPS was added after 48h of differentiation. Cells were left to differentiate for 48h or 72h as indicated. Medium was collected from the wells and centrifuged for 10 min at 1500 x g. The supernatant was transferred into a fresh tube and Tris/HCl, pH 7.4 was added up to 5 mM before storage at -20 °C. The cell pellet and cells remaining in the wells were lysed with 35 µl Cell Extraction Buffer (CEB) (see section 2.2.3.1 for details) and combined.

2.10 THP-1 cell culture on different substrates

THP-1 cells were suspended in RPMI containing 10% FBS and no antibiotics. Cells were seeded at a density of $1x10^6$ cells/well in a 24-well plate on plastic, glass coverslips or coverslips coated with collagen type I at 44 μg/ml (from rat tail, neutralized by 20 mM Tris/HCl, pH 7.4), fibronectin at 40 μg/ml (Sigma, F2006) or poly-L-lysine at 40 μg/ml (mol. weight 70000-150000, Sigma, P1274). Cells were grown on respective surfaces for 3 days and then washed once with PBS. To the cells Physiological Salt Solution (PSS) containing 10 mM HEPES/HCl, pH 7.4, 147 mM NaCl, 12 mM glucose, 2 mM $CaCl_2$, 2 mM KCl, 1 mM $MgCl_2$ was added. Cell morphology and attachment was assessed with inverted microscope and phase contrast optics (Nikon Eclipse TS100). Pictures of the cells were taken using a Panasonic Lumix (DMC-G1) camera.

2.11 THP-1 cell differentiation with ATRA in parallel with LPS priming

THP-1 cells were seeded in a 24-well plate on glass coverslips coated with poly-L-lysine as above at a density of $1x10^6$cells/well in RPMI with 10% FBS. On the next day, RA (1 μM) and LPS (0.1 μg/ml) were simultaneously added to the cells. After 48h, medium was gently aspirated, centrifuged for 10 min at 1500 x g and after transferring into fresh tube and buffering, frozen at -20 °C. Cells were washed with PBS and 0.5 ml PSS was added. Cells were then incubated in PSS with or without 1 mM ATP for 30 min or 1 hour in the incubator. Following ATP stimulation, the cell supernatant was cleared by centrifugation at 1500 x g for 10 min and after transferring into fresh tube and buffering, frozen at -20 °C.

2.12 THP-1 cell differentiation with ATRA followed by LPS priming

THP-1 cells were seeded in a 6-well plate at a density of $1x10^6$cells/well in 1 ml of RPMI with 10% FBS. Additionally, THP-1 cells were seeded in a 24-well plate at the density of $0.5x10^6$cells/well in 0.5 ml of RPMI with 10% FBS. The next day, 1 μM of ATRA or DMSO as a vehicle control was added to the wells. Cells were then differentiated for 48h. After that, the conditioned medium from the 24-well plate was collected, processed as above and frozen at -20 °C. The cell pellet was lysed on ice in 50 μl of CEB and then frozen at -20 °C. This represents the 48h time point samples.

The cells in the remaining set of wells of the 24-well plate and the ones in the 6-well plate were kept for another 24h +/- ATRA and in the absence or presence of 0.1 μg/ml LPS. The conditioned medium and cell extract fraction was prepared from the 24-well plate as previously. This represents the 72h time point samples. The cells in the 6-well plate were used for stimulation to induce IL-1β release. Cells were collected from the 6-well plate and were washed once with pre-warmed (37°C) PBS. The suspension cells was then centrifuged for 10 min at 1500 x g and the cell pellet was dissolved in 2 ml of PSS. The now fully differentiated cells were then transferred into a 24-well plate and stimulated +/- 1mM ATP in PSS for 30 min or 1 h in the incubator. After that, the cell supernatant and cell extract fraction was prepared as above and frozen at -20 °C.

2.13 Enzyme-linked immunosorbent assay (ELISA) for IL-1β

Measurements of cytokine concentration in conditioned medium from THP-1 experiments were performed using human IL-1β Ready-Set-Go reagent set (eBioscience) following the protocol provided by the manufacturer. Briefly, capture antibodies (anti-human IL-1β, CRM56) was diluted in the appropriate amount of Coating Buffer (1:250). To each well, 100 μl of capture antibodies was added and the plate incubated overnight at 4 °C. The plate was washed 5 x with TBS/Tween-20 (0.01%). In the next step wells were blocked for 1 hour with Assay Diluent (200 μl/well) to prevent non-specific binding. A 2-fold serial dilution of IL-1β standard was prepared starting from 500 pg/ml and either 100 μl of standard or 100 μl of conditioned medium/PSS transferred to the appropriate wells. Samples were incubated overnight at 4 °C, washed with TBST, and subsequently 100 μl of detection antibodies (biotin-conjugated anti-human IL-1β, CRM57) (1:250 in assay diluent) was added and the plate incubated for 1 hour at room temperature. After washing with TBST, 100 μl/well of Extravidin-peroxidase (Sigma) (1:1000 in assay diluent) was added. After 30 min, plate was washed 7 times TBST, followed by addition of 100 μl/well of Tetramethylbenzidine as substrate. The plate was left for 15 min to develop. The reaction was stopped by addition of 50 μl 1M ortho-phosphoric acid. The absorbance of the substrate at 450 nm was measured and a

background reading taken at 540 nm was subtracted. IL-1β concentrations were calculated from standards using linear regression analysis.

2.14 Stimulation of MDA-MB-231 cells to detect TG2 in the media

MDA-MB-231 cells were seeded in 24-well plates at a density of 3 x 10^4 cells/well in 1 ml of DMEM/10% FBS without antibiotics. After 2 days when the cells had reached approx. 70% confluence, cells were washed 1 x with serum free DMEM and then serum-starved for 18h. Cells were washed once with 200 µl of modified Eagle's Minimum Essential Medium (OptiMEM) (Invitrogen). The washing step was extended to 10 min when P2X7R inhibitor (A740003, Tocris) or P2X4R inhibitor (5-BDBD, Tocris) was added. Cells were stimulated with 250 µl OptiMEM containing indicated stimuli in the incubator for the indicated time. 200 µl of conditioned medium was taken from each well and then centrifuged for 10 min at 1500 x g to remove any remaining cells. Cell free supernatant from 2 wells was combined and 350 µl was transferred into a new tube. To each tube 1M Tris/HCl, pH 7.4, was added up to 5 mM final concentration before freezing at -20°C. Media were lyophilized and reconstituted in 40 µl of 8M urea and 2 x reducing sample buffer (mixed 1:1). 40 µl of conditioned medium was loaded per lane in a 10 well Tris-Glycine gel (4-20%). To visualize changes in intracellular protein levels, stimulated cells were washed once with PBS and lysed with 35 µl of CEB. Cell lysate was centrifuged for 10 min at 15, 000 x g and the supernatant was frozen at -20°C. Samples were boiled 3 min at 97 °C and 10 µg of cell lysate was loaded per lane. Proteins were resolved by electrophoresis followed by Western Blotting.

2.15 Intracellular calcium measurements in MDA-MB-231 cells

MDA-MB-231 cells were seeded at 5 x 10^4 cells/compartment in glass bottom dishes (Greiner Bio-One), pre-coated with 100 µg/ml poly-L-lysine (mol weight, 150000-300000, Sigma), washed once with PBS and air-dried before cell seeding. Fluo-4 AM (acetomethylester) (Invitrogen) calcium indicator was dissolved in DMSO containing 20% (w/v) Pluronic F-127 (Invitrogen). Cells were loaded with 3 µM Fluo-4-AM in OptiMEM for 20 min at 37°C and the medium was replaced with 200 µl fresh OptiMEM. Cells were monitored for 1 min under the confocal microscope prior to stimulation with an equal volume (to the volume in the dish) of OptiMEM

containing ATP or BzATP. The medium was carefully added to the cells to obtain a final concentration of 1 mM ATP or 100 μM BzATP. Cells were stimulated in an atmospheric control chamber kept at 37°C with 5% CO_2. The time lapse videos were recorded using the Leica SP5 confocal microscope and a 63x/1.4 NA oil objective (HCX PL Apo CS) for approx. 10 min. Sequential scanning (xyt scanning mode) was employed at a scanning rate of 2,62 s/frame. The argon laser was used to excite the Fluo-4 calcium indicator and the fluorescence emission was monitored using the FITC channel (excitation at 488 nm, emission 500-535 nm). Pictures were analyzed and exported using the LAS AF Lite program (Leica Microsystems).

2.16 Immunolocalization of TG2 in MDA-MB-231 cells

In order to investigate TG2 localization, MDA-MB-231 cells were seeded into a 24-well plate at 3 x 10^4 cells/well on sterile glass coverslips precoated with 100 μg/ml poly-L-lysine (mol weight, 150000-300000, Sigma). Cells were cultured in 1 ml of DMEM/10% FBS without antibiotics. After 2 days when cells reached approx. 70% confluence, cells were washed once with serum free DMEM and then were serum-starved for 18h. Cells were washed with 200 μl OptiMEM, followed by addition of 250 μl OptiMEM containing 1 mM ATP or 300 μM BzATP. As a control fresh OptiMEM without agonist was used. Cells were left in the incubator for 1h. Cells were then washed once with PBS, fixed with 4% PFA for 10 min at RT followed by extensive washing with PBS. To also detect intracellular TG2 cells were permeabilized with Triton-X-100 (0.1% in PBS) (Sigma) for 5 min where indicated. After washing, coverslips were blocked with 1% BSA (Cohn Fraction V, Fisher Scientific) in PBS for 60 min to prevent unspecific binding of antibodies. Coverslips were incubated for 2 h in a humidified chamber with specific mouse anti-TG2 antibodies (CUB 7402, 2 μg/ml, Thermo Scientific) diluted in PBS with 1% BSA (details of antibodies used can be found in Table 2.1 and 2.2). Diluted antibody solutions were centrifuged for 5 min at 10, 000 x g to remove any protein precypitates/aggregates prior to application to the sections. Coverslips were washed three times with PBS. Anti-mouse Alexa Fluor 594 secondary antibodies (10 μg/ml in PBS with 1% BSA) were added to the corrsponding coverslips. Incubation was performed in a humidified chamber in the dark for 1 hour. Control coverslips were incubated with only the secondary antibodies in the same manner. After washing

three times with PBS, coverslips were mounted using Vectashield with DAPI stain (Vector Laboratories) to visuallize the nucleus. Images were taken using the Leica SP5 confocal microscope and 63x objective. Sequential scanning (xy scanning mode) was adopted to collect the fluorescence from each channel. The helium-neon 543 nm laser source was used to excite Alexa Fluor 594 at 543 nm and the emission was collected at 555-620 nm. Nuclear staining was visualized by exciting the specimen at 405 nm using the diode405 laser and collecting the emmison between 430-512 nm. Pictures were analyzed and exported using the LAS AF Lite program (Leica Microsystems).

Materials and methods in Chapter 5

2.17 Cloning the P2X7R coding sequence into pcDNA 5/FRT/V5-His expression vector

Image clone (ID:4298811) containing the full-length sequence for P2X7R was purchased from GeneService, Cambridge, and was received as an *E.coli* stabculture. To prepare stocks and isolate DNA, bacteria were grown overnight in 3 ml LB medium (10 g Tryptone, 5g Yeast Extract, 10 g NaCl for 1liter) supplemented with chloramphenicol (34 μg/ml) at 220 rpm and 37 ˚C. The next day bacterial cells were collected by centrifugation at 3000 x g for 3 min and DNA was extracted using QIAprep Spin Miniprep Kit (Qiagen) according to manufacturers instructions. Plasmid DNA was finally eluted in 50 μl EB buffer (10 mM Tris/HCl, pH 8.5) and stored at -20 °C. In order to prepare glycerol stocks of transformed bacteria, 0.85 ml overnight culture was mixed with 0.15 ml glycerol and stored at -80 °C.

2.17.1 Amplifying P2X7R coding sequence by PCR

The 1.8 kb fragment encoding P2X7R was amplified using polymerase chain reaction and a forward and reverse primers (Eurofins MWG Operon) which introduced unique restriction sites into the amplified product (Tab. 2.3). For subsequent cloning, the forward primer (P2X7R-kpn-for2) was designed to add a *Kpn*I restriction site at 5' end. Reverse primers were designed to introduce a *Xho*I restriction site at 3' end. Two different reverse primers were used in order to design

two distinct P2X7R amplicons. One that contains the natural stop codon (*) of the P2X7R sequence (P2X7R-xho* primer) and a second primer that inserts the *Xho*I site immediately downstream of the coding sequence where the *Xho*I site replaces the stop codon and therefore allows for the V5-His tag to be added within the reading frame C-terminal of the P2X7R sequence (P2X7R-xho-rev primer) (Tab. 2.3). When cloned into pcDNA5/V5-His vector a C-terminal fusion protein will be producd containing a V5-is tag.

Table. 2.3 Primers used for P2X7R amplification

Name	Sequence	Melting temp.
P2X7R-**kpn**-for2	5'- TTAGGTACCTTCACCATGCCGGCCTGCTGC - 3'	72.2 ˚C
P2X7R-**xho**-rev	5'- TTTCTCGAGGTAAGGACTCTTGAAGCCACTGTACTG - 3'	70.6 ˚C
P2X7R-**xho***	5'- TTTCTCGAGTCAGTAAGGACTCTTGAAGCCACTGTA - 3'	69.5 ˚C

The P2X7R fragment was amplified using 25 cycles in a total volume of 50 µl of reaction. The amplification was performed using 1U of Phusion DNA polymerase (Finnzymes, 2U/µl) and 1 µl of each primer in the presence of 10 µl HF buffer (Finnzymes) containing 10 mM dNTPs (New England Labs) and 0.5% DMSO (Tab. 2.4).

Table. 2.4 Details of PCR program used for P2X7R amplification

	PCR program		
		temperature	time
		98 ˚C	30 sec
25 x	denaturation	98 ˚C	10 sec
	annealing	65 ˚C	20 sec
	elongation	72 ˚C	1'30 min
		72 ˚C	10 min
		4 ˚C	

For analysis, the amplified PCR fragments were separated on a 1 % agarose gel containing 1.25 mM ethidium bromide in TAE running buffer (40 mM Tris/acetate, pH 8.5, 2 mM Na_2EDTA) The agarose electorphoresis was performed under constant

voltage (100V). The PCR products were excised from the gel and extracted using QIAquick PCR Purification Kit (Qiagen). P2X7Rstop and P2X7R fragments were digested overnight at 37°C with *Kpn*I and *Xho*I restriction enzymes in NEBuffer 1 (Promega) containing 1% BSA (New England BioLabs). Digested fragments were separated using a 1% agarose gel, specific bands cut out from the gel and purified using the QIAquick GelExtraction Kit (Qiagen) according to manufacturers instructions.

2.17.2 Construction of P2X7R expression vector

A modified version of pcDNA 5/FRT vector (Invitrogen) containing the multiple cloning site from pcDNA 4/V5-His (version A) was used. This vector allows for site-specific recombination and transgene expression under the human CMV promoter, which ensures high level of constitutive expression. The vector was triple digested for 1 hour at 37°C with *Kpn*I, *BamH*I and *Xho*I restriction enzymes in NEBuffer 2 (Promega) containing 1% BSA (New England BioLabs) to reduce re-ligation of the linearised vector. The linearised plasmid was purified using the gel extraction procedure as outlined above for the P2X7R coding sequence.

The digested P2X7Rstop, P2X7R DNA fragments and linearised pcDNA 5/FRT/V5-His plasmid were separated using a 1% agarose gel in order to estimate DNA concentration of each fragment. The P2X7Rstop fragment or P2X7R fragment was mixed with linearized and digested pcDNA 5/FRT/V5-His plasmid at a ratio of 3:1 and ligated using 1U of T4 DNA ligase (Invitrogen) in the presence of 5 μl T4 DNA ligase buffer. The ligation was performed for 1 hour at RT in the total volume of 10 μl.

The ligation mix was added to 50 μl of chemically competent *E.coli* (NovaBlue GigaSingles Competent Cells, Novagen) and incubated on ice for 20 min. In the next step, bacterial cells were subjected to heat shock (42°C, 1 min) diluted in 150 μl LB, spread on agar plates containing 50 μg/ml carbenicillin (Sigma) and grown overnight at 37°C. On the following day, the bacterial colonies were transferred to 3 ml LB medium with carbenicillin (50 μg/ml) using a sterile tip and grown overnight at 37°C and 220 rpm.

Bacteria from overnight cultures were collected by centrifugation at 3000 x g for 3 min and bacterial DNA was extracted using QIAprep Spin Miniprep Kit

(Qiagen). DNA from selected colonies was digested for 1h in 37°C with *Kpn*I and *Xho*I restriction enzymes in NEBuffer 2 (Promega) containing 1% BSA (New England BioLabs). The digests were analyzed using 1% agarose gel electrophoresis. Clones containing the plasmid with the insert were transferred into 100 ml LB medium with carbenicillin (50 μg/ml) and grown overnight at 220 rpm, 37°C. Half of the overnight culture was used to extract DNA using GenElute HP Plasmid Midiprep Kit (Sigma). Glycerol stocks of the positive clones were prepared and stored at -80°C (as in subsection 1). Plasmid DNA from 2 clones for each construct was sent for sequencing (Value Read Tube, Eurofins MWG, Germany). In order to sequence the entire P2X7R insert, 4 primers were used: vector primers T7, pCR3.1-BGHrev provided by Eurofins MWG and two internal primers P2X7R-for-3, P2X7R-rev-3 primers that were *de novo* designed (Eurofins MWG) (Tab. 2.5).

Table. 2.5 Primers used for P2X7R-V5-His and P2X7Rstop sequencing

Name	Sequence	Melting temp.
P2X7R-for-3	5'- GTGCTCATCAAGAACAATATCGAC- 3'	59.3 ˚C
P2X7R-rev-3	5'- CTCCCTAGTAGCTGCTGGTTCA - 3'	62.1 ˚C

2.18 Transfection of HEK293 cells with P2X7R and P2X7R-V5-His constructs and selection of stably transfected colonies

A HEK293 host cell line that contains a Flp-In site (pFRT/lacZeo cassette) for site specific insertion using recombinase was used to generate stable cell lines (Invitrogen). This system is based on the homologous recombination that occurs between the FRT site present in the host cells and in the pcDNA 5/FRT/V5-His vector when co-expressed with Flp recombinase (Chapter 5, Fig. 5.2A). This process produces a functional hygromycin resistance cassette for selection. Integration of the expression construct into the genome is mediated by the Flp recombinase. The recombination brings the SV40 promoter and ATG initiation codon into proximity with the rest of the hygromycin gene carried by pcDNA5/FRT/V5-His, which allows for selection of cells. As the hygromycin gene transcribes the kinase that inactivates

Hygromycin B antibiotic by phosphorylation, only cells in which the integration was successful are able to grow in medium supplemented with Hygromycin B.

For generation of the stable cell line, wells in a 6-well tissue culture plate (Sarstedt) were coated with poly-L-lysine (40 μg/ml) (Sigma). HEK293 Flp-In cells were seeded at the density of 7.6 x 10^5 cells/well in 3 ml of DMEM medium supplemented with 10% FBS and antibiotics. For each construct 2 replicates were prepared. The next day, medium was replaced with 3 ml antibiotics free medium containing 10% serum. 12 μl of FuGENE 6 Transfection Reagent (Promega) reagent was added to 200 μl serum free DMEM and incubated for 5 min at RT. Meanwhile 3.6 μg of pOG44 vector encoding Flp recombinase was mixed with 0.4 μg of plasmid DNA from clone 3 or 6 of P2X7R and clone 3 or 6 of P2X7R-V5-His in a total volume of 100 μl serum free DMEM. Then each DNA mix was added into a tube containing medium and FuGENE 6 in order for the transfection reagent:DNA complexes to be formed (3:1 ratio). The incubation was continued for 30 min at RT. 150 μl of transfection reagent:DNA complex was added drop-wise into each well. The plate was gently swirled in order to evenly distribute the lipid DNA complexes. After 24h, growth medium was replaced with 5 ml antibiotics free medium with 10 % FBS containing 100 μg/ml Hygromycin B (Sigma). Growth medium supplemented with Hygromycin B was changed every day for two weeks to select transfected cells and once colonies had formed it was replaced every two days. Selection of stably transfected cells was performed for four weeks in total. Cell colonies were washed with PBS, trypsinized and transferred to a 25 cm^2 flask. After expansion in the cell culture of the HEK293 expressing P2X7R cells and HEK293 P2X7R-V5-His cells were frozen in DMEM medium containing 50% FBS and 10% DMSO. Stocks were kept in liquid nitrogen for long-term storage.

Potential changes in cell morphology were investigated using an inverted microscope (Nikon Eclipse TS100) with 20x or 40x objective and phase contrast illumination. Pictures of the stably transfected cell colonies were taken with a Panasonic Lumix (DMC-G1) camera.

2.19 Characterization of HEK293 cells stably expressing P2X7R

2.19.1 Immunolabelling of P2X7R in stably transfected HEK293 cells

In order to investigate P2X7R localization, the parental cells, P2X7R and P2X7R-V5-His stably transfected cells were seeded into a 6-well plate at 4 x 10^5 cells/well on sterile glass coverslips precoated with poly-L-lysine (100 μg/ml). Cells were grown in DMEM with 10% serum for 1 day. Cells were then washed with PBS, fixed with 2% PFA for 10 min at RT followed by extensive washing with PBS. To allow antibodies to bind to the intracellular C-terminus of P2X7R, cells were permeabilized with Triton-X-100 (0.1% in PBS) (Sigma) for 10 min. After washing, coverslips were blocked with 1% BSA (Cohn Fraction V, Fisher Scientific) in PBS for 30 min to prevent unspecific binding of antibodies. Coverslips were incubated for 2 h in a humidified chamber with specific rabbit anti-P2X7R (2 μg/ml, Santa Cruz), mouse anti-V5 (1 μg/ml, Invitrogen) antibodies reconstituited in PBS with 1% BSA or with a combination of both antibodies (details of antibodies used can be found in Table 2.1 and 2.2). Coverslips were washed three times with PBS. Anti-rabbit Alexa Fluor 488 or anti-mouse Alexa Fluor 594 secondary antibodies (both at 10 μg/ml in PBS with 1% BSA) were added separately or simultaneously to the corrsponding coverslips. Incubation was performed in a humidified chamber in the dark. Control coverslips were only stained with the secondary antibodies in the same manner. After washing three times with PBS, coverslips were mounted using Vectashield with DAPI stain (Vector Laboratories) to visuallize the nucleus. Images were taken using the Leica SP5 confocal microspope and 63x/1.4 NA oil objective (HCX PL Apo CS). Sequential scanning (xy scanning mode) was adopted to collect the fluorescence from each channel. Alexa Fluor 488 was excited at 458 nm using an argon-ion laser source and emission was captured from 494-535 nm. The helium-neon 543 nm laser source was used to excite Alexa Fluor 594 at 543 nm and the emission was read at 555-620 nm. Nuclear staining was visualized by exciting the specimen at 405 nm using the 405nm diode laser and collecting the emmison between 430-512 nm. Pictures were analyzed and exported using the LAS AF Lite program.

2.19.2 Shedding of Amphiregulin-AP upon P2X7R activation

The ADAM (a disintegrin and metalloprotease proteins) activation by P2X7R was studied using Shedding Assay. Two different approaches were performed to investigate Amphiregulin – alkaline phosphatase (AR-AP) shedding upon P2X7R activation.

2.19.2.1 Transfection of HEK293 cell lines overexpressing P2X7R with Amphiregulin-AP

The HEK293 parental cells, P2X7R and P2X7R-V5-His stable cells were seeded into 24-well plates at a density of 1.5 x 10^5 cells/well in 0.5 ml of DMEM medium supplemented with 10% FBS. For each cell type 4 replicates were prepared. The next day, growth medium was replaced with 1 ml antibiotic free medium containing serum. Cells were transiently transfected with 0.5 µg Amphiregulin-AP construct per well at a 3 µl FuGENE: 1 µg DNA ratio. Briefly, for 4 wells 6 µl of FuGENE Transfection reagent (Promega) was mixed with 450 µl serum free DMEM and incubated for 5 min at RT. Then 2 µg of the Amphiregulin-AP construct was added into the tube to allow transfection reagent:DNA complex formation during 30 min incubation at RT. 100 µl of FuGENE: DNA complex was added drop-wise into each well. The plate was gently swirled in order to evenly distribute the lipid DNA complexes.

After 48h the growth medium was removed and cells were washed with 200 µl pre-warmed PSS/well for 5 min in the incubator. Cells were stimulated with 250 µl of PSS +/- 1 mM ATP or PSS +/- 300 µM BzATP for 30 min at 37 °C in the incubator. Following stimulation, 200 µl of PSS was taken from each well and transferred into a fresh tube. The medium was centrifuged for 3 min at 10 000 x g to remove cell debris and 100 µl of the cell free supernatant was transferred into a 96 well plate. The AP buffer containing the alkaline phosphatase substrate (4NPP) was prepared as following: 100 mM Tris/HCl pH 9.5, 5 mM 4-Nitrophenyl phosphate (Sigma), 100 mM NaCl and 20 mM $MgCl_2$. 100 µl of freshly prepared AP buffer was added to each well. The increase in the absorbance of the 4NPP substrate was measured at 405 nm over time. The plate was incubated at 37 °C in between the measurements. OD values were plotted against time and analyzed by linear

regression to determine alkaline phosphatase activity, which is equivalent of the AR-AP ectodomain released into the medium upon P2X7R activation.

2.19.2.2 Co-transfection of HEK293 cells with P2X7R and Amphiregulin-AP

For co-transfection experiments the HEK293 parental cells were seeded as above and simultaneously transfected with both, 1 μg of AR-AP construct and 2 μg of P2X7R construct (clone 6) or P2X7R-V5-His construct (clone 6). The DNA mixture was prepared first and then added into serum free medium containing FuGENE 6 as outlined above. Cells co-transfected with AR-AP construct and P2X7R or P2X7R-V5-His constructs were washed and stimulated using pre-warmed and pre-gassed OptiMEM (Invitrogen) +/- 1 mM ATP or OptiMEM +/- 300 μM BzATP. Following stimulation, 200 μl of conditioned medium was taken from each well and transferred into a fresh tube and processed as previously. The alkaline phosphatase activity in the medium was determined as outlined above.

2.19.3 Calcium measurements in agonist treated HEK293 cells using confocal microscopy

HEK293 parental cells and HEK293 P2X7R cells were seeded at 7 x 10^4 cells/well in glass bottom dishes (MatTek Corporation) precoated with poly-L-lysine (100 μg/ml), washed once with PBS and air-dried before cell seeding. Fluo-4 AM (Invitrogen) calcium indicator was dissolved in DMSO containing 20% (w/v) Pluronic F-127 (Invitrogen).48 hours after cell seeding, cells were loaded with 3 μM Fluo-4 AM in OptiMEM for 20 min at 37°C and medium was replaced with 200 μl fresh OptiMEM. Cells were monitored for 1 min under the confocal microscope and prior to stimulation with an equal volume of ATP or BzATP in OptiMEM, which was carefully added to the cells to obtain a final concentration of 1 mM ATP or 100 μM BzATP.

For the experiments with the P2X7R inhibitor, HEK293 P2X7R cells were seeded at 5 x 10^4 cells/compartment in glass bottom dishes (Greiner Bio-One), precoated with poly-L-lysine (100 μg/ml). Two days later, cells were washed and loaded with 3 μM Fluo-4 AM in OptiMEM containing 5 μM P2X7R inhibitor (A740003, Tocris). After

20 min preincubation, medium was replaced with 200 µl of OptiMEM containing the same concentration of the inhibitor. Cells were then stimulated with the 100 µM BzATP in the presence of 5 µM A740003 inhibitor.
Cell stimulations were performed in the atmospheric control chamber kept at 37°C with 5% CO_2 under confocal microscope (see section 3.2.3.5.1).

2.19.3.1 Dynamic Ca^{2+} imaging

Movies were recorded using the Leica SP5 confocal microscope and a 63x/1.4 NA oil objective (HCX PL Apo CS) for approx. 10 min. Sequential scanning (xyt scanning mode) was employed at a scanning rate of 2,62 s/frame. The argon laser was used to excite the Fluo-4 calcium indicator and the fluorescence emission was monitored using the FITC channel (excitation at 488 nm, emission 500-535 nm). Pictures were analyzed and exported using the LAS AF Lite program.

2.19.3.2 Calcium measurements in agonist treated HEK293 cells using the plate reader

HEK293 P2X7R cells were resuspended in DMEM medium containing 10% FBS lacking antibiotics. A black 96-well plate (Nunc) was precoated with 100 µg/ml poly-L-lysine (Sigma), washed once with PBS and air-dried. Cells were seeded at 3 x 10^4 cells/well. The next day, growth medium was removed and cells were loaded for 20 min with 3 µM Fluo-4 AM in OptiMEM at 37°C. After 20 min, cells were washed once with OptiMEM and medium was replaced with 90 µl fresh OptiMEM. The plate was transferred to the FLUOstar OMEGA plate reader (BMG Labtech). Measurements were performed using the plate reader equilibrated to 37 °C in the presence of 5% CO_2. The Fluo-4 fluorescence was measured using the 485-12 nm excitation filter and the 520-10 nm emission filter (bottom optics, gain 2200). Fluorescence was measured in each well separately using a well-mode protocol. After measuring baseline fluorescence for 5 s (5 x 1 s interval), various volumes of BzATP stock solution in OptiMEM (1 – 10 µl) were automatically injected to yield for different concentrations of agonist and these spanned the 15 – 300 µM range. The change in Fluo-4 fluorescence was measured for 20 s after agonist addition (40 cycles of 0.1 s and then 40 cycles of 0.4 s measurement intervals). Control wells

were injected with 10 µl of OptiMEM without agonist. The change of fluorescence from 8 wells per condition was measured for each experiment. The average fluorescence of control wells was subtracted from the curves derived with agonist treatment. Each curve was analyzed by fitting the data initially using first order kinetics to estimate the value for a shared constant baseline (C) using the equation:

y=(Ymax-Ymax*exp(-k*x)+C

whereby k is the association constant and C is the shared constant for the data set. Data were then analyzed by fitting the kinetic data for the first 10s using equation:

y=(1-exp(-(A-Ymax)*k*x))/(1/Ymax-1/A*exp(-(A-Ymax)*k*x)+C,

whereby k is the association constant, A is the function of agonist concentration and C is the constant for baseline correction previously determined. This fitting was used to estimate the maximal fluorescence value (Y_{max}). The value for association constant (k) obtained from data fitting was: 1.7730^{-6} .Subsequently, Y_{max} was plotted against the agonist concentration to derive a dose-response curve.

Materials and methods in Chapter 6

2.20 Detection of TG2 in cell free supernatant using Western blotting.

Parental HEK293 cells and HEK293 cells stably expressing P2X7R were suspended in 0.5 ml of DMEM containing 10% FBS and lacking antibiotics. Cells were seeded in a 24-well plate at the density of 1.2 x 10^5 cells/well. For each condition 4 replicates were prepared. After 1 day of culture, growth medium was replaced with 0.5 ml of medium of the same composition as above. Cells were transiently transfected with 0.5 µg per well wild-type TG2 or TG2-GFP construct using FuGENE-6 transfection reagent (Promega) at a 3 µl Fugene: 1 µg DNA ratio. After 48h the growth medium was removed and each well was washed with 200 µl pre-warmed serum-free OptiMEM for 5 min in the humidified incubator. The washing step was extended up to 10 min when P2X7R inhibitor (A740003, Tocris) was present during washing. Cells were then stimulated with 250 µl of OptiMEM per well +/- 100 µM BzATP (Sigma) in the absence or presence of selected inhibitors. Cells were left at 37 °C in the humidified incubator. For each condition 800 µl of total amount of conditioned medium was collected. Briefly, 200 µl of pulse fraction was collected from each well of 4 replicates per condition and media from 2 wells

were combined in the tube. Meantime cells were washed with 200 µl of OptiMEM and then another 250 µl of OptiMEM without BzATP was added to the cells. At the indicated times, 800 µl of total amount of conditioned medium was collected. As previously, 200 µl of chase fraction was collected from each well of 4 replicates per condition and media from 2 wells were combined in the tube. Conditioned media was centrifuged for 10 min at 1500 x g at RT to remove any remaining cells. From each tube 250 µl of supernatant was transferred into a fresh tube resulting in 500 µl of cell free supernatant per condition. 1M Tris/HCl, pH 7.4, was added up to 5 mM final concentration before freezing at -20 °C. Frozen media was lyophilized and reconstituted in 50 µl of 8M urea and 2 x reducing SDS sample buffer (1:1). Samples were boiled 3 min at 97 °C and 15 µl loaded per lane of a 4-20% Tris/Glycine gel. Proteins were resolved by SDS electrophoresis followed by Western Blotting.

To visualize potential changes in cell-associated protein levels, stimulated cells were washed with PBS and lysed with 60 µl per well of Cell Extraction Buffer (as described in Materials and Methods, Chapter 2, section). Harvested cell lysate was centrifuged for 10 min at 16000 x g (4 °C) and the supernatant was decanted and frozen. Protein concentration of the cell extracts was determined using the BCA assay (as described in General Materials and methods, section 2.3.2). 10 or 5 µg of cell lysate was mixed with 2x reducing sample buffer (1:1) and loaded per lane. Proteins were resolved by SDS electrophoresis followed by Western Blotting.

2.21 Transfection of HEK293 P2X7R cells with TG2-GFP and GFP-TG2 constructs.

HEK293 P2X7R cells were seeded at 4 x 10^5 cells/well in 6-well plates on glass coverslips precoated with poly-L-lysine (100 µg/ml) (mol weight 150000-300000, P4832, Sigma). The next day, medium was changed and cells were transiently transfected with 2 µg/well TG2-GFP or GFP-TG2 constructs, respectively, using FuGENE -6 transfection reagent (Promega) at a 3 µl FuGENE: 1 µg DNA ratio. The laboratory has designed both TG2-GFP and GFP-TG2 constructs before my arrival. The coding sequences are inserted in the PrC plasmid under control of a CMV promoter (Invitrogen). After 24h, each well was washed with 200 µl pre-warmed (37 °C) OptiMEM for 5 min in the humidified incubator. The glass coverslip was

transferred from the 6-well plate and attached to a plastic holder prior to applying experimental conditions. The holder consisted of a 35mm plastic dish with a circular hole drilled into the centre (resembling those commercially available from MatTek Corporation/Greiner. Coverslips were secured to the underside of the dish with high vacuum silicone grease (Sigma) and were placed onto the microscope stage and 200 µl pre-warmed OptiMEM was added. Cells were monitored for 1 min under baseline conditions using a confocal microscope. Then a defined volume of ATP or BzATP in OptiMEM was manually added to the cells to obtain 1 mM ATP or 100 µM BzATP final concentration. Cells were stimulated in the atmospheric control chamber kept at 37°C with 5% CO_2. Movies were recorded using the Leica SP5 confocal microscope and a 63x/1.4 oil objective. Movies were recorded for approx. 10 min using sequential scanning (xyt scanning mode), taking a scan every 2,62 s/frame. The argon laser was used to excite the GFP and the fluorescence was monitored using the FITC settings (excitation at 488 nm, emission 500-535 nm). Pictures were analyzed and exported using the LAS AF Lite program (Leica Microsystems).

2.22 Annexin V labeling of the exposed phosphatidyloserine.

HEK293 P2X7R cells were seeded at 5 x 10^4 cells/compartment in glass bottom dishes (Greiner Bio-One), precoated with poly-L-lysine (100 µg/ml) (mol weight 150000-300000, P4832, Sigma). Two days later, cells were washed with 200 µl pre-warmed (37 °C) OptiMEM. To the cells 200 µl of OptiMEM containing 2 mM Ca^{2+} and FITC-conjugated Annexin V at concentration 1:100 (31490013, ImmunoTools). Cells were monitored for 1 min under baseline conditions using confocal microscopy. Movies were recorded for approx. 10 min using sequential Z-scanning (xyzt scanning mode), taking a scan every 2,62 s/frame. Then a defined volume of BzATP in OptiMEM was manually added to the cells to obtain 100 µM BzATP final concentration. Movies were recorded using the Leica SP5 confocal microscope with the atmospheric control chamber set to 37°C and 5% CO_2. The 63x/1.4 oil objective was used to visualize the cells. The argon laser was used to excite the FITC-conjugated Annexin V and the fluorescence was monitored in using the FITC channel (excitation at 488 nm, emission 500-535 nm). Pictures were analyzed and exported using the LAS AF Lite program (Leica Microsystems).

2.23 Densitometry analysis

X-ray films of ECL probed Western blots were scanned and converted into grayscale tiff images. Densitometry was performed using Image Quant analysis software (Amersham).

Materials and methods in Chapter 7

2.24 Detection of TG2 in cell free supernatant in the presence of inhibitors and at various Ca^{2+} concentrations using Western blotting.

HEK293 cells stably expressing P2X7R were seeded and transfected with wild-type TG2 or TG2 mutant $C^{277}S$ using the same transfection conditions as in Materials and Methods Chapter 6 (section 2.20). Briefly, 48h of transfection the growth medium was removed and each well was washed with serum-free OptiMEM for 5 min in the humidified incubator. The washing step was extended for up to 10 min when Calmidazolium chloride (Merck) was present during washing. Then cells were stimulated with 250 µl of OptiMEM per well +/- 100 µM BzATP in the absence or presence of Calmidazolium chloride or TG2 inhibitor (Boc-DON-QIVMeEs, Zedira). Where indicated, cell stimulation with BzATP was performed in standard OptiMEM (0.9 mM Ca^{2+}) or OptiMEM containing 2.2 mM Ca^{2+} or 1 mM EDTA. The following steps were performed according to the protocol detailed in Materials and Methods Chapter 6 (section 2.20).

2.25 Monitoring P2X7R-dependent pore formation by YO-PRO-1 uptake.

Black optical bottom 96-well plates (Nunc) were coated with 100 µg/ml poly-L-lysine, washed with PBS and air-dried. HEK293 P2X7R and parental HEK293 cells were re-suspended in DMEM containing 10 % FBS and no antibiotics. Cells were seeded at the density of 3 x 10^3 cells/well. When they reached 80% confluence, the cells were washed with pre-warmed PSS without Ca^{2+} (10 mM HEPES/NaOH, pH 7.4, 147 mM NaCl, 12 mM glucose, 2 mM KCl, 1 mM $MgCl_2$). Then, 99 µl of Ca^{2+} -free PSS containing 1 µM YO-PRO-1 (Y3603, Invitrogen) was added to each well and the plate was transferred into the plate reader equilibrated to 37°C/ 5% CO_2. YO-PRO-1 fluorescence was measured using the FLUOstar Optima instrument (BMG

Labtech). The fluorescence was read from the bottom of the plate by scanning a 4 mm orbital area in the center of the well. The probe was excited at 480 nm and the fluorescence emission was collected at 520 nm using a gain of 2200. The baseline fluorescence prior to stimulation was read every 40 s for 10 min. After cycle 14 the measurement was paused and 1 µl of BzATP at various concentrations was added to selected wells. To the control wells 1 µl of H_2O was added. YO-PRO-1 uptake by the cells was monitored for 30-60 min. The data were normalized for well-specific fluorescence and then the fluorescence of YO-PRO-1 without BzATP stimulation was subtracted form those obtained after BzATP-induced pore formation.

Chapter 3 Real-time fluorescence assay for monitoring of transglutaminase activity by determining isopeptidase activity

3.1 Introduction

In order to address the hypothesis that cells can actively externalize TG2 and that ATP stimulation (purinergic signaling) can potentiate TG2 externalization it was necessary to develop a novel method for quantifying extracellular enzyme. This will minimise cell handling or membrane perturbation caused by fixation or extensive washing and allow studying TG2 unconventional secretion and activation at the same time. Thus, in this chapter a real-time fluorescent TG2 isopeptidase assay was designed to track changes in TG2 activity. The advantage of this method is that once established as a cell-based assay, the activity of TG2 could be simultaneously measured on the outer leaflet of the cell membrane (cell associated), in the ECM or in conditioned medium. In contrast, this method should not detect intracellular TG2. As an interesting and unusual feature of TG2 is its large conformational change upon Ca^{2+} activation (Griffin et al. 2002; Pinkas et al. 2007), this transition may be an important factor regulating enzyme activity following release by the cells. Pinkas and colleagues suggest that secreted TG2 remains mainly in a closed conformation, despite low GTP and high calcium concentrations, implying that its activity is latent under normal physiological conditions (Pinkas et al. 2007). In the scratch wound assay performed on WI-38 fibroblast monolayers the activity of TG2 disappears at 12 h post wounding, although TG2 is still detected by immunostaining (Siegel et al. 2008). It was thus postulated that certain types of stress conditions lead to rapid and transient activation of extracellular TG2. On the other hand, it is well documented that physiological concentrations of Ca^{2+} in the ECM environment will keep the enzyme activated (Folk and Chung 1973; Bergamini 1988; R Király et al. 2011). Another factor that led me to design a real time assay are the recent findings about possible inactivation of TG2 through oxidation upon release (Stamnaes et al. 2010) or its fast endocytosis from the cell surface (Zemskov et al. 2007). A recent study describes a redox sensitive cysteine triad (C^{230}, C^{370}, C^{371}) involved in regulation of the oxidation state of extracellular TG2 (Stamnaes et al. 2010). The existence of a redox sensitive cysteine bond was previously postulated by Chung and Folk (1970)

and the crystal structure of TG2 confirmed the existence of a C^{370}-C^{371} disulfide bridge (Chung and Folk 1970; Pinkas et al. 2007). Investigation of Stamnaes and colleagues point at C^{230} to have a dominant role in oxidative inactivation of TG2 activity as it promotes C^{370}-C^{371} disulfide bond formation (Stamnaes et al. 2010). Interestingly, the loss of activity by oxidation is prevented in the presence of TG2 substrates or Ca^{2+} ions (at approx. 1-3 mM concentration). Ca^{2+} abolishes disulfide bond formation probably due to occupying its putative binding site, which is situated in close proximity to C^{230}. Still, once the disulfide bond is formed, addition of Ca^{2+} is unable to restore TG2 activity. Taken together this means that the level of active TG2 present in vivo can be influenced by the local oxidation state and is modulated by the presence of Ca^{2+} and substrate. On the other hand, modulation of local TG2 activation was confirmed by *in vitro* studies where incubation of WI-38 fibroblasts with oxidized glutathione markedly reduced TG2 activity around the wounded area, however TG2 activity could be restored by addition reducing agent (Jin et al. 2011). Authors of that study show evidence that the oxidative state of TG2 can be altered by specific redox-active proteins rather than by environment *per se*. They show that human thioredoxin can be a specific substrate for oxidized TG2 thus restoring its activity. Although thioredoxin is a cytosolic protein, its presence in the extracellular matrix can occur upon tissue injury and potentially this specifically drives TG2 activation. thioredoxin released from THP-1 cells primed with interferon-γ, as well as, recombinant thioredoxin were both able to induce TG2 activity on the surface of fibroblasts and on the cryosections of the mouse small intestinal biopsies. The data suggest that latent TG2 is present and can be activated.

As the transition from inactive to active TG2, and vice versa, is potentially relatively fast, the designed assay needed to detect rapid changes due to release and activation in the ECM in response to addition of P2X7R agonist, ATP. This chapter details the experimental steps that were necessary to establish a reliable method to detect the TG2 enzymatic activity of TG2 and verifies its use for the investigation of TG2 release in live cells.

The aims of the chapter:

1. Establish a sensitive real-time method to detect enzymatic activity of TG2.

2. Determine what is the influence of ATP, an allosteric regulator, on TG2 activity?

3. Investigate if the assay can be applied to live cells?

3.2 Results

3.2.1 Isopeptide substrate cleavage mediated by TG2 (assay principle)

The assay is based on measuring fluorescence changes over time with the use of a quenched substrate, with cleavage indicating the presence of TG2 activity (Fig. 3.1). The substrate was designed according to the well-known protease assays and work on isopeptidase activity by Laszlo Lorand group (Parameswaran et al. 1997). Although the predominant reaction driven by TG2 is the formation of covalent N^{ε}(γ-glutamyl)lysine bonds between or within polypeptides in the extracellular matrix (Raghunath et al. 1996; Aeschlimann and Thomazy 2000). TG2 can catalyze isopeptide bond hydrolysis in the presence of excess of an already cross-linked substrate (Parameswaran et al. 1997). To establish the isopeptidase activity assay, the Abz-APE(γ-cad-Dnp)QEA peptide, which is commercially available, was used as the substrate. This peptide is a quenched fluorescent probe derived from the osteonectin sequence (APQQEAL) that imitates an already cross-linked TG reaction product (Hohenadl et al. 1995). The backbone of the peptide is changed by attachment of the fluorophor (2-aminobenzoyl (Abz)), which is quenched by the 2,4-dinitrophenyl-cadaverine (cad-Dnp) moiety (Fig. 3.1A). The cad-Dnp substituent on the first glutamine residue mimics the Lys side chain in N^{ε}-(γ-glutamyl)lysine peptides cross-linked by TG2. TG2-catalysed hydrolysis of the isopeptide bond leads to the release of the cad-Dnp moiety from the peptide backbone resulting in a fluorescent signal from the Abz group. The isopeptidase reaction mediated by TG2 is a two-step process and ultimately results in the substrate hydrolysis or aminolysis (Fig. 3.1B). The first step is identical for both reactions and occurs when the isopeptide bonded residue in the Abz-APE(γ-cad-Dnp)QEA substrate transiently acetylates the thiol group in TG2 active site (step 1: intermediate). The thioester enzyme intermediate reacts then with the primary amine (e.g. glycine methylester provided in the buffer), which results in substrate aminolysis and release of a 'crosslinked' polypeptide (step 2a). However, this step is reversible as a new isopeptide bond is generated. In the absence of amine, TG2 can catalyze the hydrolysis reaction resulting in glutamate replacing the original isopeptide-bonded

glutamine in the substrate (step 2b). Once the substrate is cleaved, the TG2 is regenerated and able to enter into another reaction cycle.

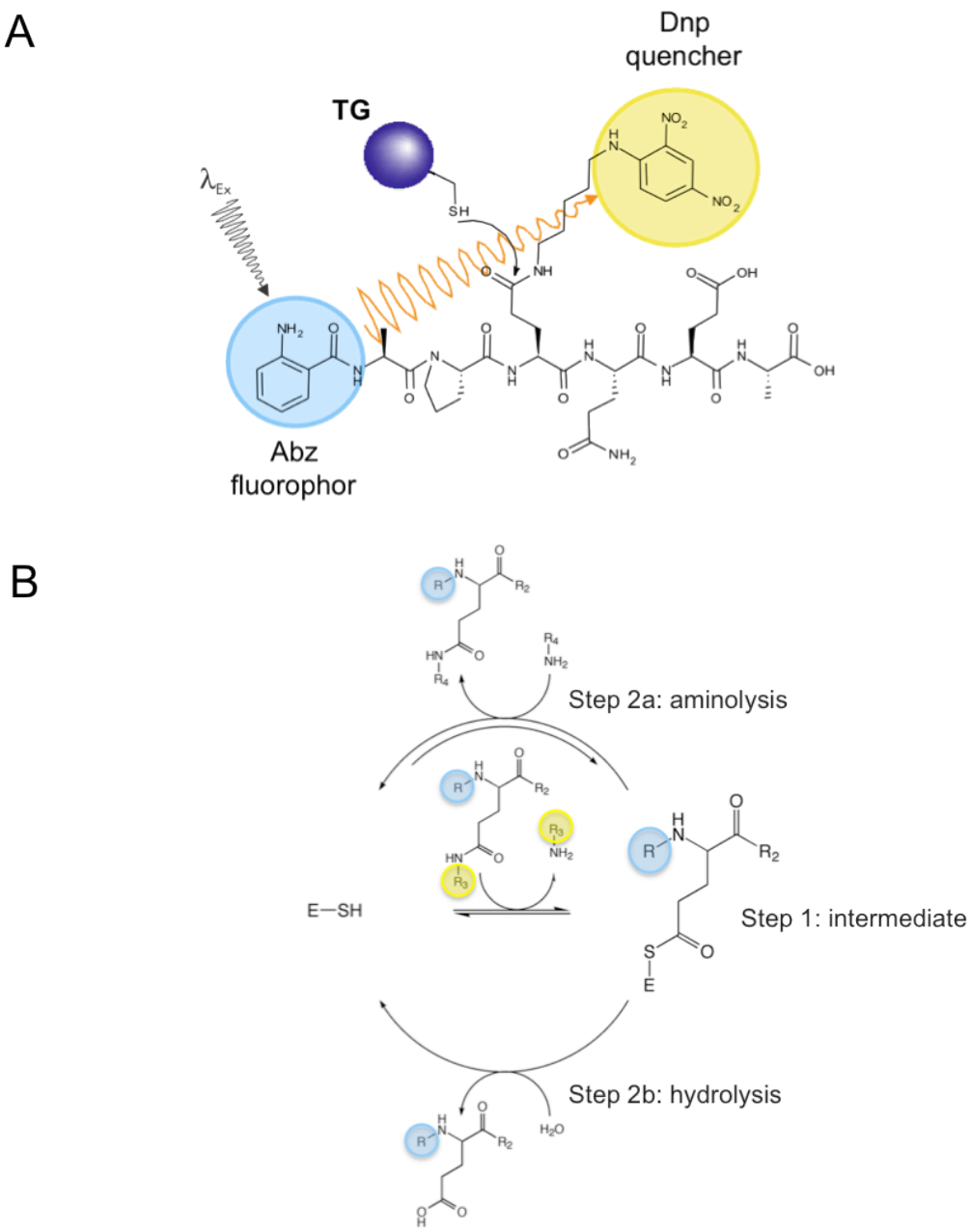

Fig. 3.1 Abz-APE(γ-cad-Dnp)QEA substrate structure and mechanism of its cleavage catalysed by TG2. A: Schematic representation of the Abz-APE(γ-cad-Dnp)QEA peptide structure with fluorescent group (2-aminobenzoyl (Abz)), the energy of which is absorbed by a quencher (2,4-dinitrophenyl (Dnp)). TG2 with active site thiol group is shown as blue sphere. **B:** The reaction starts when the isopeptide bond of the glutamine in the Abz-APE(γ-cad-Dnp)QEA substrate transiently acylates the thiol group in the TG2 active site (Step 1). This step results in the formation of the acyl-enzyme intermediate. In the absence of amine donor substrate the isopeptide bond hydrolysis occurs (Step 2b). In the presence of excess primary amine the reaction leads to aminolysis (Step 2a). Both hydrolysis and aminolysis of the fluorescent substrate allow for TG2 regeneration. (R_4-NH_2, e.g. glycine methylester). R (Abz-AP-); R_2 (-QEA); R_3 ($(CH_2)_4$-NH-Dnp); E-SH (TG2).

3.2.2 Fluorescence spectra of the Abz-APE(γ-cad-Dnp)QEA substrate

In order to measure fluorescence of the reaction product at appropriate wavelengths, the excitation and emission spectra of the quenched Abz-APE(γ-cad-Dnp)QEA substrate as well as unquenched Abz-APQQEA peptide were determined (see Appendix 1 for structure of Abz-APQQEA). According to the literature, 320 and 420 nm correspond to the excitation and emission peak maxima for the Abz group. As expected, after exciting samples at 320 nm, the fluorescence emission of the Abz-APE(γ-cad-Dnp)QEA quenched substrate was weak due to Dnp group absorbing the energy of the Abz group (Fig. 3.2A and B). On the other hand, the unquenched Abz-APQQEA peptide showed strong fluorescence emission even for 10-fold lower concentration than of the quenched. The maximum emission signal of Abz-APQQEA peptide was detected at 418 nm (Fig. 3.2B). When the Abz-APE(γ-cad-Dnp)QEA quenched substrate was incubated with 20 μg/ml TG2 in the presence of 2 mM Ca^{2+} a time-dependent increase in fluorescence emission was observed as an effect of TG2-mediated cleavage (Fig. 3.2C). A 10-fold increase in fluorescence was detected after 827 min. The increase in fluorescence was fast for approx 240 min, but slowly reached a plateau value after more than 900 min (Fig. 3.2D). Less than 10 % of substrate was converted in the first 30 min of the reaction. The maximal fluorescence signal of the reaction product was observed at 418 nm resulting in the highest detection sensitivity. However, fluorescence yield at 440 nm was > 80 % that of 418 nm. Thus, fluorescence emission coming from Abz-APE(γ-cad-Dnp)QEA cleavage mediated by TG2 could be effectively collected with 440 nm filter available with the plate reader.

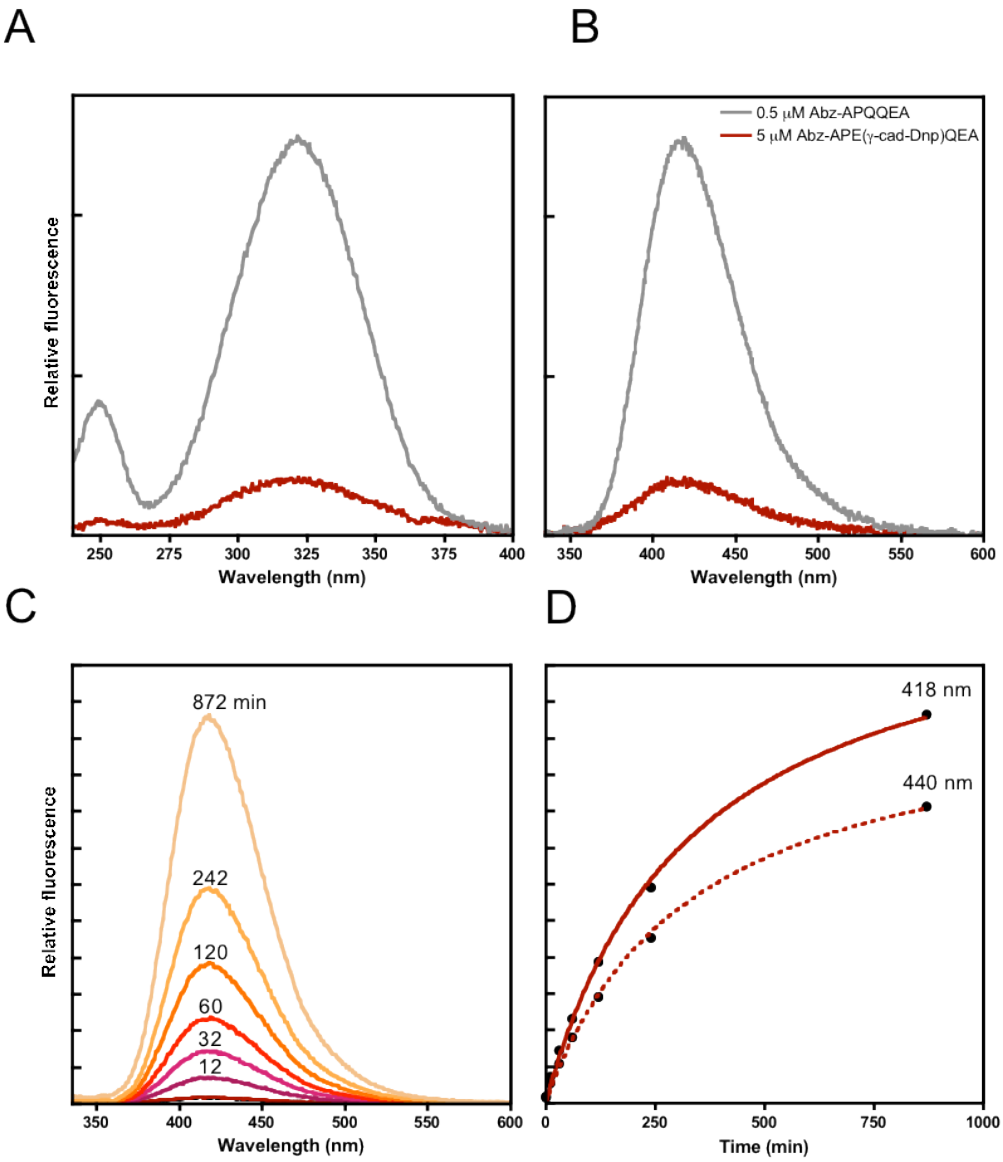

Fig. 3.2 Excitation and emission spectra of the Abz-APQQEA peptide and the Abz-APE(γ-cad-Dnp)QEA substrate and time-dependent substrate cleavage catalyzed by TG2. A, B: Unquenched Abz-APQQEA peptide (0.5 μM; grey line) and quenched Abz-APE(γ-cad-Dnp)QEA substrate (5 μM; red line) reconstituted in Assay Buffer (10 mM Gly-Me-Es, 100 mM NaCl, 50 mM Tris/HCl pH 7.5) were used to determine excitation (A) and emission spectra (B). Each line represents the mean of 5 scans of one sample after buffer subtraction. Data is representative of two independent measurements. **C:** 20 μg/ml TG2 was incubated at 37°C with 5 μM of Abz-APE(γ-cad-Dnp)QEA substrate in Assay Buffer containing 2 mM Ca^{2+}. After indicated times the fluorescence emission of the reaction mix was monitored. Baseline fluorescence of the Assay Buffer alone was subtracted from the spectra. **D:** Changes in the fluorescence upon Abz-APE(γ-cad-Dnp)QEA cleavage by TG2 were used to compare fluorescent signal at λ=418 nm and λ=440 nm collected at the same time points. Data were fitted using one site binding function: $Y = B_{max} * X / (K_d + X)$. Ticks on left y-axis correspond to 10,000 cps in all panels.

3.2.3 Optimization of the isopeptidase assay using an automated "high throughput" plate reader

The TG2 isopeptidase assay was developed to measure enzyme activity using the plate reader format. The assay optimization was performed using a FLUOstar OPTIMA instrument, which is a filter-based reader that uses excitation and emission filters in order to achieve the high sensitivity. Initially, different filters combinations were explored as filters can have different bandwidths that allow for the light to pass the filter and therefore generate different amount of signal. The light transmission through 320ex and 320-10 excitation filters that have 60 and 10 nm band pass, respectively, was measured. Moreover the light transmission through 410-80, 440-20 and 420-12 emission filters that have 80, 20 and 12 nm band pass, respectively, was measured as well. Obtained light transmission is presented in relation to the Abz-APQQEA excitation and emission spectra, respectively (Fig. 3.3A and B). The 320ex excitation and 410-80 emission filters had the best light transmission profile and were expected to give the best detection. Gain was adjusted for each filter pair to have comparable baseline conditions. The same filters were used on the FLUOstar OPTIMA instrument in order to select the best setting for the fluorescent product detection. The cleavage of Abz-APE(γ-cad-Dnp)QEA substrate with recombinant TG2 was performed in the 96-well plate format and initiated by addition of 2 mM Ca^{2+} and the reaction was captured for 1h with different combinations of filter pairs. The fluorescence value after 20 min of reaction were significantly higher when 320ex excitation filter (60 nm band pass) rather than 320-10 filter (10 nm band pass) was used (Fig. 3. 3C). By combining the 320ex excitation filter with 440-20 or 410-80 emission filters the amount of light collected with was not markedly different, when the gain values for each of pair was adjusted to give result within similar range of the scale on photomultiplier. Thus, 320ex excitation and 440-20 emission filter were chosen for the assay.

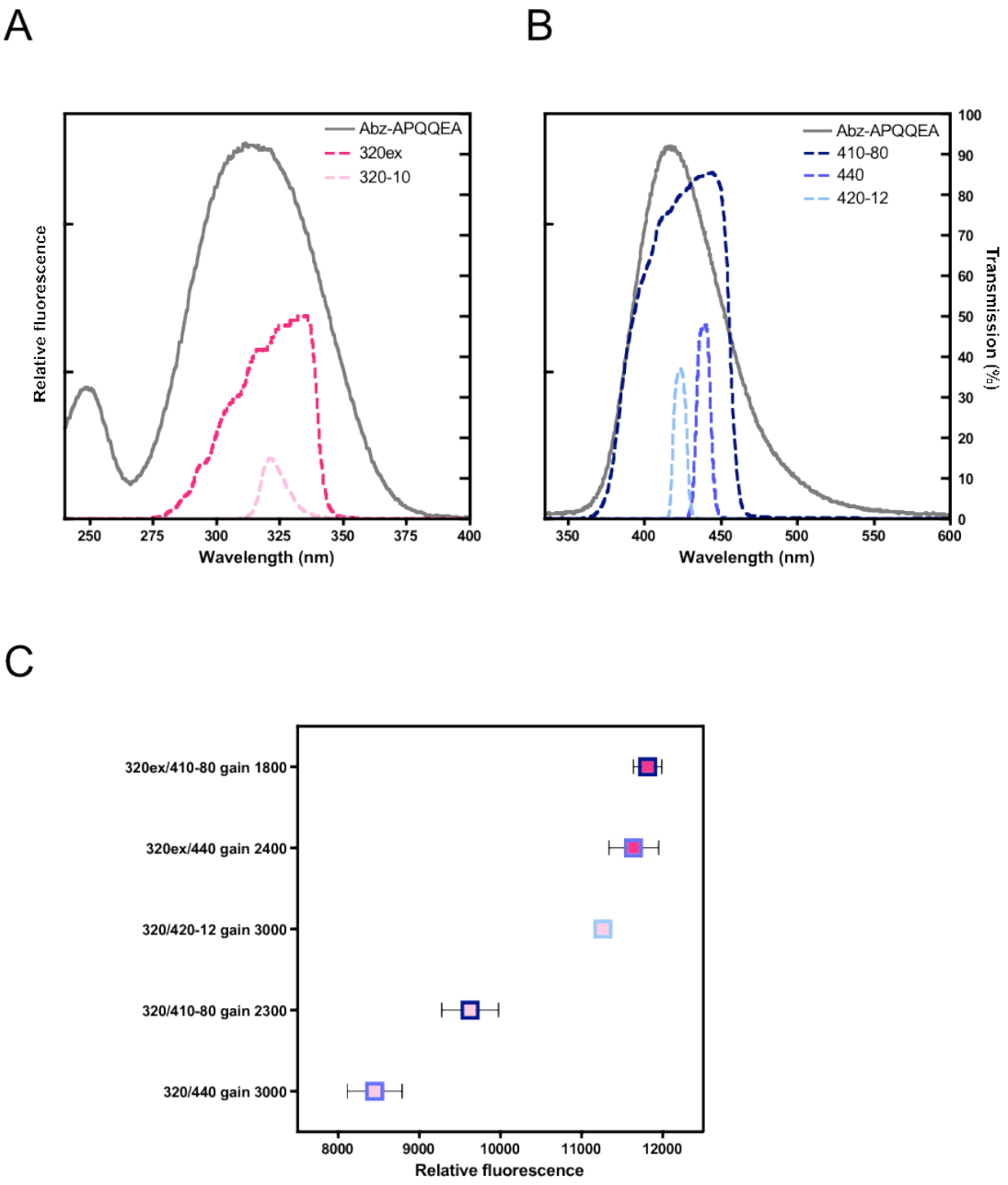

Fig. 3.3 Light transmission properties of different filters and filter selection for adaptation of TG2 isopeptidase assay for plate reader. A, B: Percent of transmitted light at different wavelength between different excitation (A) and emission filters (B) was compared. Light transmission is indicated by dashed lines (y-axis on the right). Spectrum of Abz-APQQEA peptide (0.5 µM; grey solid line) is shown as a reference. Ticks on left y-axis correspond to 10,000 cps in both panels. **C:** 10 µg/ml of recombinant TG2 was incubated at 37°C with 50 µM of Abz-APE(γ-cad-Dnp)QEA substrate in Assay Buffer containing 55 mM Gly-Me-Es, 100 mM NaCl, 50 mM Tris/HCl pH 7.5 and the cleavage was initiated by 2 mM $CaCl_2$ addition. The reaction was captured for 1h with FLUOstar OPTIMA plate reader and different filters were used to collect fluorescent signal. Gain values were adjusted for each filter pair to be at approx 30% PMT saturation level of signal at the start of the reaction. Symbols represent relative fluorescence value 20 min post reaction initiation. Each symbol color correspond to the spectrum shown in panel above where inner square represent excitation filter and the frame represent emission filter. Standard errors of the mean (± SEM) are shown for three independent measurements.

3.2.4 Isopeptidase activity of recombinant TG2

In order to establish optimal reaction conditions with regard to sensitivity and reproducibility to measure TG2 isopeptidase activity, a number of FLUOstar OPTIMA instrument settings were tested. This included choosing the plate reading mode, top or bottom optics, number of light flashes for each measurement, number of cycles and cycle time, sample mixing before and after injection, injection volume, temperature and type of 96-well plates. The detailed protocol parameters and optimized conditions that were adjusted during the assay establishment can be found in the Appendix 2. Recombinant TG2 was initially used to optimize conditions for Abz-APE(γ-cad-Dnp)QEA substrate cleavage before applying this method to assay surface TG2 activity in live cells. Here, I will discuss initially the properties of the assay. The Fig. 3.4A with the raw data represent a typical result of the isopeptidase cleavage obtained for different TG2 concentrations, where the fluorescence is proportional to the amount of TG2 used. The protocol was designed to read baseline fluorescence for 10 cycles, to account for small well-to-well differences, prior to TG2 activation with 2 mM $CaCl_2$ injection. No activity was detected in control wells, where water was injected (Fig. 3.4A). As the change in substrate concentration is small within 1h reaction time, TG2-mediated substrate conversion is linear at > 30 min and after control subtraction the fluorescence can be analyzed by linear regression (Fig. 3.4B). To verify that reaction rates are truly linear, the linear regression fit were calculated at different time intervals post Ca^{2+} injection and compared in the table (Fig. 3.4C). Table compares the reaction rates (ΔF/s), when the data were analyzed including the initial time-points of the reaction (first 5 min) or were excluded from the calculations. The data show a small log phase at the beginning of the reaction but otherwise very small differences were observed between different time intervals. This confirms linearity of the data and that a 5-35 min analysis interval provides an accurate representation of the reaction.

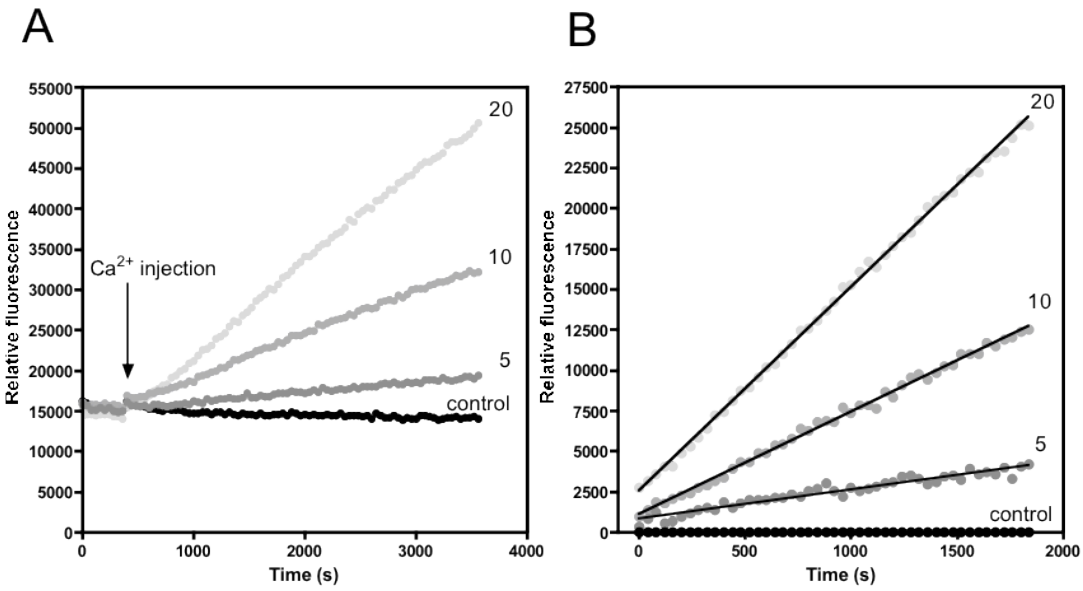

C

Reaction time (min)	Reaction rate (ΔF/s)	r^2
0-10	11.28	0.9869
0-20	12.14	0.9962
0-30	12.55	0.9978
0-40	12.64	0.9986
0-50	12.51	0.9989
5-15	11.98	0.9807
5-25	12.73	0.9960
5-35	12.86	0.9976
5-45	12.74	0.9987
5-55	12.43	0.9987

Fig. 3.4 Measurement of TG2 activity with optimized protocol for isopeptidase assay. A: Example of raw data showing Abz-APE(γ-cad-Dnp)QEA substrate conversion at different concentrations of TG2 (5 – 20 µg/ml) after 2 mM $CaCl_2$ injection. Reaction was performed at 37°C in Assay Buffer containing 50 µM Abz-APE(γ-cad-Dnp)QEA, 55 mM Gly-Me-Es, 100 mM NaCl, 50 mM Tris/HCl pH 7.5 and fluorescence was measured with FLUOstar Optima plate reader (Ex 320ex/ Em 440). Control given represents 20 µg/ml TG2 without Ca^{2+} injection (water injection). **B:** Data shown on graph A was analysed by subtracting the fluorescence in the absence of enzyme activation (no Ca^{2+}). Obtained curves were analyzed by linear regression. **C:** Cleavage of Abz-APE(γ-cad-Dnp)QEA with 20 µg/ml TG2 shown on graph A was analyzed by linear regression for different time intervals to calculate reaction rates and determine correlation coefficient.

3.2.5 TG2 activation by Ca^{2+}

As calcium binding is necessary for TG2 catalytic activity, the isopeptidase cleavage under different Ca^{2+} concentration was investigated. Under physiological concentrations of Ca^{2+} (2 mM), TG2 is highly active whereas no activity could be detected in the presence of 2 mM Mg^{2+} (Fig. 3.5A). By adding high, non-physiological concentrations of Ca^{2+} (10 mM and 50 mM) the isopeptidase cleavage was further increased (Fig. 3.5B). However, 2 mM Ca^{2+} was always used for enzyme activation in the assays, as the interest was to measure TG2 activity at physiological Ca^{2+} concentrations.

3.2.6 Buffer composition for the isopeptidase measurements

The isopeptidase assay was used to determine the influence of buffer composition on TG2 activity measurements in order to understand how the activity can be modulated and how to achieve the best assay sensitivity. TG2 is known to undergo reversible oxidative inactivation and carrying out isopeptidase cleavage in the presence of different concentrations of the reducing agent DTT confirmed a dose-dependent increase in activity. Addition of DTT up to a 10 mM concentration significantly enhanced the reaction rate and improved assay reproducibility between independent experiments (Fig. 3.6A). It was also important to determine to what extend ionic strength and pH affect the reaction. In order to do so, the isopeptidase cleavage was performed at pH 7.5 in Tris buffer containing different concentration of NaCl in the absence of glycine methylester. TG2 activity was similar in the presence of 0 – 85 mM NaCl concentration but the reaction rates started to decrease with increasing salt concentrations above 85 mM (Fig. 3.6B). In order to measure isopeptidase cleavage at various pH, MOPS and Tris buffering compounds were used and buffers prepared with or without 10 mM glycine methylester. It was expected that in the presence of an excess amine the aminolysis was the predominant reaction. However, there were no significant differences between reaction rates of hydrolysis and aminolysis at any pH (Fig. 3.6C). This was unexpected as the concentration of the reactive form of the amine (unprotonated) is clearly pH-dependent over the pH range examined, given that glycine methylester has a pKa of ~ 7.6. In both cases, the reaction was strongly pH dependent and fastest when buffer pH reached 6.5.

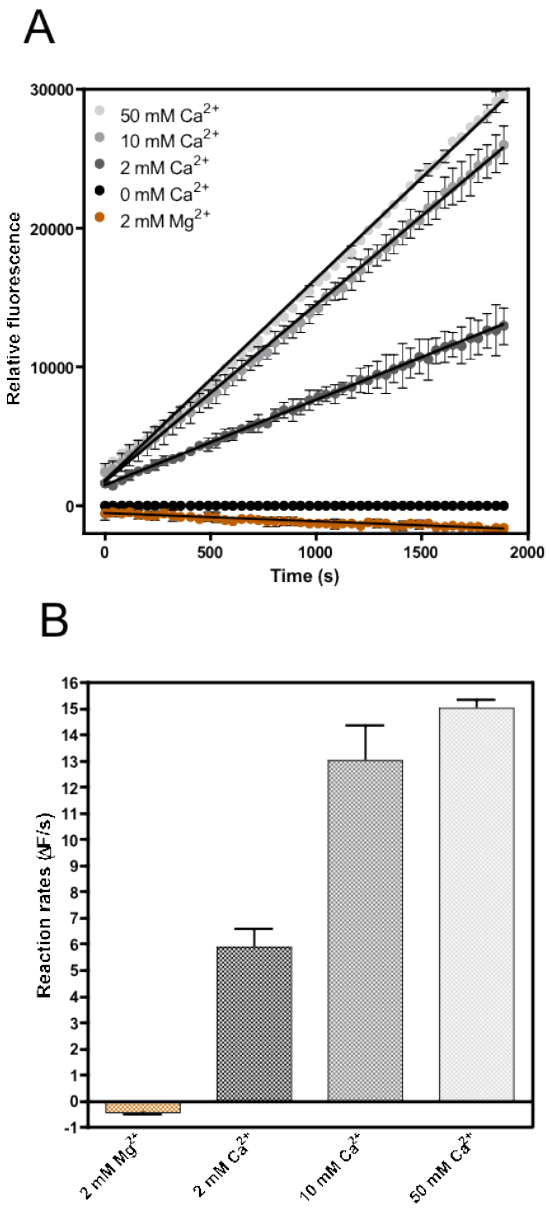

Fig. 3.5 Ca^{2+} -mediated enzyme activation analyzed by isopeptidase assay. A: Isopeptidase cleavage mediated by TG2 (20 µg/ml) in Assay Buffer after enzyme activation with different $CaCl_2$ concentrations (2, 10 or 50 mM Ca^{2+}). As a control water injection or 2 mM $MgCl_2$ was used. Fluorescence in the absence of enzyme activation (no Ca^{2+}) was subtracted and data was analyzed by linear regression. Data represent mean fluorescence over time ± SD from two independent experiments. **B:** Mean of the reaction rates ± SD from two independent experiments derived by linear regression are presented as a bar graph to illustrate changes in TG2 activity at different Ca^{2+} concentrations.

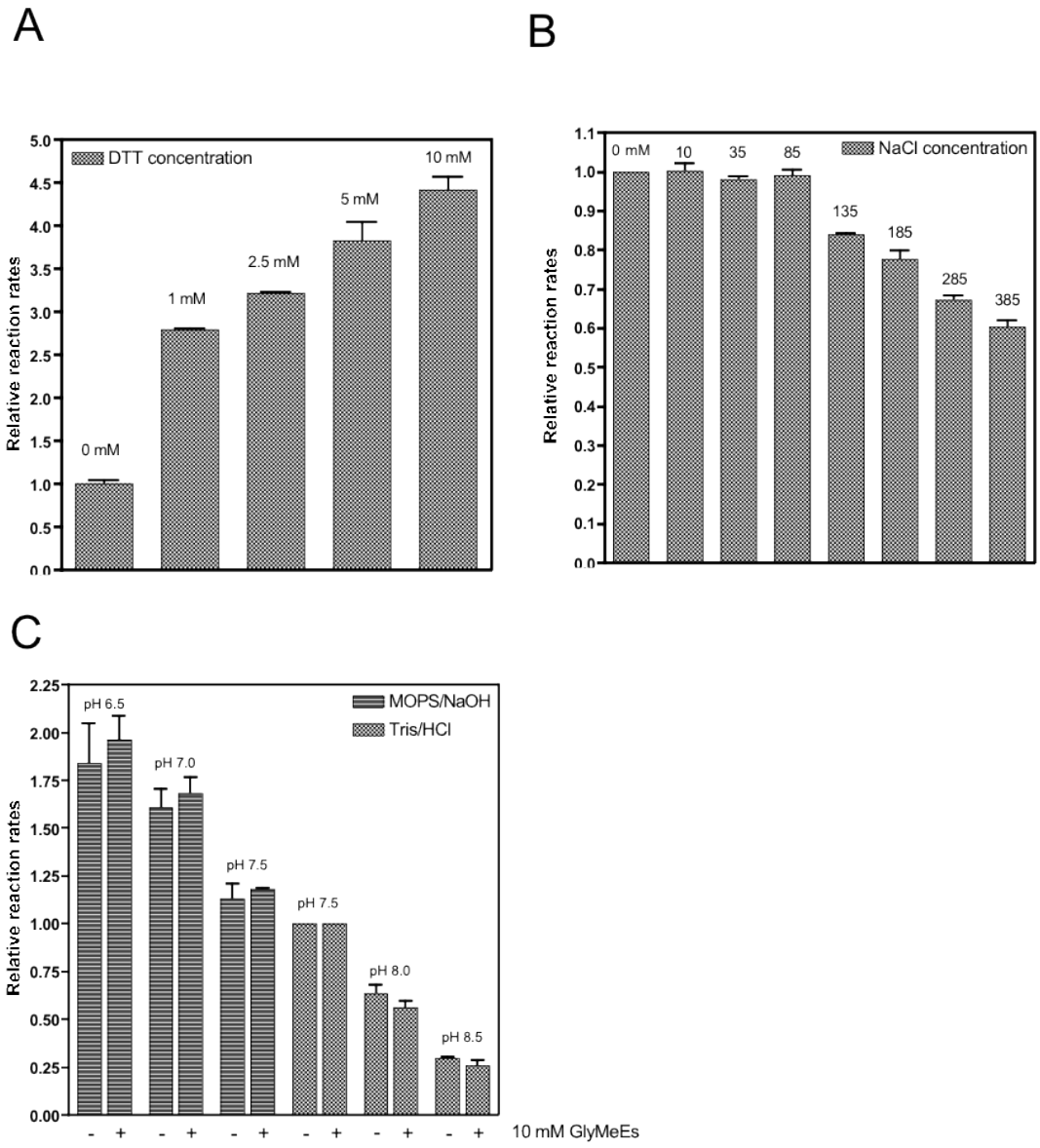

Fig. 3.6 Effect of DTT, ionic strength and pH on TG2 activity as measured with isopeptidase assay. A: TG2-mediated cleavage was performed in Assay Buffer containing different concentrations of reducing agent DTT as indicated. Fluorescence in the absence of enzyme activation (no Ca^{2+}) was subtracted and reaction rates were derived by linear regression. Graph represents the mean ± SD of the reaction rates (ΔF/s) from two independent measurements. Activity relative to that of TG2 in the absence of reducing agent is shown. **B:** Enzyme-catalyzed substrate hydrolysis was performed in Tris/HCl, pH 7.5 containing different NaCl concentrations in the absence of glycine methylester. Graph represents the mean ± SD of the reaction rates (ΔF/s) from two independent measurements. Activity is given relative to that of TG2 in 0 mM NaCl. **C:** TG2 isopeptidase activity was measured in either Tris/HCl or MOPS/NaOH at different pH. Experiments were performed in the absence or presence of 10 mM glycine methylester and reaction rates were derived by linear regression. Graphs represent mean ± SD of the reaction rates (ΔF/s) from two independent measurements. Activity is given relative to that of TG2 in Tris/HCl at pH 7.5.

3.2.7 Analysis of product of TG2-mediated isopeptidase cleavage

In the next step, it was necessary to confirm the balance between deamidated and transamidated product that is formed during the reaction, under selected conditions. Thus, the cleavage of Abz-APE(γ-cad-Dnp)QEA substrate mediated by TG2 was performed with or without amine donor. Glycine methylester was present in the buffer as previously or other donor N^{α}-acetyllysine methylester was used instead. HPLC analysis of the reaction products revealed the presence of specific peaks corresponding to the deamidated (Abz-APEQEA) or transamidated (Abz-APE(γ-N^{α}MeEster)QEA and Abz-APE(γ-N^{α}AcLysMeEster)QEA) products (Fig. 3.7). The Abz-APE(γ-cad-Dnp)QEA substrate was always detected at 17.5 min. The deamidated product was detectable in the absence of amine present (Fig. 3.7B) or at its low concentrations after approx. 11.5 min (Fig. 3.7C). Depending on the amine used, the deamidated products were eluted at slightly different positions in relation to the Abz-APE(γ-cad-Dnp)QEA substrate (Fig. 3.7C,D and E). Relative increase in the fluorescence of the deamidated vs transamidated products were similar (Fig. 3.8A and B) suggesting that differences in product formation were largely guided by amine concentration. To estimate the amine concentration required for the transition from the reaction of hydrolysis to aminolysis reaction mediated by TG2 for different amine substrates, the formation of deamidated versus transamidated product at different glycine methylester and N^{α}-acetyllysine methylester concentrations was analyzed (Fig. 3.8C). There is a big difference in the concentration of each amine necessary to yield a transamidated product (approx. 14-fold higher concentration of N^{α}-acetyllysine methylester than glycine methylester is needed) (Fig. 3.8C). Those data suggest that while the nature and concentration of the amine donor substrate has a pronounced influence on product formation.

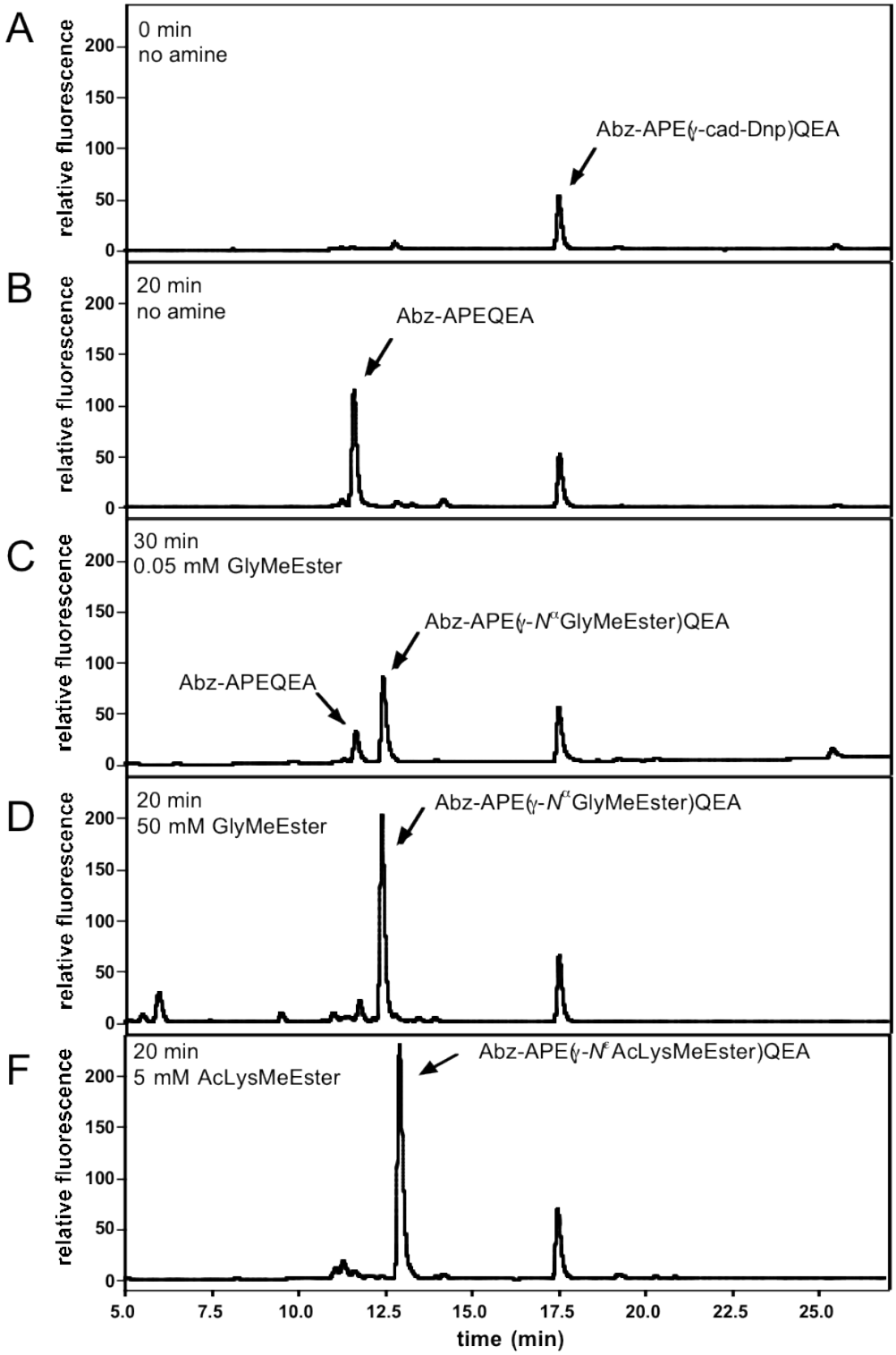

Fig. 3.7 Analysis of the reaction products upon TG2-mediated cleavage of Abz-APE(γ-cad-Dnp) QEA by HPLC. TG2 isopeptidase cleavage of Abz-APE(γ-cad-Dnp)QEA substrate was performed in Tris/HCl, pH 7.5 containing no amine, glycine methylester or N^{α}-acetyllysine methylester. Reaction products were quantified by HPLC (Phenomenex Kinetex C18/2.6 column using 7-72% acetonitrile gradient in 0.01% TFA). Peaks corresponding to the deamidated (second and third graph from the top) or transamidated (third to fifth graph from the top) product are shown in relation to the Abz-APE(γ-cad-Dnp)QEA substrate. HPLC analysis was kindly performed by Andreas Heil and data reproduced with his permission.

3.2.8 Standard reaction conditions

After evaluating a number of parameters relevant to the study of the isopeptidase activity, the standard conditions for the reaction were established. As an internal standard, the activity of 20 μg/ml TG2 in Tris/HCl at physiological pH (7.5) and in the presence of 100 mM NaCl was determined in all experiments. Enzyme activity was analyzed at 2 mM Ca^{2+} in the presence of 5 mM DTT to reverse oxidation. To avoid measuring both, the deamidated and transamidated fluorescent product, the glycine methylester concentration was kept at 10 mM to favor the reaction of aminolysis (showed on Fig. 3.8C as dashed line). Therefore, all subsequent experiments were performed under those conditions.

3.2.9 The isopeptidase assay sensitivity

The aim of developing the isopeptidase assay was to measure small changes in TG2 activity at cell surface therefore it was important to determine the detection limit of the assay. The isopeptidase cleavage was performed using standard conditions and different TG2 concentrations (1.25 – 20 μg/ml). The assay sensitivity was compared between the FLUOstar OPTIMA and FLUOstar OMEGA plate reader whereby the OMEGA instrument is supplied with a more sensitive photomultiplier (Fig. 3.9A and B). Fluorescence emission of the standard peptide Abz-APQQEA showed linear relationship when concentrations of 0.13-2.0 μM substrate were used on OPTIMA (gain 2450) and 0.016-0.5 μM (gain 2450) or 0.03-2.0 μM (gain 1883) on OMEGA instrument, respectively (Fig. 3.9C and D). The detection limit for enzymatic conversion of Abz-APE(γ-cad-Dnp)QEA was 1 μg/ml (~13 nM) TG2 on both instruments (Fig. 3.9E). This could not be enhanced by longer reaction times.

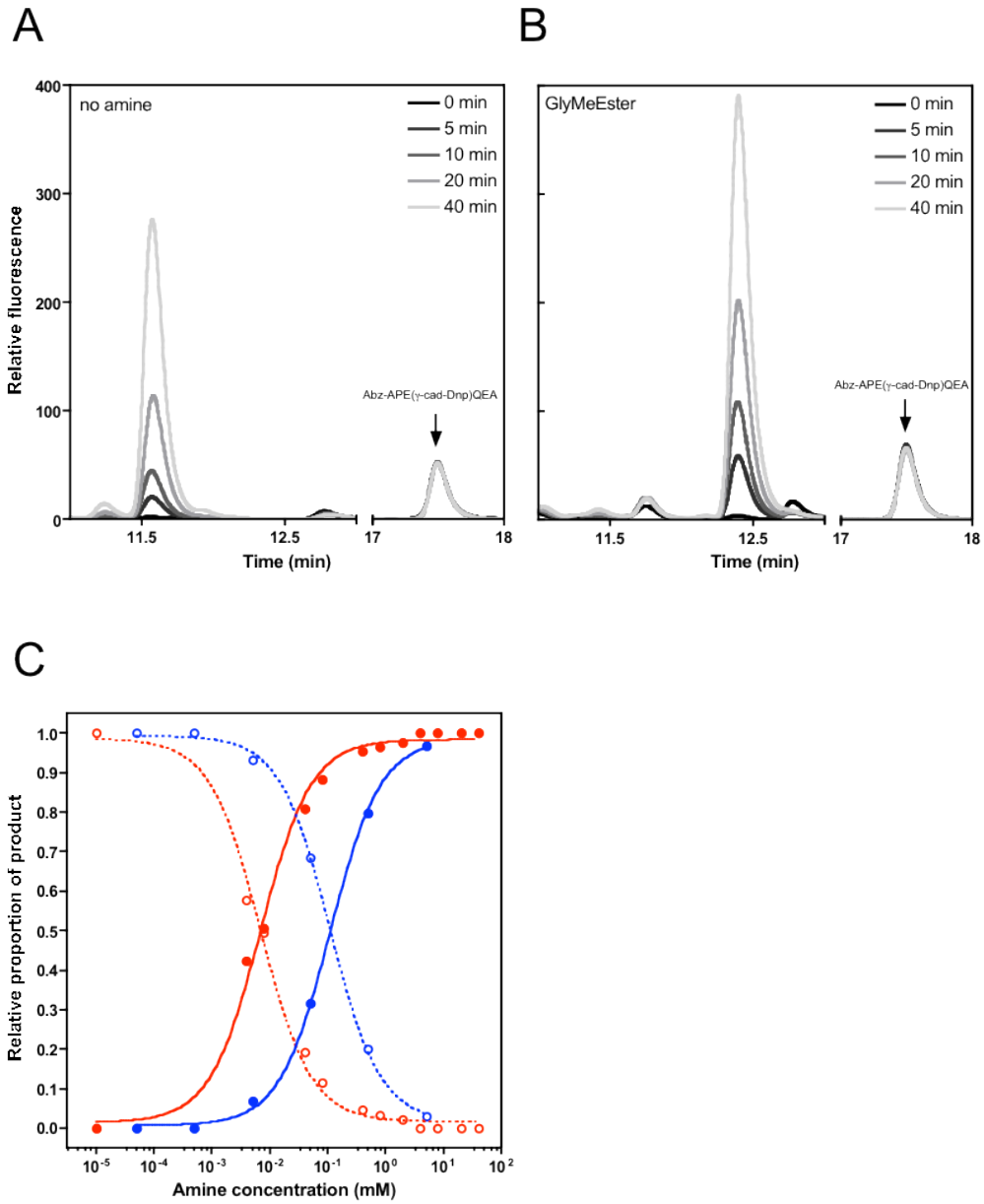

Fig. 3.8 Difference between deamidated and transamidated products formed in isopeptidase assay analyzed by HPLC. A, B: TG2 isopeptidase cleavage of Abz-APE(γ-cad-Dnp)QEA substrate was performed in Tris/HCl, pH 7.5 containing no amine or 5 mM glycine methylester. Reaction was stopped at different time points and the products were quantified by HPLC (Phenomenex Kinetex C18/2.6 column using 7-72% acetonitrile gradient in 0.01% TFA). Peaks corresponding to the deamidated (graph A) and transamidated product (graph B) are shown on the graph in relation to the Abz-APE(γ-cad-Dnp)QEA substrate. **C:** Comparison of different amine donor substrates, glycine methylester (red) and *N*-acetyllysine methylester (blue), on TG2-mediated conversion of Abz-APE(γ-cad-Dnp)QEA**.** Graph shows reaction products generated at different amine concentrations after 60 min by aminolysis (solid lines) or hydrolysis (dotted lines) of thio-ester intermediate that were quantified by HPLC. Data were fitted using sigmoidal dose response function: $Y= Y_{min} + (Y_{max} - Y_{min})/(1+10^{(logEC50-X)})$**.** HPLC analysis was kindly performed by Andreas Heil and data reproduced with his permission.

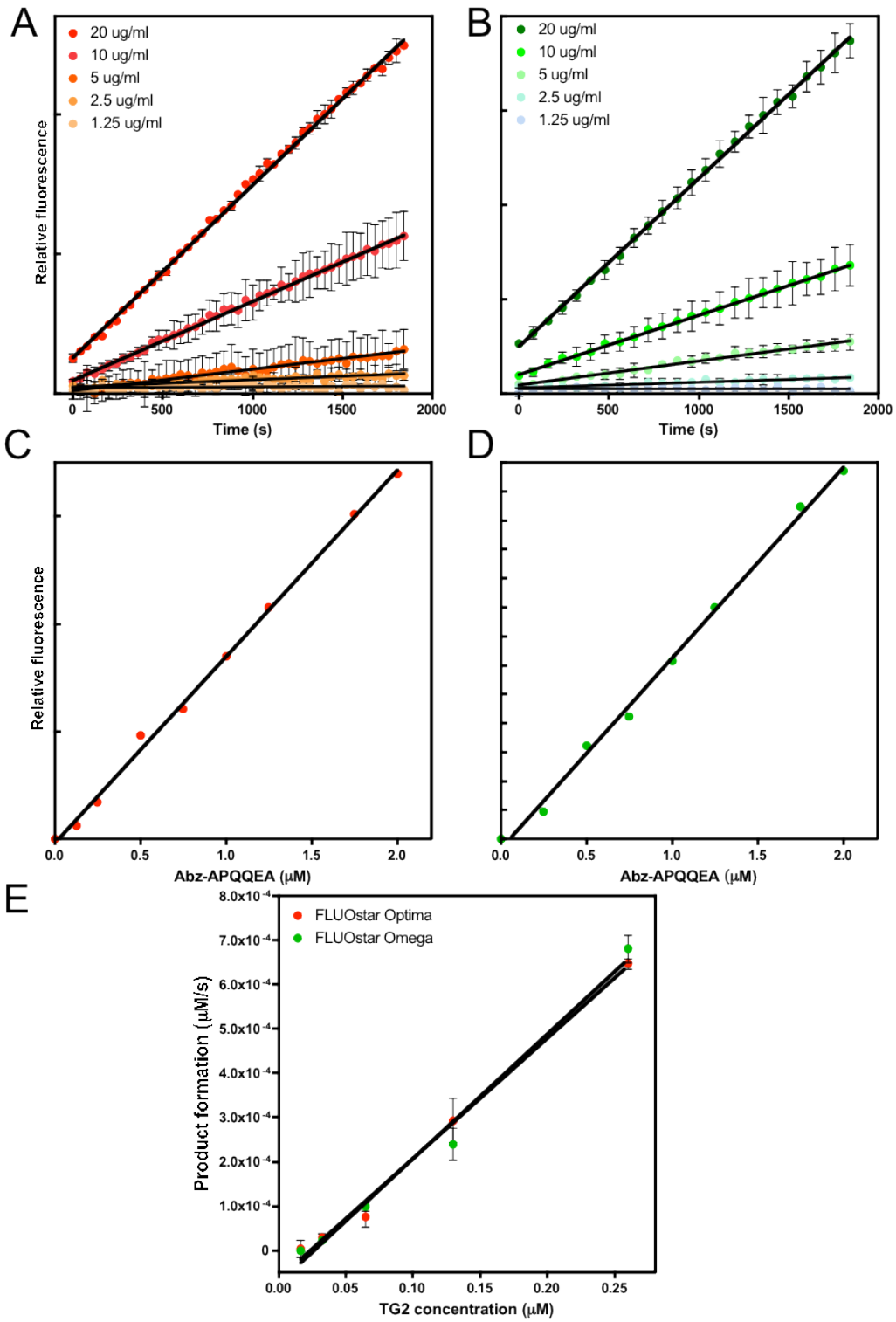

Fig. 3.9 Comparison of isopeptidase assay sensitivity between FLUOstar OPTIMA and OMEGA plate readers. A, B: Abz-APE(γ-cad-Dnp)QEA substrate cleavage was performed at different concentrations of TG2 (1.25 – 20 μg/ml) after 2 mM $CaCl_2$ injection. Fluorescence in the absence of enzyme activation (no Ca^{2+}) was subtracted and data was analyzed by linear regression. Kinetic measurements were captured with FLUOstar OPTIMA (left, gain 2450) and FLUOstar OMEGA (right, gain 2100). The OMEGA plate reader is fitted with a more sensitive PMT and therefore may detect lower concentrations of fluorophore. Graphs represent data ± SD from two independent experiments. **C, D:** Different concentrations of Abz-APQQEA peptide were measured by FLUOstar OPTIMA (left, gain 2450) and FLUOstar OMEGA (right, gain 2100) and relative fluorescence was plotted against peptide concentration to determine the linear range of detection. Data was analyzed by linear regression and slope (ΔF/μM) for each reader was determined. **E:** Reaction rates (ΔF/s) derived for each TG2 concentration measured by both readers were divided by the value of the slope for Abz-APQQEA peptide in order to calculate the product formation (μM/s). Data ± SD from two independent experiments is presented in the graph.

3.2.10 TG2 activity in the presence of nucleotides

Using the outlined reaction conditions, 20 μg/ml TG2 and different concentrations of nucleotides, the allosteric regulation of TG2 activity by nucleotides was investigated. This was important, as both ATP and BzATP will be later used as P2X7R agonists. Whereas GTP binds to TG2 structure, promotes it closed conformation and therefore acts as a high affinity regulator of TG2 activity (Achyuthan and Greenberg 1987), the data concerning ATP effect on TG2 is more debatable. The reaction was performed in the presence of Ca^{2+} and various concentrations of GTP, GTPγS, ATP and BzATP (Fig. 3.10). GTP and GTPγS (its nonhydrolyzable form) were strongly inhibiting TG2 activity, with an apparent binding affinity of 2.9 and 3.6 μM, respectively, whereas ATP and BzATP had an approx. 1000 fold lower affinity. GTP inhibition of enzyme activity was not influenced at high ionic strength (200 mM NaCl). However, it was approx. 500-fold weaker at saturating, non-physiological Ca^{2+} concentrations (50 mM Ca^{2+}).

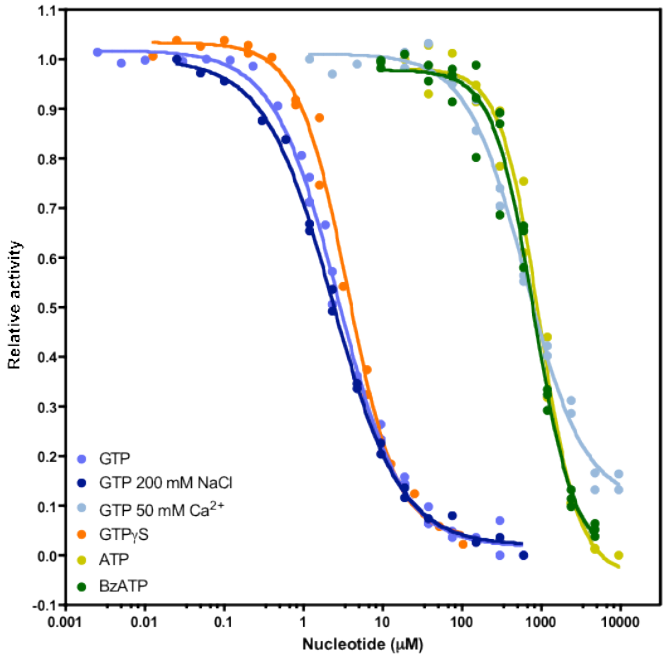

Fig. 3.10 Regulation of TG2 catalytic activity by nucleotides as measured with isopeptidase assay. Isopeptidase activity of TG2 (20 μg/ml) at 2 mM Ca^{2+}/ 100 mM NaCl in the presence of various concentrations of nucleotides as well as at non physiological concentration of Ca^{2+} (competitive allosteric regulator) and higher concentration of NaCl (altered ionic strength). For each reaction fluorescence in the absence of enzyme activation (no Ca^{2+}) was subtracted and reaction rates were derived by linear regression. Symbols represent values from two independent measurements, GTP (blue); GTP at 200 mM NaCl (dark blue); GTP in the presence of 50 mM Ca^{2+} (light blue); GTPγS (orange); ATP (light green) and BzATP (dark green). Data were fitted using sigmoidal dose response function: $Y = Y_{min} + (Y_{max} - Y_{min})/(1+10^{(logEC50-X)})$.

3.2.11 TG2 activity in live cells

After optimizing conditions for the isopeptidase assay with recombinant TG2, preliminary measurements of enzyme activity in live cells were performed to validate the use of this method for cell-based studies. The method should allow measuring activity of released TG2 in real time (Fig. 3.11). Experiments were performed in the same plate reader format but the reaction was measured in the PSS buffer (physiological salt solution). The PSS buffer is a salt solution that is mimicking the physiological extracellular conditions and is widely used to stimulate P2X7R in live cells when supplemented with ATP or BzATP (Mackenzie et al. 2005). Before performing experiments with cells the activity of recombinant TG2 in both standard Assay buffer and PSS was compared and the rate of the reaction was similar in both buffers (only approx. 1.25 x higher reaction rate in PSS than in standard assay buffer based on two independent measurements, data not shown). Two different cell lines were used: MDA-MB-231 breast cancer cells that express high levels of intracellular TG2 (see Chapter 4) and HEK293 human kidney cells stably transfected with P2X7R that are negative for TG2 (see Chapter 5 and 6). In the presence of 2 mM Ca^{2+}, the reaction rates were similar when the activity of the recombinant TG2 (10 μg/ml) was measured alone or in the presence of either cell line (Fig. 3.12). Data show that the presence of cells or cellular products does not influence the assay. In wells containing HEK293 P2X7R cells and no Ca^{2+}, there was also a small increase in fluorescence in the absence of added TG2. This likely was a non-specific event as those cells do not express TG2. Similarly, activity of TG2 was detected in MDA-MB-231 cells but only when recombinant TG2 was added indicating that the assay is not sensitive enough to detect extracellular TG2 activity in MDA-MB-231 cells or its activity is latent on the surface of cells (Fig. 3.12A and B).

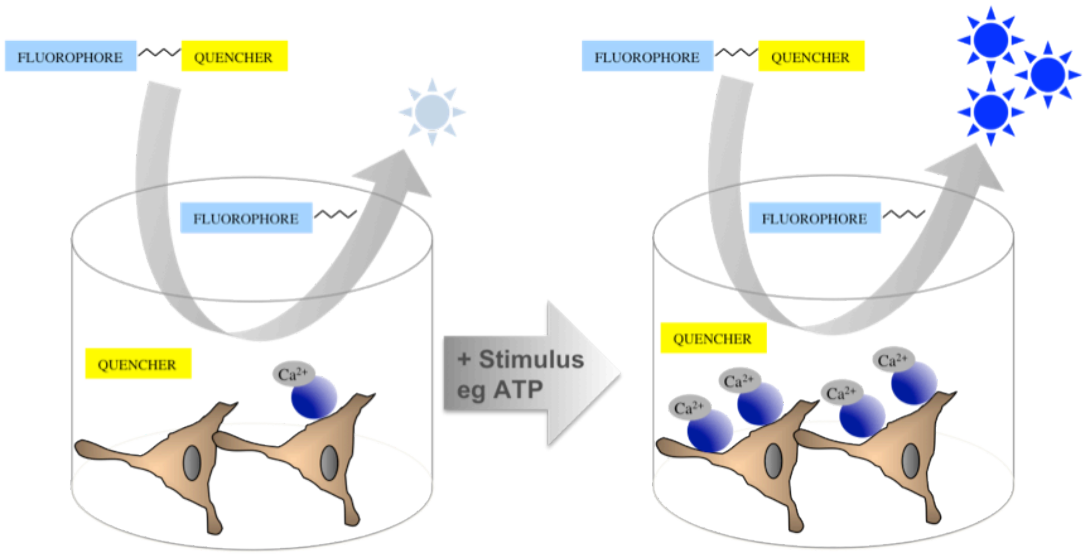

Fig. 3.11 Model of the cell-based assay to detect extracellular TG2 activity. Cells grown in the 96-well plate express low level of extracellular TG2 or surface TG2. This TG2 activity is latent even in the presence of high extracellular Ca^{2+} concentrations presumably due to enzyme oxidation and endocytosis. Upon addition of an appropriate stimulus (e.g. ATP) TG2 is externalized and activated on the cell surface. TG2 catalytic activity can potentially be monitored in real time using a fluorescent model substrate. This cell-based method would enable to study potentially active TG2 release and measure change in activity on the cell surface, in the ECM or in the conditioned medium simultaneously. TG2 is represented as blue sphere.

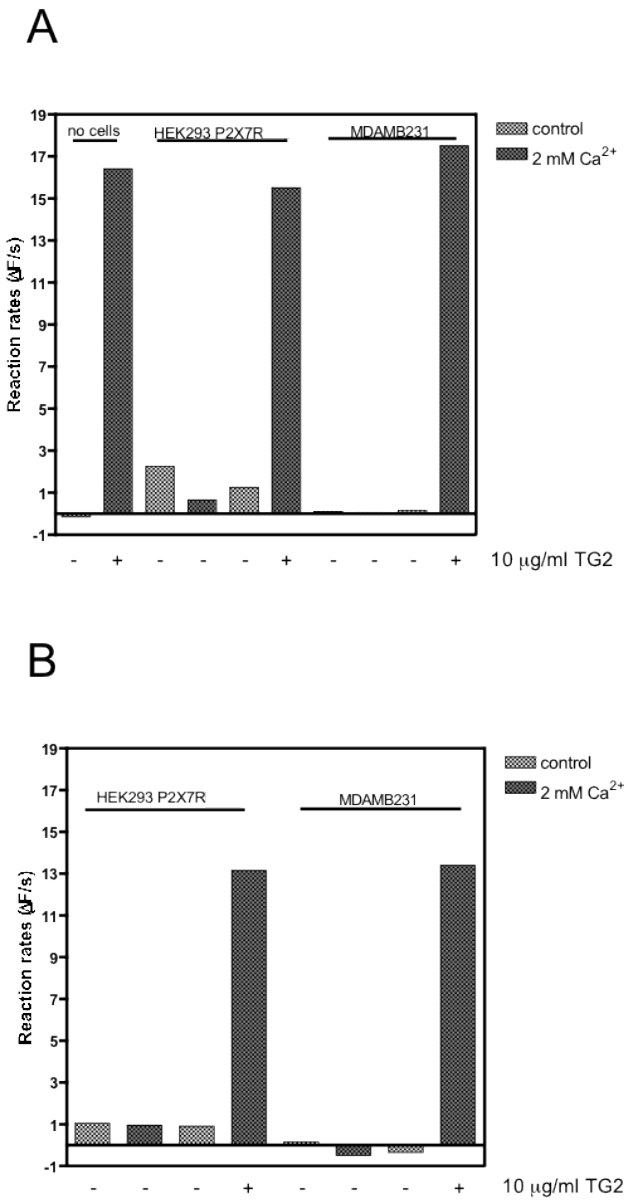

Fig. 3.12 Measurements of TG2 activity in the presence of human cells using the isopeptidase assay. A, B: The reaction was carried out with or without the presence of MDAMB231 cells or HEK293 stably expressing P2X7R. Where indicated, 10 μg/ml recombinant TG2 was added to the wells. Substrate cleavage was induced by 2 mM $CaCl_2$ injection and as the control 2 mM $MgCl_2$ was used. Baseline fluorescence was subtracted and the reaction rates derived by linear regression are shown as bars. Reaction rates from two independent experiments are given in the separate panels.

It was not clear whether insufficient sensitivity of the assay or the absence of active TG2 in the extracellular environment was responsible for the lack of signal. Therefore, Abz-APE(γ-cad-Dnp)QEA substrate cleavage was assessed after lysing the cells with Triton-X-100. The assay was performed as previously in the presence of HEK293 P2X7R and MDA-MB-231 cells and recombinant TG2 was added to one group of samples to detect potential interference with the assay. When the cell membrane of either cell types was permeabilized with Triton-X-100, the fluorescent signal increased rapidly but this process was calcium independent (Fig. 3.13A). The apparent substrate cleavage was greater in the wells where lysed MDA-MB-231 cells were present. Given that hydrolysis was Ca^{2+} independent, the reaction likely was the result of non-specific proteolytic processing of the fluorescent peptide. However, it may also possible that sufficient Ca^{2+} was released from intracellular stores to activate TG2. Therefore, the specific TG2 blocking inhibitory peptide Boc-DON-QIVMeEs (B003 inhibitor) that alkylates the active site cysteine was chosen to block TG2 activity, which was potentially released from MDA-MB-231 cells. The inhibitor concentration that can fully block recombinant TG2 activity was assessed. The addition of 1 μM of the B003 inhibitor completely prevented the cleavage of Abz-APE(γ-cad-Dnp)QEA substrate by 10 μg/ml TG2 (Fig. 3.13B). The B003 inhibitor was then used to determine to what extend intracellular TG2 released upon MDA-MB-231 permeabilization participates in the cleavage of the fluorescent substrate. Thus, 5 μM or 25 μM TG2 inhibitor was added to permeabilized MDA-MB-231 cells and only a small change in reaction rates was observed, indicating that proteolysis and not isopeptidase activity is principally responsible for the signal.

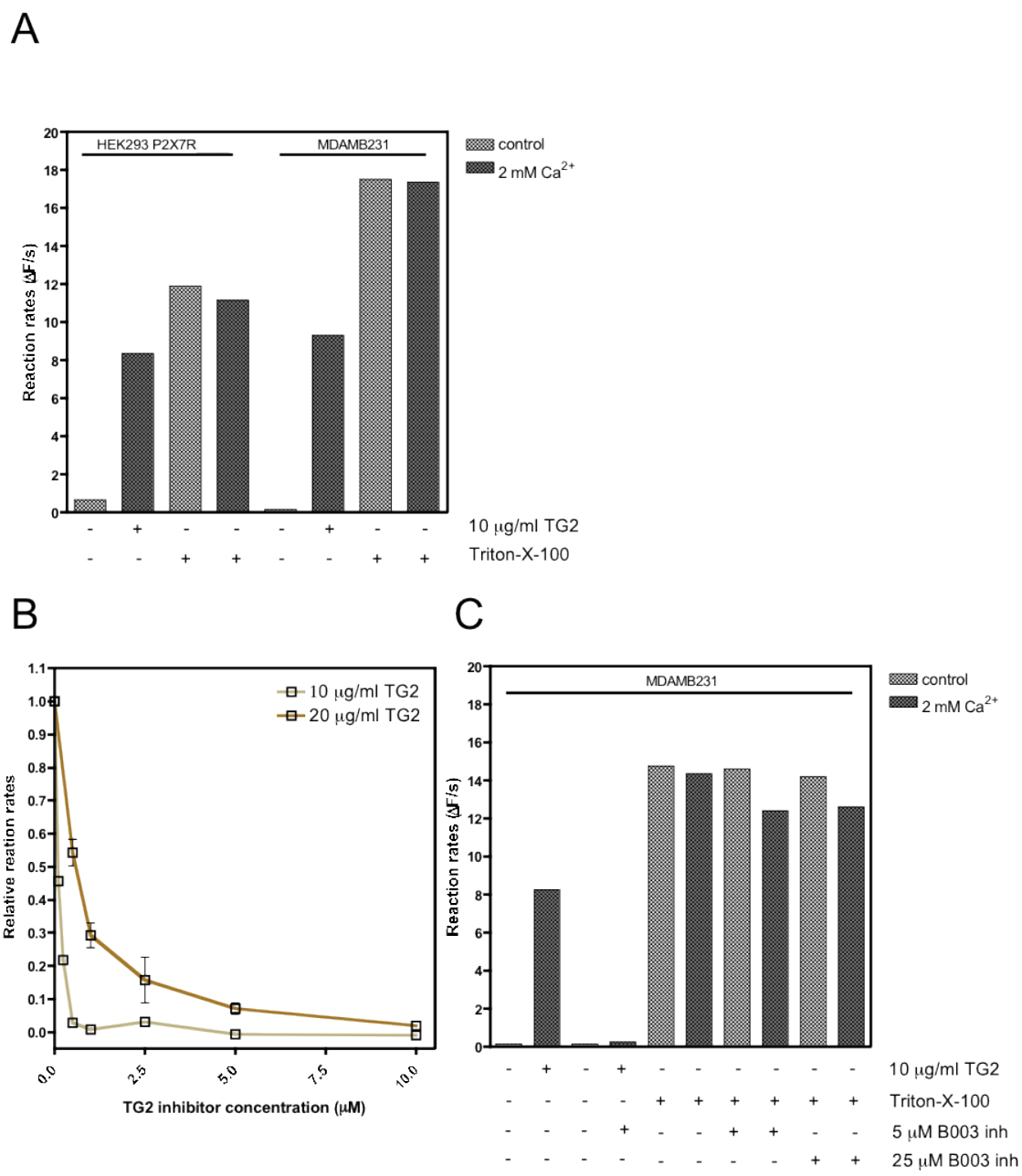

Fig. 3.13 TG2 enzymatic activity before and after cell lysis measured with the isopeptidase assay. **A:** The reaction was carried out in the presence or absence of MDAMB231 cells or HEK293 cells stably expressing P2X7R. In order to lyse the cells, the reaction was also performed in Assay Buffer containing 0.1% Triton-X-100. Where indicated, 10 µg/ml recombinant TG2 was added to the wells. Substrate cleavage was induced by 2 mM $CaCl_2$ injection and as control 2 mM $MgCl_2$ was used. Baseline fluorescence was subtracted and the reaction rates derived by linear regression and shown as bars. Data shows one representative of two independent experiments. **B:** Isopeptidase activity of TG2 was measured in the presence of various concentrations of TG2 inhibitor (Boc-DON-QIVMeEs, B003 inh). Fluorescence in the absence of enzyme activation (no Ca^{2+}) was subtracted and reaction rates were derived by linear regression. Error bars represent SD of mean of two independent experiments. **C:** 10 µg/ml recombinant TG2 was added to MDAMB231 cells and TG2 activity was measured in the presence of intact cell monolayer and upon cell lysis. Where indicated, 5 µM or 25 µM TG2 inhibitor (B003) was added to the reaction. Substrate cleavage was induced by 2 mM $CaCl_2$ injection and as the control 2 mM $MgCl_2$ was used. Baseline fluorescence was subtracted and the reaction rates derived by linear regression and shown as bars. Data of one representative experiment is shown.

3.3 Discussion

There are not many sensitive tools available to measure extracellular TG2 activity *in situ*. Different research groups are trying to develop an assay to assess TG2 activity in an intact biological system that will not disrupt cells leading to activation of possibly mostly latent TG2. Established and most widely used methods to study transglutaminase activity are based on the transamidation reaction. They are based on modified amine donor substrates such as radiolabelled putrescine incorporation into N,N-dimethylcaseine (Lorand et al. 1976; Dadabay and Pike 1987) or incorporation of dansylated cadaverine into casein (Murtaugh et al. 1984) or fibronectin (Aeschlimann and Paulsson 1991). However, those techniques require protein precipitation from cells or incubation of cells with the substrate followed by cell fixation for visualization. A number of novel techniques have recently been developed based on conformational changes of TG2 and its allosteric regulation *in situ*, trying to visualize these changes as a proxy for activity. One of the interesting examples are the "clickable" inhibitors for TG2 that can only bind the active, open conformation of the enzyme and this have been successfully used in mammalian cells and tissue experiments (Dafik and Khosla 2011). Another interesting technique is the lately described FLIM-FRET biosensor, which has mCerulean and eYFP pair attached to the N- and C- terminus of TG2. This biosensor allows to quantify changes in TG2 conformation in live cells (Caron et al. 2012). Clearly, there is a need for novel approaches to investigate TG2 activation in intact cells. The aim of this study was to evaluate whether the fluorescent substrate Abz-APE(γ-cad-Dnp)QEA was able to detect TG2 activity in real time in the absence of sample processing, in order to potentially visualize local fluctuations in activity in live cells.

It was essential to use a TG2 substrate that closely mimics the naturally occurring peptides in cartilage in order to further investigate TG2 catalytic activity. The substrate that was used to establish the assay is derived from the natural substrate for TG2, osteonectin (BM-40, SPARC). Osteonectin is a protein expressed during chondrocyte maturation and is one of the substrates for TG2 in cartilage (Aeschlimann et al. 1995). The N-terminal domain I of osteonectin was identified as a major glutamine donor substrate for TG2-mediated reactions *in* vivo. TG2 is able to modify both Q^3 and Q^4 glutamine residues in the APQQEAL sequence of

osteonectin. Q^3 and Q^4 glutamine residues are conserved in higher vertebrates, which suggests that there is a specific function of those amine acceptor sites in the cartilaginous tissue (Hohenadl et al. 1995). TG2 can catalyze isopeptide bond hydrolysis in the presence of excess of a cross-linked substrate (Parameswaran et al. 1997). In agreement with that, the established assay measures hydrolysis rate of the Abz-APE(γ-cad-Dnp)QEA substrate as an effect of acyl-enzyme intermediate formation and separation of fluorescent Abz from quenching Dnp moiety. Addition of the Abz-APE(γ-cad-Dnp)QEA to the buffer containing TG2 and Ca^{2+} results in the time-dependent increase of the fluorescence emission coming from the Abz group thus confirming that the substrate is actively converted by TG2.

A number of parameters were established to improve assay sensitivity and mimic the reaction conditions likely to occur in a physiological context. TG2 enzymatic activity is dependent on the presence of Ca^{2+} ions that can promote the open structure and allows the active site of the enzyme to react with available amine acceptor substrate (Aeschlimann and Thomazy 2000; Pinkas et al. 2007; Róbert Király et al. 2011). Similarly, TG2 isopeptidase cleavage of the Abz-APE(γ-cad-Dnp)QEA substrate is only initiated when sufficient Ca^{2+} is available but enzyme is inactive in the presence of Mg^{2+}, which is in agreement with the literature (Folk and Chung 1973; Róbert Király et al. 2011). TG2 is highly active at physiological Ca^{2+} concentrations (~2 mM) however increasing the concentrations of Ca^{2+} to 10 mM or even 50 mM enhance the isopeptidase cleavage rate, presumably due to saturation of Ca^{2+} binding sites. As those conditions do not represent the physiological situation and because it was previously reported that activation of TG2 occurs at > 200 μM Ca^{2+} (Pinkas et al. 2007; Kurta et al. 2009; Schaertl et al. 2010) increasing Ca^{2+} levels were not considered as a relevant option to improve assay sensitivity. Automated injection of Ca^{2+} for enzyme activation, combined with the ability to continuously measure linear increase of fluorescence intensity over a considerable time period enables the acquisition of kinetic data. The isopeptidase assay was proven to be a sensitive and highly specific method for measuring recombinant TG2 activity with approx. 1 μg/ml detection limit. The addition of 1 μM Boc-DON-QIVMeEs inhibitor to the reaction mixture produced complete inhibition of TG2 activity at 10 μg/ml. This inhibitor has been reported to block TG2 activity with high potency (Schaertl et al. 2010) and was successfully inhibiting TG2-dependent

substrate conversion even when activity of recombinant TG2 was measured in the presence of intact cells.

The isopeptidase assay with recombinant TG2 was useful to measure different factors that can influence TG2 activity such as oxidation, ionic strength or pH before conducting experiments in cell systems. Oxidative inactivation is an independent mechanism that does not affect C^{277} in the active site but it sterically co-strains the enzyme and thereby prevents its activation (Stamnaes et al. 2010). Recent evidence provided by Stamnaes and colleagues indicates that handling of TG2 in an oxidizing enviroment or treatment with oxidizing agents results in disulfide bond formation and consequently leads to enzyme deactivation but treatment with reducing agents such as DTT, can restore its activity. This was observed for the established isopeptidase cleavage reaction, which was significantly improved in the presence of reducing agent. The existence of redox sensitive cysteine bonds is thought to regulate the conformation of TG2 and ultimately controls TG2 activity in the extracellular environment. Hence, adding DTT to the reaction allows for maximal enzyme activity and improved assay reproducibility. TG2 was most active in low ionic strength buffer and higher concentrations of salt impaired its activity, suggesting that ionic interactions are relevant to catalysis. The hydrolysis of the substrate was strongly pH-dependent and optimal at pH 6.5. This is in agreement with the result obtained for cleavage of a similar Dns-labelled quenched substrate hydrolysed by human TG2 purified from blood cells (Parameswaran et al. 1997). There were no significant differences between reaction rates at different pH in the presence or absence of glycine methylester, which suggested that both aminolysis and hydrolysis are similarly fast. This is in agreement with the data collected by Folk and Cole where they show that pH is affecting both deamidated and transamidated product formation and that catalysis reaches a peak at pH 6 (Folk and Cole 1966). The pH will affect reactive residues involved in catalysis and change the protonation state of the amine substrate (Gross et al. 1977; Leblanc et al. 2001). HPLC analysis showed that transamidation did indeed take place and that ratio of transamidated to deamidated product depends on the nature of the amine structure and its concentration used but not the acid dissociation constant (pKa) of the amino group as such (Leblanc et al. 2001). Taken together these data show that the measurements are highly pH-dependent and therefore the tight control of reaction pH is paramount.

The plate format is ideal for investigating the effect of potential regulators or inhibitors on TG2 catalysis. Beside some of them being ligands for purinergic receptors, GTP and other nucleotides are well-characterized allosteric regulators of TG2 (Liu et al. 2002; Han et al. 2010). The IC_{50} concentrations of 2.9 μM, 3.6 μM, and ~1 mM obtained for GTP, GTPγS and ATP are in good agreement with data in the literature (Parameswaran et al. 1997). As expected, the inhibitory effect of GTP on TG2 activity was strongly dependent on the amount of Ca^{2+} present (Parameswaran et al. 1997; Mhaouty-Kodja 2004; Schaertl et al. 2010). Therefore, the IC_{50} concentration is the binding constant for GTP as this was derived in the presence of Ca^{2+}. This method was successfully used to study the allosteric regulation of a novel member of TG family – TG6 – by nucleotides (Thomas et al. 2013) (publication in Appendix 3). For this project it was important to compare TG2 activity in the presence of nucleotides in order to assess at what concentration of ATP and BzATP in the presence of 2 mM Ca^{2+} affect its activity. High ATP concentration (>1 mM) is crucial for P2X7R activation on the cell surface (Di Virgilio et al. 2001; Coddou et al. 2011). However, at 1 mM ATP half-maximal inhibition of TG2 activity was observed. As BzATP is a more potent P2X7R agonist, the concentration needed for P2X7R activation is lower (>50 μM) (North 2002; Mackenzie et al. 2005). Therefore, 100 μM BzATP can be used in experiments in order to fully activate the P2X7R receptor without blocking surface TG2 activity.

To summarize, in this chapter I have presented the experimental conditions for determination of TG2 isopeptidase activity using the fluorescent model substrate Abz-APE(γ-cad-Dnp)QEA and plate reader format (see also Appendix 2 for the Application Note for BMG LABTECH). The assay is rapid, direct and sensitive when purified TG2 is used. Small sample size and plate format make the assay cost-effective and adaptable to high-throughput analysis. The usage of the isopeptidase activity assay for cell-based studies is promising. The kinetics of the reaction was not changed when cells were present and no cell autofluorescence that would alter the baseline fluorescence was observed. However, a number of substrate modifications need to be introduced for applications beyond *in vitro* studies. Firstly, the backbone of the peptide should be further modified to avoid spontaneous Abz-APE(γ-cad-Dnp)QEA substrate cleavage by proteases when the cell membrane becomes permeable. Addition of a TG2 specific inhibitor only partially reduced substrate

conversion, and the majority of the reaction was Ca^{2+} independent. Future analysis of the cleavage products that are formed upon cell lysis are necessary in order to determine whether the products are formed due to TG2 activity. Secondly, the detection limit for measuring small changes in TG2 activity on the cell surface/in conditioned medium upon stimulation with P2X7R agonists lacked detectable activity. Replacing the Abz group on the substrate backbone for a more powerful fluorophore would likely improve sensitivity. Once the specificity and sensitivity of the assay has been addressed, the isopeptidase assay potentially could serve as a powerful tool for investigating changes in TG2 activity in live cells.

Chapter 4 TG2 upregulation and release in different cell types

4.1. Introduction

The overarching aim of the project was to investigate whether increased expression and aberrant release and activation of TG2 leads to protein modifications not normally present in extracellular matrix components. Their formation may be an indicator of compromised tissue integrity, occurring as a consequence of abnormal joint loading or in association with the inflammatory processes. In order to identify potential novel modifications formed in a physiological context, there was a need to identify a cell system that allows for induction of TG2 externalization in a defined way, which is amenable to manipulation. TG2 release can be linked with cell damage (Upchurch et al. 1987). However, there is substantial evidence to suggest that TG2 can be actively exported by cells is a context dependent manner (Aeschlimann et al. 1995; Raghunath et al. 1999). This pathway and its regulation remain enigmatic. Given the well established link to inflammation (Kim 2006), we decided to test whether secretion of TG2 is regulated by P2X7R in analogy to interleukin-1β (IL-1β)/interleukin-18 processing and release from activated monocytes/macrophages.

IL-1β belongs to a group of soluble signaling proteins that lack a signal peptide and are secreted from the cells through a non-conventional pathway (Ferrari et al. 2006; Dubyak 2012). There is some overlap between IL-1β and TG2 release from cells with regards to biological context. Therefore, it serves as a good model molecule to study alternative secretion of proteins as TG2 externalization might occur after applying similar external signals. IL-1β is an important proinflammatory cytokine released mainly by blood monocytes and tissue macrophages (Hogquist et al. 1991; Wewers et al. 1997; Mehta et al. 2001; C Andrei et al. 2004; Qu et al. 2007), dendritic cells (Pizzirani et al. 2007) or microglia (Bianco et al. 2005). During inflammation IL-1β plays a major role in regulation of important mediators: it induces synthesis of cyclooxygenase type 2, phospholipase A, nitiric oxide and adhesion molecules which can lead to systemic fever, pain and promote infiltration of inflammatory cells into the affected tissue (Dinarello 2009). There are two splice variants of IL-1 described: IL-1α and IL-1β (Singer et al. 1988). IL-1β can be found in the cytosol (Stevenson et al. 1992), where it is synthesized on free ribosomes

(Thornberry et al. 1992) and translated into a ~31-kDa pro-protein that is proteolytically cleaved by caspase-1 to give the 17 kDa active form (Mosley et al. 1987). Proteolytic processing of pro-IL-1β by caspase-1 occurs upon assembly of the multiprotein scaffold called the "inflammasome" (Rathinam et al. 2012). This complex has been suggested to be a crucial element in autoimmune and rheumatic diseases (Martinon et al. 2009). Proteolytic cleavage is necessary for IL-1β to express biological activity and effectively bind to the IL-1 receptor (Dinarello 2009). Caspase-1 is a serine protease that is able to proteolytically cleave also other cytokine precursors of the same family: IL-1α, Il-18, Il-33 and Il-1F7. In order to induce IL-1β release from cells, two distinct stimuli need to be provided: 1) an inflammatory signal such as lipopolysaccharide (LPS) (activates Toll-like receptor signaling) that leads to pro-IL-1β and pro-caspase-1 synthesis and their accumulation in the cytosol; 2) exogenous ATP that triggers ion channel-mediated K^+ efflux followed by release of mature active IL-1β. While passive IL-1β release can occur, the phenomenon of ATP-induced IL-1β release is an active and rapid process critical to inflammatory responses (Rathinam et al. 2012). Non-classical secretion of IL-1β is mediated by activation of the purinergic receptor (P2X7R) with high concentrations of extracellular ATP (Ferrari et al. 2006). Once ATP is released from injured tissue/cells it can act as a danger signal amplification system and spread the alarm within the local milieu through paracrine signaling (Grol et al. 2013). Therefore, P2X7R was considered as a potential upstream signaling receptor involved in TG2 secretion.

As TG2 may be externalized by various cell types in different ways, or its localization upon release depends on the cell type (Iismaa et al. 2009), there was a need to explore cell systems, other than connective tissue cells, in which TG2 release is likely to depend on ECM deposition. In order to study actively controlled TG2 release by cells, three different cell models were chosen for investigation. This was based on the evidence supporting TG2 release by cells and expression of P2X7R. First, the monocytic leukemia cells (THP-1) that mimic the behaviour of monocytes/macrophages (Tsuchiya et al. 1980) and second, the human breast cancer cells MDA-MB-231 that constitutively secrete TG2 into the medium and to some extend reflect the epithelial cell responses (Antonyak et al. 2011). The third model was fibroblast cell line, HCA2 cells, to represent connective tissue cells (Stephens et

al. 2004) but this was subsequently abandoned as those cells did not revealed P2X7R expression/activation.

The aims of the chapter:

1. Investigate if THP-1 cells differentiated into macrophages are able to release IL-1β upon ATP stimulation?
2. Verify whether TG2 can be detected in the conditioned medium of MDA-MB-231 breast cancer cells?
3. Identify whether TG2 release in MDA-MB-231 cells relate to constitutive P2X7R signaling?

4.2 Results

4.2.1 TG2 upregulation during THP-1 monocyte differentiation into macrophage-like cells

A monocyte/macrophage cell model was chosen in order to establish an assay for IL-1β release in response to P2X7R activation, in which potential TG2 secretion in a similar way could be monitored. The human leukemia cells THP-1 express distinct monocytic markers (Tsuchiya et al. 1980) and are fully competent in P2X7R-mediated IL-1β secretion after LPS priming (Mackenzie et al. 2001). However, in those cells TG2 is not detectable but it is possible to substantially increase TG2 levels and activity by inducing monocyte to macrophage differentiation (Mehta and Lopez-Berestein 1986). Therefore, three different differentiation factors were applied in order to upregulate TG2 expression: interleukin-6 (IL-6), 12-O-tetradecanoylphorbol-13-acetate (TPA) and *all-trans* retinoic acid (ATRA). The pro-inflammatory cytokine IL-6 was chosen as IL-6 induced differentiation was shown to effectively increase TG2 activity upon its transcription in human hepatoblastoma HepG2 cells in a time- and dose- dependent manner (Suto et al. 1993). Also, ATRA- and TPA- dependent differentiation in THP-1 cells has been proven to be accompanied by elevated TG2 expression (Mehta and Lopez-Berestein 1986). These three mediators are known to act through distinct signaling pathways.

The aim of the experiment was to optimize the conditions, such that upregulation of TG2 and pro-IL-1β synthesis in cells is simultaneously observed. THP-1 cells were grown with 10% FBS in the presence of IL-6 (0.8 nM), TPA (50 ng/ml) or ATRA (1 μM). Where indicated, cells were simultaneously incubated with LPS for 48 or 72 hours to upregulate pro-IL-1β expression, the processing and release could be monitored by ATP stimulation. Changes in cell morphology were examined during the differentiation process (Fig. 4.1A). THP-1 monocytes are rounded cells with a smooth surface that grow in suspension (see also Fig. 4.2). Upon differentiation they become adherent, have a more granular appearance and spread/migrate on the plastic surface. Simultaneous priming of cells with LPS (0.1 μg/ml) seemed to promote the process of differentiation even further as cells appeared to be more spread and activated. Among the three differentiation factors,

TPA had the fasted effect and strongest capacity to differentiate THP-1 cells into adherent macrophage-like cells (Fig. 4.1A). Cells that were treated with TPA significantly increased their size and changed morphology when compared to control or cells treated with other differentiation factors. In the case of differentiation with ATRA, some of the treated cells remained rounded but most of them started to attach and spread, which indicated monocyte to macrophage transition (Fig. 4.1A). Combination of IL-6 and LPS altered cell morphology only to some extend and IL-6 stimulation alone had little effect on THP-1 cell differentiation over the 72h time period (Fig. 4.1A).

Cell extracts from differentiated THP-1 cells were prepared in order to investigate the expression of TG2 by Western blotting. Consistent with the previous findings by Mehta and Lopez-Berestein (1986), the TG2 was not detectable in undifferentiated THP-1 cells (Fig. 4.1B). However, in my experiment after differentiation into macrophage-like cells, TG2 expression was significantly upregulated with selected agents as was anticipated (Fig. 4.1B). The calculated molecular mass of TG2 is ~77 kDa but the migration of the band in SDS-PAGE is approx. corresponding to 80-85 kDa when compared with the protein marker, which is consistent with the literature (Hadjivassiliou et al. 2008). TPA and ATRA alone were able to markedly upregulate TG2 expression and this was visible after both, 48h and 72h of differentiation (Fig. 4.1B). TG2 expression was even more potentiated in the presence of simultaneous priming with LPS. Note, the absence of the TG2 band after 48h simultaneous stimulation of cells with ATRA and LPS occurred only in this particular experiment. An increase in TG2 expression was only observed in IL-6 differentiated cells after 48h in the presence of LPS but TG2 could not be detected any more at 72h, which was consistent between replicate experiments (Fig. 4.1B). For further experiments, ATRA was selected for THP-1 differentiation as it effectively upregulated TG2 expression without causing enhanced release of IL-1β in the absence of ATP stimulation from LPS-primed cells as was the case with TPA (data not shown). ATRA was also more effective than IL-6 to induce the anticipated changes in cell morphology associated with cell differentiation.

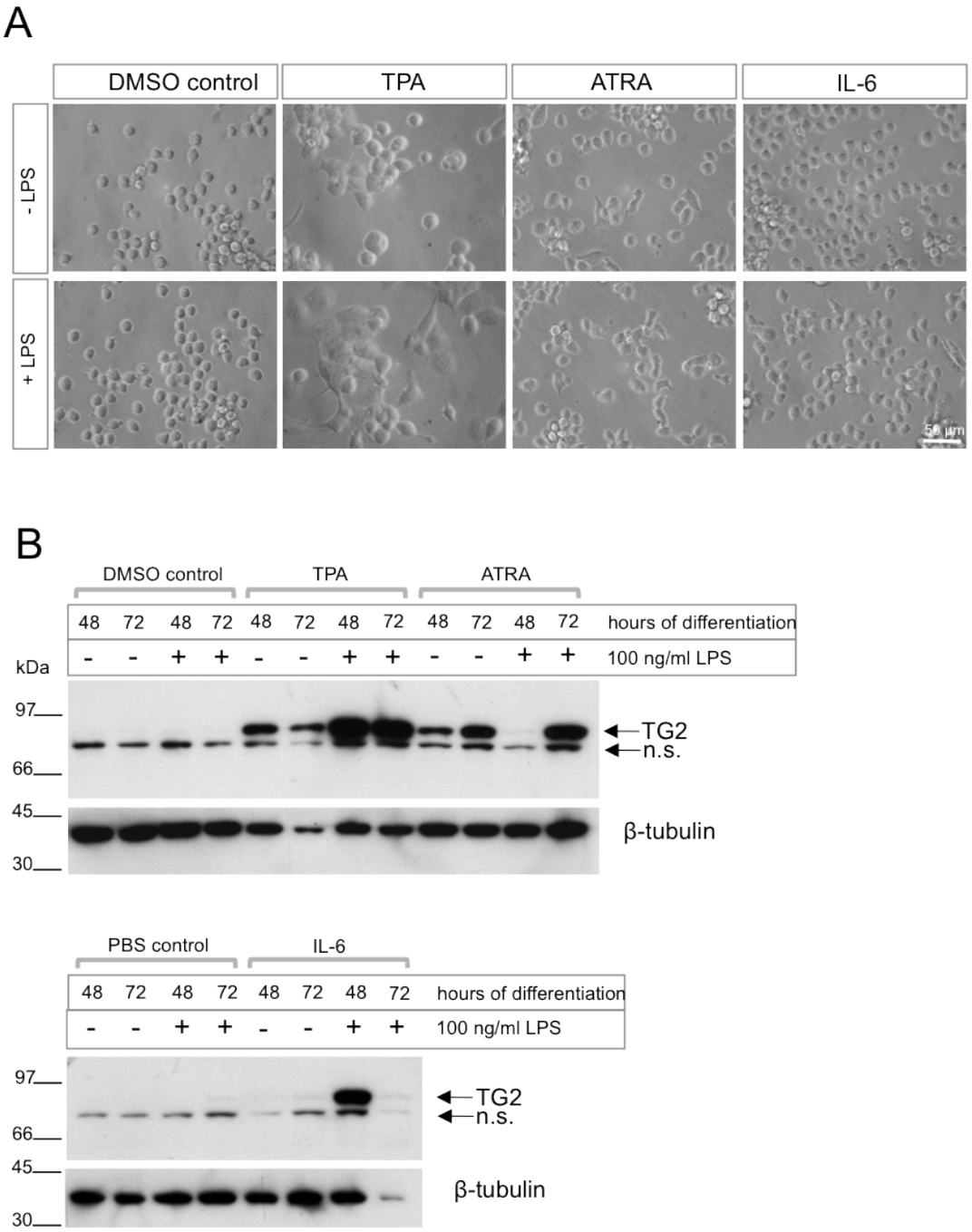

Fig. 4.1 TG2 upregulation during differentiation of THP-1 cells into macrophage-like cells. A: THP-1 cells were grown for 72h in the presence of 0.8 nM IL-6, 50 ng/ml TPA or 1 µM a*ll-trans* retinoic acid (ATRA). DMSO (0.1%) was used as a carrier control. However, IL-6 was made up in PBS. Where indicated, cells were simultaneously stimulated with 0.1 µg/ml LPS. Phase contrast pictures show gross morphological appearance of cells at the end of the differentiation process. **B:** THP-1 cells were lysed after 48 or 72h of differentiation and 10 µg of protein was loaded per lane of a 4-20% SDS polyacrylamide gel under reducing conditions and proteins were separated followed by Western blotting. Nitrocellulose membrane was stained with anti-TG2 antibodies. β-tubulin antibody staining was used to estimate the loading. The identity of the band labeled "n.s." is unclear and might be non-specific. The migration of the molecular size marker is indicated on the left.

4.2.2 Establishing the assay for analysis of ATP-induced IL-1β release from LPS-primed THP-1 cells

4.2.2.1 Optimization of THP-1 cell differentiation with ATRA

In order to optimize conditions for cell handling such as cell washing and buffer exchange necessary for ATP stimulation, THP-1 cells were grown on different substrates for 3 days to determine which surface effectively immobilized THP-1 cells without causing changes in their morphology associated with cell activation. Cells were seeded on tissue culture plastic, the glass or surface pre-coated with collagen type I or fibronectin or poly-L-lysine (Fig. 4.2A). Culture of THP-1 cells on glass, collagen type I and fibronectin induced cell spreading and activation. The plastic and poly-L-lysine coated surfaces were the best substrates for THP-1 cell growth as they did not induce cell activation (Fig. 4.2A). After culture for 3 days on the different surfaces, the cells were washed and the PSS buffer required for subsequent experimental steps was added in order to see how well the cells attached to each substrate (Fig. 4.2B). As poly-L-lysine was the only substratum that did not induce cell activation while at the same preventing cells from being lost during cell washing, this substratum was selected for future experiments (Fig. 4.2B).

To verify that the best conditions for ATP stimulation of differentiated THP-1 cells had been selected, two different experimental protocols for cell priming were performed in order to induce TG2 and pro-IL-1β synthesis and compared: 1) 48h differentiation of cells with ATRA in the presence of LPS performed on cells attached to poly-L-lysine and 2) 48h differentiation with ATRA followed by 24h LPS priming on cells grown on plastic. This direct comparison is the result of a series of optimization experiments that were conducted.

4.2.2.2 ATRA-mediated THP-1 cell differentiation simultaneous with LPS priming

THP-1 cells were grown on glass coverslips coated with poly-L-lysine and were stimulated for 48h in the absence or presence of ATRA (1 μM) and LPS (0.1 μg/ml)

simultaneously. After 48h, conditioned medium was gently harvested and the concentration of IL-1β was measured by capture ELISA (Fig. 4.2C). Surprisingly, THP-1 monocytes (DMSO control) and macrophage-like cells (ATRA treated) were able to spontaneously release a low amount of IL-1β into the medium upon LPS treatment. This markedly upregulated extracellular IL-1β levels to approx. 20 pg/ml released within an hour (Fig. 4.2C). It is likely that this represents a passive release of non-processed pro-IL-1β as the antibodies used for ELISA can recognize both the pro-and mature form (data not shown). This unstimulated release of IL-1β seemed to be slightly upregulated in cells differentiated into macrophage-like cells (Fig. 4.2C). The same cells were now used to perform P2X7R stimulation with ATP. After gentle washing with PBS, PSS buffer -/+ 1 mM ATP was added to each well. Cells were stimulated in the incubator for 30 min or 1 hour and the conditioned medium was used for quantification of the cytokine. The result showed that the cells even without ATP stimulation can spontaneously release a substantial amount of cytokine under this conditions (Fig. 4.2D). ATP treatment of cells resulted in differences in the kinetics of IL-1β release from ATRA differentiated cells as compared to DMSO control cells (Fig. 4.2D). Whereas the addition of ATP to non-differentiated cells increased IL-1β secretion approx. 2-fold after 30 and 60 min, the differentiated cells showed more variable and lower secretion of IL-1β. It appeared that prolonged treatment of cells with LPS might lead to spontaneous IL-1β secretion and that this effect was enhanced in ATRA differentiated cells.

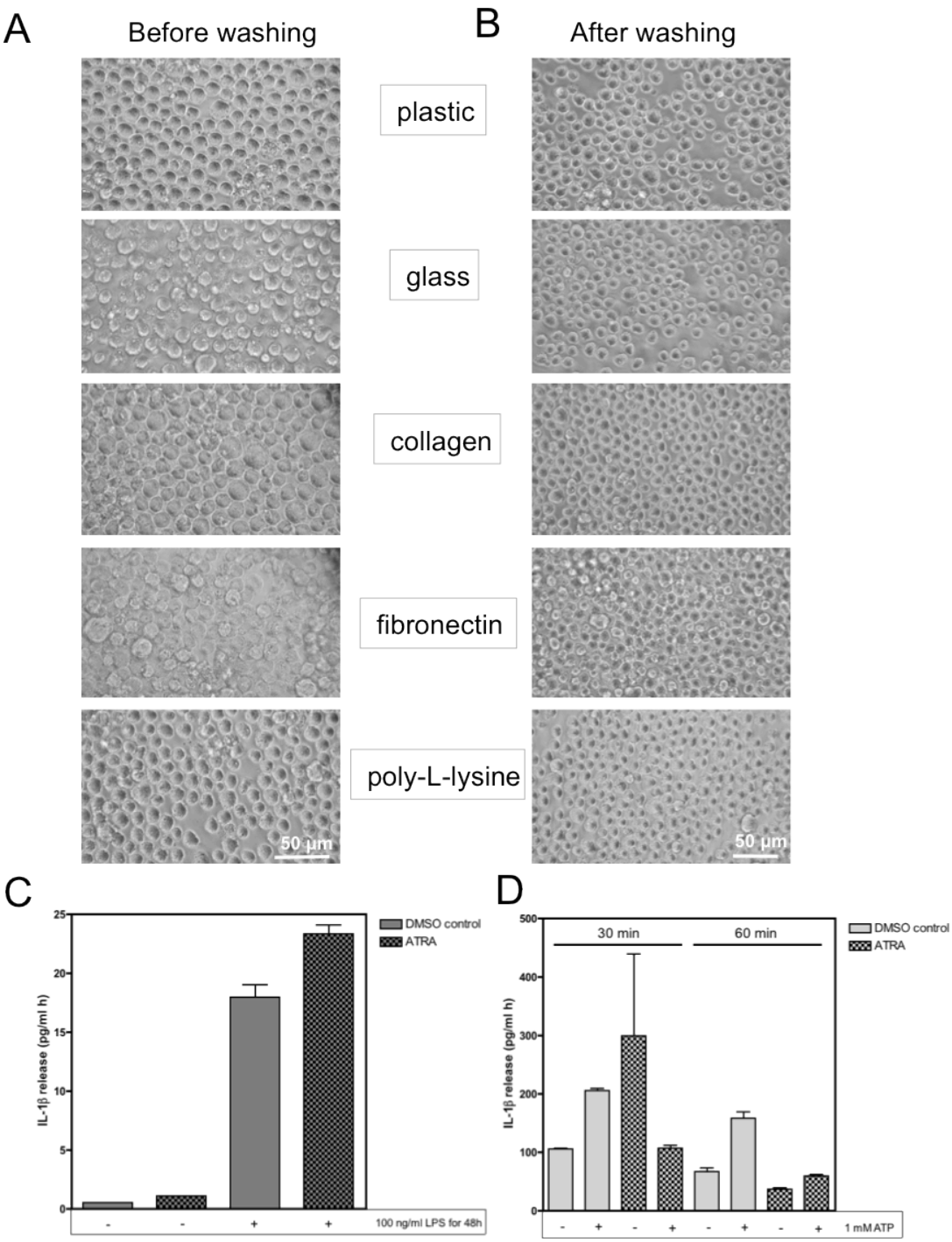

Fig. 4.2 Optimizing conditions for THP-1 cell stimulation. A, B: THP-1 cells were suspended in RPMI medium containing 10% FBS. Cells were seeded in 6-well plates on different surfaces: plastic, glass or glass coated with collagen type I (44 µg/ml), fibronectin (40 µg/ml) or poly-L-lysine (40 µg/ml). Cells were left to grow on respective surfaces for 3 days and after that time phase contrast images were taken (**A**). Cells that were growing on different substrates were washed with PBS and then incubated in PSS buffer. Cell attachment on different substrates was investigated. Phase contrast images on the right show cell monolayer after a washing step (**B**). **C:** THP-1 cells were seeded in 24-well plates on poly-L-lysine (40 µg/ml). Cells were differentiated with ATRA (1 µM) for 48h in the presence of LPS (0.1 µg/ml). After 48h of cell differentiation, the conditioned media were collected and the release of IL-1β was measured by capture ELISA. The data show values from one experiment with four experimental repeats in ELISA plate (mean ± SEM). **D:** After 48h, differentiated cells were collected, washed and stimulated with 1 mM ATP in PSS for 30 and 60 min or were incubated in PSS without agonist. The release of IL-1β into the cell supernatant during cell stimulation was measured by capture ELISA. The data show values from one experiment with duplicates in ELISA plate (mean ± SEM).

4.2.2.3 THP-1 cell differentiation with ATRA followed by LPS priming

In the second approach, THP-1 cells were grown for 48h on the plastic surface in the absence or presence of ATRA (1 μM) and then primed for another 24h with or without LPS (0.1 μg/ml). After 48 and 72h, the cell supernatant was used to measure IL-1β concentration by ELISA. Cells were lysed in order to confirm TG2 and IL-1β upregulation at different stages of cell differentiation. Detection of immunoreactive species of the cell extract showed that ATRA can effectively upregulate TG2 expression after 48 and 72h and when acting alone, does not stimulate synthesis of pro-IL-1β (Fig. 4.3A). ELISA analysis of conditioned medium showed that ATRA-mediated differentiation elevated IL-1β secretion from LPS treated monocytes (20 pg/ml per hour) compared with the DMSO control (8 pg/ml per hour) (Fig. 4.3B). The rate of IL-1β release at baseline was similar to that observed in the previous experiment (Fig. 4.2C). After 72h, the cells were transferred gently from the 24-well plate into tubes and collected by centrifugation. For P2X7R stimulation, cells were washed with PBS prior to re-suspending in PSS buffer -/+ 1 mM ATP and after transferring to a 24-well plate, incubated for 30 min or 1 hour at 37 ˚C/5% CO_2. At the end of the experiment, cell supernatant was used for IL-1β quantification by ELISA and the cells were lysed to analyse TG2 levels by Western blotting. It was predicted that the ATP stimulation might lead to TG2 secretion but that this is unlikely to substantially decrease its intracellular concentration in such a short treatment time. Furthermore, even if TG2 was externalized efficiently it may largely remain cell associated as has previously been reported for macrophages (Hodrea et al. 2010) and therefore invisible to this analysis. As expected, the ATP stimulation had no overt effect on cellular TG2 levels as indicated by the fact that the TG2 band remained of the same intensity (Fig. 4.3C). On the other hand, there was a slight reduction in the amount of the intracellular pull of pro-IL-1β after ATP addition in both DMSO treated control cells and ATRA differentiated cells primed with LPS thus suggesting that P2X7R activation lead to pro-IL-1β processing and release in mature form (Fig. 4.3C). In fact, quantification of IL-1β in the conditioned medium confirmed that addition of ATP lead to an increase in the amount of IL-1β being secreted by the cells (Fig. 4.3D). ATRA differentiated cells released more IL-1β

compared to the DMSO control when stimulated with ATP (Fig. 4.3D). However, spontaneous release of IL-1β by ATRA differentiated cells into the PSS was also increased. The difference in cytokine concentration in the supernatant in response to P2X7R receptor activation was more significant after 1 hour of stimulation and this is in agreement with the results from Western blotting on the cell extracts (Fig. 4.3C and D). Examination of cell morphology at the end of the experiment revealed that ATRA differentiated and LPS primed cells were already clustered, spread and activated prior to ATP stimulation, unlike the control ones (Fig. 4.3E). This may explain the high rate of baseline IL-1β secretion and might suggest some endogenous P2X7R activation. The ATP treatment lead to gross morphological changes and potentially some cell death. The original intend was to quantify TG2 activity in real time during ATP stimulation using the isopeptidase assay developed in Chapter 3. However, sensitivity of the substrate to proteolysis prevented this approach.

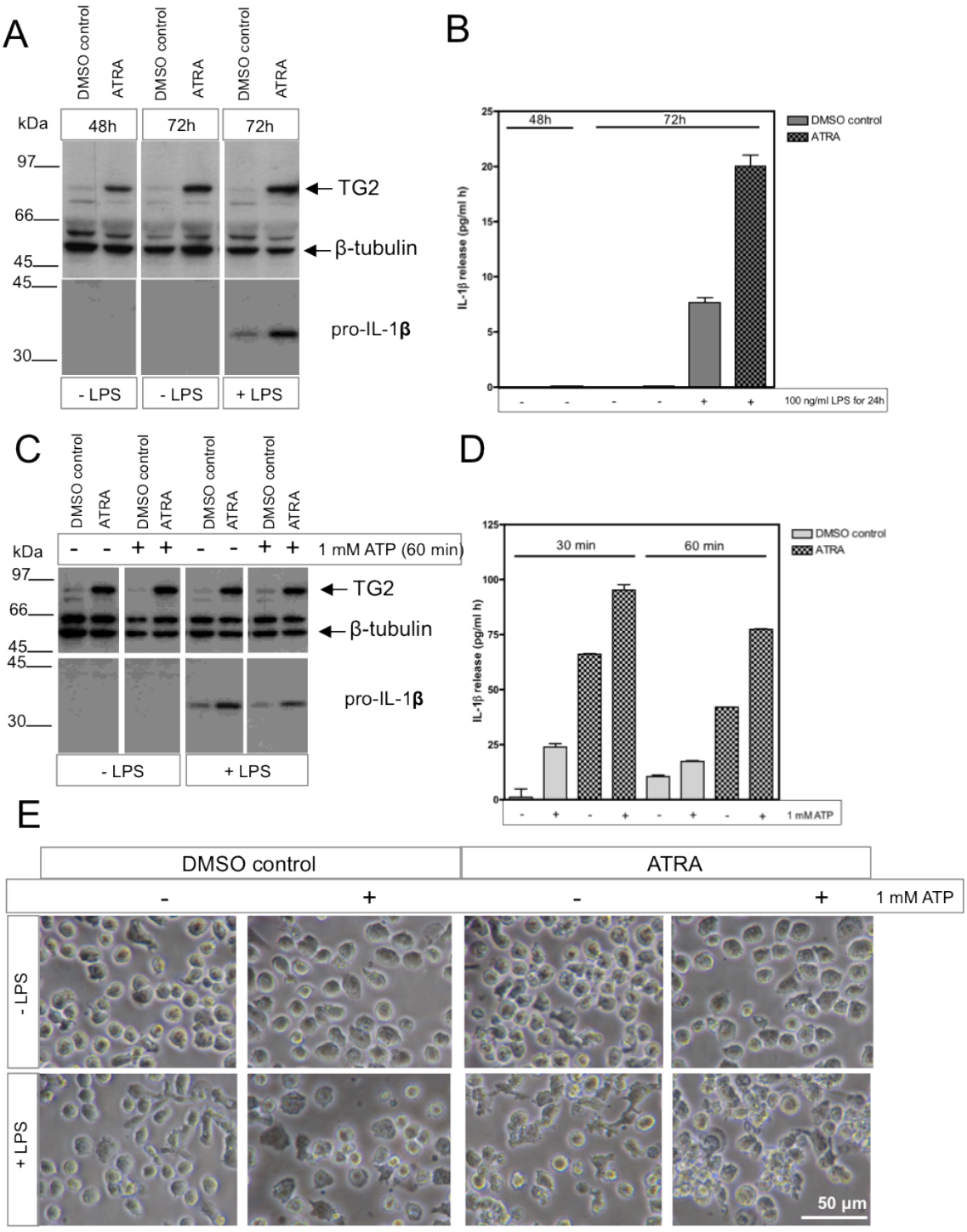

Fig. 4.3 Changes in TG2 expression and IL-1β secretion during THP-1 cell differentiation/ activation. A, B: THP-1 cells were differentiated with ATRA (1 µM) for 48h followed by 24h stimulation with or without LPS (0.1 µg/ml). Cells were lysed after 48h and 72h and 10 µg of protein was processed as previously described and analyzed by Western blotting for TG2 and β-tubulin (antibodies added simuntaneously). The membrane was then re-probed for the presence of pro-IL-1β (**A**). After 48 and 72h of cell differentiation, the conditioned media were collected and the release of IL-1β was measured by capture ELISA. The data show values from one experiment with duplicates in ELISA plate (mean ± SEM) (**B**). **C, D:** After 72h, differentiated cells were collected, washed and stimulated with 1 mM ATP in PSS for 30 or 60 min, or were incubated in PSS without agonist. Cell extracts were prepared as previously described and analyzed by Western blotting for TG2 and β-tubulin (added simuntaneously). The membrane was then re-probed for IL-1β (**C**). The release of IL-1β into the cell supernatant during cell stimulation was measured by capture ELISA. The data show values from one experiment with duplicates in ELISA plate (mean ± SEM). Only LPS stimulated cells released detectable levels of IL-1β (**D**). **E:** At the end of the 60 min ATP stimulation phase contrast images were taken to look for changes in cell morphology that would indicate cell activation.

4.2.3 Constitutive TG2 release into the medium by serum starved MDA-MB-231 breast cancer cells

At this point of the study another research group interested in non-conventional release of TG2 published a manuscript showing that serum starved MDA-MB-231 breast cancer cells can constitutively secrete TG2 into the medium via microvesicle shedding (Antonyak et al. 2011). Therefore, I decided to test whether this could be confirmed in our hands and whether a protocol for TG2 analysis in medium could be optimized based on the same cell model (MDA-MB-231 cells). Additionally, this would allow me to examine if ATP or BzATP elevate the levels of TG2 in the medium as some of the reports suggested that these cells express purinergic receptors (Kawai et al. 2008). This could give me the scope to obtain the answers and than later return to the THP-1 cell model and investigate if TG2 is secreted into the conditioned medium in parallel with IL-1β processing and release.

4.2.3.1 TG2 expression by MDA-MB-231 cells and its localization upon ATP and BzATP treatment

The aim was to use the MDA-MB-231 cells to trigger TG2 externalization by P2X7R activation. However, before performing this experiment, cell lysate from MDA-MB-231 cells was prepared to investigate the expression levels of TG2 and P2X7R by Western blotting (Fig. 4.4A). The cell lysate of MDA-MB-231 cells was compared with THP-1 cell extract as those monocyte-like cells express P2X7R at detectable amounts. As expected, undifferentiated THP-1 cells were lacking TG2 whereas in MDA-MB-231 cells anti-TG2 antibodies recognized a strong band for TG2 of approx. 80 kDa. THP-1 and MDA-MB-231 cells expressed P2X7R at comparable levels, and the anti-P2X7R antibodies recognized the glycosylated wild-type receptor of approx. 77 kDa in size, which is consistent with the literature (Nicke 2009). This indicated that the MDA-MB-231 cells could be used to test P2X7R involvement in triggering TG2 secretion as those cells express both components necessary for the study. In next step, the TG2 expression in serum starved MDA-MB-231 cells was examined by immunolocalization (Fig. 4.4B). Permeabilization of cells with Triton-X-100 was performed in order to investigate total TG2 distribution and possible association with intracellular organelles. Staining of the cells with anti-

TG2 antibodies revealed a ubiquitous cytoplasmic distribution of TG2 within the cytosol and lack of specific compartments enriched with TG2. Cells were then incubated in the presence or absence of 1 mM ATP or 300 μM BzATP and at the end of the experiment fixed and stained with anti-TG2 antibodies. The staining of cells was performed without cell permeabilization to see if changes in TG2 on the cell surface on in the ECM can be seen. The MDA-MB-231 cells revealed an interesting pattern of surface TG2 expression (Fig. 4.4C). TG2 seemed to be localizing to specific focal areas of the cell membrane (Fig. 4.4C, 60 min control). When the cells were stimulated for 60 min with the P2X7R agonist ATP or BzATP, the immunolabelling of TG2 revealed its accumulation at specific membrane subdomains that might be the sites of newly forming microvesicles (Fig. 4.4B, 60 min ATP and BzATP, respectively).

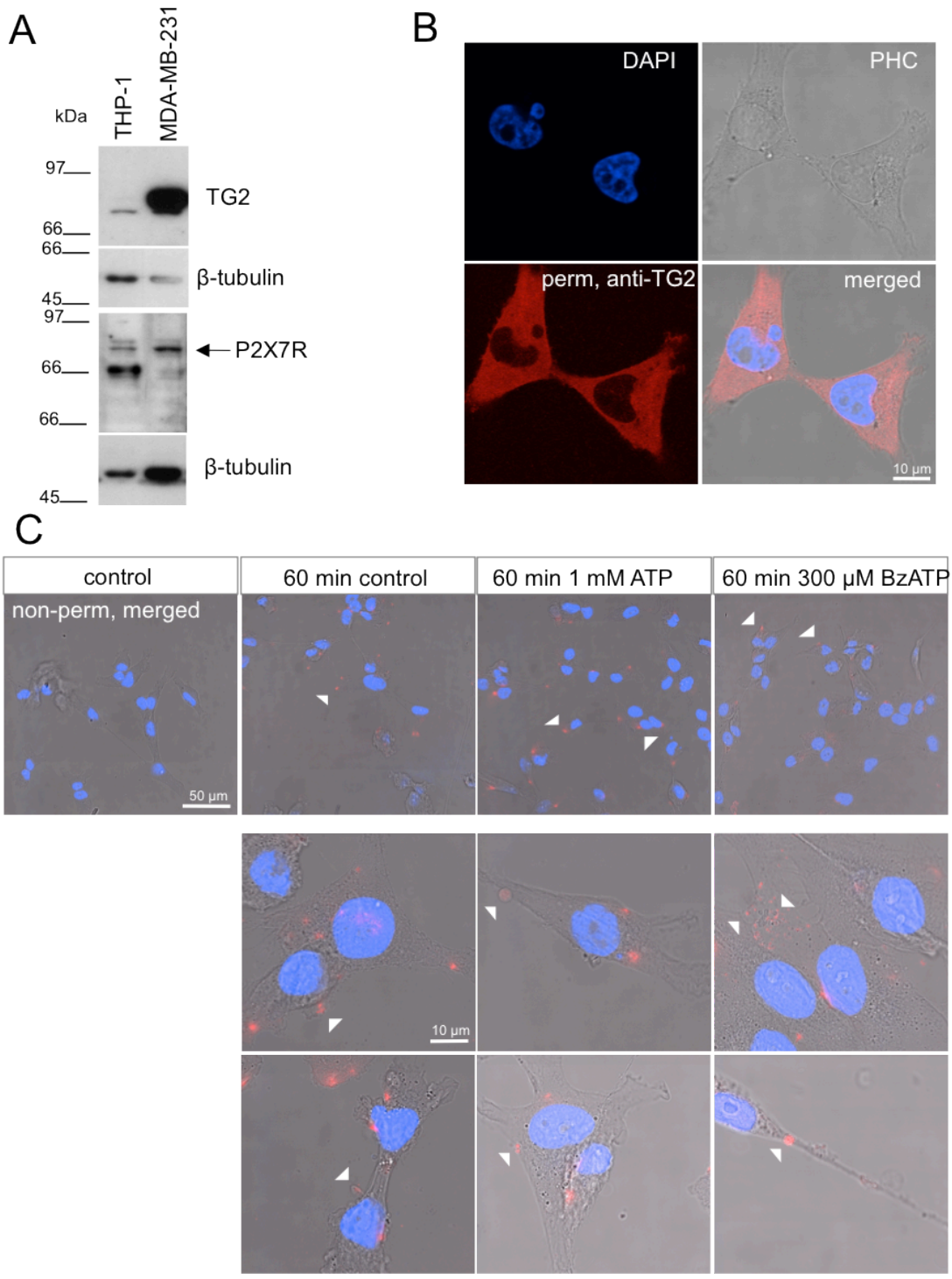

Fig. 4.4 TG2 expression and localization in MDA-MB-231 cells upon P2X7R stimulation. A: Total levels of TG2 and P2X7R was compared in cell extracts of THP-1 monocytes and MDA-MB-231 cells. 10 µg of protein was processed as previously described and analyzed by Western blotting for TG2 and β-tubulin (loading control). **B:** Serum starved MDA-MB-231 cells were washed and incubated for 60 min in OptiMEM. After fixation, TG2 expression was visualized in permeabilized cells using anti-TG2 antibodies and Alexa Fluor 594 secondary antibodies. Images represent an optical section acquired by confocal microscopy. Nuclei were stained with DAPI, and fluorescence images overlaid on phase contrast images (PHC) to help visualize TG localization. **C:** Serum starved MDA-MB-231 cells were washed and stimulated in the presence or absence of 1 mM ATP or 300 µM BzATP in OptiMEM. After 60 min cells were fixed and TG2 surface expression was visualized in non-permeabilized cells using anti-TG2 antibodies and Alexa Fluor 594 secondary antibodies. As a control, coverslips were stained with secondary antibodies only. Images represent an optical section acquired by confocal microscopy and merged as in B.

4.2.3.2 Enhanced secretion of TG2 in MDA-MB-231 cells stimulated with ATP

The change in TG2 surface staining upon ATP and BzATP stimulation indicated its potential association with shedding microvesicles (MVs) (Fig. 4.4). Therefore, to quantify any potentially secreted TG2 the analysis of conditioned medium from serum starved MDA-MB-231 cells with and without P2X7R stimulation was performed (Fig. 4.5). Antonyak and colleagues (2011) reported that treatment of HeLa cells with epidermal growth factor (EGF) enhanced formation of MVs on their surface. Thus, MDA-MB-231 cells were serum starved for 18h and then stimulated for 60 min in serum free OptiMEM with or without EGF, BzATP and ATP. Moreover, recombinant TG2 was added to the cells to check if it can be retrieved from the medium and detected by Western blotting after the duration of the experiment. The same amount of conditioned medium were harvested, lyophilized and analyzed by Western blotting (Fig. 4.5A). A serial dilution of recombinant TG2 in OptiMEM was lyophilized as well and separated next to the conditioned medium to estimate the concentration of TG2 released by the cells. Analysis of the nitrocellulose membrane with anti-TG2 antibodies confirmed that serum starved MDA-MB-231 cells are able to spontaneously secrete TG2 into the conditioned medium to a concentration of approx. 10 ng/ml in 1 hour (Fig. 4.5A). ATP stimulation increased its release into the medium (Fig. 4.5A, see also Fig. 4.5B) whereas BzATP and EGF were not able to increase its extracellular levels. As it was previously reported that microvesicles and exosomes contain specific proteins of the cytoskeletal network including actin (Théry et al. 2002; Burnier et al. 2009; Antonyak et al. 2011), the membrane was re-probed for the presence of actin. Both, ATP and BzATP stimulation noticeably induced actin release into the conditioned medium. Actin was running at the expected size of approx. 42-45 kDa (Fig. 4.5A, see also Fig. 4.5B). This indicated that both agonists are likely to have caused microvesicles shedding and therefore were effective in activating P2X7R. The membrane was negative for β-tubulin (~55 kDa in size), which was included as a control of nonspecific release of cellular proteins due to possible cell damage (Fig. 4.5A). Similarly, the membrane was probed for GAPDH that should be running at approx. 37 kDa and was found to be absent in the conditioned medium of MDA-MB-231 cells (Fig. 4.5B) thus suggesting that TG2 and actin increase upon ATP stimulation is not related to non-specific loss in membrane integrity.

To better understand the kinetics of agonist-mediated TG2 release, medium was collected after 15, 60 or 120 min from cells that were left unstimulated or were stimulated with 1 mM ATP (Fig. 4.5C). The analysis confirmed that TG2 and actin are constitutively secreted into the medium and accumulate over time. Treatment of cells with 1 mM ATP lead to faster TG2 and actin accumulation in the medium (Fig. 4.5C). This might indicate that there is constitutive upregulation of the process of MVs shedding from serum-starved cells and that stimulation with ATP accelerates the kinetics of their accumulation. This therefor further suggested that TG2 secretion into the extracellular space triggered by stimulation with ATP was mediated by purinergic receptor activation on the surface of MDA-MB-231 cells. However, the finding that BzATP was unable to trigger TG2 release was not consistent with a P2X7R dependent process.

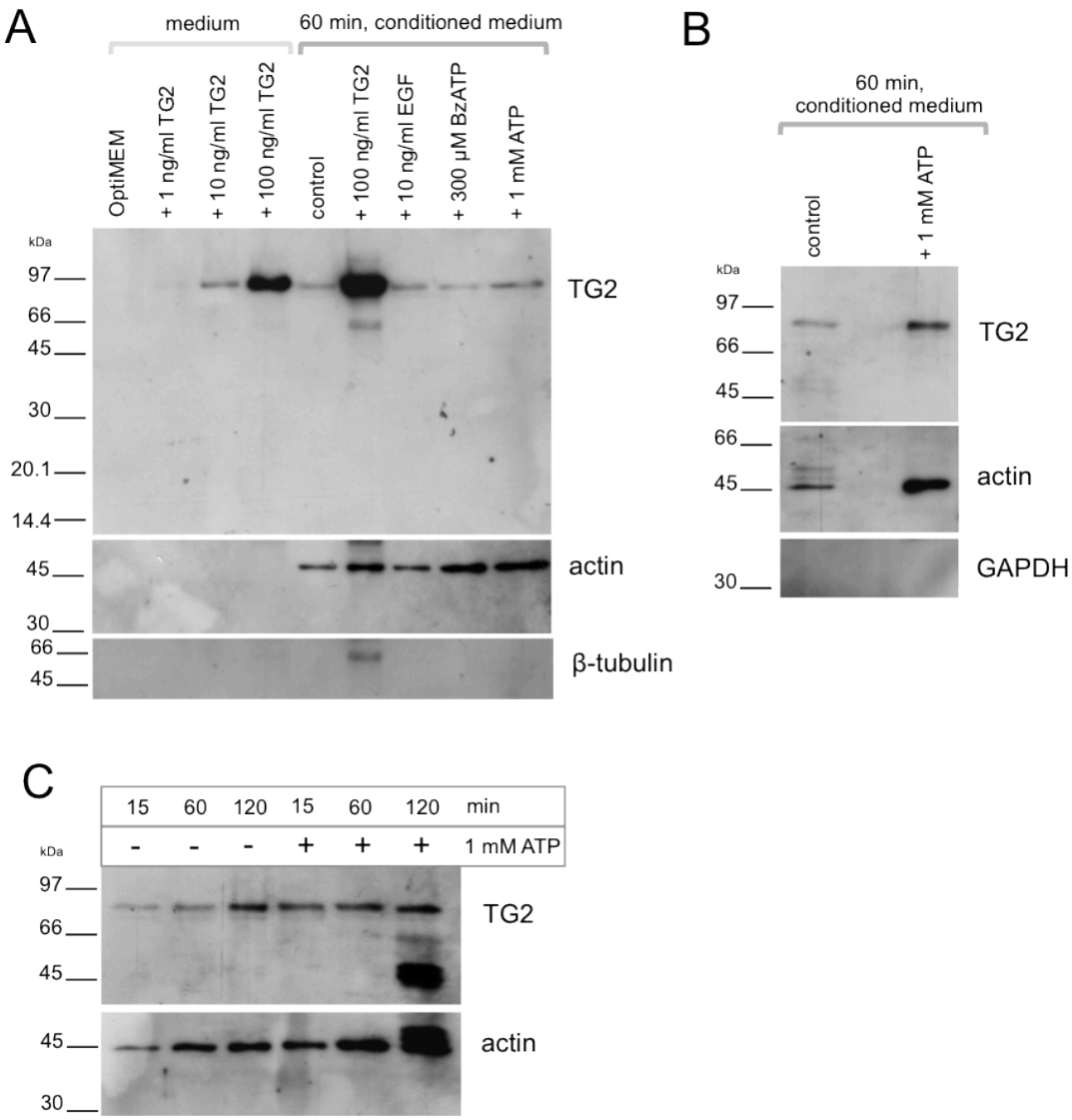

Fig. 4.5 Changes in TG2 and actin levels in cell free supernatant upon ATP stimulation of MDA-MB-231 cells as analyzed by Western blotting. A: MDA-MB-231 cells were serum starved for 18h. Then cells were washed and stimulated with 100 ng/ml TG2, 10 ng/ml EGF, 300 µM BzATP or 1 mM ATP for 60 min in OptiMEM. Conditioned medium from duplicate wells (400 µl) was collected and cleared of cells/cell debris by centrifugation (1500 x g, 10 min). 350 µl of conditioned media and fresh OptiMEM containing different concentrations of TG2 were lyophilized, resuspended in sample cocktail containing urea and analyzed by Western blotting for TG2, actin and β-tubulin. **B:** Serum starved MDA-MB-231 cells were stimulated for 60 min in the presence or absence of 1 mM ATP in OptiMEM. Conditioned medium was collected and cleared by centrifugation as above. Samples were analyzed by Western blotting for the presence of TG2, actin and GAPDH. **C:** Serum starved MDA-MB-231 cells were stimulated for different times in the presence or absence of 1 mM ATP in OptiMEM. Conditioned medium was processed as previously described and analyzed by Western blotting for TG2 and actin.

4.2.3.3 Changes in intracellular calcium induced by ATP and BzATP stimulation

In order to further confirm purinergic receptor activation in MDA-MB-231 cells, changes in intracellular Ca^{2+} concentrations were measured using Fluo-4 calcium indicator. The aim of the experiment was to check if stimulation with both 1 mM ATP and 100 μM BzATP lead the expected increase in intracellular calcium levels. The comparison of the two agonists was important as ATP can not only act on receptors of the P2X family but also on P2Y receptors, which evoke G-protein coupled responses (Grol et al. 2013), whereas BzATP is a potent agonist for P2X7R but can potentially also activate other members of the P2X family (Jarvis and Khakh 2009). MDA-MB-231 cells were loaded with Fluo-4 calcium indicator and then stimulated with either agonist in order to monitor potential changes in fluorescence intensity using confocal microscopy (Fig. 4.6). Stimulation of MDAMB231 cells with 1 mM ATP induced a rapid transient increase in intracellular Ca^{2+} that returned to baseline levels after approx 2 minutes (Fig. 4.6 left panel and graph). Treatment of cells with 100 μM BzATP lead to a substantially smaller increase in fluorescence and showed a different biphasic desensitization kinetics. Agonist treatment failed to produce sustained high calcium levels nor induce "cell blebbing", which are the characteristic cell responses observed upon P2X7R activation. This may suggest that MDA-MB-231 cells do not express functional P2X7R or express it at low level and that Ca^{2+} spikes are predominantly driven by activation of different surface receptors.

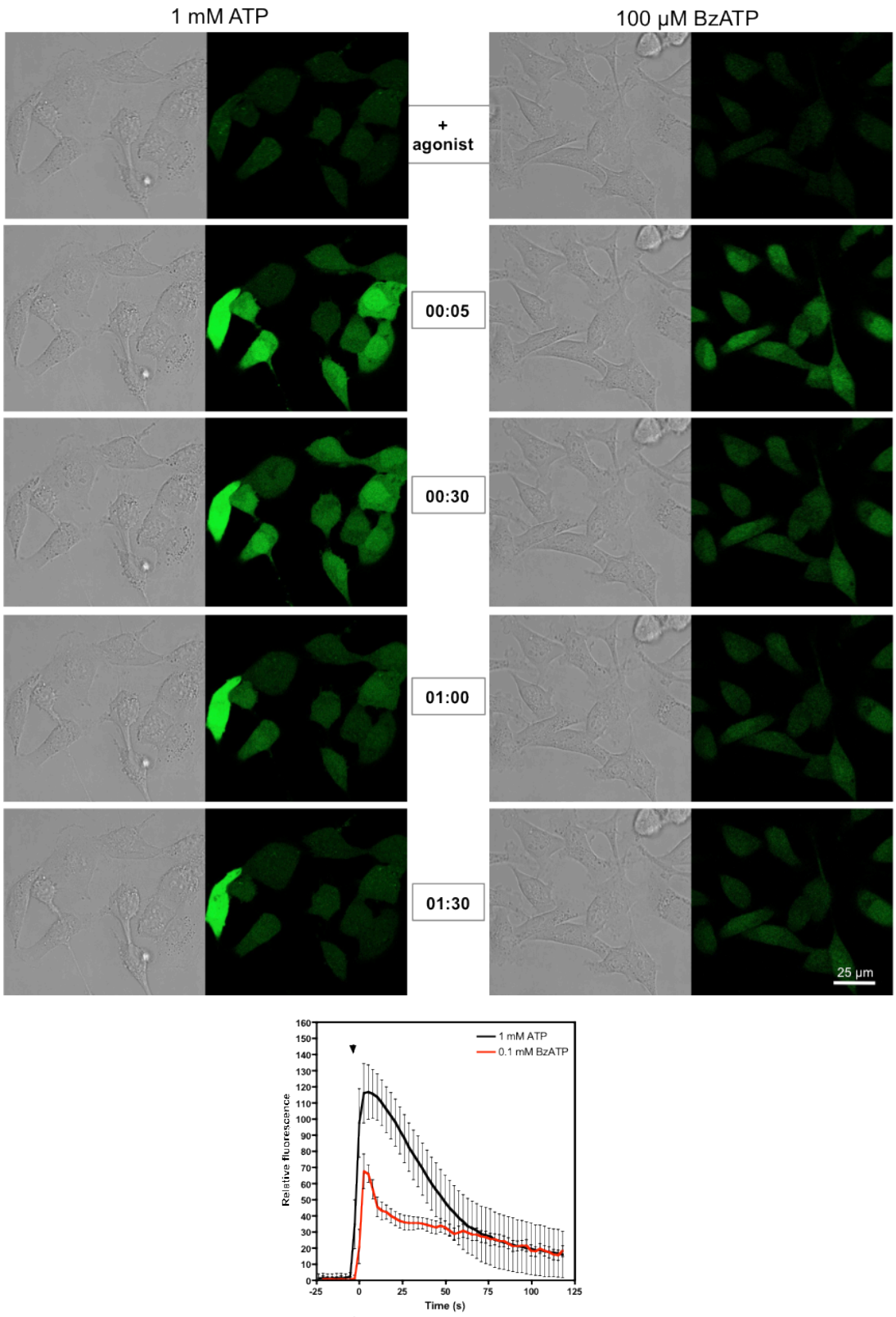

Fig. 4.6 Changes in intracellular Ca^{2+} concentration in MDA-MB-231 cells upon stimulation with P2X receptor agonists. MDA-MB-231 cells were incubated with 3 µM Fluo-4 calcium indicator in OptiMEM for 20 min and thereafter stimulated with 1 mM ATP or 100 µM BzATP. Changes in fluorescence were monitored for up to 10 min using confocal microscopy. Time after stimulation is given in the middle column in minutes. Pictures represent an optical section acquired by confocal microscopy. Data shown is result of one experiment. The graphs represent changes in Fluo-4 fluorescence upon application of ATP or BzATP (arrowhead). Line represents mean fluorescence values ± SEM from the experiment above (ATP, n= 11; BzATP, n= 12 cells).

4.2.3.4 Attempt to inhibit TG2 secretion with P2X7R and P2X4R inhibitor

To identify if P2X7R was involved in the process of rapid TG2 release upon ATP stimulation of MDA-MB-231 cells, a potent P2X7R inhibitor was used (A740003) (Honore et al. 2006). It was further predicted that the addition of inhibitor might decrease the levels of constitutively released TG2. Detection of immunoreactive species analysis of TG2 in the conditioned medium confirmed previous findings that ATP was able to upregulate its release (Fig. 4.7A). Flotillin-2 is a scaffolding protein that is involved in formation of lipid-raft microdomains (Otto and Nichols 2011) but was also describe to be localizing in exosomes (Trajkovic et al. 2008) and microvesicles (Antonyak et al. 2011) and was used as a marker of shedding membrane-bound vesicles. However, the addition of the P2X7R inhibitor failed to block TG2 as well as flotillin-2 secretion into the conditioned medium of cells stimulated with either ATP or BzATP (Fig. 4.7A). Surprisingly, the addition of inhibitor seemed to induce TG2 translocation in both non treated control and ATP stimulated cells (Fig. 4.7A). A similar trend was observed in the next experiment where the concentration of the P2X7R inhibitor was increased from 5 to 100 μM to be confident that the lack of an effect was not due to insufficient inhibitor concentration (Fig. 4.7B). Cells stimulated with 1 mM ATP in the presence of inhibitor were still able to secrete TG2 at a similar level to control and P2X7R inhibition did also not seem to affect release of actin (Fig. 4.7B). Therefore, it was predicted that another member of the P2X family might be involved in regulating ATP-dependent signaling in those cells. P2X4 receptor was the assumed candidate. Thus, the stimulation of MDA-MB-231 cells was repeated using ATP and BzATP as agonists but this time in the presence of P2X7 inhibitor (A740003), P2X4 inhibitor (5-BDBD) or a combination of both inhibitors (Fig. 4.7C). The concentration of P2X7R inhibitor was reduced back to 5 μM. Western blotting analysis of conditioned medium was not fully conclusive, as both inhibitors seemed to promote its secretion rather than inhibiting TG2 translocation when applied individually. However, partial reduction in released TG2 levels was observed in ATP treated cells in the presence of both inhibitors. Though, it was not clear why release was increased in unstimulated cells in the presence of the inhibitors as compared to vehicle control (Fig. 4.7C). Therefore, the studies with the P2X7R inhibitor did not clearly answer the question if

TG2 release can be P2X dependent but rather suggested that it maybe caused at least in part by P2Y-dependent responses in MDA-MB-231 cells.

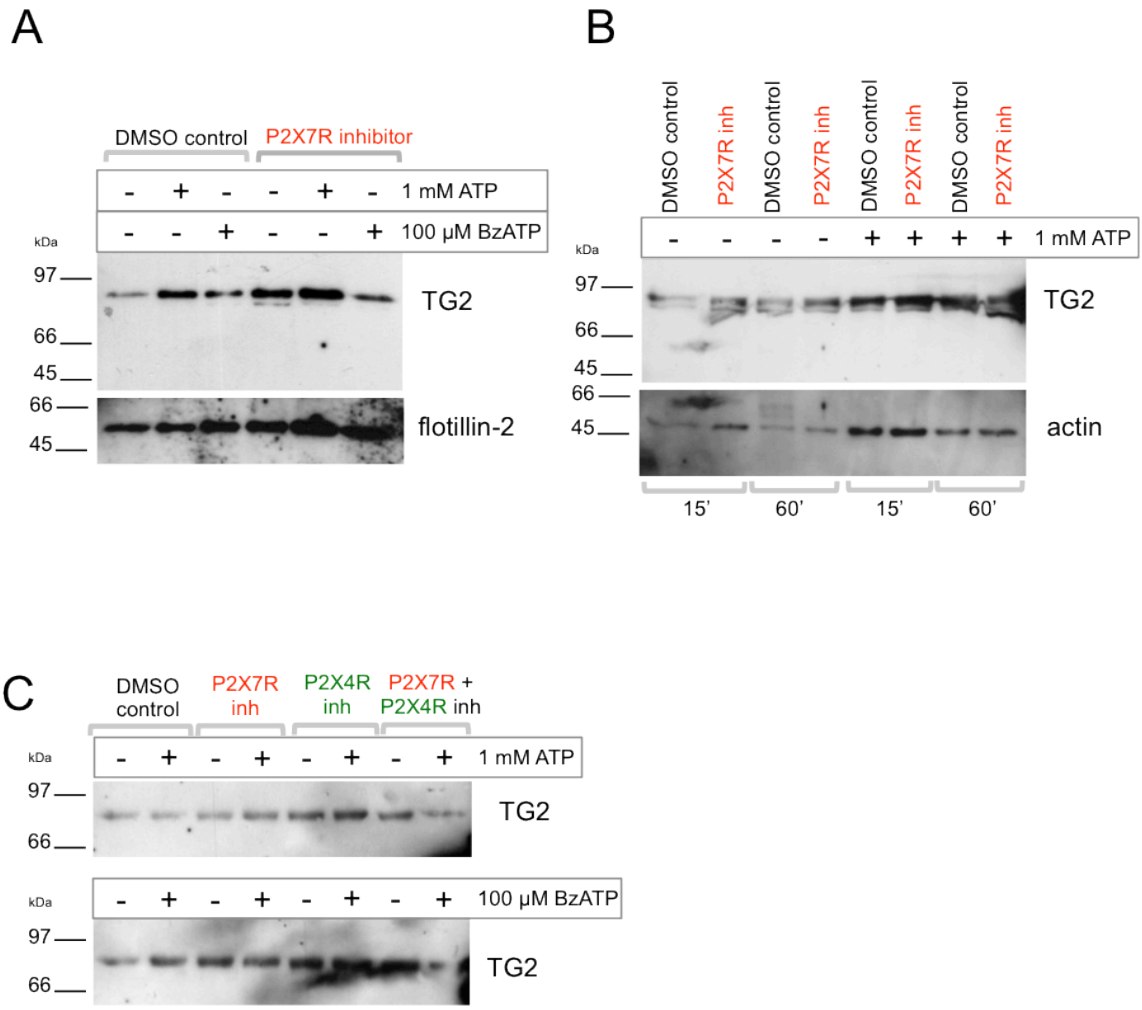

Fig. 4.7 Detection of agonist-mediated TG2 release in the presence or absence of P2X7R and P2X4R inhibitor. A: Serum starved MDA-MB-231 were washed and pre-treated for 10 min with control medium (0.05% DMSO) or 5 µM P2X7R inhibitor (A740003 in DMSO). Then cells were incubated for 30 min in the absence or presence of 1 mM ATP or 100 µM BzATP in fresh OptiMEM. Where indicated, the respective inhibitor or DMSO as a carrier control was present during stimulation. Conditioned medium was cleared by centrifugation, lyophilized, resuspended and analyzed by Western blotting as above. Anti-TG2 and anti-flotillin-2 antibodies were used to probe the membrane. **B:** Serum starved MDA-MB-231 were washed and pre-treated for 15 min with control medium (1% DMSO) or 100 µM P2X7R inhibitor (A740003 in DMSO) in OptiMEM. After pre-incubation, to half of the wells 1 mM ATP in OptiMEM was added and cells were stimulated for another 15 or 60 min. Conditioned medium was cleared by centrifugation and analyzed by Western blotting as in Fig. 5. Anti-TG2 and anti-actin antibodies were used to stain the membrane. **C:** Serum starved MDA-MB-231 were washed and pre-treated for 10 min with control medium (0.1% DMSO), 5 µM P2X7R inhibitor (A740003 in DMSO), 10 µM P2X4R inhibitor (5-BDBD in DMSO) or a combination of both inhibitors. Then cells were incubated for 30 min in the absence or presence of 1 mM ATP (top membrane) or 100 µM BzATP (bottom membrane) in fresh OptiMEM. Where indicated, the respective inhibitors or DMSO as a carrier control was present during stimulation. Conditioned medium was cleared by centrifugation and analyzed by Western blotting as above. Anti-TG2 antibodies were used to stain the membrane.

4.3 Discussion

In this chapter, P2X7R-mediated IL-1β processing and release was studied in the monocytic THP-1 cells using ELISA and Western blotting techniques. Moreover, the induction of TG2 expression during differentiation of monocyte into macrophage-like cells was investigated to enable the investigation of TG2 upregulation in the context of a physiologically relevant model. This gave interesting insights into regulation of TG2 expression by various modulators that are involved in the process of inflammation or terminal cell differentiation. At the beginning of this study, it was important to select a relevant cell model to investigate P2X7R-dependent TG2 externalization. A monocyte/macrophage cell model was chosen in order to establish an assay for IL-1β release and to later study non-conventional TG2 release. It is well supported by experimental evidence that synovial macrophages are key players in driving destructive inflammatory responses in rheumatoid arthritis (Brennan and McInnes 2008) as well as in osteoarthritis (Bondeson et al. 2010). Furthermore, macrophages were found to express catalytically active TG2 on the cell surface (Murtaugh et al. 1984; Hodrea et al. 2010) and also P2X7R (Qu et al. 2007), which makes this cell type a good candidate to investigate the consequence of ATP treatment on TG2 externalization. THP-1 cells are able to secrete active IL-1β (Mackenzie et al. 2001), express P2X7R in the plasma membrane (Humphreys and Dubyak 1996) and upregulate P2X7R expression after stimulation with inflammatory mediators such as LPS (Falzoni et al. 1995). Regulation of TG2 expression was explored in the context of THP-1 differentiation into macrophage-like cells using three different differentiation agents: IL-6, TPA and ATRA. Both, IL-6 and ATRA mediate effector binding to the their respective response elements in the *TMG2* promoter and therefore directly regulate TG2 expression (Aeschlimann and Thomazy 2000). However, regulation of TG2 by proinflammatory IL-6 is dependent on NFκB signaling (Suto et al. 1993; Kuncio et al. 1998), whereas retinoids regulate TG2 expression through activating RAR and RXR binding enhancer element upstream of the *TMG2* gene (Nagy et al. 1996; Aeschlimann and Thomazy 2000). Retinoids are being a differentiation signal mostly associated with developmental process. On the other hand, TPA, which is a derivate of the phorbol ester is indirectly acting on TG2 expression levels by activating the protein kinase C α (PKCα) signaling cascade and ultimately FAK phosphorylation (Stephens et al. 2004; Iismaa et al. 2009). PKCα

outside-in signaling promotes cell spreading and motolity (Verderio et al. 2003; Telci et al. 2008). Enhanced transcription of *TGM2* can be regulated by other molecules such as EGF, TNF-α, TGFβ1 or IL-1β itself, depending on the cell type and biological context (Mehta and Eckert 2005; Mehta and Han 2011b; Nurminskaya and Belkin 2012). However, the selected mediators were chosen because of their role in macrophage differentiation. In my experiments, THP-1 cell differentiation with ATRA proved to be effective in inducing TG2 expression during differentiation into macrophage-like cells (Mehta and Lopez-Berestein 1986). Thus, this model was chosen for optimizing the assay for ATP-dependent IL-1β release.

ATP stimulation and measurement of secreted IL-1β from differentiated monocytes was investigated using two different conditions 1) when TG2 and pro-IL-1β expression was simultaneously upregulated; 2) when TG2 induction was followed by pro-IL-1β upregulation with LPS. In both cases, the capture ELISA showed that ATP enhanced IL-1β release from LPS-primed macrophage-like cells which is in agreement with the literature (Mackenzie et al. 2001; Mehta et al. 2001; Qu et al. 2007). It was not possible to fully confirm that ATP caused release of the processed 17 kDa form of IL-1β as I did not manage to detect mature IL-1β in the conditioned buffer by Western blotting. However, the fact that in LPS-primed cells a decreased level of intracellular pro-IL-1β was detected after 1 hour of ATP stimulation suggests that pro-IL-1β is processed and released. LPS treatment of THP-1 cells lead to a low level of IL-1β release in the absence of ATP stimulation. Differentiation with ATRA enhanced baseline IL-1β release. ATRA can have both stimulatory and inhibitory influence on IL-1β as well as IL-6 release by LPS-challenged monocytes, depending on the length of the stimulation (Gross et al 1993). This is in line with my results, which showed that the differentiation protocol affected the susceptibility of the cells to ATP stimulation. The differentiation status of the cell could determine the response to ATP. P2X7 receptors were shown to be upregulated on the mRNA levels during THP-1 stimulation with LPS and interferon-γ and this increased the formation of membrane pores (Humphreys and Dubyak 1998). Oppositely, Gudipaty and colleagues (2001) showed that there are no differences in P2X7R mRNA levels between freshly isolated monocytes and those differentiated into macrophages. However, the function of P2X7R was greatly enhanced in macrophages. This response is cell type specific as ATRA downregulates P2X7R expression in human

neuroblastoma cells and inhibits both P2X7R expression and function in mouse Neuro2A cells (Bilbao et al. 2012). The second model in which monocyte differentiation was followed by LPS treatment would be preferably chosen as under those conditions THP-1 cells showed greater potency for ATP-dependent IL-1β secretion. In pathology of arthritis, the monocytes are attracted to the affected joint where they undergo differentiation into macrophages and start to secrete proinflammatory IL-1β (Pope 2002). Our model of cell differentiation could then reflect the *in vivo* process of monocyte recruitment and activation. However, to fully understand whether the experimental conditions are relevant to the *in vivo* situation, further experiments would need to be performed.

In this chapter, the conditions for TG2 release and its detection in the supernatant of serum starved MDA-MB-231 cells were also established. This enabled me to show for the first time that purinergic signaling might be linked to non-conventional secretion of TG2. Specifically, Western blotting analysis revealed that serum starved breast cancer cells secrete TG2 into the conditioned medium in a time-dependent manner and that ATP stimulation markedly potentiated TG2 externalization. Some recent reports seem to be indicating that P2X7R activation can promote growth and survival of cancer cells by tonic regulation of Ca^{2+} fluxes (Francesco Di Virgilio et al. 2009; Di Virgilio 2012). Increased expression of P2X7R might promote cell survival in severe stress conditions such as serum deprivation. ATP driven growth is mediated by an autocrine-paracrine loop, and removal of extracellular ATP by apyrase that degrades it, leads to the arrest of cancer cell growth. It has been postulated that this activity of P2X7R is unrelated to the "pore formation" phenomenon but relates to P2X7R constant channel activity. However, it is still unclear how very low concentrations of ATP mediate P2X7R activation despite the low ATP affinity of P2X7R (North 2002). There is substancial evidence that TG2 is upregulated during metastatic cell transformation is the number of different cell types (Mehta and Eckert 2005; Iismaa et al. 2009). For example, TG2 is involved in the invasive phenotype of pancreatic cancer cells (Mehta and Han 2011b). TG2 was also found to be secreted into the ascites fluid surrounding ovarian tumour cells (Yakubov et al. 2013). Also TG2 is upregulated during epithelial to mesenchymal transition following persistent activation of NFκB signaling (Kumar and Mehta 2012). Interestingly, the screening of various cancer cells showed that

upregulation of TG2 correlates with increased IL-6 production (Keunhee Oh et al. 2011). Moreover, knocking-down the TG2 expression with shRNA significantly reduced IL-6 secretion into the medium in MDA-MB-231 cells and reduced anchorage-independent cell growth. Taken together, this indicates that cytokine production and TG2 expression may be linked and may form an important feedback loop not only for cells of immune origin. Antonyak and colleagues (2011) showed that MDA-MB-231 breast cancer cells are able to secrete TG2 that localizes on the surface of budding microvesicles (MVs). Yet, not all cell types known to secrete TG2 were able to produce those structures. Serum starved HeLa cervical carcinoma cells required EGF treatment to produce such MVs and NIH3T3 fibroblasts were incapable to form MVs even upon serum starvation or EGF stimulation (Antonyak et al. 2011). Therefore, the authors of that study speculated that this type of TG2 release might be the dominant pathway of TG2 secretion in highly metastatic cancer cells. In my experiments I could not find clear evidence that would estabilished a link between MV's and TG2 release as differential ultracentifugation (results not shown) suggest it localization in the soluble, non vesicular fraction even though TG2 showed a localized surface topology in non-permeabilized cells.

In my experiments, ATP was able to trigger rapid TG2 secretion into the conditioned medium of serum starved MDA-MB-231 cells. Interestingly, actin was found to be co-released with TG2, which is in agreement with data shown by Antonyak and colleagues (2011). Actin belongs to the proteins, which are found in released MVs (Burnier et al. 2009) and exosomes (Théry et al. 2002). Other intracellular proteins such as β-tubulin or GAPDH could not be detected in the same medium fractions where TG2 and actin were accumulating. This suggests that release of TG2 and actin is not simply due to cell damage but is triggered by purinergic signaling. The P2X7R was a candidate receptor driving the active TG2 release into the medium. Western blotting analysis confirmed P2X7R expression in these cells. However, the studies with the selective P2X7R inhibitor were unable to block TG2 externalization and in some instances even seemed to promote its release. The more prominent intracellular Ca^{2+} fluxes evoked by ATP stimulation compared to BzATP as well as the higher sensitivity of cells to ATP versus BzATP suggested a P2X4R response rather than a P2X7R response. However, a P2X4R inhibitor was also unable to clearly block TG2 accumulation in medium in response to ATP treatment.

The partial inhibition observed upon ATP stimulation when both P2X7R and P2X4R inhibitors were present might indicate the presence of P2X7R/P2X4R hetero-oligomers in the membrane of MDA-MB-231 cells. Although P2X7R was believed not to form hetero-oligomeric assemblies with any of the P2X family members (Torres et al. 1999; North 2002), recent functional data indicate that those hetero-oligomers can exist in the cell membrane of HEK293 when co-expressed and primary murine bone marrow derived macrophages (Guo et al. 2007). It was further shown that P2X7R stabilized the surface expression of P2X4R and those complexes remained sensitive to BzATP stimulation but were less active than P2X7R on its own. Another explanation of our finding might be that MDA-MB-231 cells do not express a fully functional P2X7R or express a distinct splice variant that has aberrant activity. Cervical cancer cells express the truncated P2X7R(j) isoform lacking part of the extracellular domain and the entire second transmembrane domain as well as C-terminus (Feng et al. 2006). When expressed in HEK293 cells, this naturally occurring splice variant, shows reduced channel function and fails to mediate dye uptake, which is characteristic feature of P2X7R-dependent 'pore formation".

The fact that cells were more sensitive to ATP than BzATP stimulation, which consequently triggered TG2 release, could also suggest activation of metabotrophic purinergic receptors of the P2Y receptor family (Baroja-Mazo et al. 2012; Grol et al. 2013). This is further supported by the fact that BzATP is an approx. 10-fold stronger agonist than ATP for P2X7R (Rassendren et al. 1997) but not for P2Y receptors (Burnstock 2007). The reduced intracellular Ca^{2+} signaling in response to BzATP was observed and this is not consistent with a P2X7R activation profile. P2Y receptors are likely to be activated by lower concentrations of ATP and this may lead to release of Ca^{2+} from intracellular stores (Grol et al. 2013). Thus, the TG2 release in those cells may be mediated by P2YR. This should be further investigated to determine if P2X or P2Y-dependent signaling is responsible for TG2 secretion.

P2X7R was shown to be present in both THP-1 and MDA-MB-231 cells and some encouraging results were obtained in those cell models. However, it was difficult to clearly establish a link between P2X7R function and TG2 release given the experimental conditions and possibly expression of different types of receptors. Therefore, there was a need to produce a stable cell line with P2X7R expression,

channel function and “pore” forming” capacity to have a model, in which our questions could be addressed more directly. Stably transfected HEK293 cells expressing wild-type P2X7R were considered to be a useful tool to study the intracellular events upon P2X7R activation and a possible link to TG2 externalization. This is outlined in the next chapter.

Chapter 5 Establishing cell model expressing functional P2X7R

5.1 Introduction

Understanding the pathway leading to TG2 externalization that could be both linked with P2X7R activation and be common for different cell types was important at the stage of this study. Stably transfected HEK293 cells are a widely used model to investigate P2X7R biology, as this cell type lacks other P2X receptor family members (Wilson et al. 2002; Mackenzie et al. 2005). In fact, HEK293 cells overexpressing rat P2X7R or human P2X7R were used to analyze electrophysiology, receptor gating, the kinetics of dye uptake and served as a good model to describe the distinct features of P2X7R (Surprenant et al. 1996; Rassendren et al. 1997; Virginio et al. 1999; MacKenzie et al. 2001; Mackenzie et al. 2005). The aim of this part of the study was to establish cell lines stably expressing functional P2X7R, untagged wild-type and V5 tagged receptor, that could be later used for investigating TG2 release upon P2X7R stimulation.

In HEK293 cells overexpressing P2X7R, ATP triggers remarkable morphological changes called “cell blebbing” and the presence of cell membrane ruffling indicates P2X7R activation (A Morelli et al. 2003; Adinolfi et al. 2010). Therefore the term “blebbing” is commonly used to describe large membrane reorganization events such as rapid formation of protrusions or plasma membrane projections that follow P2X7R stimulation (MacKenzie et al. 2001). These are thought to occur due to cytoskeletal rearrangements. It was observed that cell blebbing is a secondary response to the cation permeation through the P2X7R pore. This indicates that changes in cell morphology are occurring after P2X7R channel opening or subsequent large membrane pore formation (A Morelli et al. 2003; Mackenzie et al. 2005). However those authors also showed that cell blebbing is reversible and no longer visible after agonist removal. The cell blebbing is usually characterized by initial formation of numerous microvesicles (<0.5 μm) that precede development of the large blebs (>1 μm) (Solle et al. 2001; Mackenzie et al. 2005). Mackenzie and colleagues describe that microvesicles are actively shed from the cell surface and consequently lead to loss in membrane area (Mackenzie et al. 2005). On the other hand, large but organellum free membrane blebs stay attached to the cell

surface and remain intact even during prolonged agonist application. However, they also can be retracted from the plasma membrane. They called this type of cell activation the "zeotic" membrane movement to indicate that such changes may also be associated with an apoptotic response. However, they have shown that only prolonged stimulation of P2X7R with a potent agonist like BzATP (≥ 30 min) can induce cell death as measured by lactate dehydrogenase (LDH) release (MacKenzie et al. 2001). Also, it has been suggested that very high agonist concentrations might cause cell leakage and LDH release from P2X7R overexpressing cells (Ferrari et al. 1997). Therefore, careful selection of the optimal conditions for P2X7R stimulation is necessary in order to investigate the physiological cell response. This chapter details the experimental steps that were used to establish and characterize two stable HEK293 cell lines expressing P2X7R that were subsequently used as a cell model to investigate TG2 externalization.

The aims for the chapter:

1. Establish cell lines stably expressing wild-type or V5-His tagged P2X7R
2. Confirm that P2X7R is expressed and functional in the stably transfected cell lines
3. Establish optimal conditions for P2X7R activation and optimize concentrations of agonists, ATP and BzATP

5.2 Results

5.2.1 Cloning of the P2X7R coding sequence into mammalian cell expression vector

The purpose of the experiment was to design two DNA vectors containing the P2X7R coding sequence: one to be translated into wild-type P2X7R with its natural stop codon (P2X7R) and the other with a V5-His tag attached to the C-terminus (P2X7R-V5-His). Fig. 5.1A shows the experimental steps that were necessary to clone the P2X7R sequence into pcDNA/FRT/V5-His plasmid. Five and four positive bacterial clones were obtained for pcDNA5/FRT/V5-His with subcloned P2X7Rstop and P2X7R, respectively (data not shown). The complete coding sequence from 2 positive clones of P2X7Rstop and P2X7R was sent for Sanger dideoxy sequencing, which confirmed that no mutations were present in the selected clones according to the NCBI GenBank reference P2X7R sequence (BC011913; gi_33877741). The complete sequencing results are shown in Appendix 4. The sequencing also confirmed the presence of the stop codon downstream of the P2X7R coding sequence in P2X7Rstop and its lack in the second construct that should be translated into protein with V5-His epitope (Fig. 5.1B).

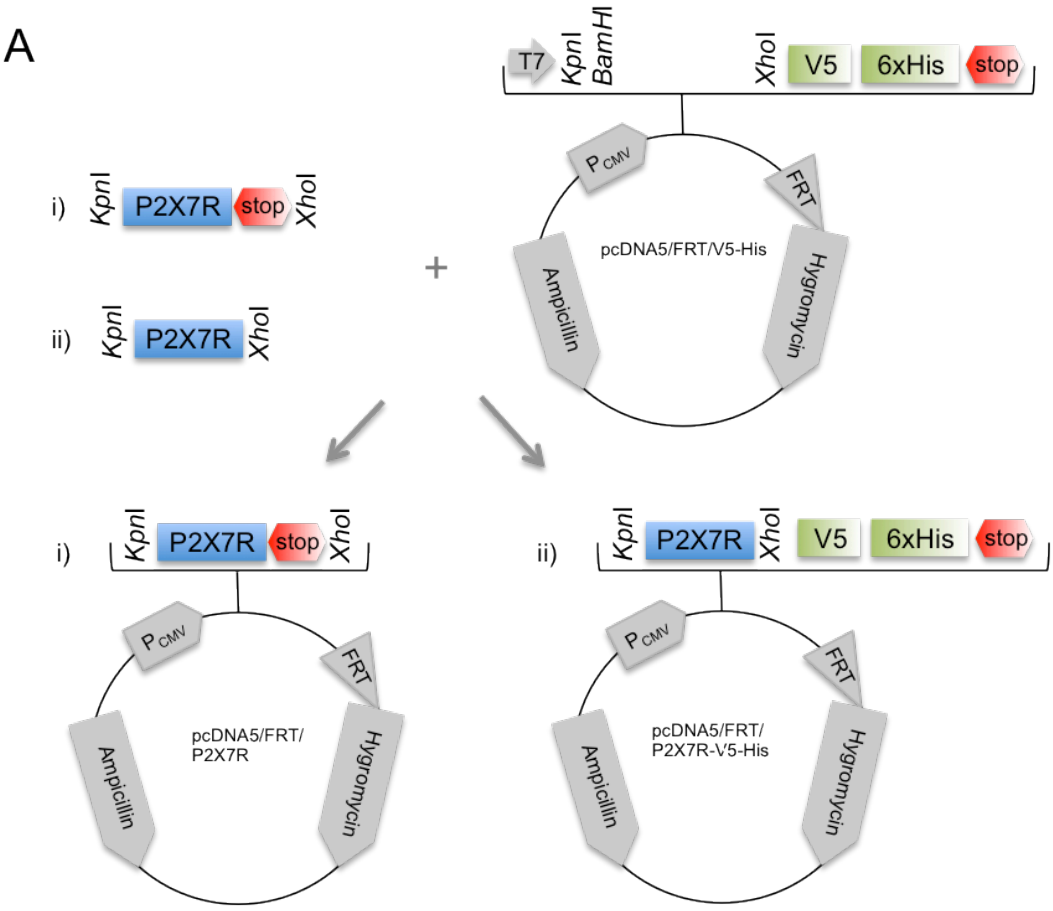

B

P2X7R (with stop codon)

AGTCCTTACTGACTCGAGTCTAGAGGGCCCTTCGAAGGTAAGCCTATCCCTAACCCTCTCCTCGGTCTCGATTCTACGCGTACCGGT
TCAGGAATGACTGAGCTCAGATCTCCCGGGAAGCTTCCATTCGGATAGGGATTGGGAGAGGAGCCAGAGCTAAGATGCGCATGGCCA
S P Y *
CATCATCACCATCACCATTGA
GTAGTAGTGGTAGTGGTAACT

P2X7R-V5-His (with V5-His tag on C-terminus)

AGTCCTTACCTCGAGTCTAGAGGGCCCTTCGAAGGTAAGCCTATCCCTAACCCTCTCCTCGGTCTCGATTCTACGCGTACCGGTCAT
TCAGGAATGGAGCTCAGATCTCCCGGGAAGCTTCCATTCGGATAGGGATTGGGAGAGGAGCCAGAGCTAAGATGCGCATGGCCAGTA
S P Y L E S R G P F E G K P I P N P L L G L D S T R T G H
CATCACCATCACCATTGA
GTAGTGGTAGTGGTAACT
H H H H H *

Fig. 5.1 Cloning of the P2X7R coding sequence into pcDNA 5/FRT/V5-His vector. A: To generate the human P2X7R and human P2X7R tagged with V5-His on the C-terminus, the full length coding sequence of P2X7R was amplified in PCR reactions. Primers that introduce *Kpn*I and *Xho*I restriction sites at the 5' and 3' ends, respectively, were used. One of them was designed to omit the stop codon of the native P2X7R sequence. PCR fragments encoding P2X7R were digested with *Kpn*I and *Xho*I and ligated into pcDNA5/FRT/V5-His vector linearized by triple digest with *Kpn*I, *BamH*I and *Xho*I. The obtained ligation mixtures were used to transform competent *E.coli*, followed by selection for Ampicillin resistance. Plasmid DNA extracted from individual clones was subjected to restriction analysis and dideoxy sequencing in order to identify clones with the appropriate insert. **B:** Figure shows the comparison of the C-terminal sequence between wild-type P2X7R (top) and V5-His tagged P2X7R (bottom). P2X7R sequence (blue), stop codon (red), *Xho*I restriction site (grey), V5 tag and 6xHis (green).

5.2.2 Stable transfection of HEK293 cells with P2X7R and P2X7R-V5-His expression constructs

Given that both P2X7R and P2X7R-V5-His constructs were successfully obtained, they were used for stable transfection of HEK293 Flp-In cells as they contain an integrated FRT site (Fig. 5.2A). The principle of the stable cell line generation using this cell line is detailed in the Materials and Methods (section 2.18). HEK293 Flp-In host cells were co-transfected with pOG44 vector encoding the Flp recombinase and the P2X7R or P2X7R-V5-His constructs and after 24h subjected to selection with 100 μg/ml Hygromycin B. Selection was carried out for four weeks until cell colonies were big enough to be transferred to a new culture dish. As integration is site-specific there is no difference to be expected between individual cell clones. At the end of stable cell line generation, there were no evident differences in cell morphology between established cell lines and parental cells (Fig. 5.2B). Cell colonies that were formed after transfection with different DNA preparation (*E.coli*, clones 3 and 6) of P2X7R construct were gently trypsinized and combined. Similarly, cell colonies formed for P2X7R-V5-His construct were also combined and transferred to another dish. The resulting cell lines will be referred to as HEK293 P2X7R and HEK293 P2X7R-V5-His.

After establishing HEK293 P2X7R and P2X7R-V5-His cell lines, cell extracts were obtained and P2X7 expression was analyzed by Western blotting to confirm expression of the receptor. As a negative control cell extract from parental HEK293 cells was used. Proteins were separated by SDS polyacrylamide gel electrophoresis and subsequently transferred to a nitrocellulose membrane. Membranes were stained with anti-V5 or anti-P2X7R antibodies to investigate protein expression levels and antibodies specificity (Fig. 5.2C). Expression of P2X7 was confirmed in both stable cell lines using the P2X7R antibodies and no signal was detected in the lane where protein extract from parental cells was separated. The anti-P2X7R antibodies recognized a protein band of approximately 77 kDa calculated from the relative migration of the protein marker. This is in agreement with previous reports and corresponds to the glycosylated wild-type receptor (Nicke et al. 2009). The P2X7R-V5-His version of the receptor was running with a slightly higher

apparent MW which is due to the V5-His tag that adds approx 3.5 kDa in molecular mass. It seems that the P2X7R-V5-His variant is expressed at a slightly higher level than wild-type receptor. The increased signal intensity for P2X7R-V5-His was not due to loading differences as β-tubulin levels were equivalent in lysates from P2X7R or P2X7R-V5-His expressing cells (Fig. 5.2C, P2X7R staining, left membrane). Staining with anti-V5 antibodies was only positive for P2X7R-V5-His cells and recognized a protein band of the same band as the anti-P2X7R antibodies (Fig. 5.2C, V5 staining, right membrane).

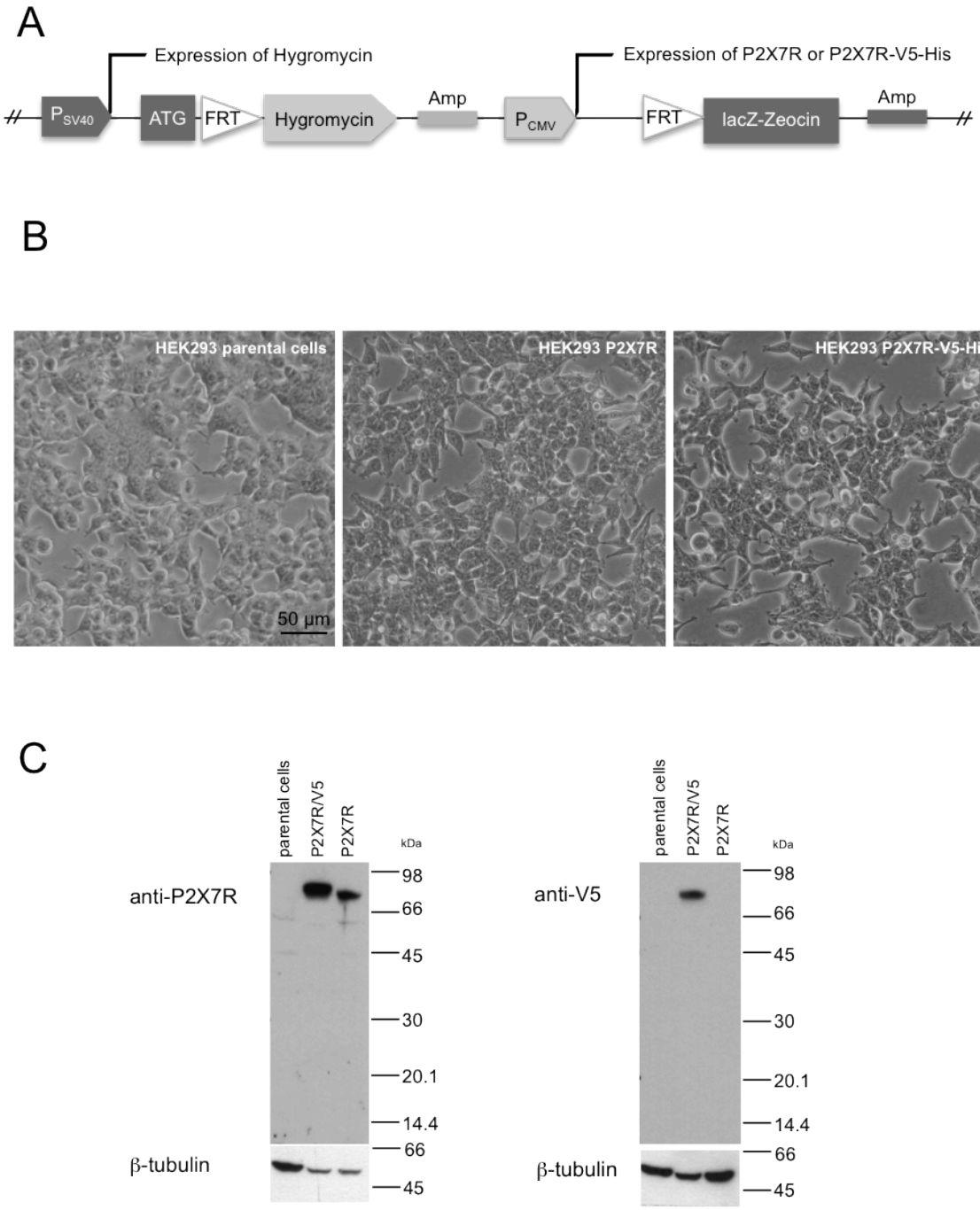

Fig. 5.2 Cells stably transfected with P2X7R. A: Schematic representation of the integrated P2X7R and P2X7R-V5-His expression constructs after homologus recombination between FRT sites mediated by Flp recombinase. Expression of Hygromycin gene will only occur after correct integration of construct into the Flp site as Hygromycin gene lacks the promoter and the ATG initiation codon. **B:** HEK293 Flp-In cells (parental cells) were transfected with pOG44 vector encoding Flp recombinase and P2X7R or P2X7R-V5-His constructs using DNA from 2 different bacterial clones. Cells were growing for 2 weeks in the presence of 100 µg/ml Hygromycin B. Pictures show morphology of parental cells and cells stably expressing P2X7R or P2X7R-V5-His. **C:** Established HEK293 cell lines expressing P2X7R or P2X7R-V5-His and parental cells were seeded in a 6-well plate. After 24h, cells were lysed with extraction buffer containing 20 mM HEPES, pH 7.4, 150 mM NaCl, 1 mM EGTA, 1% Triton X-100, 0.25% Deoxycholic acid, 10% glycerol, 1 mM PMSF and 1 mM NEM. 25 µg of protein extract per lane was separated on a 4-20% SDS polyacrylamide gel under reducing conditions followed by Western blotting. Nitrocellulose membrane was stained with anti-P2X7R (left) or anti-V5 antibodies (right). Membrane was then re-probed with anti-β-tubulin antibodies to confirm equal protein loading. Migration of the LMW protein standard is indicated on the right.

5.2.3 Accessing functionality of transgene in HEK293 cells

5.2.3.1 P2X7R immunolocalization

The Western blotting experiment confirmed that P2X7R is expressed in both established cell lines. However, it was now important to confirm that the P2X7R is trafficked to the cell surface. Therefore, cells were analyzed by immunolocalization to study P2X7R expression pattern. HEK293 parental and P2X7R overexpressing cells were permeabilized and stained with anti-P2X7R and whereas P2X7R-V5-His cells were stained with anti-V5 antibodies to investigate P2X7R localization. Fluorescent labelling with secondary antibodies confirmed that in both P2X7R and P2X7R-V5-His cell types P2X7R was detectable in the plasma membrane and absent from the parental cells (Fig. 5.3A). Detection of a fluorescent signal in the nucleus with anti-P2X7R antibodies was not considered specific as it was also detected in parental cells, which do not express P2X7R and which were negative for the P2X7R membrane staining (Fig. 5.3A, top panel). Wild-type and V5- tagged receptor levels in the cell membrane were comparable suggesting that the tag does not interfere with receptor trafficking. Then P2X7R and P2X7R-V5-His cells were analyzed by immunolocalization to examine if P2X7R and the V5-tag co-localize in P2X7R-V5-His cells. When anti-P2X7R and anti-V5 antibodies were used simultaneously the co-localization of the staining could be detected in cells expressing P2X7R-V5-His but not in those expressing P2X7R as expected (Fig. 5.3B).

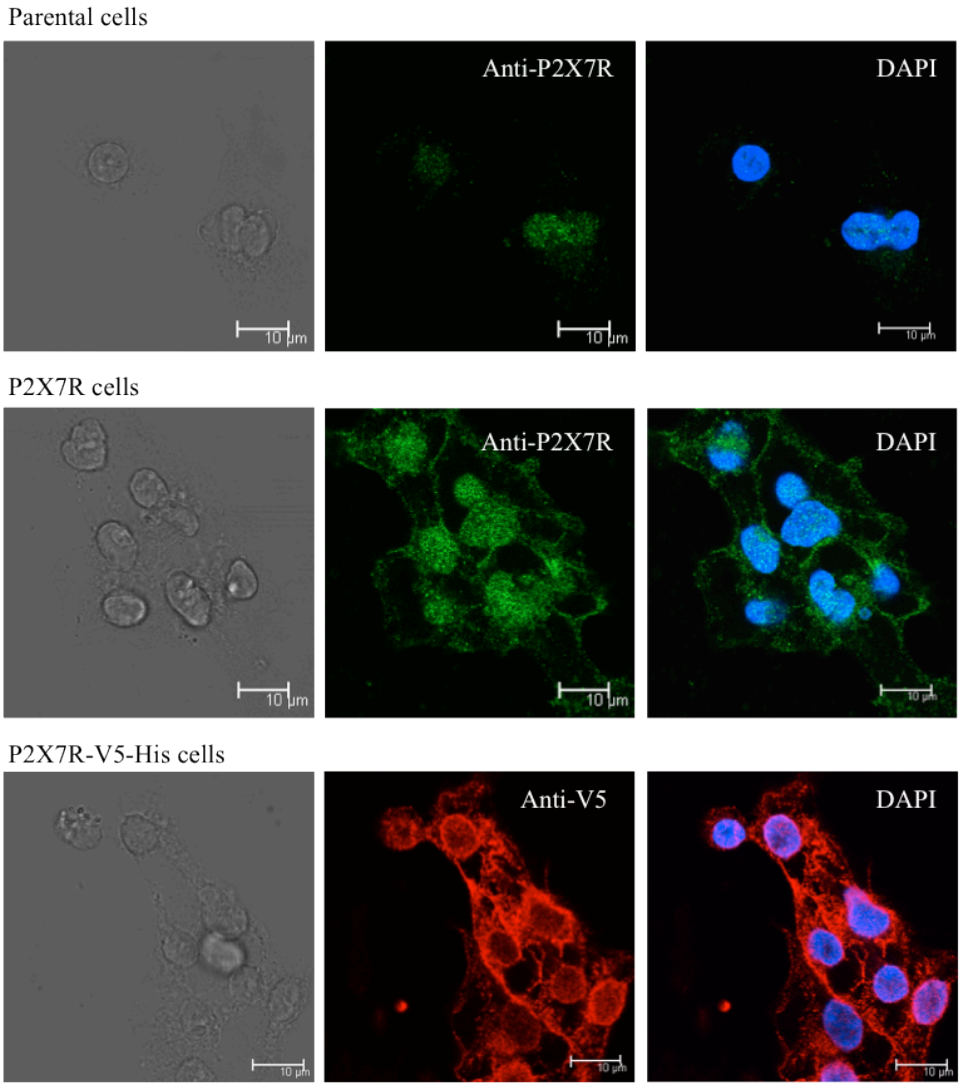

Fig. 5.3A Immunolocalization of P2X7R in HEK293 cell lines. Parental cells and P2X7R and P2X7R-V5-His stably transfected cells were seeded on glass coverslips coated with poly-L-lysine. Cells were fixed with PFA and permeabilized with Triton-X-100 before staining with anti-P2X7R that recognizes the intracellular C-terminal sequence or anti-V5 antibodies. Alexa Fluor 488 (P2X7R, green) or Alexa Fluor 594 (V5, red) secondary antibodies were used. Mounting medium with dapi stain was used to visuallize the nucleus. Images represent an optical section acquired by confocal microscopy.

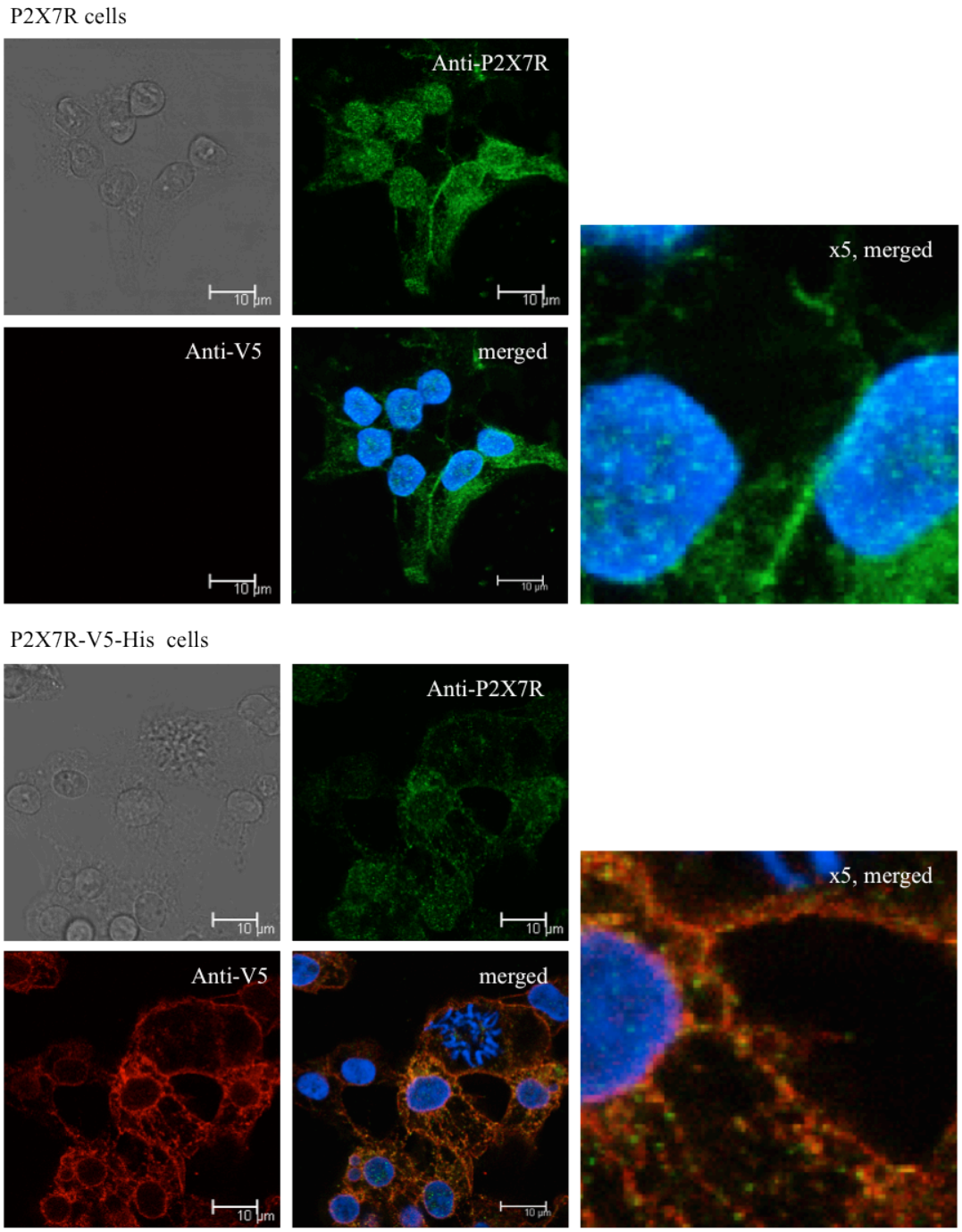

Fig. 5.3B Immunolocalization of P2X7R in HEK293 cell lines (continued). In order to confirm P2X7R and V5 colocalization, the cells were co-stained with anti-P2X7R or anti-V5 antibodies simutaneously followed by addition of Alexa Fluor 488 (green) or Alexa Fluor 594 (red) secondary antibodies to detect the respective primary antibodies. Mounting medium with dapi stain was used to visuallize the nucleus. Images represent an optical section acquired by confocal microscopy. Yellow colour in merged images identify colocalization.

5.2.3.2 ADAM activation by P2X7R

Once cell surface P2X7R expression was confirmed it was important to investigate functionality of the receptor in the cell membrane. For this purpose, a shedding assay was selected based on the knowledge that stimulation of P2X7R activates ADAM-10 metalloproteinases in the cell membrane (Le Gall et al. 2009). The release of functional EGFR ligands from the precursor proteins by ADAM10 can be easily monitored. Amphiregulin tagged with alkaline phosphatase (AR-AP) was used as an ADAM substrate to monitor ADAM activity. The presence of AP activity in the conditioned medium will indicate that ADAM-dependent cleavage occurred. Therefore, the stimulation of P2X7R with agonists should result in enhanced release of AP and its activity in the conditioned medium (Fig. 5.4A). Parental cells, P2X7R and P2X7R-V5-His were transiently transfected with an AR-AP construct and after 48h, stimulated with 1 mM ATP or 300 μM BzATP for 30 min in physiological salt solution (PSS). BzATP is an ATP analogue that shows a high degree of selectivity for P2X7R and is not a ligand for P2Y receptors (Coddou et al. 2011). Cells from both established cell lines (P2X7R and P2X7R-V5-His) showed increased levels of AP activity present in the conditioned medium after agonist treatment, suggesting that P2X7R activation is able to induces ADAM-mediated cleavage of AR-AP (Fig. 5.4B and C). Parental cells were unable to respond to 300 μM BzATP and only a negligible increase in the AP activity was detectable after challenge with 1 mM ATP (Fig. 5.4B and C). Throughout the experiments a similar trend of relative AR-AP shedding activity after agonist addition was observed. However, the absolute AP activity was greatly variable between transfections of the stable cell lines between different experiments, which was possibly due to differences in transfection efficiency and made it difficult to clearly compare the P2X7R and P2X7R-V5-His response (Fig. 5.4B and C). Moreover, the cell stimulation was performed in the PSS buffer that contains 2 mM Ca^{2+} and consequently the P2X7R activation might not be maximal. Therefore, a second approach was used to investigate AR-AP shedding. To have more equal concentration of P2X7R and AR-AP reporter a co-transfection of parental HEK293 cells with P2X7R or P2X7R-V5-His constructs together with AR-AP was performed. Additionally, cell stimulation was performed in OptiMEM that contains 0.9 mM Ca^{2+}, which should enhance P2X7R response to agonists. The co-

transfection experiments were reproducible and clearly confirmed that wild-type P2X7R and P2X7R-V5-His are functional. In both cases the addition of 300 μM BzATP for 30 min lead to a dramatic, approximately 20-fold for P2X7R and 17-fold for P2X7R-V5-His increase in AR-AP shedding over the unstimulated control (Fig. 5 4D and E). Stimulation of cells with 1 mM ATP was also able to significantly induce AR-AP shedding in cells expressing wild-type receptor (approx. 13-fold). In this case, the activation of cells expressing P2X7R-V5-His was 5 fold different to control but the difference did not reached statistical significance (Fig. 5.4D and E). These data confirm that trends observed in the stable cell lines and indicate that ADAM activation is increased in P2X7R cells when compared to P2X7R-V5-His although both support ADAM activation to a degree.

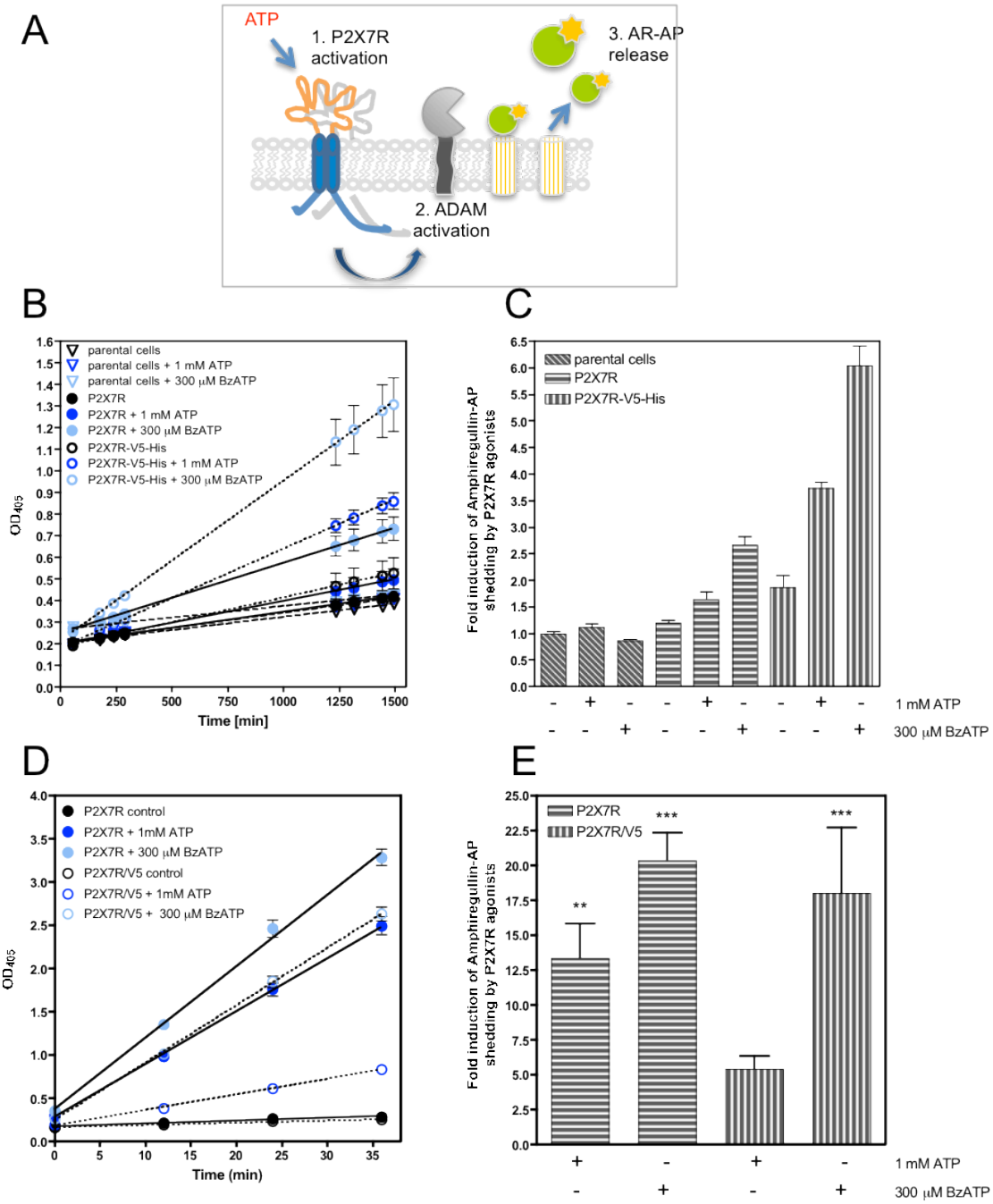

Fig. 5.4 Testing receptor functionality: Amphiregulin-AP shedding induced by P2X7R agonists. **A:** Schematic representation of the ADAM-dependent cleavage of AR-AP ectodomain from the cell surface upon P2X7R activation. 1: P2X7R ligand binding, 2: P2X7R triggered intracellular signalling activating ADAM sheddase, 3: ADAM-mediated processing of AR-AP to release ectodomain (AP = alkaline phosphatase) **B,C:** Parental, P2X7R or P2X7R-V5-His cells transiently transfected with AR-AP were treated for 30 min with 1 mM ATP or 300 µM BzATP in PSS. Conditioned medium was collected and assessed for alkaline phosphatase activity. Substrate conversion was monitored for 24 h and analyzed by linear regression to determine AP activity. The graph B shows the result from one representative experiment with four experimental repeats ± SEM. Graph C shows the mean value of the slope (± 95 % confidence interval) relative to untreated parental cells. **D, E:** Parental cells were transiently co-transfected with P2X7R or P2X7R-V5-His constructs and AR-AP. After 2 days cells were treated for 30 min with 1 mM ATP or 300 µM BzATP in OptiMEM. Conditioned medium was collected and assessed for alkaline phosphatase activity as above. The graph D shows the result from one represetnative experiment with four experimental repeats ± SEM. Graph E shows the mean value of the slope ± SEM expressed relative to respective untreated cells and represent results from three independent experiments (** $p<0.01$, *** $p<0.001$).

5.2.3.3 Changes in intracellular calcium

In order to assess if P2X7R activation leads to Ca^{2+} influx in the established P2X7R cell line, changes in intracellular Ca^{2+} concentrations upon ATP and BzATP application were investigated. Fluo-4 calcium indicator was used to monitor the intracellular free [Ca^{2+}] concentrations. Parental cells and cells stably expressing wild-type P2X7R were loaded with Fluo-4 indicator and then stimulated with the agonists to observe fluorescence transients using confocal microscopy. An increase in fluorescence, representing a rise in intracellular [Ca^{2+}] was observed within seconds of agonist application and was much more pronounced in cells expressing the P2X7R receptor (Fig. 5.5 and 6). Moreover, in cells overexpressing P2X7R, the increase in intracellular Ca^{2+} concentration upon 1 mM ATP (Fig. 5.5 and 7A) or 100 μM BzATP application (Fig. 5.6 and 7C) was followed by fast and extensive cell blebbing (within 30 s). The P2X7R overexpressing cells were able to respond to both agonists in a similar way but the response to 100 μM BzATP was stronger and lead to sustained calcium influx that was maintained even up to 10 min as long as agonist was present. High intracellular Ca^{2+} levels only returned to baseline when BzATP was washed away. 10 μM BzATP application was tested as well but failed to induce sustained Ca^{2+} influx or cell blebbing (data not shown). Stimulation of parental cells with 1 mM ATP induced smaller and transient oscillations in intracellular Ca^{2+} that returned to baseline levels after a few minutes (Fig. 5.5 and 7A). It was speculated that this response reflects activation of P2Y receptors in HEK293 cells. In agreement with this, treatment with 100 μM BzATP was unable to cause a similar response (Fig. 5.6 and 7B).

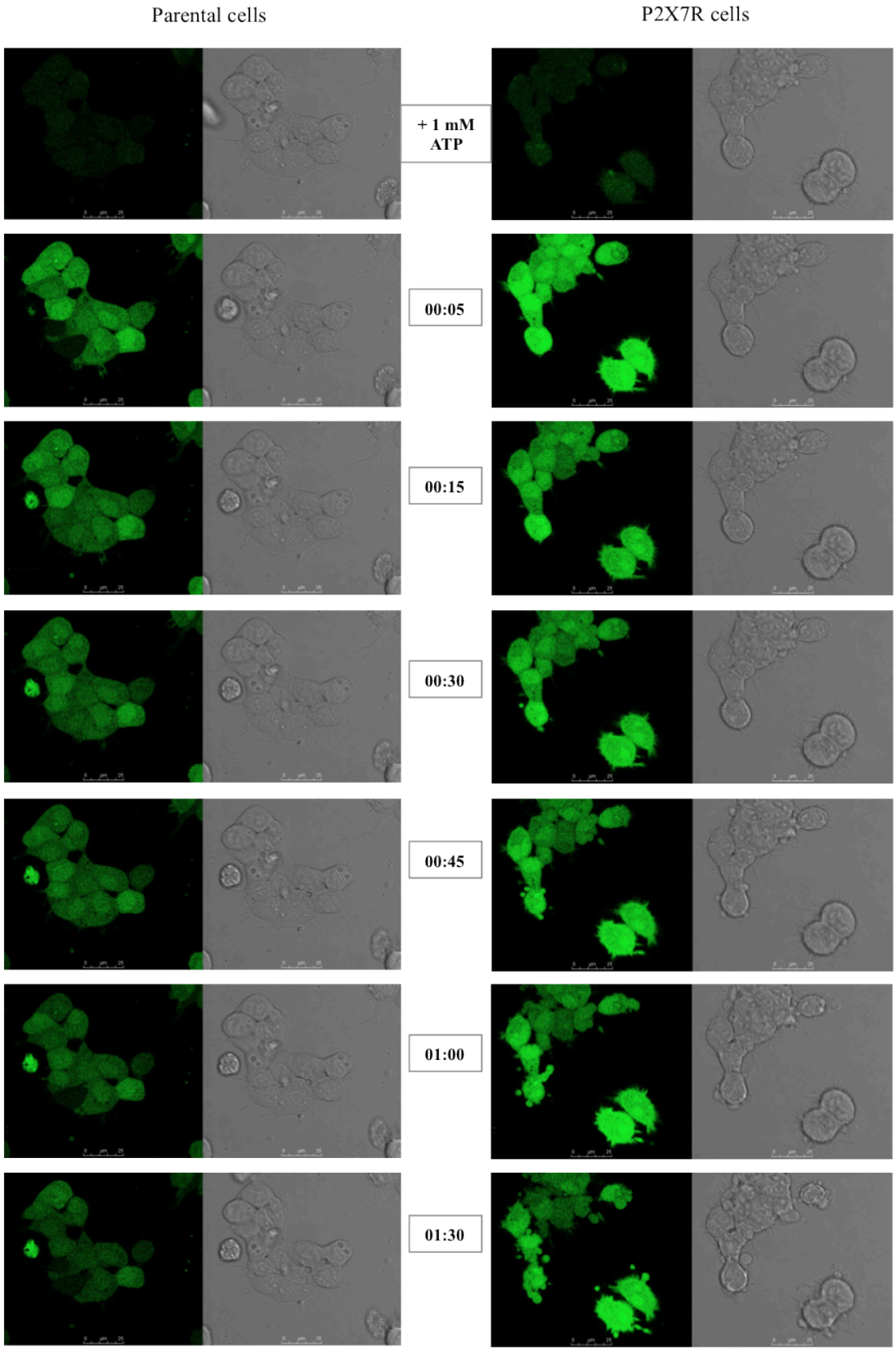

Fig. 5.5 Testing receptor functionality: changes in intracellular Ca^{2+} concentrations. Parental cells and cells stably expressing wild-type P2X7R were incubated with 3 µM Fluo-4 calcium indicator in OptiMEM for 20 min and thereafter stimulated with 1 mM ATP. Changes in fluorescence were monitored for up to 10 min using confocal microscopy. Time after stimulation is given in the middle column in minutes. Pictures represent an optical section acquired by confocal microscopy. Data shown is representative for two independent experiments. The bar size is 25 µm.

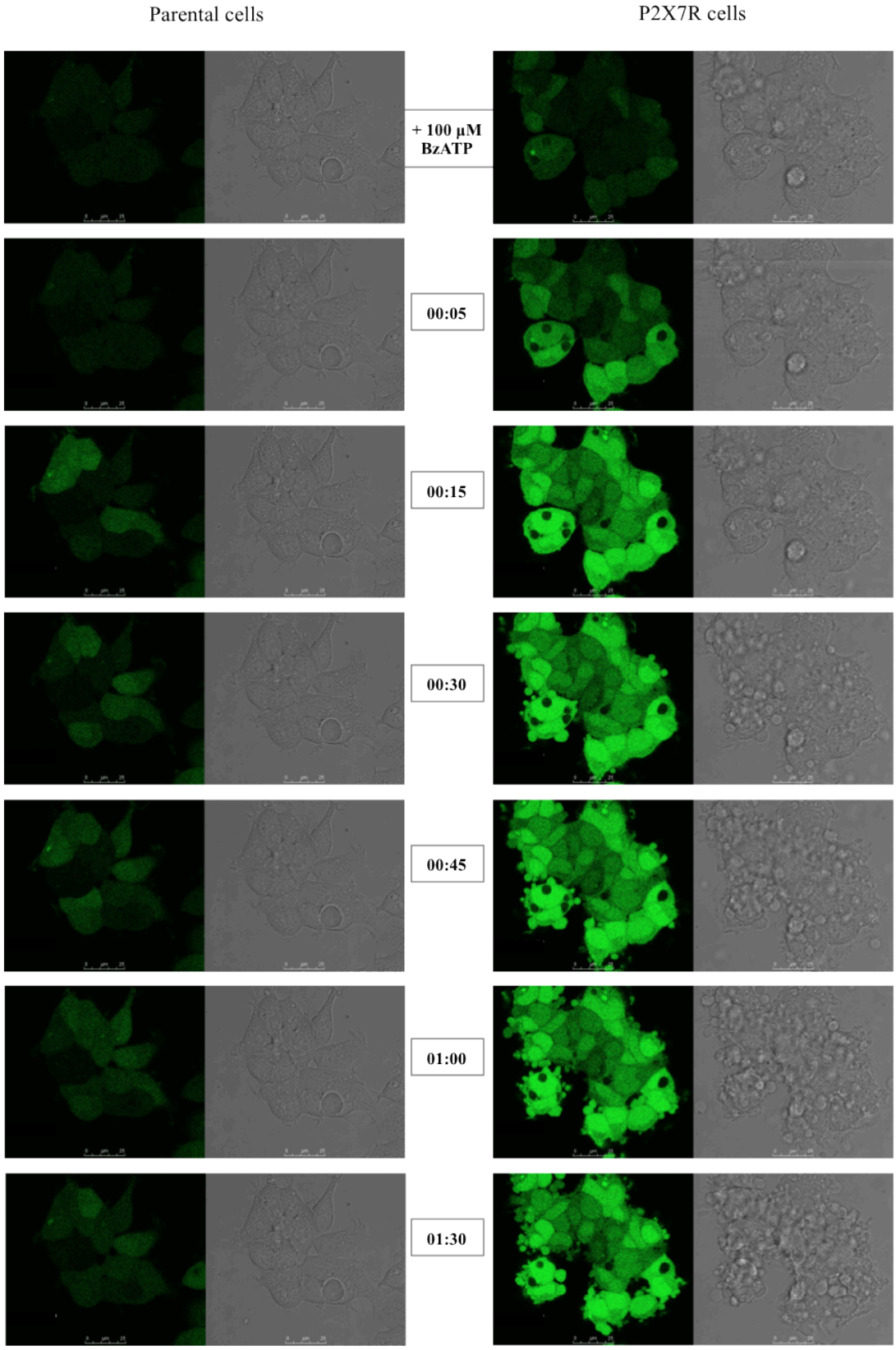

Fig. 5.6 Testing receptor functionality: changes in intracellular Ca^{2+} concentrations. Parental cells and cells stably expressing wild-type P2X7R were incubated with 3 µM Fluo-4 calcium indicator in OptiMEM for 20 min and thereafter stimulated with 100 µM BzATP. Changes in fluorescence were monitored for up to 10 min using confocal microscopy. Time after stimulation is given in the middle column in minutes. Pictures represent an optical section acquired by confocal microscopy. Data shown is representative for two independent experiments. The bar size is 25 µm.

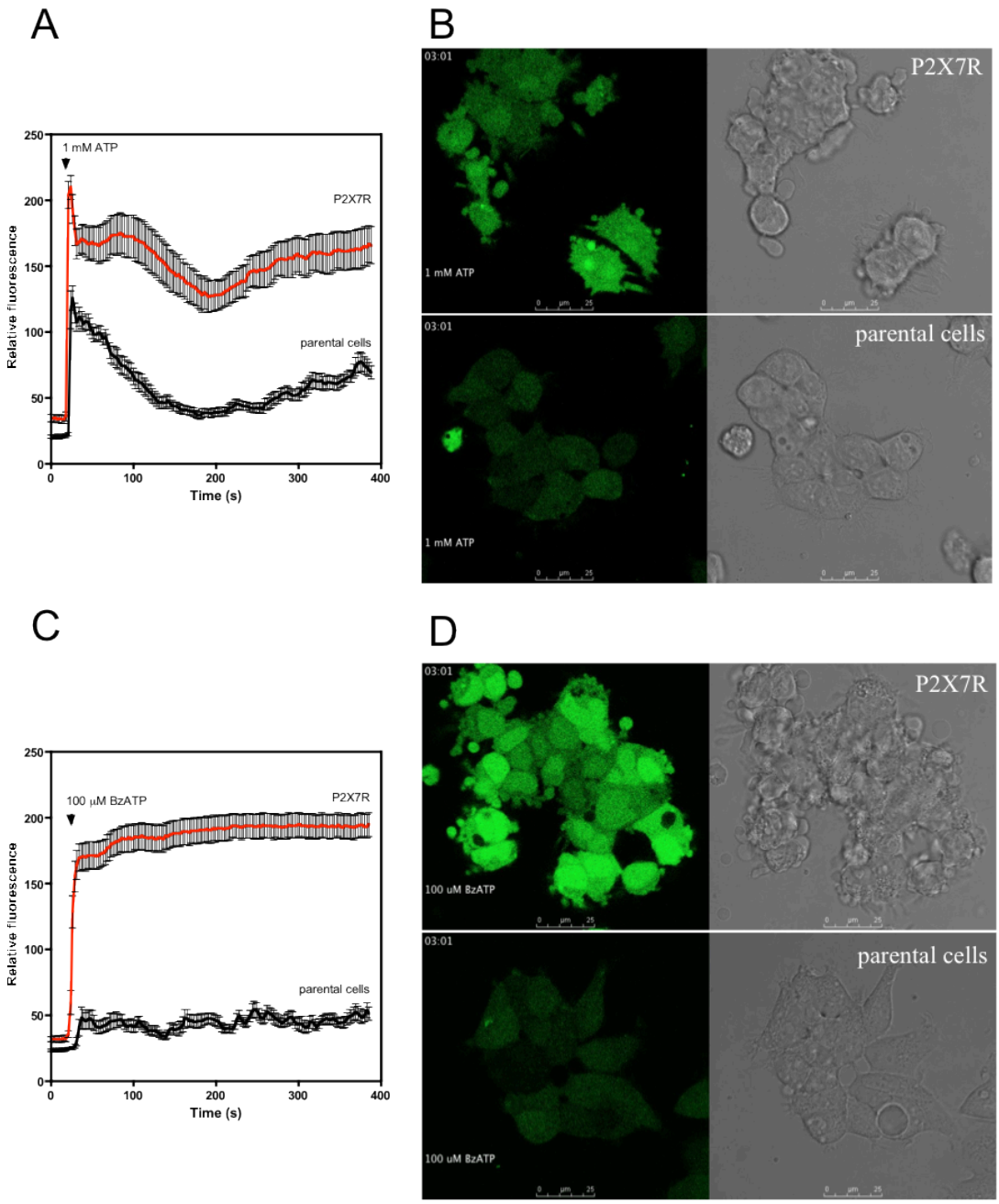

Fig. 5.7 Comparison of intracellular Ca^{2+} changes in HEK293 cells that are negative or positive for P2X7R. **A,C:** The graphs represent changes in Fluo-4 fluorescence upon application of ATP or BzATP. Line represent mean fluorescence values ± SEM from a representative experiment (ATP, n=8; BzATP, n=12 cells). **B,D:** Pictures show changes in Fluo-4 fluorescence and cell morphology of parental cells and cells stably expressing P2X7R 3 min post stimulation with 1 mM ATP (B) or 100 µM BzATP (D). Images represent an optical section acquired by confocal microscopy. The bar size is 25 µm.

In order to further confirm that changes in [Ca^{2+}] and cell blebbing were induced by P2X7R and not other changes in transfected cells, a potent and competitive inhibitor of P2X7R (A740003) was used. This inhibitor was shown to be highly selective as it blocks intracellular Ca^{2+} signaling, pore formation and IL-1β release (in monocytes differentiated into macrophages) (Honore et al. 2006). Cells were loaded with Fluo-4 indicator in the presence of P2X7R inhibitor and stimulated with BzATP as described previously. Preincubation of cells with 5 μM inhibitor followed by stimulation in its presence completely blocked intracellular Ca^{2+} spikes after addition of BzATP agonist (Fig. 5.8). Furthermore, P2X7R inhibitor treatment also inhibited cell membrane blebbing. The sensitivity to BzATP was partially restored after removing the inhibitor from the cells demonstrating reversibility but the response was markedly reduced (Fig. 5.8 A and C). Collectively, this demonstrates that BzATP induces a rise in [Ca^{2+}] and membrane reorganization via P2X7R activation in HEK293 P2X7R cells.

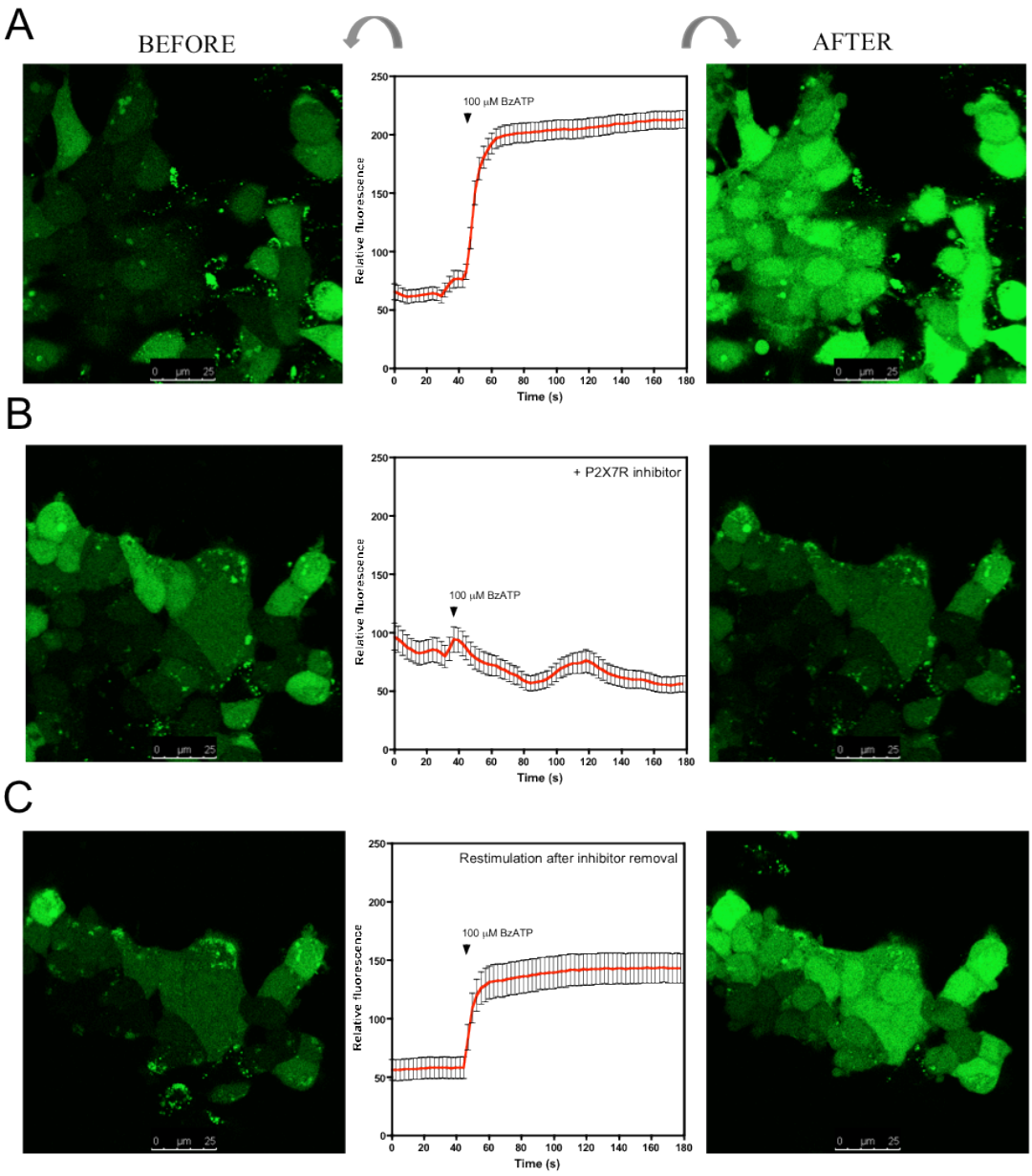

Fig. 5.8 Demonstrating specificity of Ca^{2+} response with P2X7R inhibitor. A: Cells stably expressing P2X7R were incubated with 3 µM Fluo-4 calcium indicator for 20 min in OptiMEM. Changes in intracellular Ca^{2+} concentrations were subsequently monitored upon 100 µM BzATP application. **B:** Cells were preloaded with 3 µM Fluo-4 for 20 min in the presence of 5 µM A740003 P2X7R inhibitor and then stimulated with 100 µM BzATP in the presence of 5 µM A740003. **C:** Cells from the same optical field as shown in B were washed once to remove the inhibitor and left for 10 min in fresh medium. Then the addition of 100 µM BzATP was repeated. Images represent an optical section acquired by confocal microscopy taken before (0 s) and after (180 s) agonist addition. Graphs represent mean value of Fluo-4 fluorescence ± SEM measured in a representative experiment (n = 30). The bar size is 25 µm.

5.2.3.4 BzATP dose response measured by changes in intracellular Ca^{2+}

A BzATP dose response of in HEK293 P2X7R cells was determined by measuring intracellular [Ca^{2+}] signaling as readout for P2X7R activation using a plate reader format (Fig. 5.9). Cells were loaded with Fluo-4 Ca^{2+} indicator as described previously and the change in fluorescence was measured after automated injection of different concentrations of BzATP (9 - 300 μM range). At concentrations lower than 13 μM, intracellular [Ca^{2+}] increase was not detected. When the BzATP concentration was close to the apparent K_d (< 50 μM), the cell response was quite variable between individual wells probably due to the fact that a specific threshold needs to be reached for membrane depolarization and allowing Ca^{2+} entry. This is illustrated in Fig. 5.9A, which shows the response obtained from 8 replicate wells in a single experiment that were treated with either 200 or 40 μM BzATP concentration. The variable response between each well can be caused by a small difference in cells responding, the delay in response of some cells or unequal cell loading with the Fluo-4 indicator. Nevertheless, there was a clear dose-dependence in the response, both in terms of the number of wells that responded and the magnitude of the signal. Given the variability, a larger number of repeats was performed in each experiment to obtain acceptable results (n=8 wells). The data analysis were performed without excluding any repeat. Therefore no response was also considered as valid result. As intracellular [Ca^{2+}] increase is only an indirect measure for P2X7R activation and is regulated through many different pathways within the cell, only the first 10s of the Ca^{2+} influx were considered. Those data should most accurately represent ligand binding to the receptor that directly triggers a rapid increase in Ca^{2+} influx without interference from subsequent cell response. Each curve was analyzed by fitting the data initially with first order kinetics to estimate the value for a shared constant C. This analysis was done to perform the baseline correction of data set obtained in each experiment. Then the data were fitted with a second order kinetics equation in order to determine the Y_{max} (maximal fluorescence) for specific BzATP concentrations (Fig. 5.9B). The obtained Y_{max} was then plotted against the BzATP concentrations to estimate the minimal effective BzATP dose required for P2X7R activation as measured by Ca^{2+} influx. The 100 μM BzATP concentration, which was used in the previous experiments was able to

induce an intracellular [Ca^{2+}] spike that was close to maximal P2X7R activation (Fig. 5.9C, dashed green line). Thus, this BzATP concentration was used in Chapter 6 and 7, where TG2 release was investigated. Additionally, the K_d for BzATP binding to P2X7R was estimated at approx. 80 μM. This is in line with literature data, which report EC_{50} from 40 to 100 μM BzATP concentration measured as the peak current using P2X7R expressed in HEK293 cells in the presence of 0.3 and 2 mM extracellular Ca^{2+}, respectively (Rassendren et al. 1997).

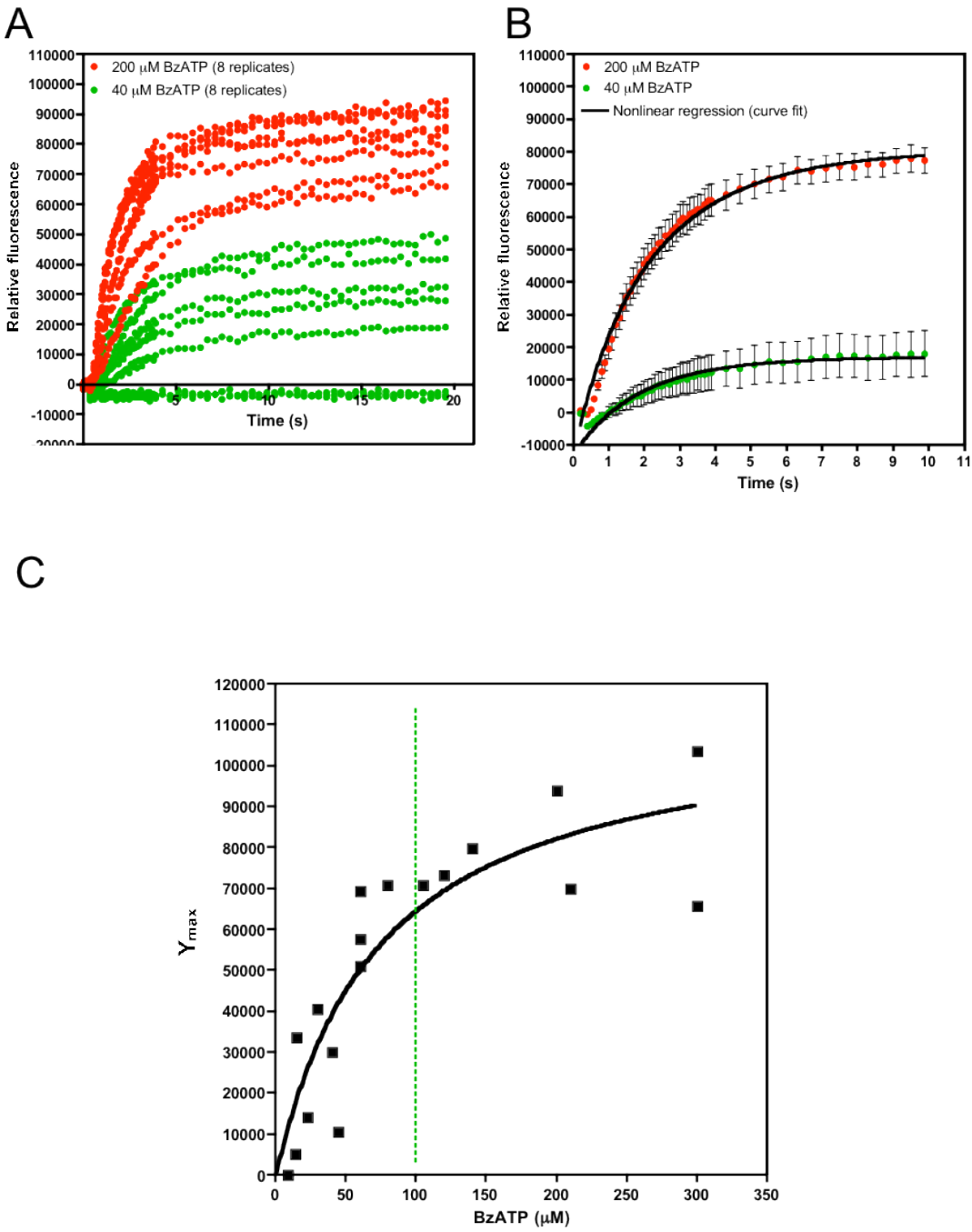

Fig. 5.9 Dose response of HEK293 P2X7R cells to BzATP application as measured by changes in intracellular Ca^{2+} concentrations. A, B: Cells stably expressing wild-type P2X7R were incubated with 3 µM Fluo-4 in OptiMEM for 20 min and after medium change stimulated with various concentrations of BzATP in OptiMEM (9 – 300 µM). Note, concentrations <13 µM were unable to elicit Ca^{2+} responses. Baseline fluorescence was monitored for 5s followed by automated injection of different concentrations of BzATP. Graph shows the changes in fluorescence upon 200 and 40 µM BzATP injection into eight replicate wells of one representative experiment. For each curve, the baseline fluorescence before injection and the fluorescence of the control curve (OptiMEM injection) was subtracted (**A**) Changes in fluorescence intensity during initial 10 s post injection were used for analysis. Data was fitted using the second order kinetics equation as outlined in details in Materials and Methods to derive Y_{max} value for specific concentration of BzATP (**B**). **C:** Y_{max} values obtained in five independent measurements (each performed using eight experimental repeats) was plotted against BzATP concentrations tested. Data were fitted using a one site binding function: $y = B_{max} * x / (K_d + x)$. Each P2X7R subunit binds one ATP molecule and hence P2X7R mediated channel function is related to 1:1 binding event in a simple approximation. Green dashed line represents 100 µM BzATP concentration, which was selected for subsequent experiments.

5.3 Discussion

Two HEK293 cell lines stably expressing human P2X7R were established: cells that express wild-type P2X7R and cells with P2X7R containing a V5-His tag carboxy terminal. Western blotting using anti-V5 antibodies and anti-P2X7R antibodies confirmed the expression of P2X7R in both established cell lines. Moreover, staining the V5 tag on P2X7R with anti-V5 antibodies was helpful to confirm the specificity of anti-P2X7R antibodies. Thus, the anti-P2X7R antibodies were subsequently used to investigate P2X7R expression by immunocytochemistry. Both, wild-type and V5 tagged receptor were expressed in the cell membrane as demonstrated by colocalization studies using confocal microscopy. This indicates that the wild-type P2X7R and V5 variant are properly trafficked to the cell surface. The observed P2X7R expression pattern is in agreement with data in the literature where cells transfected with rat P2X7R expressed it in the lipid bilayer, with some staining for P2X7R also detected in the cytosolic compartment (Smart et al. 2002; Wilson et al. 2002).

Functionality of the P2X7R in the membrane of HEK293 cells was initially confirmed using the shedding assay. Cells which co-express AR-AP and P2X7R or the V5-tagged version of P2X7R showed a significant increase of alkaline phosphatase activity in the conditioned medium following agonist stimulation. The cleavage of AR-AP ectodomain is likely mediated by members of ADAMs family (a disintegrin and metalloprotease proteins), which are membrane proteineses responsible for cleaving the ectodomains of growth factors, cytokines or receptors (Blobel 2005; Murphy 2008). ADAM-10 and ADAM-17 are metalloproteinases expressed in HEK293 cells (Ali and Knaüper 2007) and the literature suggests that ADAM-17 is the main one responsible for releasing the AR-AP domain because it regulates shedding of a number of EGFR ligands including AR (Murphy 2008). On the other hand, it has previously been shown that cleavage of Betacellulin from the surface of CHO cells endogenously expressing P2X7R is potentiated upon 300 μM BzATP addition and that this is due to ADAM-10 activation (Le Gall et al. 2009). It is more likely that ADAM-10 regulates AR-AP shedding in my experiments as it is activated by Ca^{2+} influx (Horiuchi et al. 2007), which is one of the consequences of P2X7R channel function (North 2002). Further experiments would be required to determine the relative contribution of different ADAMs to shedding as this was

outside the main focus of the PhD the involvement of ADAMs sheddases was not further investigated. The higher increase in shedding induced by BzATP in comparison to ATP likely relates to the fact that BzATP is an approx 10-fold better agonist than ATP to activate P2X7R (Rassendren et al. 1997). The reduced response of P2X7R-V5-His cells to ATP when compared with cells expressing wild-type receptor may result from reduced activity of the receptor due to the attachment of the V5-His tag. This is possible even when the surface expression between established cell lines was comparable. The approach to introduce a tag on the C-terminus was successfully used in the past and P2X7R with FLAG or HA epitope showed comparable functional properties as the wild-type receptor (Torres et al. 1999). On the other hand, it was also reported that an EGFP tag on the C- but not on the N-terminus of P2X7 required higher concentrations of the ATP-dose response as C-terminal EGFP alters ion transduction through the channel (Smart et al. 2002; A Morelli et al. 2003). In order to exclude a possible effect of the V5-His-tag on receptor function, the cells expressing wild-type receptor were used for further experiments.

P2X7R activity in the membrane of HEK293 was additionally investigated using calcium imaging. In the established HEK293 P2X7R cell model, application of 1 mM ATP or 100 μM BzATP caused sustained high intracellular Ca^{2+} levels that were followed by cell blebbing characteristic for P2X7R mediated cell responses. These results are in agreement with previous reports, which show that stimulation of HEK293 cells expressing homomeric rat P2X7R with 30 μM BzATP causes massive membrane blebbing after appox. 1 min of agonist addition (Virginio et al. 1999) and that addition of BzATP at a concentration of 100 μM causes sustained increase in intracellular calcium (Wilson et al. 2002). Elevation of intracellular Ca^{2+} concentration is an effect of Ca^{2+} influx through the open channel. However, the release of Ca^{2+} from intracellular stores as a part of the response cannot be ruled out and might contribute to the overall fluorescence signal measured. P2X7R activation is known to also cause intramitochondrial Ca^{2+} increase and swelling (Mackenzie et al. 2005). The spike in intracellular Ca^{2+} observed in parental cells upon 1 mM ATP application is likely due to activation of P2YR as P2Y1 and P2Y2 receptors are constitutively expressed in HEK293 cells and their maximal activation can occur at 100 μM ATP concentration (Schachter et al. 1997). The P2YR response is however

distinct from P2X7R activation and does not involve sustained Ca^{2+} influx but is caused by release of Ca^{2+} from intracellular stores and therefore displays rather fast desensitization kinetics, that do not correlate with cell blebbing (Smart et al. 2002; Wilson et al. 2002; Stokes et al. 2006). Application of 100 μM BzATP was not able to evoke the same intracellular Ca^{2+} spike in parental cells, which is consistent with the literature (Stokes et al. 2006). Therefore, with BzATP as an agonist, a significant P2Y response can be excluded (Jacobson et al. 2002; Coddou et al. 2011). According to the literature, the EC_{50} value for ATP and BzATP varies from 100-720 and 20-55 μM, respectively, depending on the levels of Ca^{2+} present in the external solution, using human P2X7R expressed in HEK293 cells (Stokes et al. 2006; Jarvis and Khakh 2009). In our system, the cells were stimulated in the presence of OptiMEM that contains 0.9 mM Ca^{2+} and therefore 1 mM ATP and 100 μM BzATP induced a response close to maximal receptor activation. Those concentrations of agonists were used throughout further experiments.

Chapter 6 TG2 externalization upon P2X7R activation

6.1 Introduction

In the previous chapter the conditions for optimal P2X7R activation in the HEK293 cell model were determined. Cells overexpressing P2X7R were able to open a membrane channel that allows Ca^{2+} influx and were forming plasma membrane vesicles in the presence of P2X7R agonists, hence showed the classical response to P2X7R activation. I was therefore now in a position to investigate whether P2X7R-activation has an effect on TG2 externalization. Thus, the purpose of this chapter was to examine the mechanism of TG2 secretion in analogy to P2X7R-dependent IL-1β release, although IL-1β secretion requires inflammasome assembly (Dinarello 2009; Dubyak 2012). If a functional inflammasome is required for TG2 release, then further components such as CARD domain proteins would need to be introduced into P2X7R HEK293 cells, as previously shown for human fibroblasts lacking CARD domain of Nlrp1 inflammasome complex (Liao and Mogridge 2009). Soluble IL-1β was shown to be directly secreted into conditioned medium by various cell types (Brough and Rothwell 2007; Dinarello 2009). Several alternative pathways for its secretion have been proposed that might participate in generating extracellular active cytokine. The first model proposes that IL-1β secretion is due to shedding of microvesicles filled with pro- and mature IL-1β from a specific site of the plasma membrane (MacKenzie et al. 2001). The second hypothesis suggests exosomes as the main pathway for rapid IL-1β release (Qu et al. 2007). The third model suggests IL-1β processing in the lysosomal compartment from which it is secreted by membrane fusion and exocytosis (Cristina Andrei et al. 2004; Bianco et al. 2005). Also, some recent reports are indicating participation of autophagy-dependent release as another way for IL-1β secretion (Deretic et al. 2012). Recent hypothesis on non-conventional TG2 export from the cells involves its association with microvesicles (Antonyak et al. 2011) or microparticles (van den Akker et al. 2011). Therefore, it was important to test whether P2X7R-mediated vesicle shedding leads to TG2 externalization in established HEK293 P2X7R cells.

The field of microvesicles and exosomes is growing fast. For a long time as these cell structures were considered an artifact, cell debris or necrotic cell bodies but

they are now thought to have specific roles in various biological processes (Al-nedawi et al. 2009; Cocucci et al. 2009). Small cytoplasmic protrusions eventually shed as small vesicles can carry receptors, signaling molecules, cytoskeletal proteins and consequently they are involved in surface-membrane trafficking, transfer of proteins and mRNA, coagulation cascade mediators released by platelets, release of cytokines during inflammation or tumor metastasis and cell transformation. The nomenclature is not yet well established in the literature and there are many terms to describe those small membrane-bound particles (Burnier et al. 2009; Al-nedawi et al. 2009). The term "shedding vesicles", "microvesicles" (MVs) or "microparticles" (MPs) is used to describe 100-1000 nm diameter vesicles that directly bleb from the membrane of viable cells (Al-nedawi et al. 2009; Cocucci et al. 2009). The term "microparticle" (MPs) is generally a more cell type specific term as it defines the particles shed from activated blood cells or vascular endothelial cells that can be found circulating in blood (Piccin et al. 2007). Clearly, this process is actively controlled by cells and occurs in response to specific signals. MVs and MPs originate from specific cells and consequently carry certain antigens on their surface (Burnier et al. 2009). They usually contain lipid raft proteins (flotillin-1, tissue factors, lineage markers or receptors e.g. EGFR) (Al-nedawi et al. 2009). They are usually formed due to phospholipid bi-layer re-arrangements. In this process enzymes such as calpain, flippase, floppase, aminophospholipid translocase and acidic sphingomyelinase are taking an active part. Their activation leads to flipping of phospholipids and cytoskeletal changes that allow blebbing of newly formed MVs. In contrast, the term "exosomes" relates to a smaller type of membrane vesicles, these are 40-100 nm in size and are retained inside the multivesicular bodies of the endosomal system (MVBs) (Al-nedawi et al. 2009; Cocucci et al. 2009). They are transported via the endosomal sorting complexes as early endosomes and might be released from MVBs to the extracellular space upon cell stimulation. Those small vesicles are considered to be more specialized and carry slightly different cargo than MVs or MPs (HSP70, CD63, mRNA). Both, microvesicles and exosomes have been suggested to be involved in the non-conventional release of specific proteins that lack a signal sequence for ER import and hence are candidate mechanisms for TG2 externalization.

The aims of the chapter:

1. Investigate if P2X7R by itself is sufficient to enable agonist-mediated TG2 externalization?
2. Investigate if P2X7R activation leads to re-distribution of intracellular TG2?
3. Examine if TG2 is externalized via microvesicle shedding?

6.2 Results

6.2.1 Time-dependent release of TG2 into the medium upon P2X7R activation

The purpose of this study was to investigate if HEK293 cells stably expressing functional P2X7R are able to secrete TG2 into the conditioned medium during or after P2X7R activation. As HEK293 lack endogenous TG2 expression, cells were transiently transfected with wild-type TG2 and then stimulated in the presence or absence of the potent and selective P2X7R agonist BzATP. As 100 μM BzATP was sufficient to fully activate P2X7R activation as demonstrated by Ca^{2+} influx (see Chapter 5, section 5.2.3.3, Fig. 5.6), this concentration was used to study TG2 release. In order to determine the stimulation time necessary to detect changes in extracellular TG2 levels, but at the same time minimize cellular damage caused by prolonged P2X7R activation, the initial experiment was designed to collect conditioned medium at different time-points of P2X7R stimulation (Fig. 6.1A). Medium was collected at the end of BzATP stimulation (pulse fraction) and also harvested 30 min after agonist removal (chase fraction) to see if there is potentially a delay in TG2 release. Analysis of the conditioned medium collected from HEK293 P2X7R cells expressing TG2 by Western blotting showed that low levels of TG2 can be detected in cell supernatant under baseline conditions. BzATP treatment markedly (~ 10-fold) increased TG2 levels in the medium (Fig. 6.1B and C). Time course analysis of the pulse fractions indicated gradual accumulation of TG2 in the medium caused by P2X7R activation. 5 min pulse was not sufficient to detect TG2 externalization, however, after 10 min BzATP treatment TG2 export into the medium was triggered and TG2 accumulated further in the supernatant when BzATP was present for 30 min. Interestingly, after removal of the agonist, elevated levels of TG2 in the chase fractions were still observed, even in cells that were initially only challenged for 5 min. This indicates that there is a delay upon which TG2 is recruited for externalization. It seems that the initial P2X7R activation, even a pulse as short as 5 min, might be sufficient to trigger active release of TG2, and the presence of the agonist at later stages might not be required. However, cells that were challenged with BzATP for 10 or 30 min were able to release marginally more TG2 than those stimulated for 5 min only, which can be seen in the chase fractions that are of equal

duration (Fig. 6.1B and C). The increased TG2 levels detected in the medium were not caused by intracellular TG2 depletion, as the total TG2 levels were similar between the control and BzATP treated cells at the end of the experiment (Fig. 6.1D; see also Fig. 6.4B). Moreover, the BzATP evoked signaling did not apparently change total P2X7R levels associated with the cells nor was receptor degradation evident, even after 30 min of stimulation (Fig. 6.1D).

Shedding of TG2 and flotillin-2 containing MVs was previously reported by Antonyak and colleagues (2010). Hence, the presence of the lipid raft protein, flotillin-2, in the cell-free supernatant was monitored in my experiments (Fig. 6.1B). As expected and consistent with results obtained for TG2, elevated levels of flotillin-2 were only detected upon P2X7R activation, suggesting that MVs release correlates with receptor activation (Fig. 6.1B). However, it seems that the timing of flotillin-2 release is different to that of TG2. After 30 min of P2X7R stimulation, in medium collected during 30 min of chase, the TG2 levels are still maximally upregulated whereas flotillin-2 could not be detected (Fig. 6.1B, see also Fig. 6.2A).

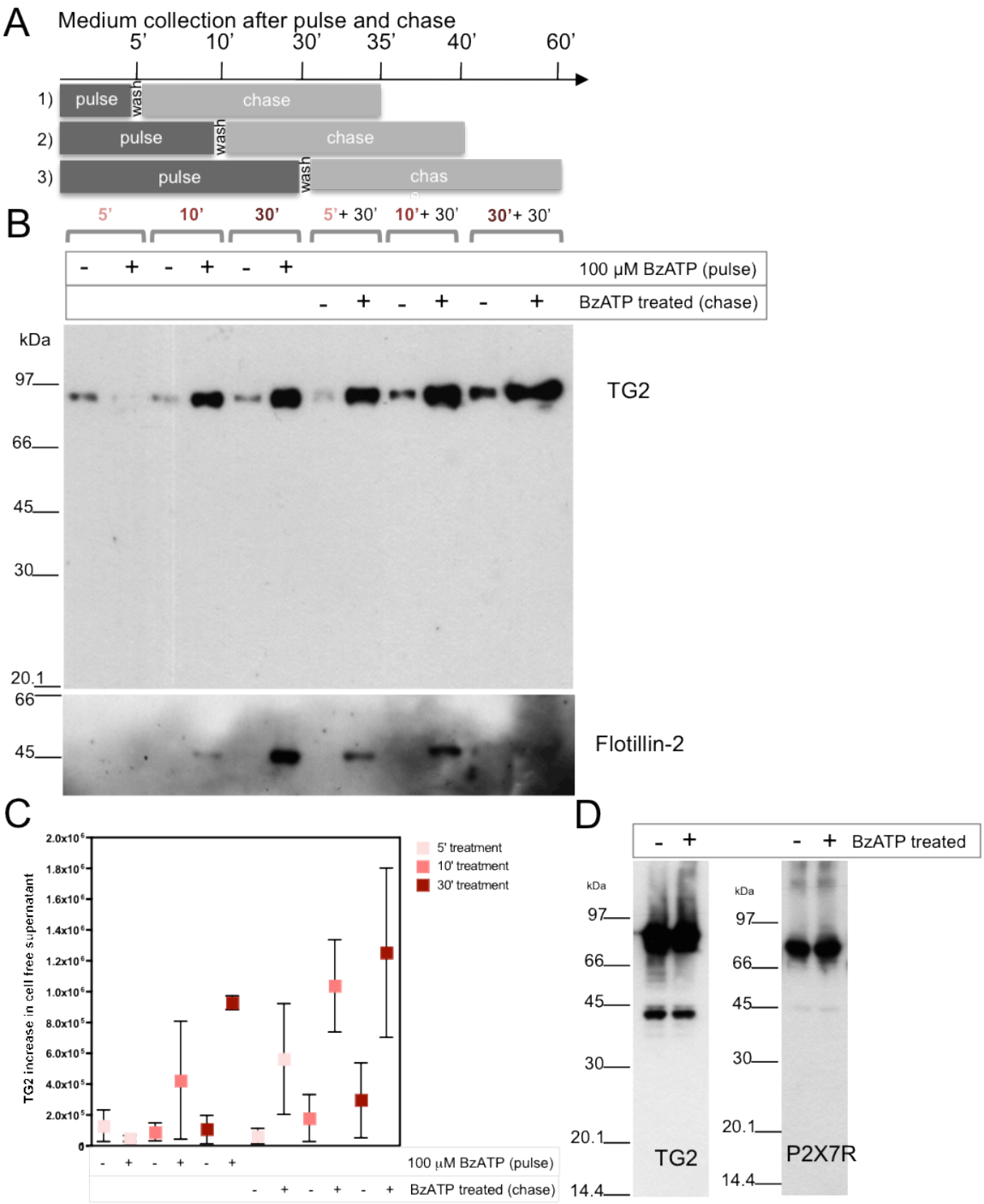

Fig. 6.1 Detection of TG2 in cell supernatant with or without P2X7R activation as analyzed by Western blotting. A: In order to investigate whether TG2 is released upon P2X7R activation as well as study the kinetics of the process, an experiment was designed to collect medium fractions from the initial phase of BzATP stimulation (pulse) and a subsequent phase after BzATP removal (chase). **B:** HEK293 P2X7R cells were seeded in a 24-well plate at the density of 1.2 x 10^5 cells/well and the next day transiently transfected with TG2. After 48h cells were stimulated for 5, 10 or 30 min in the absence (vehicle control) or presence of 100 µM BzATP in OptiMEM. Cells were washed and left for an additional 30 min in fresh OptiMEM without BzATP. Conditioned medium was cleared by centrifugation (1500 x g, 10 min), lyophilized and analyzed by Western blotting. TG2 antibodies were used to stain the membrane. Then, membrane was re-probed for flotillin-2. **C:** TG2 levels in the medium were estimated by densitometry and the volume of the bands was calculated. Graph represent mean value of the volume ± SEM from two independent experiments. **D:** After medium collection, cells that were untreated or stimulated with 100 µM BzATP (30 min pulse + 30 min chase) were extracted as described in Materials and Methods. 10 µg of protein was loaded per lane and separated on 4-20% SDS polyacrylamide gel under reducing conditions followed by Western blotting. Nitrocellulose membrane was stained with anti-TG2 and P2X7R antibodies.

6.2.2 Inhibition of TG2 release with P2X7R inhibitor

In order to further confirm that P2X7R activation is responsible for TG2 translocation, HEK293 P2X7R cells were stimulated for 30 min with BzATP in the presence of 5 μM P2X7R inhibitor (A740003). This inhibitor concentration has previously been shown to be sufficient for blocking BzATP-evoked calcium signaling in respective cells (see Chapter 5, section 5.2.3.3, Fig. 5.8). Cells that were pre-treated with P2X7R inhibitor and later stimulated with BzATP in its presence were no longer able to accumulate TG2 as well as flotillin-2 in the medium (Fig. 6.2A and B). Inhibition of P2X7R abolished TG2 externalization during stimulation as well as subsequent release in the chase fraction. This demonstrates that the agonist BzATP by itself has no unspecific effect on TG2 externalization and thereby confirms it to be a P2X receptor-dependent process (Fig. 6.2, see also Fig. 6.4A and C). In addition, similar to results shown in Fig. 6.2B, flotillin-2 could not be detected in the 30 min chase fraction that still contain TG2 at high concentration, thus further indicating that the mechanism of TG2 export from the cells might be distinct to flotillin-2 release.

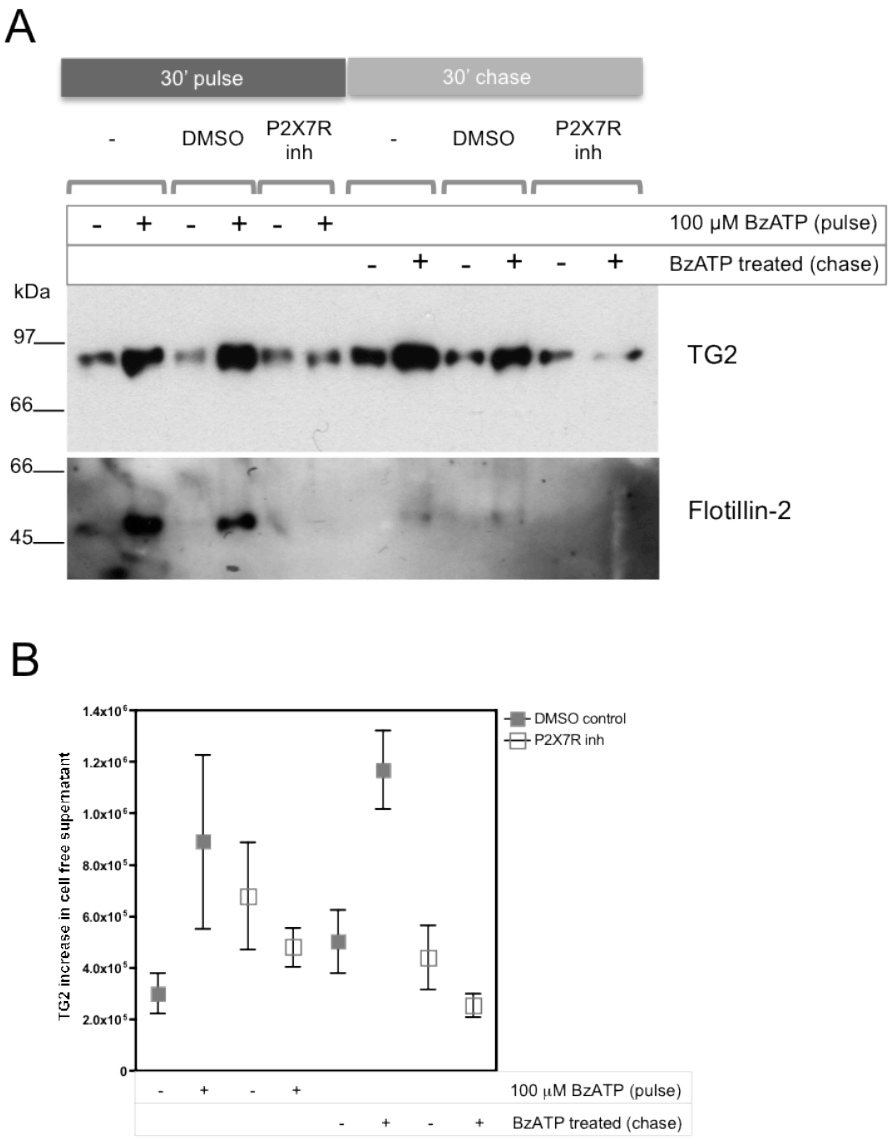

Fig. 6.2 Detection of BzATP-mediated TG2 release in the presence and absence of P2X7R inhibitor. A: HEK293 P2X7R cells transiently expressing TG2 were pre-treated for 10 min with normal medium, DMSO (0.05%) or 5 µM P2X7R inhibitor (A740003 in DMSO) before stimulation. Then cells were kept for 30 min in the absence or presence of 100 µM BzATP in OptiMEM. Where indicated, 5 µM P2X7R inhibitor or DMSO as a carrier control was present. Cells were washed and left for an additional 30 min in the respective media without agonist. Conditioned medium was cleared by centrifugation, lyophilized and analyzed by Western blotting as in Fig. 1. TG2 and Flotillin-2 antibodies were used to stain the membrane. **B:** TG2 levels in the medium were estimated by densitometry and the volume of the bands was calculated. Graph represent mean value of the volume ± SEM from three independent experiments.

6.2.3 Effect of BzATP treatment on cell viability

It is known that prolonged stimulation of cells expressing P2X7R with high concentrations of BzATP or ATP may lead to cell death (Surprenant et al. 1996; Di Virgilio et al. 2001). However, previous reports also indicate that stimulation with 100 μM BzATP for up to 10 min is not associated with increased cell necrosis, apoptosis or non-controlled lysis (Mackenzie et al. 2001). It was therefore important to investigate whether short BzATP stimulation affects viability of P2X7R expressing and non-expressing cells. Hence, the parental HEK293 cells and HEK293 cells overexpressing P2X7R were challenged with 100 μM BzATP in OptiMEM for 5, 10 and 30 min, then washed and left for 24h in DMEM containing 10% FBS. At the end of each time-point of stimulation and after 24h phase contrast images of cells were taken to observe gross changes in cell morphology and estimate cell numbers (Fig. 6.3). As expected, BzATP addition induced cell rounding and extensive blebbing in cells expressing P2X7R but not in the parental cells, as I have previously shown in Chapter 5 (section 5.2.3.3, Fig. 5.6). After 24h, significant cell loss was observed only in P2X7R cells that were stimulated with BzATP for 30 min (Fig. 6.3, bottom panel). The 30 min BzATP treatment did not affected the cell number in the parental cells. One of the reasons for the observed cell loss of P2X7R expressing cells is that BzATP treatment induces remarkable changes in cytoskeleton organization (Mackenzie et al. 2005) that lead to loss of cell attachment to the plate surface. Therefore, some cell loss occurs from cell handling during medium replacement. On the other hand, the observed cell loss might come from the fact that 30 min BzATP treatment induced some cell death and this cannot be ruled out at this stage. As 10 min BzATP treatment did not cause detectable cell loss and because this stimulation time is sufficient to detect TG2 in the cell supernatant, those conditions were chosen for all following experiments.

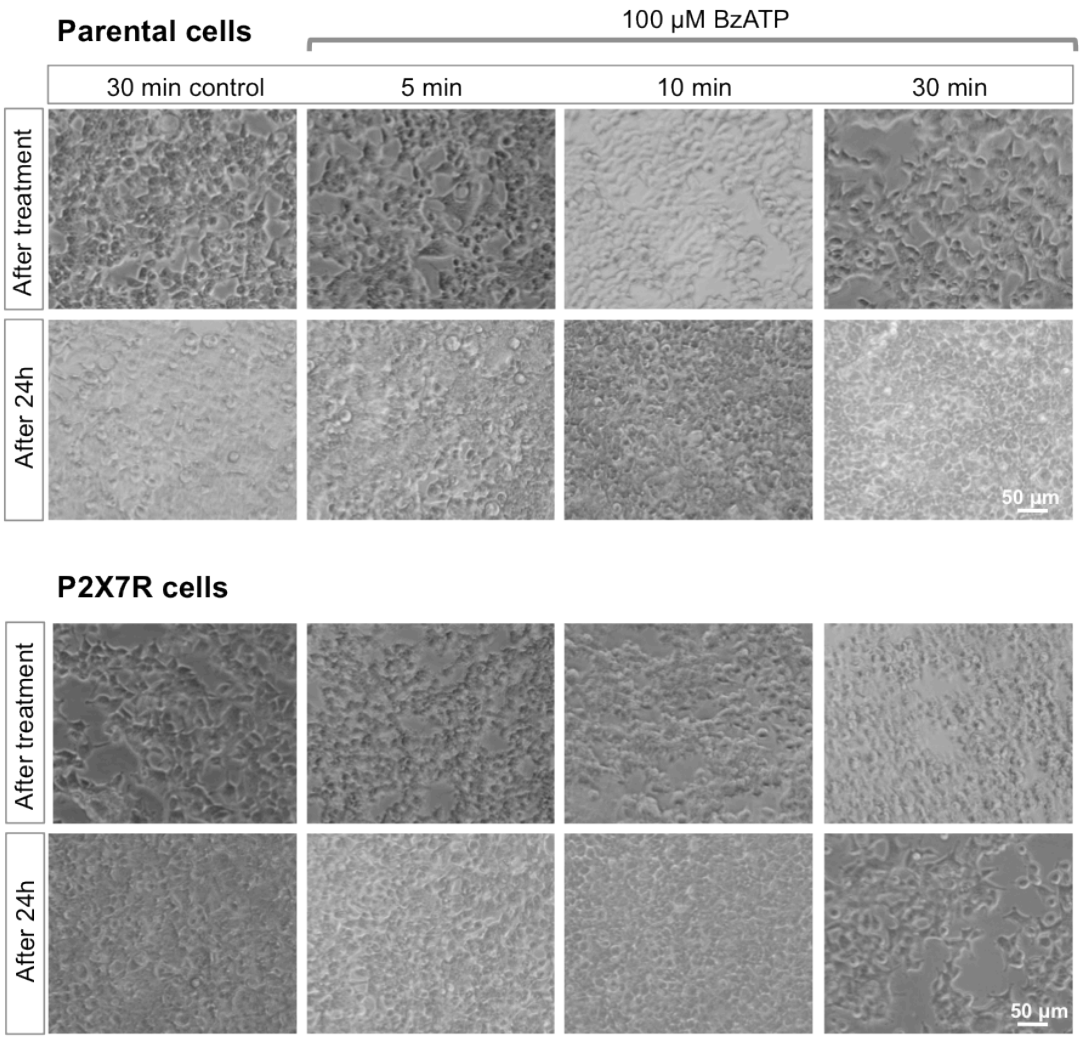

Fig. 6.3 Monitoring of gross morphological changes in HEK293 cultures that are negative or positive for P2X7R upon BzATP addition. Parental cells and cells stably expressing P2X7R were stimulated for indicated times in the absence or presence of 100 µM BzATP in OptiMEM. Following treatment, OptiMEM was removed and replaced with DMEM containing 10 % FBS and cells were left to recover for 24h. Phase contrast images of the cells were taken after each time point of stimulation and after 24h.

6.2.4 P2X7R-mediated secretion of TG2 from HEK293 cells is not linked to loss of cell membrane integrity

The experiment with the P2X7R inhibitor confirmed that active TG2 release was dependent on P2X7R function in cells overexpressing P2X7R. However, I also had to exclude that the same is possible in parental cells treated with BzATP. Thus, parental and P2X7R cells were transiently transfected with wild-type TG2 and stimulated with 100 μM BzATP as previously. The response to stimulation was observed only in P2X7R cells where an initial increase of TG2 and flotillin-2 in the pulse fraction was followed by rapid accumulation of both proteins in the chase fraction (Fig. 6.4A and C). Parental cells were unable to secrete TG2 or flotillin-2 in a similar manner during BzATP treatment or after agonist removal and TG2 clearly remained at the baseline level. Lysis of cells at the end of the experiment confirmed that both parental and P2X7R cells were expressing TG2 and flotillin-2 at similar levels and hence a lack of release was not due to a lack of protein expression (Fig. 6.4B). This result clearly shows that in HEK293 cells, active TG2 secretion requires P2X7R activation.

To eliminate the possibility that TG2 release might occur as an effect of cell lysis, membrane damage or unspecific release of their cytoplasmic content, a membrane containing both medium fractions and total cell extracts from a single experiment (separated in parallel on the same gel) was probed for the presence of IκBα (Fig. 6.4A and B). The same approach was previously used by Antonyak and colleagues (2011) where IκBα staining was used to distinguish between microvesicle and cytosolic protein fractions. As shown in Fig. 6.4 A, B and D, IκBα was only present in the cell lysate but was absent in the conditioned medium. This indicates that TG2 release is occurring in a selective manner and is not related to cell damage or transient loss of plasma membrane integrity.

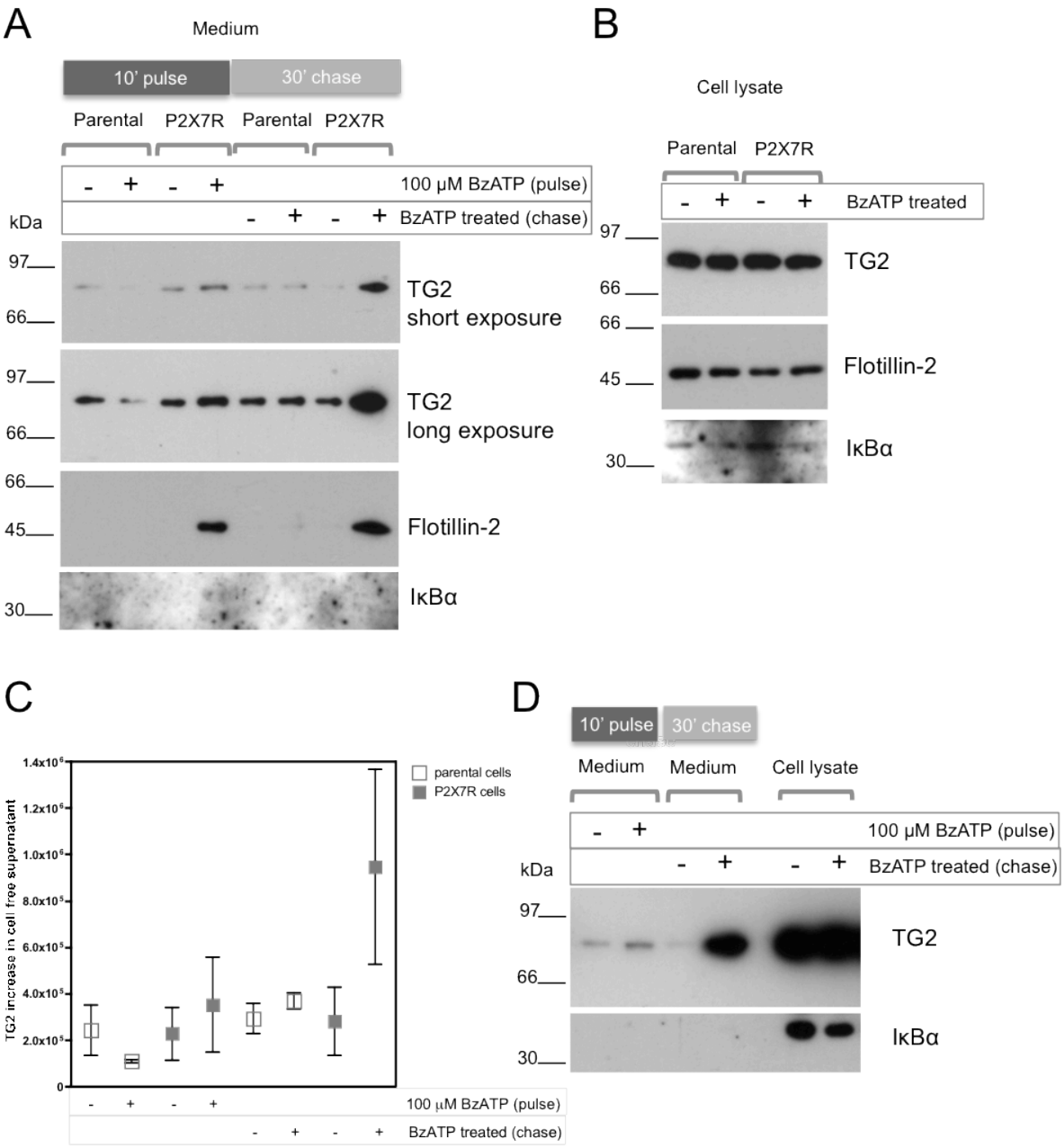

Fig. 6.4 Comparison of BzATP-mediated TG2 release between HEK293 cells that are negative or positive for P2X7R. **A:** Parental cells and cells stably expressing P2X7R were transiently transfected with TG2. After 48h cells were stimulated for 10 min in the absence or presence of 100 µM BzATP in OptiMEM. Cells were washed and left for an additional 30 min in fresh medium. Conditioned medium was processed and analyzed by Western blotting as in Fig.1. TG2, flotillin-2 and IκBα antibodies were used to stain the membrane. **B:** At the end of the experiment cells that were untreated or stimulated 100 µM BzATP (10 min pulse + 30 min chase) were lysed with cell extraction buffer. 5 µg of protein was loaded per lane and and analyzed by Western blotting as in panel A. **C:** TG2 levels in the medium were estimated by densitometry and the volume of the bands was calculated. Graph represent mean value of the volume ± SEM from two independent experiments. **D:** HEK293 P2X7R cells transiently expressing TG2 were were stimulated for 10 min in the absence or presence of 100 µM BzATP in OptiMEM. Cells were washed and left for additional 30 min in fresh medium. Conditioned medium was processed as described above and 10 µg of protein was loaded per lane and and analyzed by Western blotting for TG2 and IκBα.

6.2.5 TG2 localization upon P2X7R-stimulation

To further investigate whether shedding of TG2-containing microvesicles could be observed in real-time upon P2X7R activation, GFP labeled TG2 was used to track its localization during cytoskeleton rearrangements and plasma membrane blebbing. Transfection of P2X7R cells with TG2-GFP (GFP on C- terminus) showed a clear ubiquitous TG2 cytoplasmic distribution (Fig. 6.5A). Most of the transfected cells did not reveal any specific localization of TG2-GFP within particular intracellular compartments. However, in occasional cells where the expression was quite low, small fluorescent spots were visible suggesting that TG2-GFP might associate with specific organelles. As the presence of the bulky GFP tag was considered to potentially affect TG2 secretion, the P2X7R cells were transiently transfected with wild-type and TG2-GFP constructs and the cell supernatant analyzed for TG2 release after stimulation with BzATP as previously. Analysis of the conditioned medium by Western blotting revealed that P2X7R activation is also triggering secretion of TG2-GFP as evident by the accumulation of approx. 110 kDa protein that was detected with anti-TG2 antibodies in the 30 min chase fraction (Fig. 6.5B and C).

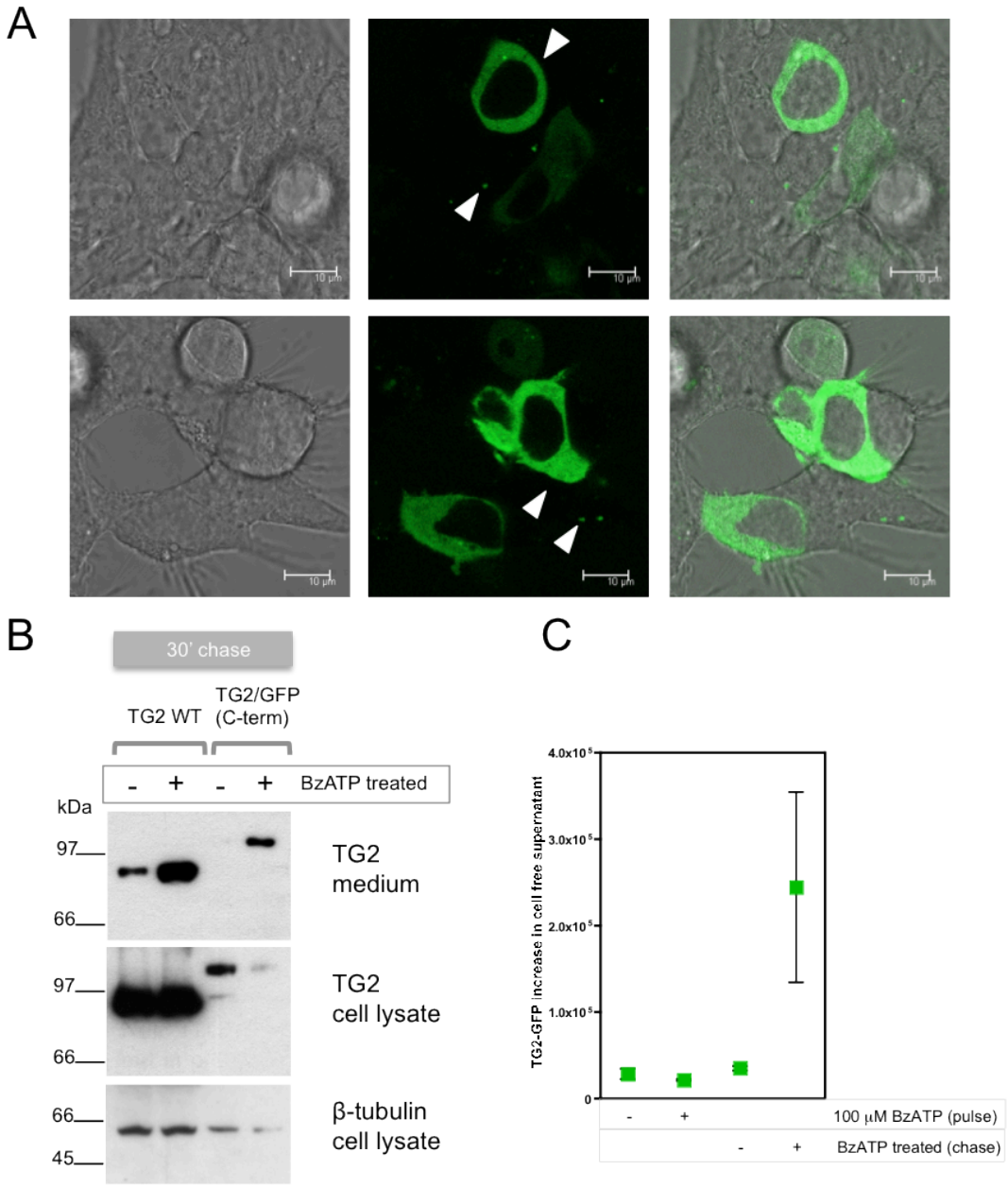

Fig. 6.5 GFP-tagged TG2: intracellular localization and BzATP-mediated release into cell supernatant. A: HEK293 P2X7R-V5-His cells were transiently transfected with TG2-GFP (C-terminus). After 24h the expression of TG2-GFP was analyzed. Images represent an optical section acquired by confocal microscopy (phase contrast, left; fluorescence, middle; overlay, right). Arowheads indicate the localization of TG2-GFP that is mainly distributed within the cytoplasm. **B:** HEK293 P2X7R cells were transiently transfected with wild-type TG2 or TG2 tagged with GFP at the C-terminus. After 48h, cells were stimulated for 10 min in OptiMEM with vehicle or 100 μM BzATP. Cells were washed and left for an additional 30 min in fresh medium. Conditioned medium was processed as in Fig. 1 and 10 μg of protein was loaded per lane and analyzed by Western blotting for TG2. Membrane was also probed for β-tubulin to estimate protein loading. Result shown is representative for two independent experiments. **C:** TG2-GFP levels in the medium were estimated by densitometry and the volume of the bands was calculated. Graph represent mean value of the volume ± SEM from two independent experiments.

As TG2-GFP was externalized form the cells, presumably in the same manner as the wild-type TG2, it served as a model to investigate changes in TG2 localization upon P2X7R activation. Thus, in the next step cells overexpressing P2X7R were transfected with TG2-GFP (C-term) and stimulated with 1 mM ATP or 100 μM of BzATP to study the dynamics of membrane changes and possibly associated TG2 re-distribution by time-lapse microscopy (Fig. 6.6). Monitoring of cells revealed that they remained responsive to application of the agonist (comparable with Chapter 5). Moreover, even high levels of TG2 expression did not seem to have an effect on morphological changes and cell blebbing. Redistribution of TG2-GFP within cells was fastest at the initial timepoints when the Ca^{2+} influx is observed (Fig. 6.6; see Chapter 5, Fig. 5.6 and 5.7). However, this appeared to relate to changes in cell morphology rather than specifically alter the localization of TG2 *per se*. On the other hand, there was a noticeable reduction in fluorescence levels over time suggesting that TG2 was released although this could not be visualized. At later time points, the cytoplasmic TG2 localization remained largely unchanged. Detailed analysis showed that upon stimulation, TG2-GFP was also localizing in membrane blebs and was freely translocating to sites where new membrane blebs formed (Fig. 6.7). It was difficult to clearly confirm shedding of vesicles with fluorescent TG2. Careful inspection revealed that despite abundant "cell blebbing" in most cases the membrane protrusions remained continuous with the plasma membrane and some blebs were eventually retracted by the cells. It appears therefore that the big vesicles that are formed post P2X7R activation are still a part of the cellular membrane and that TG2-GFP can diffuse between the cytosol and the lumen of newly formed blebs. This was further confirmed by a set of bleaching approaches where a small area inside the "bleb" was bleached and the redistribution of fluorescence was investigated (data not shown).

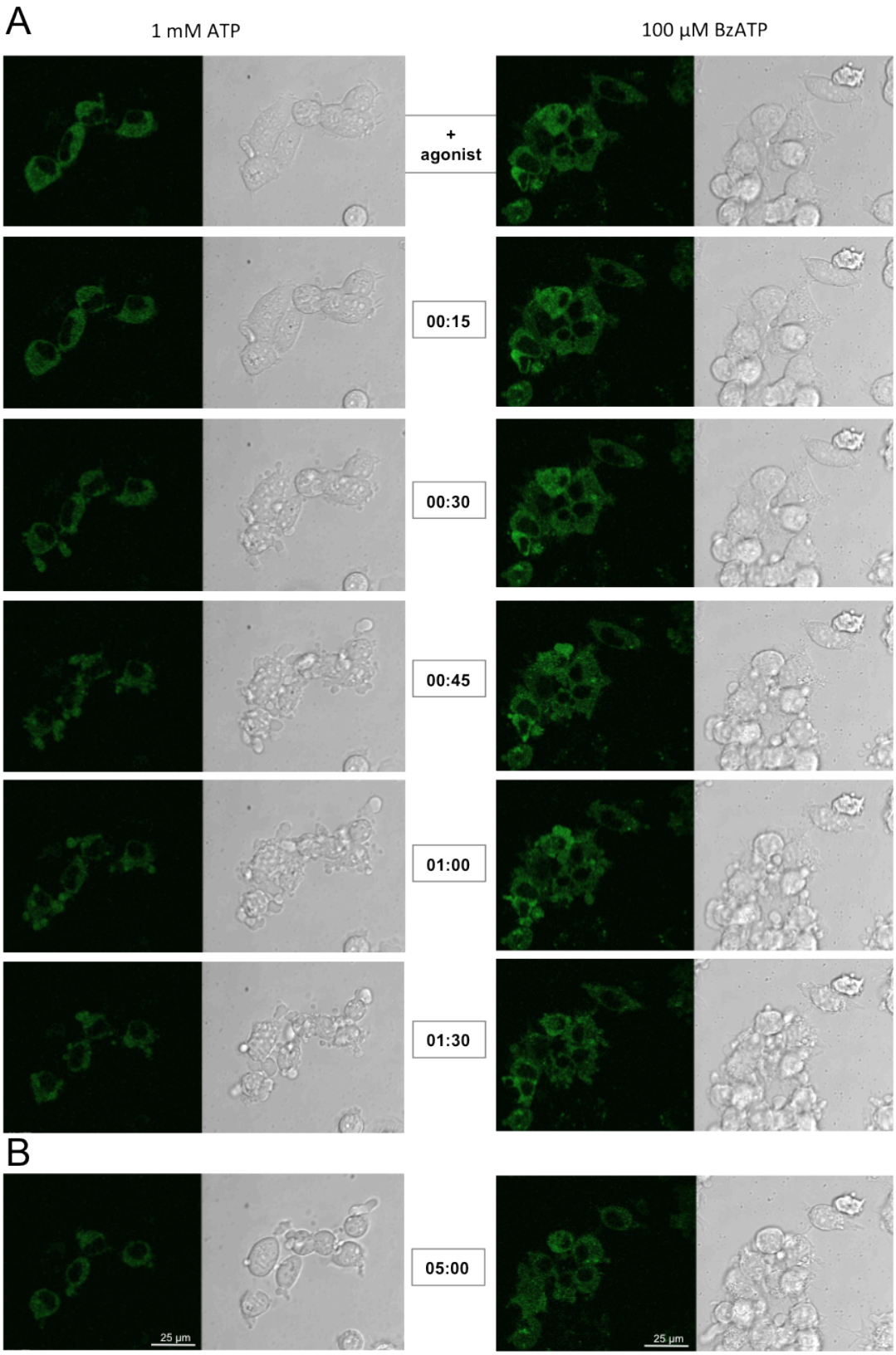

Fig. 6.6 TG2-GFP localization in HEK293 P2X7R cells upon agonist stimulation. Cells were transiently transfected with TG2 C-terminally tagged with GFP. 24h post-transfection cells were treated with 1 mM ATP or 100 µM BzATP in OptiMEM. Changes in fluorescence were monitored for up to 10 min using timelapse microscopy. Time following stimulation is given in between image panels in minutes: seconds. Pictures represent an optical section acquired by confocal microscopy. Panel A shows initial time intervals during which the rise in intracellular Ca^{2+} is observed whereas panel B shows a later time interval (after 5 min) towards the end of which TG2 starts to be detected by Western blotting.

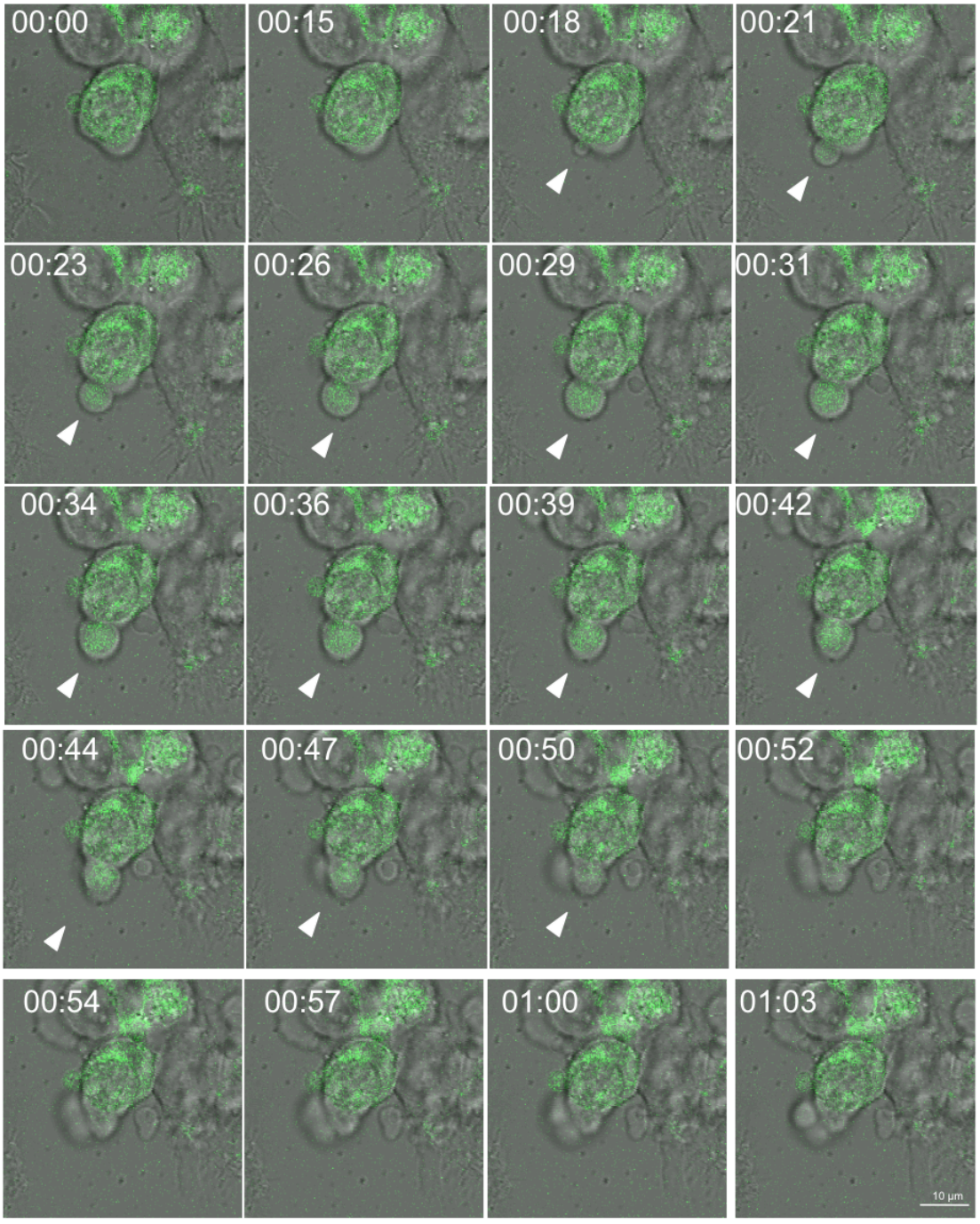

Fig. 6.7 TG2-GFP redistribution in HEK293 P2X7R cells upon agonist stimulation. Cells were transiently transfected with TG2 C-terminally tagged with GFP. 24h post-transfection cells were treated with 100 µM BzATP in OptiMEM. Changes in fluorescence were monitored using timelapse microscopy. Pictures represent an optical section acquired by confocal microscopy. Time following stimulation is given in between image panels in minutes: seconds. Fluorescent and phase contrast images were overlaid to correlate the re-distribution of tagged TG2 with morphological changes. Arrowhead highlights the formation of a cell „bleb" filled with fluorescent TG2.

The same set of experiments were also performed with or GFP-TG2 to investigate if the GFP attachment to the N-terminus of TG2 would alter its localization and to exclude any tag related artefacts. The stimulation of HEK293 P2X7R cells expressing GFP-TG2 with 1 mM ATP or 100 μM of BzATP gave the same pattern of cell behaviour as previously revealed with the C-terminally tagged TG2 (Fig. 6.8). Similarly, GFP-TG2 was uniformly distributed within the cytosol and was freely translocated between cell body and protruding membrane upon cell challenge with both ATP and BzATP.

Taken together, the data suggest that TG2 tagged with GFP is externalized as indicated by a loss of fluorescence over time and by its presence in the conditioned medium confirmed by Western blotting. However, either vesicles containing TG2 are very small, beyond available resolution or that TG2-GFP is directly translocated across the membrane and not vesicle bound.

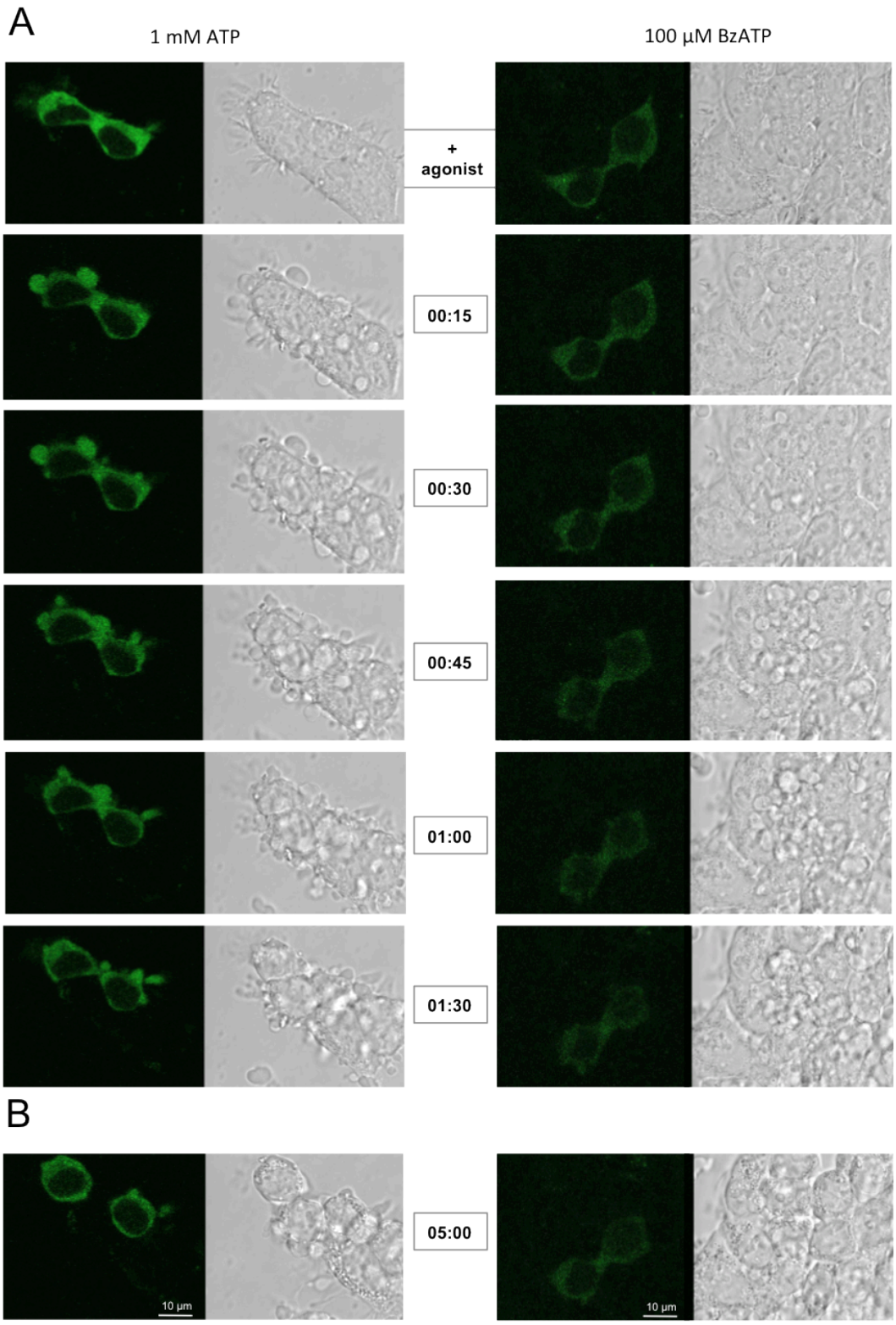

Fig. 6.8 GFP-TG2 localization in HEK293 P2X7R cells upon agonist stimulation. Cells were transiently transfected with TG2 N-terminally tagged with GFP. 24h post-transfection cells were treated with 1 mM ATP or 100 µM BzATP in OptiMEM. Changes in fluorescence were monitored for up to 10 min using timelapse microscopy. Pictures represent an optical section acquired by confocal microscopy. Time following stimulation is given in between image panels in minutes: seconds.

6.2.6 Exposure of phosphatidyloserine evoked by BzATP stimulation

P2X7R activation can lead to transient pseudoapoptosis that manifests by the phosphatidyloserine (PS) flipping to the outer leaflet of the cell membrane (MacKenzie et al. 2001). This can be visualized by adding fluorescently labelled annexin V, which binds to exposed PS. The aim of the experiment was to test if upon selected conditions i.e. 100 μM BzATP stimulation, the spontaneous flip of PS in the membrane bilayer can be observed. Hence, P2X7R cells were stimulated in the presence of FITC labelled annexin V and the process was monitored under the confocal microscope in real time. Images of activated cells were collected using Z-stack analysis and revealed the presence of Annexin V positive clusters of cell membrane that are developing following P2X7R activation (Fig. 6.9). This is reminiscent of the localization of extracellular TG2 immunostaining in MDA-MB-231 cells presented in Chapter 4. However, it remains to be experimentally shown that these membrane subdomains where PS is exposed are the sites of TG2 translocation.

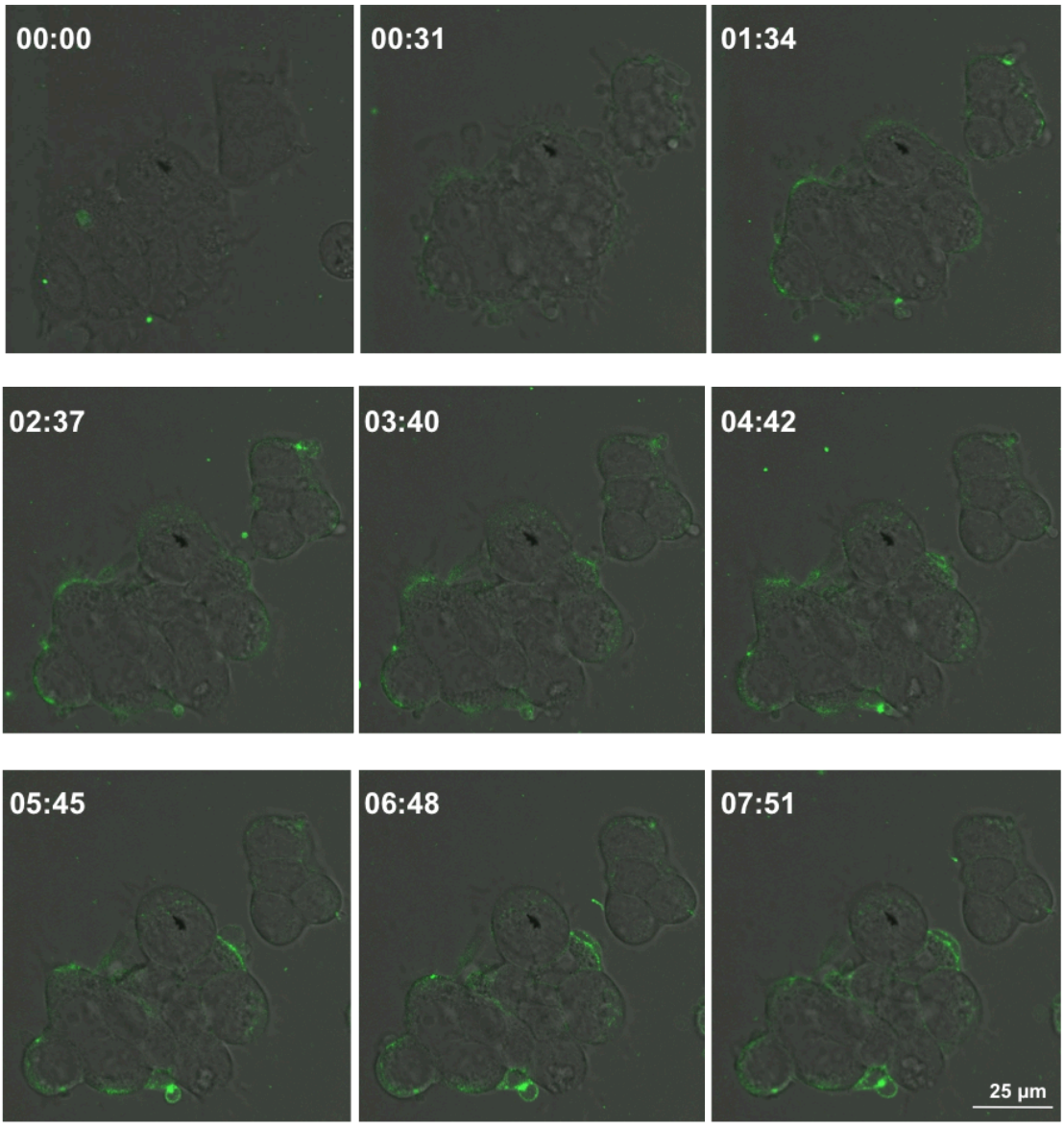

Fig. 6.9 Monitoring of lipid asymmetry in the plasma membrane with Annexin V labeling after P2X7R activation. HEK293 cells were stimulated with 100 µM BzATP in OptiMEM containing 2 mM Ca^{2+} in the presence of FITC-conjugated Annexin V. Changes in Annexin V binding to exposed phosphatidylserines was monitored for up to 10 min using confocal microscopy. Pictures represent an optical section selected from a one Z-stack acquired by timelapse microscopy. Fluorescent and phase contrast images were overlaid to correlate the Annexin-V localization with morphological changes. Data shown is result of one experiment. Time following stimulation is given in between image panels in minutes: seconds.

6.3 Discussion

The most important finding of this part of the study is that P2X7R stimulation induces rapid release of TG2 from HEK293 cells stably expressing functional receptor. This mechanism identifies a novel pathway of active TG2 release that is relevant in the context of tissue damage. As TG2 externalization occurs in the HEK293 P2X7R cells that are devoid of the inflammasome components (Bryan et al. 2010; Lu et al. 2012), this might represent a general mechanism that regulates presence of biologically active TG2 outside of the cells also in absence of inflammation. Beside cell injury, ATP can be released by cells in response to different stimuli such as mechanical stress, which activates purinergic signaling (Garcia and Knight 2010; Rumney et al. 2012). BzATP-evoked TG2 release was abolished by P2X7R inhibitor clearly indicating that P2X7R is an important player in the process of non-classical secretion of proteins other than IL-1β. The absence of the cytosolic marker IκBα in the cell supernatant of stimulated cells suggests, that rapid TG2 translocation is independent of cell damage and represents a specific mechanism for active TG2 delivery to the extracellular space.

Our current understanding of TG2 function suggests its close association with the cell surface and quick deposition into ECM upon release (Nurminskaya and Belkin 2012). These observations come from many studies that look at cross-linking and transamidation activity of TG2 in the presence of high extracellular Ca^{2+} and its interaction with the numerous ECM proteins such as fibronectin, collagen, syndecan-4 or heparin (Aeschlimann and Thomazy 2000; Telci et al. 2008; Scarpellini et al. 2009; Belkin 2011). However, those extracellular/membrane interactions demonstrate how TG2 may be retained on the cell surface or ECM but does not explain the trafficking mechanism through the membrane (Nurminskaya and Belkin 2012). There are already a number of studies showing that TG2 can be collected from cell medium; however, the common pathway of this type of secretion remains elusive (Balklava et al. 2002; van den Akker et al. 2011; Antonyak et al. 2011; Chou et al. 2011). Additionally, enzymatically active TG2 was found in the ascites of the ovarian cancer and potentially plays a role in cancer cell growth (Satpathy et al. 2007; Yakubov et al. 2013).

Zemskov and colleagues recently proposed a model of TG2 unconventional export, which says that the recycling endosomes are the intracellular machinery required for TG2 release (2011). They state a hypothesis that TG2 is recruited to the endosomes prior its externalization and captured inside vesicles on its way to the cell surface. Therefore the deposited TG2 and endocytosed TG2 remains in the state of equilibrium. In order to investigate TG2 surface trafficking, authors of the study used embryonic mouse fibroblasts (NIH3T3) with an inducible TG2 expression system and compared the externalization pathway with human endothelial cells (HUVEC) endogenously expressing TG2. They observed that in fibroblasts *de novo* synthesized TG2 was accumulating in perinuclear vesicles after approx. 4h and after reaching the cell surface TG2 was deposited into the ECM (after approx. 8h). The same timing of release was observed for HUVEC cells, however only NIH3T3 fibroblast were able to release TG2 into the growth medium after approx. 24h post induction of expression. They have also looked more closely at the non-canonical secretory pathway of TG2 from the cells by using various inhibitors of protein trafficking. Agents that block the ER/Golgi pathway or secretion of other non-classically released proteins, such as FGF2 and IL-1β unable to inhibit TG2 release from NIH3T3 fibroblasts. However, they showed that inhibition of *N*-ethylmaleimide-sensitive factor (NSF), which is an ATPase involved in intracellular membrane fusion between synaptosomal-associated protein (SNAP) and SNARE, reduces total levels of cell surface TG2. Thus, authors concluded that association of TG2 with the membrane of intracellular organelles is necessary event for its proper externalization. By blocking the VAMP3 and SNAP23 SNAREs proteins, with which NSF can interact they showed that TG2 failed to reach the cell membrane. The model suggested by Zemskov and colleagues explains how TG2 could be secreted from the cells in a constitutive manner, however does not answer the question if TG2 secretion can be triggered by any specific external signal. It also does not give a hint on how TG2 can cross the lipid membrane barrier of perinuclear endosomes. However their work suggests that unconventional export of TG2 is a tightly controlled process that involves membranous organelles inside fibroblasts and endothelial cells.

Evidence collected in this chapter suggests that TG2 release might occur together with microvesicles shedding from activated cells. The analysis of

microvesicles is challenging due to the lack of standardized methods for their isolation that does not affect release of their content and break down (Burnier et al. 2009). Because of their small size, there are many limitations on how to visualize and analyse the specific fraction of microvesicles that contain specific biological information. In order to determine the presence of TG2 in the supernatant of HEK293 P2X7R cells a similar approach to the medium collection from MDA-MB-231 was used (as described in Chapter 4). Cell-free medium analysis by Western blotting using specific markers is not ideal to distinguish between soluble protein, microvesicles or exosome populations. However, it gave a handle to sensitively and reproducibly show that P2X7R activation leads to downstream signaling necessary for TG2 and flotillin-2 accumulation in the cell supernatant.

Antonyak and colleagues proposed a model of TG2 release that involves its association with cell-derived microvesicles (MVs), which represents a pathway of TG2 transfer between cells (Antonyak et al, 2010). They observed that MVs containing TG2 of approx. 0.2-2 μm in diameter are actively shed from a subset of serum starved MDA-MB-231 breast cancer cells and U87 human glioma cells (from 35 and 25% of cells, respectively). However their model does not address the question of TG2 translocation from cytosol to the outer leaflet of budding membrane vesicle. Nevertheless, they draw an interesting possible function of MVs shed from highly progressive tumours. They show that MVs have a transforming effect on normal recipient cells and this mechanism might be important for cancer metastasis (REF).

A similar approach to study TG2 secretion was used by van der Akker and colleagues (2011), where they report the secretion of TG2/eGFP-containing microparticles (MPs) from human embryonic kidney cells (HEK293) and from mouse vascular smooth muscle cells (MOVAS). In order to capture TG2 release, they have transiently transfected cells with TG2 tagged with eGFP and used confocal microscopy and growth medium collection to assess for released MPs. They have observed that in HEK293 cells, TG2/eGFP containing MPs accumulate in the medium post transfection and show an example of fluorescent MPs being detached from the surface of a smooth muscle cell. Surprisingly, smooth muscle cells required the addition of FBS for 24h or 2h treatment with Ca^{2+} ionophore was necessary for the MPs to be observed and collected in the growth medium. The secretion of wild-

type TG2/eGFP was positively correlating with the presence of Annexin V positive staining on the cell surface measured by flow cytometry thus confirming that MPs might be released during spontaneous PS flips.

At this point it is uncertain whether TG2 release is linked to microvesicles formation in the HEK293 cells overexpressing P2X7R. Studies with GFP tagged TG2 confirmed that in the presence of P2X7R activation, the cytosolic form of TG2 can freely translocate within the cell and localize at sites of extensive blebbing. I was however unable to clearly observe shedding of fluorescently labelled vesicles packed with TG2. Furthermore, the dynamics of flotillin-2 release differed from those of TG2 secretion, which suggests that TG2 may not be associated with microvesicles. On the other hand, those experiments confirmed that cells expressing both TG2 and P2X7R at high levels are still able to respond to BzATP treatment in a similar manner to those non-expressing TG2. Hence, TG2 does not apparently affect P2X7R activation.

It has been reported that intracellular TG2 is not only present in the cytosol but also can be found associated with nuclear and mitochondrial membranes in some types of cells (Lorand and Graham 2003; Nurminskaya and Belkin 2012). Yet, the transfection with GFP labelled TG2 seemed to upregulate mainly the cytosolic form of the protein. Similar results were obtained by van den Akker and colleagues (2011) when they transfected HEK293 cells with TG2 C-terminally tagged with eGFP and showed a comparable distribution of TG2 within the cytosol. Localization of TG2 to subcellular compartments may be cell-type specific (Thomazy and Fesus 1989) or modulated by the cell cycle (Mian et al. 1995). It would be interesting to see if different forms of TG2 could undergo different surface trafficking and recycling within the cell. At the moment, it appears that the cytosolic fraction of TG2 is the main source of secreted TG2 in response to P2X7R activation. However, this needs to be further confirmed.

In conclusion, my work reveals that the presence of TG2 in the cell supernatant might relate to an excess of TG2 being released and be an important novel mechanism for fast TG2 delivery to the extracellular space, which happens under certain conditions i.e. the activation of danger-sensing P2X7R.

Chapter 7 The role of Ca^{2+} signaling in TG2 secretion

7.1 Introduction

P2X7R are ligand–gated ion channels that after millisecond of ATP stimulation dilate and allow Ca^{2+}, Na^{+} entry and K^{+} efflux, leading to membrane depolarization (North 2002). However, the receptor activation is also linked with the formation of large membrane pores upon prolonged stimulation with ATP or high agonist concentrations. This complex mechanism is not fully understood (Ferrari et al. 2006; Pelegrín 2011). As HEK293 cells expressing functional P2X7R are able to actively release TG2 upon BzATP stimulation, it was important to investigate which activity of P2X7R is required to induce TG2 externalization.

The P2X7R is highly polymorphic, and it becomes increasingly clear that some amino acid substitutions predispose to disease. SNP linkage analysis in an rheumatoid arthritis (RA) cohort revealed the presence of P2X7R gene mutations that impair receptor function, which correlate with the presence of rheumatoid factor or C-reactive protein in patients carrying those alleles (Al-Shukaili et al. 2011). Interestingly, mutations in P2X7R that disable membrane pore formation have also been associated with reduced chronic pain in osteoarthritis (OA) patients (Sorge et al. 2012). This suggests that sustained P2X7R activation could also contribute to arthritis pathogenesis, and inhibiting P2X7R-mediated pore formation but not channel activity may therefore have therapeutic potential.

Opening of the P2X7R membrane pore is usually manifested by entry of large cations such as N-methyl-D-glucamine (MW 195) or dyes such as ethidium bromide (MW 394) or YO-PRO-1 (MW 629) through the membrane of viable cells (Virginio et al. 1999; Pelegrín 2011; Browne et al. 2013). Currently, there are two hypothesis trying to explain the phenomenon of P2X7R-dependent increase in membrane permeability commonly called “pore formation” (Costa-Junior et al. 2011; Pelegrín 2011; L. H. Jiang et al. 2013). The first one suggests that prolonged application of ATP induces further conformational changes within P2X7R subunits leading to dilation of the channel itself. The channel dilates to the stage where ultimately a pore is formed that is large enough so that dyes can permeate the channel. Gradual occupation of all ATP binding sites on the trimeric P2X7R receptor

may be involved in a transition from activated receptor toward pore formation (Jiang et al. 2013). The second model suggests that proteins such as pannexins and connexins are coupling with activated P2X7R and are responsible for dye translocation across the membrane.

The first hypothesis is supported by findings that activation of P2X7R evokes a large inward cation current that has a "double" nature (Roger et al. 2010; Browne et al. 2013). The initial fast rise in the current is followed by a slower rise in "current", which suggests further channel dilation to the point when dye uptake is possible (Yan et al. 2011). Gradual opening of the P2X7R channel rather than a one-step switch mechanism implies that further agonist binding is essential for the channel expanding leading to possible pore formation (Virginio et al. 1999). This is also consistent with high agonist concentrations promoting high current facilitation and pore formation i.e potential saturation of ligand binding sites. Electropysiology data on the P2X7R show that repeated application of ATP is needed to reach the full capacity for ion flux and only sustained application of agonist is necessary to reach the steady-state current and cell blebbing (Roger et al. 2010). Recently, Browne and colleagues (2013) suggested that dyes permeate the P2X7R channel in the same manner as passing ions. When the YO-PRO-1 entry was simultaneously measured with the changes in membrane current, dye uptake was greatest at -60 mV membrane potential, which produced the largest inward cation current. By changing the membrane potential to +60 mV and inducing an outward ionic current, they reported reduced dye uptake, which confirms that YO-PRO-1 translocation is also voltage dependent. Moreover, they have observed that introduction of a positive charge inside the channel decreases the entry of positively charged ethidium bromide and increases translocation of negatively charged FITC. The opposite was observed when the respective residue was exchanged for a negatively charged amino acid. Therefore, the authors speculated that dyes (up to 1.4 nm in diameter) can permeate directly through the P2X7R pore in the same way as ions do. However, they do not fully exclude the possibility that other proteins might be involved.

The second model proposes an interaction of P2X7R with the membrane hemichannel, Pannexin-1 as a possible pathway explaining "pore formation" (Pelegrin and Surprenant 2006). Pannexin-1 is a transmembrane protein closely related to family of gap-junction proteins, the connexins, however it is not acting in

the same manner as gap-junction that are quickly delivered and internalized from the cell surface and therefore seems to mediate different types of cell-cell communication (Penuela et al. 2007). Pannexin-1 was suggested to mediate the observed dye uptake upon P2X7R activation. It was shown that the initial dye uptake is abolished after blocking Pannexin-1 with antagonistic peptides or reducing its expression with siRNA in HEK293, which did not affect ionic currents due to P2X7R activation. Similarly, inhibition of Pannexin-1 also successfully blocked initial rapid dye uptake after ATP stimulation of J774 macrophages endogenously expressing P2X7R (Pelegrin and Surprenant 2007). Moreover when overexpressed, Pannexin-1 was shown to co-immunopecipitate with P2X7R (Pelegrin and Surprenant 2006). The addition of colchicine had similar effects and prevented pore formation without altering membrane currents through P2X7R clearly suggesting the presence of distinct molecular events regulating those two states (Marques-da-Silva et al. 2011). However, there are also some data that argue against pannexin-1 involvement (Jiang et al. 2013). Macrophages from Pannexin-1 KO mice are still able to take up dye and therefore, there must be a different mechanism allowing for the pore to be formed (Qu et al. 2011; Baroja-Mazo and Pelegrín 2012). Also, the presence of some differences between HEK293 cells and macrophages in the dye uptake process suggest, that separate permeation pathways might be involved depending on the cell type (Schachter et al. 2008; Cankurtaran-sayar et al. 2009). Despite the fact that there are conflicting data about the role of Pannexin-1 in pore formation, it is possible that both receptor channel dilation and hemichannel interaction contribute to the phenomenon and that different hemichannels are involved in the passage of anionic or cationic dyes through the membrane, depending on cell type (Pelegrín 2011). As P2X7R displays this interesting dual function in the cell membrane it was important to further investigate whether the initial ion current through the P2X7R channel itself or the subsequent pore formation is the necessary element for TG2 release in the HEK2393 cell model.

The aims for the chapter:

1. Investigate if TG2 release is dependent on extracellular Ca^{2+} entry upon P2X7R activation?
2. Investigate if TG2 externalization is dependent on P2X7R pore formation?

7.2 Results

7.2.1 Possible mechanisms of P2X7R-evoked signaling mediating TG2 externalization

At this point of study it was essential to consider which component of P2X7R-evoked signaling may be involved in TG2 externalization (Fig. 7.1). One possible hypothesis was, that the initial P2X7R channel opening resulting in a fast Ca^{2+} influx, is the important element driving TG2 secretion (see Chapter 5, Fig. 5.5-5.7) (Ca^{2+} signaling). As this step results in membrane depolarization and is accompanied with Na^{+} entry and K^{+} depletion, those changes in ion concentrations might influence non-conventional TG2 release. A third possible mechanism for TG2 release might involve formation of large membrane pores by P2X7R itself that is known to develop upon prolonged BzATP stimulation. In addition, we predicted that ATP-evoked signaling could lead to P2Y activation, which is associated with subsequent release of Ca^{2+} from intracellular ER stores and this downstream step could contribute to TG2 externalization in addition to extracellular Ca^{2+} influx. The possible mechanisms of non-classical TG2 secretion involves its translocation across the membrane with the help of specific transporters or microvesicle shedding from the cell surface. As extracellular enzymatic activity of TG2 is regulated by Ca^{2+} ions and associated with substantial changes in enzyme conformation, it seemed possible that external Ca^{2+} plays an important role in the process of rapid TG2 translocation through the plasma membrane. Thus, the effect of extracellular Ca^{2+} on TG2 secretion and activation was first studied.

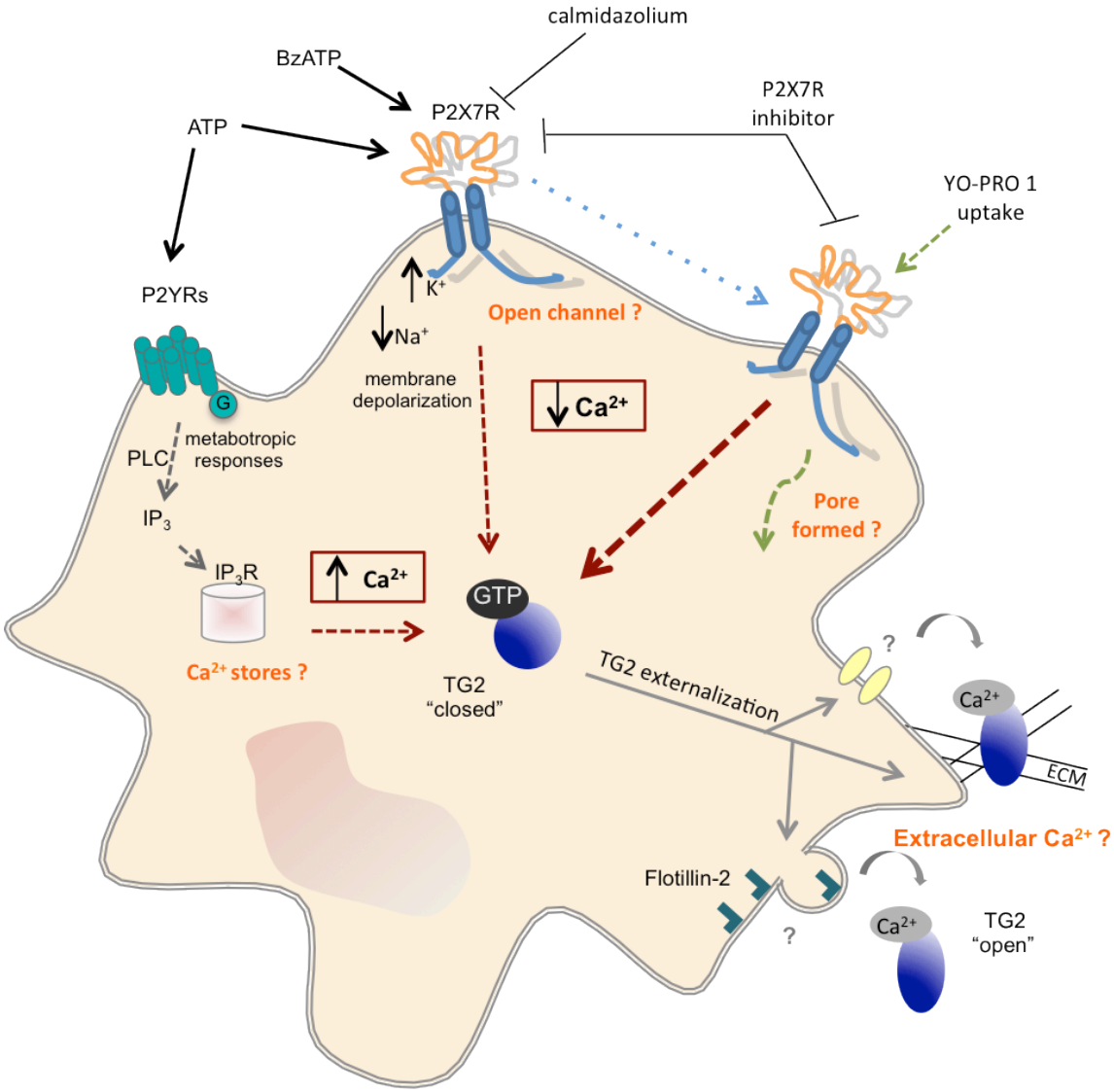

Fig. 7.1 Schematic representation of the proposed signalling leading to TG2 release from the cell. The P2X7 receptor can be activated by high extracellular ATP/BzATP concentrations. Binding of agonist to P2X7R opens a membrane channel leading to Na^+ influx and K^+ efflux, subsequent Ca^{2+} influx and cell membrane depolarization. Increase in intracellular Ca^{2+} may recruit TG2 for release, potentially through microvesicle shedding (as flotillin-2) or yet unknown membrane transporters. Prolonged stimulation of P2X7R and/or high concentrations of agonist further dilates the channel and leads to formation of a large membrane pore that can be visualized by dye uptake (e.g. YO-PRO-1). It is uncelar whether P2X7R activation alone or pore formation might be a necessary step for fast TG2 release. Purinergic signalling mediated by ATP can lead to activation of P2Y receptors and release of Ca^{2+} from intracellular stores via IP_3 production, which might be involved in TG2 release. Within the cell, TG2 is inactive due to tight regulation by GTP. Ca^{2+}-binding serves as a molecular "switch" for activation and induces the conformational change from its 'closed' to an 'open' conformation. Once externalized, TG2 might bind to and calatyze cross-linking of cell surface and ECM proteins. Inhibitors selectively blocking specific molecular events were employed to understand the contribution of these events to TG2 externalization.

7.2.2 Regulation of TG2 externalization by extracellular Ca^{2+}

The first hypothesis was that entry of extracellular Ca^{2+} through the P2X7R channel or membrane pore is regulating availability of TG2 in the extracellular space. The fact that TG2 was found to be present in the growth medium of HEK293 P2X7R cells was an interesting observation itself (see Chapter 6, Fig. 6.1-6.4), as most of the cells that externalize TG2 will express it only on the cell surface or deposit it directly into the ECM (Lorand and Graham 2003). Upon P2X7R stimulation, TG2 secretion was observed in medium (OptiMEM) that contained a Ca^{2+} concentration of 0.9 mM, which is slightly below the estimated free ionised extracellular Ca^{2+} is 1.1-1.3 mM (Riccardi and Kemp 2012). Therefore, the first question was whether TG2 release is still observed when extracellular Ca^{2+} concentrations are altered. Consequently, stimulation of HEK293 P2X7R cells with 100 μM BzATP was performed in OptiMEM supplemented with varying extracellular Ca^{2+} concentrations (0, 0.9 and 2.2 mM Ca^{2+}) (Fig. 7.2A and B). As shown in Chapter 6, BzATP stimulation under standard conditions (0.9 mM Ca^{2+}) led to an increase of TG2 secretion into the culture supernatant in both pulse and chase fractions. Surprisingly, stimulation of cells at 2.2 mM Ca^{2+} completely abolished TG2 externalization to the growth medium. The amount of TG2 released was highest in the pulse fraction when cells were stimulated in the absence of Ca^{2+} (OptiMEM with 1 mM EDTA). However, TG2 levels dropped back to baseline levels in the chase fraction. This suggests that TG2 release was fastest but not sustained at lower Ca^{2+} concentrations. To further elucidate whether TG2 release into the medium might be associated with microvesicle shedding, the nitrocellulose membrane was probed for the presence of flotillin-2. The amount of flotillin-2 released was greatest at 0.9 mM Ca^{2+} and greatly reduced in cells stimulated with BzATP at 0 or 2.2 mM Ca^{2+} (Fig. 7.2A). This further confirms that TG2 and flotillin-2 secretory pathway may be distinct and hence differentially affected by extracellular Ca^{2+}.

Interestingly, HEK293 P2X7R cells transiently expressing TG2 that were challenged with BzATP at different extracellular Ca^{2+} concentrations revealed distinct morphological changes upon P2X7R activation (Fig. 7.2C). In standard conditions (0.9 mM Ca^{2+}), cells stimulated with 100 uM BzATP became strongly activated and started to extensively bleb, whereas the same treatment at 2.2 mM Ca^{2+}

had a much less pronounced effect on cell morphology. Cells remained more spread and did not form visible membrane blebs seen in cells at 0.9 mM Ca^{2+}. On the other hand, cells that were stimulated in OptiMEM containing 1 mM EDTA started to detach from the plate and become rounded even without BzATP stimulation, thus suggesting that cation chelation has effects besides those related to P2X7R activation.

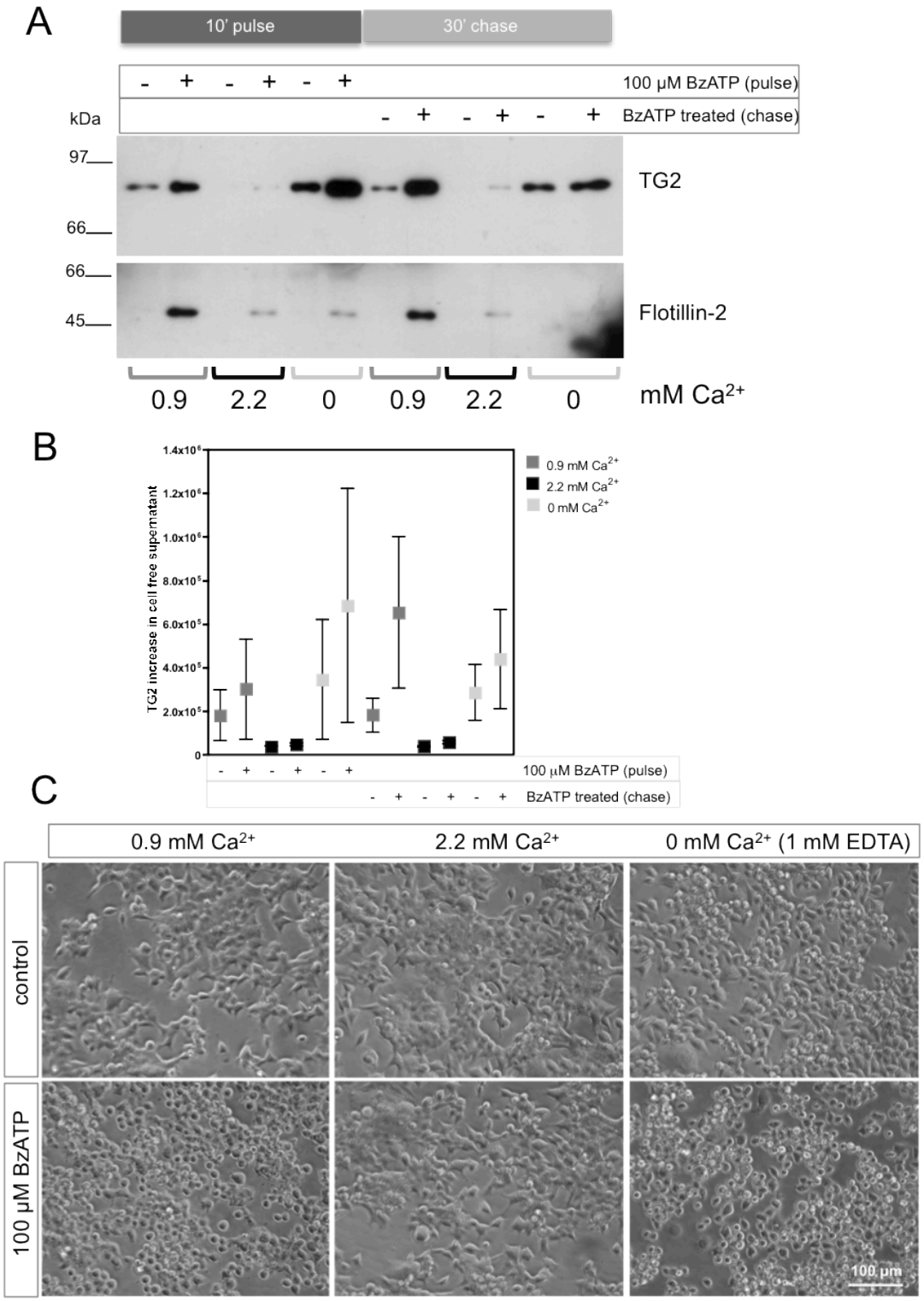

Fig. 7.2 P2X7R-mediated TG2 release at different extracellular Ca^{2+} concentrations. HEK293 P2X7R cells transiently expressing TG2 were stimulated for 10 min, in the absence or presence of 100 µM BzATP in OptiMEM containing 0.9 mM Ca^{2+}, 2.2 mM Ca^{2+} or 1 mM EDTA . Cells were washed and left for an additional 30 min in respective media without agonist. **A:** Conditioned medium was processed as previously described and analyzed by Western blotting for TG2 and flotillin-2. Result shown is a representative blot of two independent experiments. **B:** TG2 levels in the medium were estimated by densitometry and the volume of the bands was calculated. Graph represent mean value of the volume ± SEM from two independent experiments. **C:** At the end of the experiment, phase contrast images of cell monolayer were taken to look for changes in cell morphology that would indicate cell activation.

7.2.3 Investigation of the role of Ca^{2+}-mediated TG2 activation on its externalization

There were several possibilities of how extracellular Ca^{2+} levels may influence TG2 release into medium upon P2X7R activation. One of the hypothesis being that secreted TG2 was activated to a varying extent in the presence of different Ca^{2+} concentrations and may be crosslinked and therefore retained at the cell surface (pericellular ECM) at high but not low Ca^{2+} concentrations. Therefore, at high Ca^{2+} TG2 may no longer be detectable in the culture supernatant despite being translocated across the membrane. Thus, the aim of the experiment was to examine if addition of a potent TG2 inhibitor can restore its release into the medium at 2.2 mM Ca^{2+} by blocking its activity and therefore possible interaction/crosslinking to cell surface or ECM upon release. HEK293 P2X7R cells transiently expressing TG2 were stimulated with BzATP in 0.9 and 2.2 mM Ca^{2+} in the presence of a carrier (DMSO control) or 25 μM TG2 inhibitor (Boc-DON-QIVMeEs) (Fig. 7.3A). This concentration was previously found to be effective in blocking in situ TG2 activity in culture models (see Chapter 3, section 3.2.11, Fig. 3.13B and C). However, the presence of TG2 inhibitor during BzATP stimulation had no effect on TG2 amounts in medium. This indicated that the expected TG2 activation at 2.2 mM Ca^{2+} might not be the reason for why it is not present in the cell free supernatant at high Ca^{2+} concentration. Nonetheless, it is possible that crosslinking occurred in a compartment inaccessible to inhibitor. Therefore, another approach was used to exclude that TG2 enzymatic activity is an important factor influencing its release from the cells. This time externalization of wild-type TG2 was compared with secretion of TG2 that contains a mutation in the cysteine of the active site ($C^{277}S$) (Fig. 7.3B). Release of mutant lacking transamidation activity should occur independent of extracellular Ca^{2+} concentrations if the role of Ca^{2+} in externalization relates to regulation of enzyme itself. The secretion was compared at both, 0.9 and 2.2 mM of extracellular Ca^{2+}. BzATP stimulation induced both TG2 as well as TG2 $C^{277}S$ mutant translocation into the medium at 0.9 mM Ca^{2+} but not at 2.2 mM Ca^{2+} (Fig. 7.3B). This indicates that the observed differences in TG2 release at specific Ca^{2+} concentrations are not associated with altered TG2 activity, but might be related with differences in P2X7R activation or possibly pore formation.

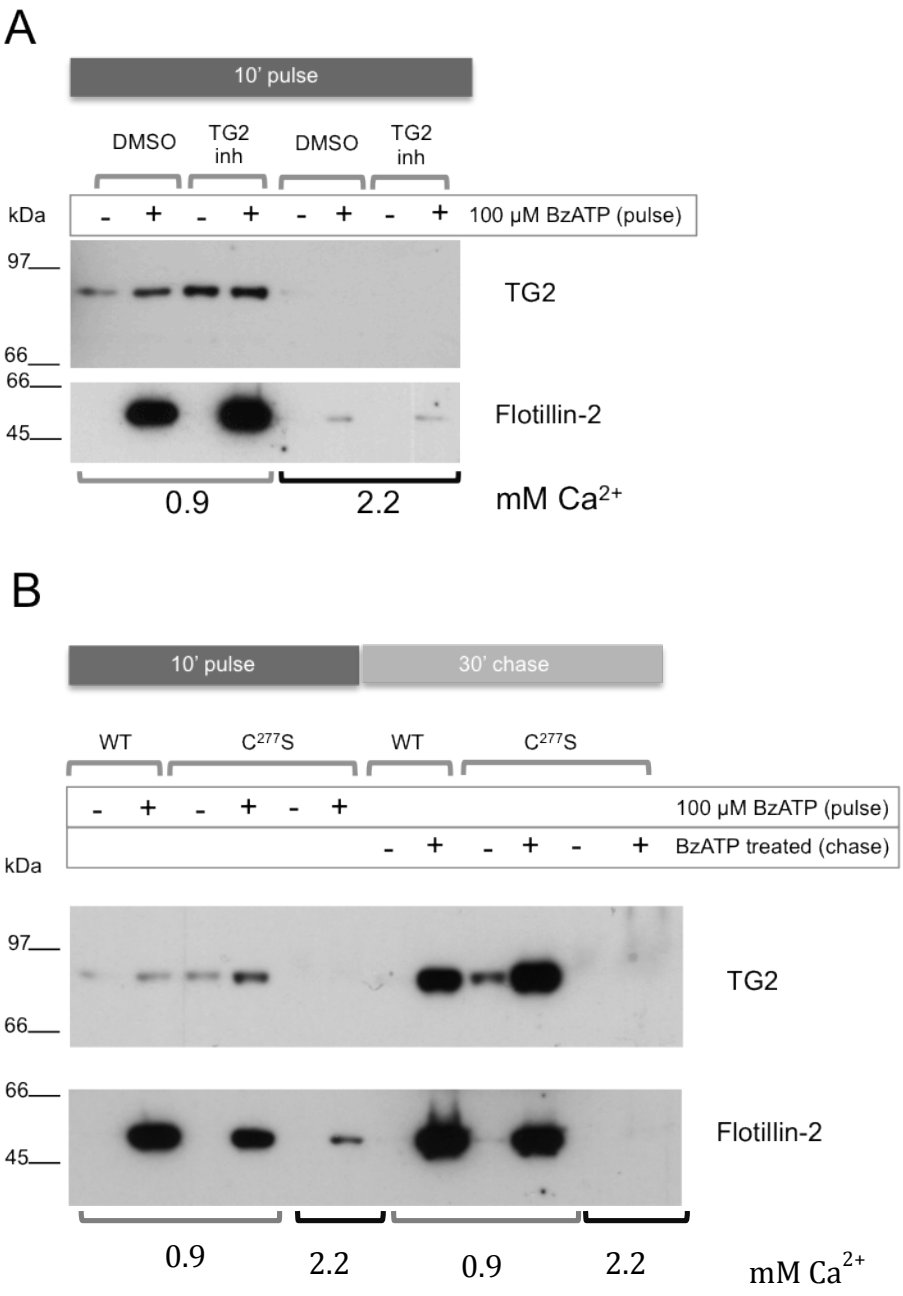

Fig. 7.3 Investigating whether TG2 catalytic activity is necessary for P2X7R-mediated enzyme release. A: HEK293 P2X7R cells transiently expressing TG2 were stimulated for 10 min in the absence or presence of 100 µM BzATP in OptiMEM containing 0.9 mM Ca^{2+} or 2.2 mM Ca^{2+}. Where indicated, 25 µM TG2 inhibitor (Boc-DON-QIVMeEs) was added and DMSO (0.05%) was used as a carrier control. Conditioned medium was processed as before and analyzed by Western blotting for TG2 and flotillin-2. **B:** HEK293 P2X7R cells were transiently transfected with wild-type TG2 or TG2 mutant $C^{277}S$. After 48h, cells were stimulated for 10 min in the absence or presence of 100 µM BzATP in OptiMEM containing 0.9 mM Ca^{2+} or 2.2 mM Ca^{2+}. Cells were washed and left for an additional 30 min in respective media without agonist. Conditioned medium was processed as before and analyzed by Western blotting for TG2 and flotillin-2. Result shown is a representative blot of two independent experiments.

7.2.4 TG2 release after blocking the P2X7R ion channel

Previous experiments using A740003 P2X7R inhibitor confirmed that TG2 secretion could be specifically blocked in HEK293 overexpressing P2X7R cells (see chapter 5, section 5.2.3.3, Fig. 5.8). This competitive P2X7R inhibitor abolishes both P2X7R-dependent current and pore formation at the same time (Honore et al. 2006). However, it was interesting to further distinguish which of those two intrinsic functions of P2X7R are necessary for mediating TG2 secretion. To assess the contribution of the initial ion flux on TG2 secretion calmidazolium chloride was chosen. Calmidazolium is a non-specific inhibitor of Ca^{2+} and Na^{+} membrane channels that is able to inhibit the initial ATP-evoked current through P2X7R without affecting the dye uptake by the cells (Virginio et al. 1997). The release of wild-type TG2 was assessed in standard conditions (OptiMEM with 0.9 mM Ca^{2+}) in the presence and absence of 1 μM calmidazolium chloride (Fig. 7.4A). The collection point of the chase fraction was reduced from 30 min to 10 min to be able to see if the presence of calmidazolium might delay TG2 release and be more apparent during the initial burst of TG2 release. Treatment of cells with BzATP in the presence of calmidazolium had no effect on TG2 release. However, calmidazolium was effective in blocking flotillin-2 secretion. This might indicate that the secretion of TG2 is dependent on the P2X7R-dependent pore formation, but not the initial ion flux and associated currents.

7.2.5 Analyzing the role of Ca^{2+} in regulation of P2X7R pore formation

Given that the observed TG2 release could be linked with the formation of the large P2X7R pore it was important to investigate if HEK293 P2X7R cells are able to undergo membrane pore formation when stimulated with 100 μM BzATP. Additionally, it was important to investigate whether the kinetics of this process correlated with TG2 release. Measurement of YO-PRO-1 uptake is one of the common methods used to study pore formation evoked by P2X7R activation. YO-PRO-1 fluorescence assay was adapted to measure pore formation in HEK293 P2X7R cells in real-time to test various conditions. Uptake was examined in PSS buffer containing 0 mM Ca^{2+} in order to evoke maximal P2X7R activation. The pore formation abilities were first compared between parental HEK293 cells and P2X7R

stable transfectants. A fluorescence increase indicative dye entry into the cells was visible only in P2X7R cells and developed within 30 seconds of BzATP addition (Fig. 7.4B). Hence, pore formation occurred surprisingly fast and closely followed by Ca^{2+} signaling in these cells. Parental cells were unable to form the membrane pores and consequently failed to uptake YO-PRO-1 even at high BzATP concentrations (300 μM) as expected. In P2X7R positive cells the YO-PRO-1 uptake was clearly dose-dependent and the response potentiated at higher (300 μM) BzATP concentrations (Fig. 7.4B). We therefore decided to examine dose dependence in more detail (Fig. 7.4C and D). Dye uptake showed a bi-phasic concentration-dependence profile. Unexpectedly, fast uptake followed by a much slower reaction but only when high BzATP concentrations were administered (>300 μM) (Fig. 7.4D). It seems that above a certain threshold of agonist concentration, P2X7R can further dilate or change conformation, which allows increased YO-PRO-1 uptake. However, this later change seems not to be required for TG2 release, as 100 μM BzATP is sufficient to trigger enzyme export.

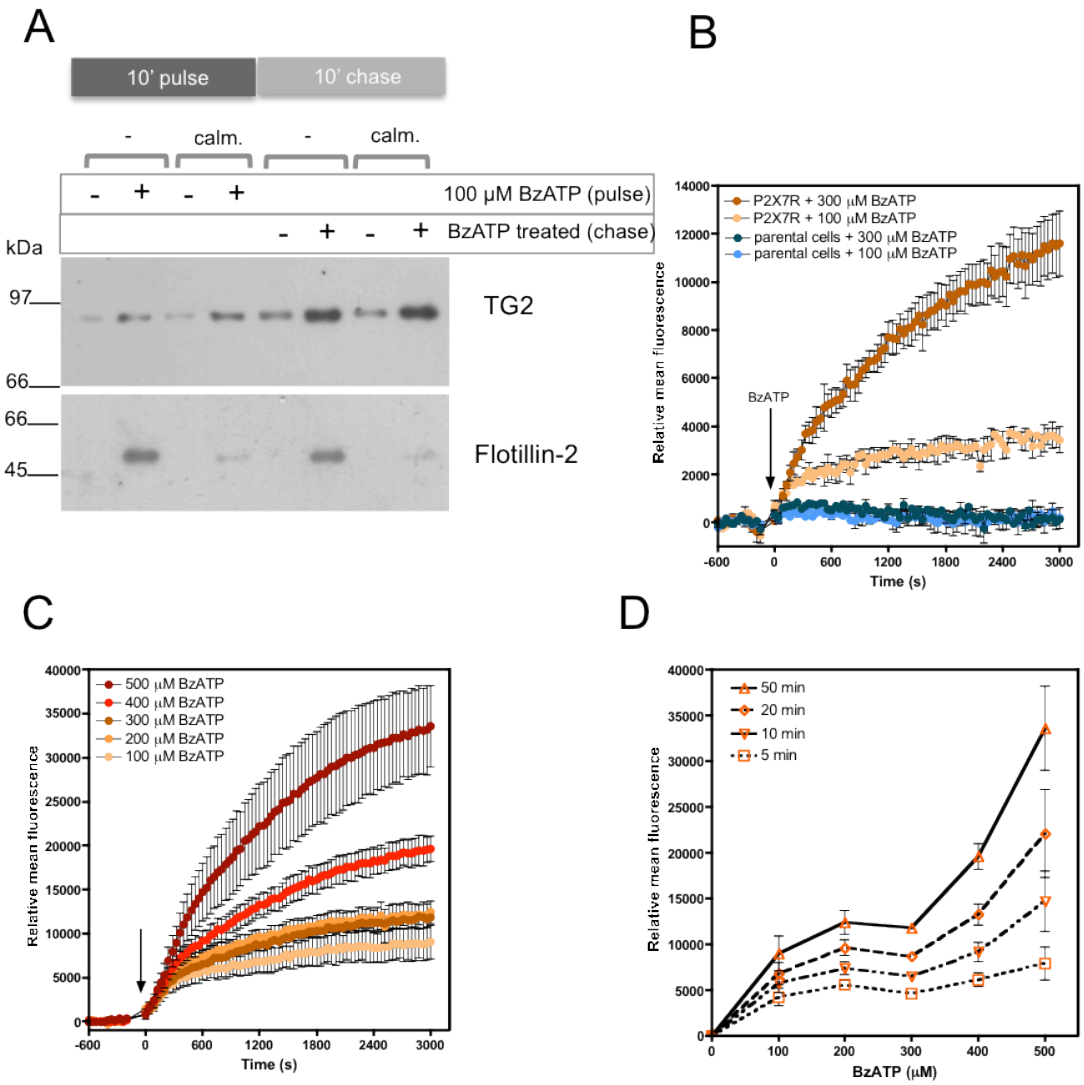

Fig. 7.4 Investigating the role of P2X7R ion channel function and P2X7R pore formation for TG2 release. A: HEK293 P2X7R cells transiently expressing TG2 were pre-treated for 10 min with or without 1 µM Calmidazolium chloride prior to P2X7R stimulation. Then cells were kept for 10 min in the absence or presence of 100 µM BzATP in OptiMEM. Where indicated, 1 µM Calmidazolium chloride was also present. Cells were washed and left for an additional 10 min in respective media without agonist. Conditioned medium was processed as before and analyzed by Western blotting for TG2 and flotillin-2. Result shown is a representative Western blot of two independent experiments. **B:** HEK293 parental cells and cells stably expressing P2X7R were seeded in a 96-well plate at the density of 3 x 10^3 cells/well. After 2 days cells were washed and 1 µM YO-PRO-1 in PSS without Ca^{2+} was added. Then cells were stimulated with 100 or 300 µM BzATP, respectively, and the YO-PRO-1 uptake was monitored (excitation 480 nm, emission 520 nm). Each point is the mean fluorescence ± SEM from two wells. Graph is a representative result of two independent experiments. **C, D:** Cells stably expressing P2X7R were stimulated with various concentrations of BzATP. Measurements were performed in PSS without Ca^{2+} in the presence of 1 µM YO-PRO-1. Changes in YO-PRO 1 uptake were monitored and each point is the mean fluorescence ± SEM from two wells (**C**). The YO-PRO-1 fluorescence obtained after different times of continuous P2X7R stimulation was plotted against BzATP concentrations (**D**).

In the next stage, it was important to understand if the presence of various concentrations of external Ca^{2+} will influence the process of pore formation. It has previously been shown that the removal of Ca^{2+} from the external solution can slow the increase of pore dilation (Virginio et al. 1999). As TG2 externalization was dependent on the levels of extracellular Ca^{2+} but not related with its catalytic activity, differences in P2X7R pore formation at various external Ca^{2+} concentrations could offer a potential explanation. The P2X7R response was therefore compared after addition of 500 μM BzATP in the presence of 0 or 2 mM Ca^{2+}. Surprisingly, treatment of cells at 2 mM Ca^{2+} evoked a transient unexpected spike of fluorescence, that was not observed at 0 mM Ca^{2+} (Fig. 7.5A). However, this transient spike was not observed at lower Ca^{2+} concentrations (Fig. 7.5B). Furthermore, this spike was not related with P2X7R as this initial spike in fluorescence at 2 mM Ca^{2+} was also observed in parental HEK293 stimulated with 100 μM BzATP (Fig. 7.5D). It is unclear what causes the fluorescence change but it is unlikely related to dye uptake by cells. YO-PRO-1 accumulation over time was observed only in P2X7R overexpressing cells, even when stimulation at 2 mM Ca^{2+} (Fig. 7.5A and D). After reducing the BzATP concentration to 300 μM, the changes in YO-PRO-1 uptake at different Ca^{2+} concentrations was analyzed and indicated that the presence of Ca^{2+} is directly modulating the rate of dye uptake in those cells (Fig. 7.5C). When the initial reaction rates were compared the data indicated that dye uptake is inversely proportional to the Ca^{2+} concentration (Fig. 7.5D).

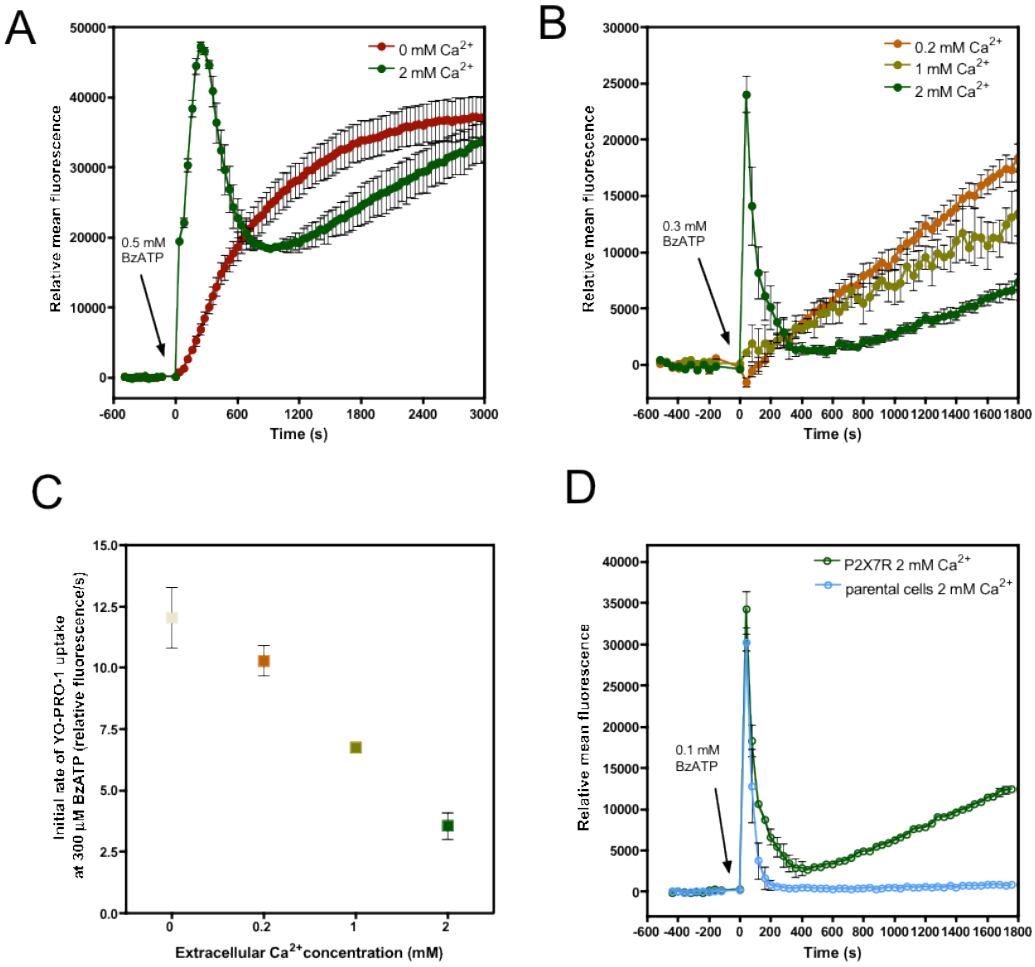

Fig. 7.5 P2X7R-mediated dye uptake at different extracellular Ca^{2+} concentrations. A-C: HEK293 P2X7R were seeded in a 96-well plate at a density of 3 x 10^3 cells/well. When cells reached approx 80 % confluency, medium was replaced with PSS containing various concentrations of Ca^{2+} and 1 µM YO-PRO-1. Then, cells were stimulated with 500 µM BzATP in PSS containing 2 or 0 mM Ca^{2+} and dye uptake was monitored. Each point is the mean fluorescence ± SEM from two wells **(A)**. HEK293 P2X7R were stimulated with 300 µM BzATP in PSS containing 2, 1 or 0.2 mM Ca^{2+}. Each point is the mean fluorescence ± SEM from two wells (**B**). The data points after BzATP administration were analyzed by linear regression and the value of reaction rate was plotted against the concentration of extracellular Ca^{2+} present during YO-PRO-1 uptake. Error bars represent SEM of mean obtained from multiple measurements (**C**). **D:** Parental cells and cells stably expressing P2X7R were washed and medium was replaced with PSS containing 2 mM Ca^{2+} and 1 µM YO-PRO-1 prior to stimulation with 100 µM BzATP. Each point is the mean fluorescence ± SEM from two wells.

7.3 Discussion

The main focus of this chapter was to study the role of extracellular Ca^{2+} on rapid TG2 externalization triggered by P2X7R activation. The aim of this part of study was to investigate if TG2 enzymatic activity is required for secretion. Moreover it was investigated whether increase in extracellular TG2 levels are occurring due to the initial BzATP-evoked Ca^{2+} influx through P2X7R open channel or happen as a consequence of membrane pore formation. Collected evidence is suggesting that intracellular sustained rise in intracellular Ca^{2+}, mediated by membrane pore, might be a possible mechanism leading to TG2 delivery into extracellular space.

Extracellular activity of TG2 is dependent on Ca^{2+} ions that facilitate the transition of TG2 into an active, open conformation that exposes the catalytic core (Bergamini 1988; Pinkas et al. 2007). It has been previously proposed that TG2 unconventional secretion might be linked with Ca^{2+} signaling (Zemskov et al. 2011). It was shown that intracellular Ca^{2+} chelator (BAPTA) reduces the level of surface TG2, whereas Ca^{2+} ionophore (Ionomycin) upregulates its presence at the surface of HUVEC endothelium cells and WI-38 fibroblast endogenously expressing TG2. However, the detailed mechanism that connected intracellular [Ca^{2+}] changes with non-classical TG2 secretion has not been proposed. In this part of study, the stimulation of cells with BzATP at different concentrations of Ca^{2+} suggested that extracellular Ca^{2+} levels are important for TG2 externalization process and regulate its availability in the growth medium. During P2X7R stimulation, the amounts of released TG2 were decreasing with increasing concentrations of extracellular Ca^{2+}. Therefore, it was hypothesized that at 2.2 mM Ca^{2+}, a condition when TG2 should be fully active (Király et al. 2011), it might immediately bind to ECM and be no longer detected in the growth medium. However, the experiment with active site mutant ($C^{277}S$) revealed that the $C^{277}S$ mutant was also secreted in the same manner as wilt-type protein. Thus, the increased enzymatic activity of TG2 is not the reason why its no longer present in the medium at 2.2 mM Ca^{2+}. Moreover, it showed that the catalytic activity of TG2 is not a requirement for its rapid release. Similar results were previously reported by van den Akker and colleagues (2011), which showed gradual accumulation of TG2-conatinaing microvesicles in the growth medium of transiently transfected HEK293 cells. They also showed that $C^{277}S$ inactive mutant

was localizing in the conditioned medium similarly to wild-type TG2. Alike, Antonyak and collagues (2011) reported that TG2 enzymatic activity was not essential for its release from MDA-MB-231 cells. Blocking TG2 surface activity by monodansylcadaverine or T101 inhibitor did not interfere with microvesicle formation**.** Different approach to detect TG2 in the medium was used by Balklava and colleagues (2002) where the conditioned medium from serum-starved 3T3 fibroblasts was pre-cleared by centrifugation and protein precipitated or lyophilized in order to assess wild-type TG2 and $C^{277}S$ mutant levels by ELISA (Balklava et al. 2002). However, they have observed that only wild-type TG2 could be deposited in the ECM and localize in conditioned medium, whereas $C^{277}S$ was retained on the surface of fibroblasts (Balklava et al. 2002). It is therefore likely that enzymatic activity of TG2 might be important factor controlling TG2 availability outside the cells and vary between different cell types.

The experiment with variable concentrations of extracellular Ca^{2+} also suggested that the sustained increase of intracellular Ca^{2+} might be necessary element of the pathway recruiting TG2 for release. Increased levels of TG2 were detected in cells in OptiMEM with 0.9 mM Ca^{2+} even after removal of the BzATP but this was not the case at 0 mM Ca^{2+}. One of the explanations why further TG2 accumulation is not seen is that lack of external Ca^{2+} might induce complete depletion of Ca^{2+} from intracellular stores during first 10 min of BzATP stimulation. On the other hand, it was previously shown that BzATP stimulation induced intracellular [Ca^{2+}] rise in HL-60 promyleocytes but only when cells were kept at 2.2 mM Ca^{2+} (Suh et al. 2001). BzATP treatment at 0 mM external Ca^{2+} was not sufficient to induce rise in intracellular Ca^{2+} which indicate that P2X7R stimulation does not lead to IP_3 generation and PLC-dependent signaling in those cells. However, they showed that BzATP addtition was still able to evoke membrane depolarization even without external Ca^{2+}, which indicates that P2X7R activation is still prominent at this state. Thus, to fully understand involvement of intracellular [Ca^{2+}] rise on TG2 externalization the experiments with PLC and IP_3 inhibitors should be perform to investigate if only influx through P2X7R channel rather that [Ca^{2+}] mobilization from intracellular stores is playing an important role in observed prolonged TG2 release not seen without external Ca^{2+}.

Ca^{2+} signaling is a known inducer of MV shedding and activator of cytoskeletal rearrangements. The release of [Ca^{2+}] from intracellular stores can activate plasma membrane enzymes such as flippase, floppase and scrambalase, which in stady-state are regulating phospholipid membrane asymmetry (Burnier et al. 2009). Changes in enzymes distribution lead to loss of aminosphingolipids anchorage to the cytosleleton and it dissociation. Therefore local [Ca^{2+}] increase takes an active part in the process of membrane blebbing. Interstingly, the levels of extracellular Ca^{2+} were also regulating the release of flotillin-2, which were optimal at 0.9 mM Ca^{2+}. Decreased levels of in flotillin-2 in EDTA treated medium might be explained by the reduced shedding of membrane vesicles upon removal of extracellular Ca^{2+}. Mackenzie and colleagues (2001) observed that in the lack of external Ca^{2+} cell blebbing is reduced but no loss of membrane area is seen in both HEK293 expressing rat P2X7R cells and THP-1 monocytes. Moreover in a Ca^{2+} free medium, the release of IL-1β from LPS primed THP-1 cells was abolished after challenge with BzATP and no longer detected at early time points when IL-1β is postulated to be secreted via microvesicle pathway. Similarly microvesicles shedding is reduced in dendritic cells in the lack of external Ca^{2+} (Pizzirani et al. 2007). Morelli and colleagues (2003) showed that in the presence of EGTA the cells are not undergoing extensive blebbing but become more swollen and rounded. They speculate that this might be an effect of large Na^{+} influx that permeates the channel in the shortage of Ca^{2+}. Therefore Ca^{2+} signaling through P2X7R is an important component of the microvesicles shedding (Morelli et al. 2003) and presence of Ca^{2+} seems to be required to induce their rapid formation.

As the Ca^{2+} seems to be necessary element for microvesicles release and cell blebbing it was important to understand why TG2 and Flotillin-2 secretion was abolished at physiological Ca^{2+} concentrations (2.2 mM) when sustained Ca^{2+} entry should be expected. It was hypothesized that lack of TG2 and Flotillin-2 secretion might be due to insufficient P2X7R activation. It was previously shown that presence of divalent cations in the extracellular solution is reducing P2X7R channel opening and pore formation and speculated that cations are influencing the availability of free acidic form of ATP^{4-} to activate P2X7R (Virginio et al. 1997; Coddou et al. 2011). The acidic form of ATP is the true ligand to activate P2X7R but not the cation bound ATP (North 2002; Yan et al. 2011). In the presence of Ca^{2+} there is a rightwards shift

in agonist concentration dependence indicating that presence of Ca^{2+} decrease the potency of the agonist acting on P2X7R (Yan et al. 2008; Yan et al. 2011). However authors of that study show that Ca^{2+} is allosterically affecting P2X7R gating rather than only reducing the availability of $BzATP^{4-}$ (Yan et al. 2011). The same pattern of current facilitation response is observed when Ca^{2+} is present thus suggesting that extracellular Ca^{2+} itself does not affect transition from open to dilated receptor state. But the presence of Ca^{2+} significantly affected the P2X7R deactivation by altering the rate. Repeated stimulation of cells with 100 μM BzATP followed by washing periods showed that the deactivation of P2X7R is much slower in cells that were kept without extracellular Ca^{2+}. Therefore, it is possible that due to reduced P2X7R activation at high external Ca^{2+} TG2 release is not visible any more whereas at lower Ca^{2+} the effect is prolonged due to slower P2X7R deactivation. It will be interesting to further investigate differences in $[Ca^{2+}]$ signaling upon different extracellular Ca^{2+} concentrations to understand how TG2 secretion is linked with rapid Ca^{2+} influx.

The large C-terminus of P2X7R is involved in the process of pore formation possibly through interaction with hemichannels and proteins of cytoskeleton (Mackenzie et al. 2005; Costa-Junior et al. 2011; Baroja-Mazo et al. 2012). Thus, the observed changes in TG2 secretion might be as well linked with the changes in pore formation upon different Ca^{2+} concentrations but not initial Ca^{2+} influx. The preliminary experiments with YO-PRO-1 uptake seem to support this hypothesis as the initial rate of dye uptake was much lower at high Ca^{2+}. However, it seems that there might be a formation of transient fluorescent product at 2 mM Ca^{2+} and in the presence of BzATP that is not related to the P2X7R pore formation that should be further investigated. But if this peak is ignored, the kinetics of dye uptake differs between zero extracellular Ca^{2+} and when some Ca^{2+} is present in the bath solution. In the lack of Ca^{2+} the YO-PRO-1 uptake was quick and seemed to reach a plateau faster, but in the presence of Ca^{2+} the uptake was gradually increasing. At the moment there is not enough data to explain how pore formation might influence TG2 release at different extracellular Ca^{2+} levels. The experiment with calmidazolium suggest that the initial Ca^{2+} and Na^{+} entry might not be needed for TG2 releases but only pore formation is the key element. It is however not known what is the exact mechanism of calmidazolium chloride acting on P2X7R. This agent was previously used to block channel of cyclic-nucleotide-gated receptors and shows to inhibit the

initial current of rat P2X7R channel without affecting the pore formation (Virginio et al. 1997). Therefore, ATP is possibly able to bind to P2X7R and induce changes necessary for the pore to be formed even in the presence of calmidazolium. It is possible that its inhibition is similar to the action of another inhibitor, Invermectin. It was suggested that Ivermectin, which is an allosteric regulator of P2X4 receptor, might bind inside the open channel when the transmembrane domains slightly shift away from each other during receptor activation (Hattori and Gouaux 2012).The Invermectin could then bind to the lipid molecules of the membrane bilayer that fill the gap between the TM domains and modulate the function of the pore. In analogy, it is possible that binding of calmidazolium to P2X7R changes ions permeation pathway or delays their translocation but at the same time allow for the pore to be formed. As flotillin-2 but not TG2 release was affected by calmidazolium this further confirms that their release pathways are not the same.

In summary, literature and collected evidence suggest that extracellular Ca^{2+} is an important regulator of TG2 membrane translocation and this might be due to Ca^{2+} ions regulating the degree of P2X7R activation rather than enzymatic activity of TG2. Further studies are necessary to fully answer whether TG2 externalization is linked with P2X7R-dependnent pore formation or transient Ca^{2+} influx and membrane depolarization.

Chapter 8 General discussion

The aim of this disscussion is to briefly summarise the different hypothesis regarding TG2 export and contrast them to my findings. I am proposing a novel mechanistic link between P2X7R activation and TG2 release. P2X7R activation triggers the delivery of TG2 after cell injury, when ATP levels are elevated and act through paracrine signaling. The results presented in this thesis show for the first time that introduction of functional P2X7R alone is sufficient to reconstitute rapid non-conventional TG2 export in a cell model. The evidence presented here suggests that TG2 externalization is linked to P2X7R dependent Ca^{2+} signaling and might be due to the ability of P2X7R to form a pore.

Revealing the precise mechanism of TG2 externalization is a crucial task given the role of extracellular transamidation activity in disease proceses. This would potentially allow pharmacological modulation of TG2 secretion at specific stages of disease. It is likely that additional molecules are released through the same non-classical mechanism but their discovery is slow (Dinarello 2009). Non-conventional release triggered by activation of P2X7R might apply to other proteins, as it was shown for IL-1β (MacKenzie et al. 2001) and HMGB1 (Lu et al. 2012). This pathway may represent an important mechanism for regulating the presence of mediators at the sites of inflammation and injury. Moreover, it is likely that other members of the transglutaminase family are secreted using the same pathway, especially structurally closely related TG3 and TG6. This mechanism may also apply to FXIIIa, a protein with a well-definied extracellular function in hemostasis but which is also highly expressed in skeletal tissues like TG2 (Nurminskaya and Kaartinen 2006). The secretion of TG2 triggered by P2X7R might play a role in many diseases linked to inflammation, such as rheumatoid arthritis, osteoarthritis, coeliac disease and various types of cancers.

Another very important question linked to this topic that requires further investigation is whether TG2 activation is linked to externalization, or whether it occurs independently. Our current understanding suggests that TG2 is rapidly converted into the activated form by high extracellular Ca^{2+} concentrations (Pinkas et al. 2007). However, potentially secreted TG2 could remain in GTP/GDP-associated

closed conformation and this may depend on the microenvironment encountered in the externalization process (Johnson and Terkeltaub 2005). Several lines of recent evidence suggest that autocrine signaling in chondrocytes in fact requires extracellular GTP/GDP-bound enzyme (Johnson and Terkeltaub 2005). Additionally, antibodies against TG2 found in coeliac disease patients display and unexpected specificity (Iversen et al. 2013). Clonal antibodies isolated from CD patients were shown to bind the one of 4 different regions of the N-terminal part of TG2. Despite the fact that theoretically these N-terminal epitopes of TG2 are available in both open and closed conformations, antibodies only recognise TG2 when present in free form in solution but not when cell surface associated. These data suggest that both forms of TG2 are available in the extracellular space and might be mediating different responses.

8.1 Proposed mechanism: Rapid TG2 release is triggered by danger signals in osteoarthritis

I propose the hypothesis that ATP-dependent P2X7R activation triggers TG2 release, which may occur during development of osteoarthritis (Fig. 8.1). Both, P2X7R-mediated inflammatory cytokines release (Labasi et al. 2002) and extracellular TG2 action are likely to be implicated in joint pathology (Huebner et al. 2009). However, a link between these events is an entirely novel concept. It is still unclear which cell type is the main source of active TG2 released to the extracellular milieu during joint disease. Chondrocytes (Johnson et al. 2001), macrophages (Hodrea et al. 2010) as well as fibroblasts (Balklava et al. 2002) are all able to externalize TG2 and may independently contribute to the enzyme pool. A possible scenario that predisposes TG2 for the secretion during osteoarthritis might be the increased ATP concentrations released during aberrant mechanical loading of cartilage (Garcia and Knight 2010) (Fig. 8.1). Chondrocytes were shown to respond to purinergic signaling (Garcia and Knight 2010) and express P2X7R (Knight et al. 2009). This leads to TG2 export as well as activation and might promote tissue mineralization and induce chondrocyte hypertrophy. As specyfic P2X7R polymorphisms have been linked with both rheumatoid arthritis (Al-Shukaili et al. 2011) and osteoarthritis (Sorge et al. 2012), it is likely that patients with allelic variants of P2X7R may differ with regards

to TG2 export. This should be further investigated and may identify specific patient populations that are naturally deficient in certain activities of TG2.

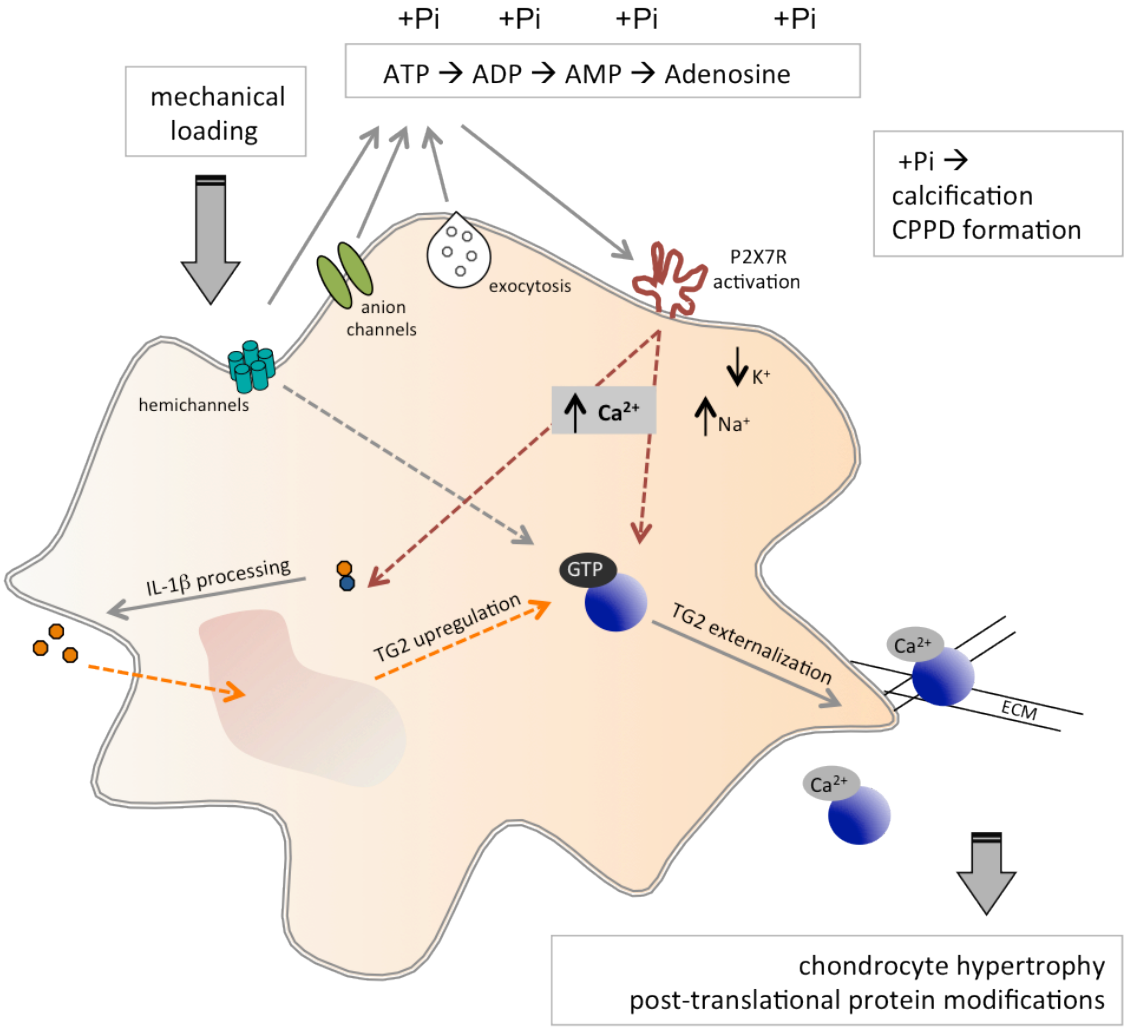

Fig. 8.1 Schematic representation of the P2X7R signalling leading to TG2 release from chondrocytes during osteoarthritis. Mechanical loading of cells releases ATP to the extracellular compartment. ATP is rapidly hydrolysed on the cell surface by ectoenzymes and inorganic phosphate (Pi) molecules are generated. Nevertheless, the P2X7 receptor can be activated by high local extracellular ATP concentrations. Binding of agonist to P2X7 opens a membrane channel leading to Na^+ influx and K^+ efflux, subsequent Ca^{2+} influx and ultimately cell membrane depolarization. Increase in intracellular Ca^{2+} may recruit TG2 for release. IL-1β is rapidly secreted after P2X7R stimulation and acts in an autocrine way to upregulate TG2 transcription. Inorganic phosphate (Pi) drives matrix calcification and deposition of calcium pyrophosphate dehydrate crystals (CPPD). Ca^{2+}-binding upon TG2 externalization serves as a molecular "switch" for its activation, and ultimately leads to aberant protein modifications, chondrocyte differentiation and matrix mineralization.

8.2 Current understanding of constitutive TG2 release

8.2.1 TG2 release via recycling endosomes

Non-conventional export of TG2 by fibroblasts and endothelial cells seems to occur in a constitutive manner and involve different membranous organelles (Zemskov et al. 2011). It was shown that after three hours of induction of TG2 expression, TG2 was found co-localized with perinuclear vesicles prior to their export. At the initial step of TG2 synthesis, TG2 appear to be targeted into the vesicles expressing the recycling endosomal marker (Rab11). Therefore, newly synthesized cytosolic TG2 needs to somehow fuse with recycling endosomes and be captured inside the vesicles. This was verified by the fact that both TG2 and Rab11 were shown to be protected from proteolytic degradation due to their endosomal localisation (Zemskov et al. 2011). The authors suggested that the fusion process involves an interaction of TG2 with phosphoinositides localized on recycling vesicles. The ^{590}KIRILGEPKQRKK^{602} sequence motif in TG2 is possibly responsible for the interaction with phosphoinositides. However, as this is not a conserved sequence motif among other members of the TG family, this type of export would only apply to TG2. Mutation of the phosphoinositide binding site present in TG2 on a second β-barrel domain, apparently lead to reduced TG2 recruitment into recycling endosomes and decreased TG2 surface levels (Zemskov et al. 2011). Therefore, the authors concluded that this interaction is crucial for proper TG2 export. This is in contradiction to data presented by Chou and colleagues (2011). They showed that epithelial cells are able to secrete both wild-type TG2 as well as a mutant TG2 lacking β-barrel 2 into the conditioned medium (Chou et al. 2011). Both enzymes were efficiently deposited into the ECM upon serum starvation. In contrast, TG2 lacking the N-terminal β-sandwich domain was not deposited into the ECM and not secreted into the medium (Chou et al. 2011). Other groups have also shown that the intact N-terminal part of TG2 is necessary for TG2 trafficking and required for cell surface localization (Balklava et al. 2002; Telci et al. 2008) as binding of the N-terminal part of TG2 to FN facilitates its presence on the cell surface and in the ECM (Gaudry et al. 1999). Residues in the N-terminal domain, responsible for the FN

interaction were also described (Chou et al. 2011). $D^{94}A$ and $D^{97}A$ point mutations in the putative FN binding sequence were shown to inhibit TG2 secretion (Chou et al. 2011). However, silencing the FN expression had no effect on TG2 export. Thus, the authors concluded that TG2 translocation through the membrane is FN-independent in epithelial cells (Chou et al. 2011). However, it is not known how these point mutations affect TG2 folding and conformation as well as activity and therefore, the lack of TG2 may be due to misfolding of the protein. It is possible that constitutive TG2 secretion is cell-type specific or different experimental approaches between research groups lead to some contradicting findings and this requires further studies.

8.2.2 TG2 endocytosis from the cell surface

It was also suggested that the pool of TG2 on the cell surface is dynamic. TG2 association with peripheral endocytic vesicles was proposed, allowing fast TG2 recycling and trafficking into the cell (Zemskov et al. 2007). In fibroblasts, endocytosed TG2 was shown to associate with early endosomes (after 5 min), followed by progression to Rab7 positive late endosomes (after 30 min) and eventual translocation into lysosomes expressing LAMP-1 (after 90 min). However, the previously discussed report on TG2 export (Zemskov et al. 2011) suggests that at the initial step of TG2 biosynthesis, TG2 is targeted into the recycling endosomes with Rab11 expression (Zemskov et al. 2011). This indicates that a different subset of vesicles may be involved in TG2 delivery to the cell surface when compared to internalization. These findings makes the model quite complex and does not fully explain how these processes are separated. TG2 is believed to share the same endocytic pathway with β1 integrin, although only proteolytically cleaved TG2 can be detected upon its internalization (Zemskov et al. 2007). TG2 endocytosis is dependent on cholesterol and needs dynamin-2 GTPase activity for intracellular trafficking. Moreover, TG2 co-localization with transferrin was detected suggesting a clathrin-dependent mechanism of endocytosis (Zemskov et al. 2007). However, involvement of lipid rafts or caveolae cannot be ruled out, as inhibitors of this type of internalization blocked TG2 endocytosis and proteolysis (Zemskov et al. 2007). The interaction of the TG2 catalytic domain with low–density lipoprotein receptor-related protein 1 (LRP1) is believed to be required for TG2 endocytosis. This observation

was based on the fact that LRP1 deficient cells showed an increased cell surface transamidation activity. This may constitute a mechanism that regulates TG2 extracellular activity in fibroblasts. However, another route for TG2 internalization was recently discovered in our lab. It might be mediated by its interaction with membrane G-coupled receptor, GPR56 (data of Bauer et al. in our lab). TG2 was shown to be a ligand for GPR56 and to undergo clathrin-mediated endocytosis upon GPR56 binding (Bauer et al). GPR56 and was shown to regulate melanoma metastasis by as yet unknown mechanism (Xu et al. 2006). However, TG2 may only be one of several potential ligands and the respective interactions are likely to have different functional roles.

8.2.3 TG2 shed form cells in microvesicles and microparticles

Apoptosis, direct membrane blebbing or exosome formation represent different pathways for membrane-bound cargo delivery from cell to cell (Al-nedawi et al. 2009). The release of TG2 in microparticles was already discussed in previous chapters and this type of constitutive release has been reported in mouse vascular smooth muscle cells (van den Akker et al. 2011). There is also evidence of TG2 captured inside the shed microvesicles, as seen in cancer cells (Antonyak et al. 2011). This type of release was potentiated by serum deprivation, or by EGF treatment of some cancer cells. It is still unclear how TG2 is specifically targeted into these vesicles for export and whether this process is different in normal versus cancer cells.

8.3 Modulators of TG2 availability on the cell surface/ECM

8.3.1 TG2 release regulated by nitric oxide

Nitric oxide (NO)-dependent S-nitrosylation is a proposed mechanism regulating TG2 export in the vascular wall (Santhanam et al. 2010; Jandu et al. 2013). There are some recent reports showing that NO inhibits TG2 externalization in vascular endothelial cells and fibroblasts (Telci et al. 2009; Santhanam et al. 2010; Jandu et al. 2013). NO was previously shown to nitrosylate free cysteine residues of TG2 (Lai

et al. 2001). In the presence of Ca^{2+} ions, the S-nitrosylation was even more profound, probably resulting in TG2 "unfolding" that allows for more cysteine residues being exposed on the surface of the molecule (Lai et al. 2001). As S-nitrosylation inhibits TG2 activity, NO is thought to be an important allosteric regulator of TG2 activity. Jandu and colleagues show that under conditions promoting nitric oxide formation, addition of an NO synthase inhibitor restores TG2 cell surface localization and its export to ECM in human aorta endothelial cells (Jandu et al. 2013). The inhibitor was able to decrease the S-nitrosylation of TG2 in a time-dependent manner, which allowed gradual extracellular TG2 accumulation. In analogy, addition of NO donor to smooth muscle cells or human fibroblasts not only significantly reduced TG2 surface and ECM presence, but also inhibited its extracellular cross-linking activity. Telci and colleagues obtained similar results when they treated human fibroblasts with an agent continuously releasing NO and noticed decreased extracellular TG2 localization and reduced FN deposition in treated fibroblasts (Telci et al. 2009). NO treated cells had some TG2 on the cell surface but were apparently not able to deposit it into ECM (Telci et al. 2009). There might be some differences between fibroblasts and vascular endothelial cells in TG2 export. Interestingly, the S-nitrosylation of TG2 is reversible by addition of reducing agent, such as DTT, which increases the activity of TG2 in epithelial cells (Santhanam et al. 2010). However, it is unclear whether S-nitrosylation is reversible *in situ*. Moreover, the gain of TG2 activity is in agreement with other reports suggesting that the redox potential clearly affects TG2 extracellular activity (Stamnaes et al. 2010). In summary, laminar shear stress reduce TG2 surface levels and activity by inducing S-nitrosylation of TG2, and abolishes its deposition into the ECM (Santhanam et al. 2010; Jandu et al. 2013). However, it is currently not known if this mechanism of regulating TG2 bioavailability in the extracellular space would apply to other cell types or is specific to endothelial cells and fibroblasts.

8.4 Final conclusions

In summary, the results presented in this thesis have advanced our understanding of non-conventional export of TG2 from cells. The data provided an excellent basis for additional research in this area as it identifies a signal that controls the export

mechanism. Although, not answering the question of TG2 membrane translocation it characterizes a novel mechanism that triggers TG2 externalization, which was not reported before in the literature. This mechanism might exist alongside the other proposed mechanisms of constitutive TG2 release. However, an answer to this awaits further experimental evaluation.

Further understanding of how biologically active TG2 is generated is of fundamental importance. Firstly, non-conventional protein export is likely a conserved pathway shared by potent biological signaling molecules including IL-1β, thioredoxin, HMGB-1, FGF2, TG2 and possibly many more. Secondly, pharmacological intervention of this pathway has clear potential for therapy and pain control in arthritis. Lastly, there is substantial evidence that post-translational modifications of specific proteins might be generated by TG2 in the context of the osteoarthritis once released. This potentially may serve as a biological indicator describing a specific stage of the disease.

I have decided to continue my efforts in this direction of research and developed a fellowship application based on my PhD studies. The purpose of the research is to understand if TG2 release in cartilage is occurring as a consequence of abnormal joint loading or in association with the inflammation, which both processes are linked with P2X7R activation. The specific objectives I intend to address in the future are:

- To determine whether P2X7R in response to mechanical loading is sufficient to activate TG2 release in human cartilage.
- To identify whether $P2X7R^{-/-}$ mice are protected from IL-1β mediated TG2 signaling.
- To investigate which molecular event downstream of P2X7R activation is necessary or sufficient to trigger rapid TG2 externalization.
- To investigate whether TG2 externalization and enzyme activation are linked together or are independently controlled events.

References

Abbracchio, M.P. and Burnstock, G. 1994. Purinoceptors: are there families of P2X and P2Y purinoceptors? *Pharmacol Ther* 64, pp. 445–475.

Achyuthan, K.E. and Greenberg, C.S. 1987. Identification of a guanosine triphosphate-binding site on guinea pig liver transglutaminase. Role of GTP and calcium ions in modulating activity. *J Biol Chem* 262, pp. 1901–1906.

Ademowo, O.S., Staunton, L., Fitzgerald, O. and Pennington, S.R. 2013. *Biomarkers of Inflammatory Arthritis and Proteomics, Genes and Autoimmunity - Intracellular Signaling and Microbiome Contribution*. Stanilova, P. S. ed.

Adinolfi, E., Cirillo, M., Woltersdorf, R., Falzoni, S., Chiozzi, P., Pellegatti, P., Callegari, M.G., Sandonà, D., Markwardt, F., Schmalzing, G. and Di Virgilio, F. 2010. Trophic activity of a naturally occurring truncated isoform of the P2X7 receptor. *FASEB journal : official publication of the Federation of American Societies for Experimental Biology* 24(9), pp. 3393–404.

Aeschlimann, D., Kaupp, O. and Paulsson, M. 1995. Transglutaminase-catalyzed matrix cross-linking in differentiating cartilage: identification of osteonectin as a major glutaminyl substrate. *J Cell Biol* 129, pp. 881–892.

Aeschlimann, D., Mosher, D. and Paulsson, M. 1996. Tissue transglutaminase and factor XIII in cartilage and bone remodeling. *Semin Thromb Hemost* 22(5), pp. 437–43.

Aeschlimann, D. and Paulsson, M. 1991. Cross-linking of laminin-nidogen complexes by tissue transglutaminase. A novel mechanism for basement membrane stabilization. *J Biol Chem* 266, pp. 15308–15317.

Aeschlimann, D. and Paulsson, M. 1994. Transglutaminases: protein cross-linking enzymes in tissues and body fluids. *Thrombosis and Haemostasis* 71(4), pp. 402–15.

Aeschlimann, D. and Thomazy, V. 2000. Protein crosslinking in assembly and remodelling of extracellular matrices: the role of transglutaminases. *Connect Tissue Res* 41, pp. 1–27.

Ahvazi, B., Boeshans, K.M., Idler, W., Baxa, U. and Steinert, P.M. 2003. Roles of calcium ions in the activation and activity of the transglutaminase 3 enzyme. *J Biol Chem* 278, pp. 23834–23841.

Ahvazi, B., Kim, H.C., Kee, S.H., Nemes, Z. and Steinert, P.M. 2002. Three-dimensional structure of the human transglutaminase 3 enzyme: binding of calcium ions changes structure for activation. *EMBO J* 21, pp. 2055–2067.

Akimov, S.S. and Belkin, a M. 2001. Cell-surface transglutaminase promotes fibronectin assembly via interaction with the gelatin-binding domain of fibronectin: a

role in TGFbeta-dependent matrix deposition. *Journal of cell science* 114(Pt 16), pp. 2989–3000.

Van den Akker, J., van Weert, A., Afink, G., Bakker, E.N.T.P., van der Pol, E., Böing, A.N., Nieuwland, R. and VanBavel, E. 2011. Transglutaminase 2 is secreted from smooth muscle cells by transamidation-dependent microparticle formation. *Amino Acids* 42(2-3), pp. 961–73.

Al-nedawi, K., Meehan, B. and Rak, J. 2009. Microvesicles. 8(13), pp. 2014–2018.

Al-Shukaili, A., Al-Kaabi, J., Hassan, B., Al-Araimi, T., Al-Tobi, M., Al-Kindi, M., Al-Maniri, A., Al-Gheilani, A. and Al-Ansari, A. 2011. P2X7 receptor gene polymorphism analysis in rheumatoid arthritis. *Int J Immunogenet* 38, pp. 389–396.

Ali, N. and Knaüper, V. 2007. Phorbol ester-induced shedding of the prostate cancer marker transmembrane protein with epidermal growth factor and two follistatin motifs 2 is mediated by the disintegrin and metalloproteinase-17. *The Journal of biological chemistry* 282(52), pp. 37378–88.

Andrei, C, Margiocco, P., Poggi, A., Lotti, L. V, Torrisi, M.R. and Rubartelli, A. 2004. Phospholipases C and A(2) control lysosome-mediated IL-1 beta secretion: Implications for inflammatory processes. *Proceedings of the National Academy of Sciences of the United States of America* 101, pp. 9745–9750.

Andrei, Cristina, Margiocco, P., Poggi, A., Lotti, L. V, Torrisi, M.R. and Rubartelli, A. 2004. Phospholipases C and A2 control lysosome-mediated IL-1 beta secretion: Implications for inflammatory processes. *Proceedings of the National Academy of Sciences of the United States of America* 101(26), pp. 9745–50.

Antonyak, M.A., Li, B., Boroughs, L.K., Johnson, J.L., Druso, J.E., Bryant, K.L., Holowka, D.A. and Cerione, R.A. 2011. Cancer cell-derived microvesicles induce transformation by transferring tissue transglutaminase and fibronectin to recipient cells. *Proc Natl Acad Sci U S A* 108, pp. 4852–4857.

Arandjelovic, S., McKenney, K.R., Leming, S.S. and Mowen, K.A. 2012. ATP induces protein arginine deiminase 2-dependent citrullination in mast cells through the P2X7 purinergic receptor. *J Immunol* 189(8), pp. 4112–4122.

Baldwin, T.A. and Ostergaard, H.L. 2002. The protein-tyrosine phosphatase CD45 reaches the cell surface via golgi-dependent and -independent pathways. *J Biol Chem* 277, pp. 50333–50340.

Balklava, Z., Verderio, E., Collighan, R., Gross, S., Adams, J. and Griffin, M. 2002. Analysis of tissue transglutaminase function in the migration of Swiss 3T3 fibroblasts: the active-state conformation of the enzyme does not affect cell motility but is important for its secretion. *The Journal of biological chemistry* 277(19), pp. 16567–75.

Baroja-Mazo, A., Barberà-Cremades, M. and Pelegrín, P. 2012. The participation of plasma membrane hemichannels to purinergic signaling. *Biochimica et biophysica acta* 1828(1), pp. 79–93.

Baroja-Mazo, A. and Pelegrín, P. 2012. Modulating P2X7 Receptor Signaling during Rheumatoid Arthritis: New Therapeutic Approaches for Bisphosphonates. *Journal of osteoporosis* 2012, p. 408242.

Begg, G.E., Carrington, L., Stokes, P.H., Matthews, J.M., Wouters, M. a, Husain, A., Lorand, L., Iismaa, S.E. and Graham, R.M. 2006. Mechanism of allosteric regulation of transglutaminase 2 by GTP. *Proc Natl Acad Sci U S A* 103(52), pp. 19683–19688.

Belkin, A.M. 2011. Extracellular TG2: emerging functions and regulation. *FEBS J* 278, pp. 4704–4716.

Berenbaum, F. 2012. Osteoarthritis as an inflammatory disease (osteoarthritis is not osteoarthrosis!). *Osteoarthritis and cartilage / OARS, Osteoarthritis Research Society* 21(1), pp. 16–21.

Berenbaum, F. 2013. Osteoarthritis as an inflammatory disease (osteoarthritis is not osteoarthrosis!). *Osteoarthritis and cartilage / OARS, Osteoarthritis Research Society* 21(1), pp. 16–21.

Bergamini, C. 1988. GTP modulates calcium binding and cation-induced conformational changes in erythrocyte transglutaminase. *FEBS letters* 239(2), pp. 255–8.

Bergamini, C., Dondi, A., Lanzara, V., Squerzanti, M., Cervellati, C., Montin, K., Mischiati, C., Tasco, G., Collighan, R., Griffin, M. and Casadio, R. 2010. Thermodynamics of binding of regulatory ligands to tissue transglutaminase. *Amino acids* 39(1), pp. 297–304.

Bianchi, M.E. and Agresti, A. 2005. HMG proteins: dynamic players in gene regulation and differentiation. *Curr Opin Genet Dev* 15, pp. 496–506.

Bianco, F., Pravettoni, E., Colombo, A., Schenk, U., Moller, T., Matteoli, M. and Verderio, C. 2005. Astrocyte-derived ATP induces vesicle shedding and IL-1 beta release from microglia. *Journal of Immunology* 174, pp. 7268–7277.

Bilbao, P.S., Katz, S. and Boland, R. 2012. Interaction of purinergic receptors with GPCRs, ion channels, tyrosine kinase and steroid hormone receptors orchestrates cell function. *Purinergic signaling* 8(1), pp. 91–103.

Blobel, C.P. 2005. ADAMs: key components in EGFR signaling and development. *Nat Rev Mol Cell Biol* 6, pp. 32–43.

Bonaldi, T., Talamo, F., Scaffidi, P., Ferrera, D., Porto, A., Bachi, A., Rubartelli, A., Agresti, A. and Bianchi, M.E. 2003. Monocytic cells hyperacetylate chromatin protein HMGB1 to redirect it towards secretion. *EMBO J* 22, pp. 5551–5560.

Bondeson, J., Blom, A.B., Wainwright, S., Hughes, C., Caterson, B. and van den Berg, W.B. 2010. The role of synovial macrophages and macrophage-produced mediators in driving inflammatory and destructive responses in osteoarthritis. *Arthritis Rheum* 62, pp. 647–657.

Brennan, F.M. and McInnes, I.B. 2008. Evidence that cytokines play a role in rheumatoid arthritis. *Journal of Clinical Investigation* 118, pp. 3537–3545.

Brough, D. and Rothwell, N.J. 2007. Caspase-1-dependent processing of pro-interleukin-1beta is cytosolic and precedes cell death. *Journal of cell science* 120(Pt 5), pp. 772–81.

Browne, L.E., Compan, V., Bragg, L. and North, R.A. 2013. P2X7 receptor channels allow direct permeation of nanometer-sized dyes. *The Journal of neuroscience : the official journal of the Society for Neuroscience* 33(8), pp. 3557–66.

Browne, L.E., Jiang, L.-H. and North, R.A. 2010. New structure enlivens interest in P2X receptors. *Trends in pharmacological sciences* 31(5), pp. 229–37.

Bruce, A., Alexander, J., Julian, L., Martin, R., Roberts, K. and Peter, W. 2002. *Molecular Biology of the Cell*. 4th ed. New York: Garland Science.

Bryan, N.B., Dorfleutner, A., Kramer, S.J., Yun, C., Rojanasakul, Y. and Stehlik, C. 2010. Differential splicing of the apoptosis-associated speck like protein containing a caspase recruitment domain (ASC) regulates inflammasomes. *Journal of inflammation (London, England)* 7, p. 23.

Burnier, L., Fontana, P., Kwak, B.R. and Angelillo-Scherrer, A. 2009. Cell-derived microparticles in haemostasis and vascular medicine. *Thrombosis and Haemostasis*, pp. 439–451.

Burnstock, G. 2007. Physiology and Pathophysiology of Purinergic Neurotransmission. *Physiol Rev* 87, pp. 659–797.

Burnstock, G. 1972. Purinergic nerves. *Pharmacol Rev* 24, pp. 509–581.

Burnstock, G. 2008. Purinergic signaling and disorders of the central nervous system. *Nature reviews. Drug discovery* 7(7), pp. 575–90.

Caja, S., Mäki, M., Kaukinen, K. and Lindfors, K. 2011. Antibodies in celiac disease: implications beyond diagnostics. *Cellular & molecular immunology* 8(2), pp. 103–9.

Candi, E., Oddi, S., Paradisi, A., Terrinoni, A., Ranalli, M., Teofoli, P., Citro, G., Scarpato, S., Puddu, P. and Melino, G. 2002. Expression of transglutaminase 5 in normal and pathologic human epidermis. *J Invest Dermatol* 119, pp. 670–677.

Cankurtaran-sayar, S., Sayar, K. and Ugur, M. 2009. P2X7 Receptor Activates Multiple Selective Dye-Permeation Pathways in RAW 264 . 7 and Human Embryonic Kidney 293. *Molecular pharmacology* 76(6), pp. 1323–1332.

Caron, N.S., Munsie, L.N., Keillor, J.W. and Truant, R. 2012. Using FLIM-FRET to measure conformational changes of transglutaminase type 2 in live cells. *PLoS One* 7(8), pp. 1–7.

Cecil, D.L. and Terkeltaub, R. 2008. Transamidation by Transglutaminase 2 Transforms S100A11 Calgranulin into a Procatabolic Cytokine for Chondrocytes. 180(12), pp. 8378–8385.

Chaumont, S. and Khakh, B.S. 2008. Patch-clamp coordinated spectroscopy shows P2X2 receptor permeability dynamics require cytosolic domain rearrangements but not Panx-1 channels. *Proceedings of the National Academy of Sciences of the United States of America* 105(33), pp. 12063–8.

Chou, C.-Y., Streets, A.J., Watson, P.F., Huang, L., Verderio, E. a M. and Johnson, T.S. 2011. A crucial sequence for transglutaminase type 2 extracellular trafficking in renal tubular epithelial cells lies in its N-terminal beta-sandwich domain. *The Journal of biological chemistry* 286(31), pp. 27825–35.

Chung, S.I. and Folk, J.E. 1970. Mechanism of the inactivation of guinea pig liver transglutaminase by tetrathionate. *J Biol Chem* 245(4), pp. 681–689.

Cockcroft, S. and Gomperts, B.D. 1979. ATP induces nucleotide permeability in rat mast cells. *Nature* 279, pp. 541–542.

Cocucci, E., Racchetti, G. and Meldolesi, J. 2009. Shedding microvesicles: artefacts no more. *Trends in cell biology* 19(2), pp. 43–51.

Coddou, C., Yan, Z., Obsil, T., Huidobro-Toro, J.P. and Stojilkovic, S.S. 2011. Activation and regulation of purinergic P2X receptor channels. *Pharmacol Rev* 63(3), pp. 641–683.

Costa-Junior, H.M., Sarmento Vieira, F. and Coutinho-Silva, R. 2011. C terminus of the P2X7 receptor: treasure hunting. *Purinergic signaling* 7(1), pp. 7–19.

Dadabay, C.Y. and Pike, L.J. 1987. Rapid increases in the transglutaminase activity of A431 cells following treatment with epidermal growth factor. *Biochemistry* 26(21), pp. 6587–91.

Dafik, L. and Khosla, C. 2011. Dihydroisoxazole analogs for labeling and visualization of catalytically active transglutaminase 2. *Chem Biol* 18, pp. 58–66.

Degryse, B. and de Virgilio, M. 2003. The nuclear protein HMGB1, a new kind of chemokine? *FEBS Letters* 553(1-2), pp. 11–17.

Denlinger, L.C., Fisette, P.L., Sommer, J.A., Watters, J.J., Prabhu, U., Dubyak, G.R., Proctor, R.A. and Bertics, P.J. 2001. Cutting edge: the nucleotide receptor P2X7 contains multiple protein- and lipid-interaction motifs including a potential binding site for bacterial lipopolysaccharide. *J Immunol* 167(4), pp. 1871–1876.

Deretic, V., Jiang, S. and Dupont, N. 2012. Autophagy intersections with conventional and unconventional secretion in tissue development, remodeling and inflammation. *Trends in cell biology* 22(8), pp. 397–406.

Dinarello, C.A. 2009. Immunological and inflammatory functions of the interleukin-1 family. *Annu Rev Immunol* 27, pp. 519–550.

Dinarello, C.A. 2004. Unraveling the NALP-3/IL-1beta inflammasome: a big lesson from a small mutation. *Immunity* 20, pp. 243–244.

Doyle, H. a and Mamula, M.J. 2005. Posttranslational modifications of self-antigens. *Annals of the New York Academy of Sciences* 1050, pp. 1–9.

Doyle, H.A. and Mamula, M.J. 2002. Posttranslational protein modifications: new flavors in the menu of autoantigens. *Curr Opin Rheumatol* 14, pp. 244–249.

Dubyak, G.R. 2012. P2X7 receptor regulation of non-classical secretion from immune effector cells. *Cellular microbiology* 14(11), pp. 1697–706.

Dzhambazov, B., Lindh, I., Engström, A. and Holmdahl, R. 2009. Tissue transglutaminase enhances collagen type II-induced arthritis and modifies the immunodominant T-cell epitope CII260-270. *Eur J Immunol* 39, pp. 2412–2423.

Falzoni, S., Munerati, M., Ferrari, D., Spisani, S., Moretti, S. and Di Virgilio, F. 1995. The purinergic P2Z receptor of human macrophage cells. Characterization and possible physiological role. *J Clin Invest* 95, pp. 1207–1216.

Fatal, N., Karhinen, L., Jokitalo, E. and Makarow, M. 2004. Active and specific recruitment of a soluble cargo protein for endoplasmic reticulum exit in the absence of functional COPII component Sec24p. *J Cell Sci* 117, pp. 1665–1673.

Feng, Y.-H., Li, X., Wang, L., Zhou, L. and Gorodeski, G.I. 2006. A truncated P2X7 receptor variant (P2X7-j) endogenously expressed in cervical cancer cells antagonizes the full-length P2X7 receptor through hetero-oligomerization. *The Journal of biological chemistry* 281(25), pp. 17228–37.

Ferrari, D., Chiozzi, P., Falzoni, S., DalSusino, M., Melchiorri, L., Baricordi, O.R. and DiVirgilio, F. 1997. Extracellular ATP triggers IL-1 beta release by activating the purinergic P2Z receptor of human macrophages. *Journal of Immunology* 159, pp. 1451–1458.

Ferrari, D., Pizzirani, C., Adinolfi, E., Lemoli, R.M., Curti, A., Idzko, M., Panther, E. and Di Virgilio, F. 2006. The P2X(7) receptor: A key player in IL-1 processing and release. *Journal of Immunology* 176(7), pp. 3877–3883.

Folk, J.E. and Chung, S.I. 1973. Molecular and catalytic properties of transglutaminases. *Adv Enzymol Relat Areas Mol Biol* 38, pp. 109–191.

Folk, J.E. and Cole, P.W. 1966. Transglutaminase: mechanistic features of the active site as determined by kinetic and inhibitor studies. *Biochim Biophys Acta* 122, pp. 244–264.

Fountain, S.J. and Burnstock, G. 2009. An evolutionary history of P2X receptors. *Purinergic Signal* 5, pp. 269–272.

Fuller, S.J., Stokes, L., Skarratt, K.K., Gu, B.J. and Wiley, J.S. 2009. Genetics of the P2X7 receptor and human disease. *Purinergic signaling* 5(2), pp. 257–62.

Le Gall, S.M., Bobe, P., Reiss, K., Horiuchi, K., Niu, X.D., Lundell, D., Gibb, D.R., Conrad, D., Saftig, P. and Blobel, C.P. 2009. ADAMs 10 and 17 represent differentially regulated components of a general shedding machinery for membrane proteins such as transforming growth factor alpha, L-selectin, and tumor necrosis factor alpha. *Mol Biol Cell* 20, pp. 1785–1794.

Garcia, M. and Knight, M.M. 2010. Cyclic loading opens hemichannels to release ATP as part of a chondrocyte mechanotransduction pathway. *J Orthop Res* 28, pp. 510–515.

Gardella, S., Andrei, C., Ferrera, D., Lotti, L. V, Torrisi, M.R., Bianchi, M.E. and Rubartelli, A. 2002. The nuclear protein HMGB1 is secreted by secretory pathway. 3(10), pp. 995–1001.

Gaudry, C. a, Verderio, E., Jones, R. a, Smith, C. and Griffin, M. 1999. Tissue transglutaminase is an important player at the surface of human endothelial cells: evidence for its externalization and its colocalization with the beta(1) integrin. *Experimental cell research* 252(1), pp. 104–13.

Goldring, M.B. 2000. The role of the chondrocyte in osteoarthritis. *Arthritis and rheumatism* 43(9), pp. 1916–26.

Goldring, M.B. and Goldring, S.R. 2010. Articular cartilage and subchondral bone in the pathogenesis of osteoarthritis. *Annals of the New York Academy of Sciences* 1192, pp. 230–7.

Goldring, M.B. and Goldring, S.R. 2007. Osteoarthritis. (July), pp. 626–634.

Grenard, P., Bates, M.K. and Aeschlimann, D. 2001. Evolution of transglutaminase genes: identification of a transglutaminase gene cluster on human chromosome 15q15. Structure of the gene encoding transglutaminase X and a novel gene family member, transglutaminase Z. *The Journal of biological chemistry* 276(35), pp. 33066–78.

Griffin, M., Casadio, R. and Bergamini, C.M. 2002. Transglutaminases: nature's biological glues. *Biochem J* 368, pp. 377–396.

Grol, M.W., Pereverzev, A., Sims, S.M. and Dixon, S.J. 2013. P2 receptor networks regulate signaling duration over a wide dynamic range of ATP concentrations. *Journal of cell science* 126(Pt 16), pp. 3615–26.

Gross, M., Whetzel, N.K. and Folk, J.E. 1977. Amine binding sites in acyl intermediates of transglutaminases. Human blood plasma enzyme (activated coagulation factor XIII) and guinea pig liver enzyme. *J Biol Chem* 252(11), pp. 3752–3759.

Gudipaty, L., Humphreys, B.D., Buell, G. and Dubyak, G.R. 2001. Regulation of P2X 7 nucleotide receptor function in human monocytes by extracellular ions and receptor density Regulation of P2X 7 nucleotide receptor function in human monocytes by extracellular ions and receptor density. *Am J Physiol Cell Physiol* 280, pp. C943–C953.

Guo, C., Masin, M., Qureshi, O.S. and Murrell-lagnado, R.D. 2007. Evidence for Functional P2X 4 / P2X 7 Heteromeric Receptors. *Molecular pharmacology* 72(6), pp. 1447–1456.

Hadjivassiliou, M., Aeschlimann, P., Strigun, A., Sanders, D.S., Woodroofe, N. and Aeschlimann, D. 2008. Autoantibodies in gluten ataxia recognize a novel neuronal transglutaminase. *Ann Neurol* 64, pp. 332–343.

Hadjivassiliou, M., Sanders, D.S., Grünewald, R.A., Woodroofe, N., Boscolo, S. and Aeschlimann, D. 2010. Gluten sensitivity: from gut to brain. *Lancet Neurol* 9, pp. 318–330.

Han, B.G., Cho, J.W., Cho, Y.D., Jeong, K.C., Kim, S.Y. and Lee, B.I. 2010. Crystal structure of human transglutaminase 2 in complex with adenosine triphosphate. *Int J Biol Macromol*.

Hasdemir, B., Fitzgerald, D.J., Prior, I.A., Tepikin, A. V and Burgoyne, R.D. 2005. Traffic of Kv4 K+ channels mediated by KChIP1 is via a novel post-ER vesicular pathway. *J Cell Biol* 171(4), pp. 459–469.

Hattori, M. and Gouaux, E. 2012. Molecular mechanism of ATP binding and ion channel activation in P2X receptors. *Nature* 485(7397), pp. 207–12.

Hodrea, J., Demény, M.A., Majai, G., Sarang, Z., Korponay-Szabó, I.R. and Fésüs, L. 2010. Transglutaminase 2 is expressed and active on the surface of human monocyte-derived dendritic cells and macrophages. *Immunol Lett* 130, pp. 74–81.

Hogquist, K.A., Unanue, E.R. and Chaplin, D.D. 1991. Release of IL-1 from mononuclear phagocytes. *J Immunol* 147, pp. 2181–2186.

Hohenadl, C., Mann, K., Mayer, U., Timpl, R., Paulsson, M. and Aeschlimann, D. 1995. Two adjacent N-terminal glutamines of BM-40 (osteonectin, SPARC) act as amine acceptor sites in transglutaminaseC-catalyzed modification. *J Biol Chem* 270, pp. 23415–23420.

Honore, P., Donnelly-Roberts, D., Namovic, M.T., Hsieh, G., Zhu, C.Z., Mikusa, J.P., Hernandez, G., Zhong, C., Gauvin, D.M., Chandran, P., Harris, R., Medrano, A.P., Carroll, W., Marsh, K., Sullivan, J.P., Faltynek, C.R. and Jarvis, M.F. 2006. A-740003 [N-(1-{[(cyanoimino)(5-quinolinylamino) methyl]amino}-2,2-dimethylpropyl)-2-(3,4-dimethoxyphenyl)acetamide], a novel and selective P2X7 receptor antagonist, dose-dependently reduces neuropathic pain in the rat. *J Pharmacol Exp Ther* 319, pp. 1376–1385.

Horiuchi, K., Le Gall, S., Schulte, M., Yamaguchi, T., Reiss, K., Murphy, G., Toyama, Y., Hartmann, D., Saftig, P. and Blobel, C.P. 2007. Substrate selectivity of epidermal growth factor-receptor ligand sheddases and their regulation by phorbol esters and calcium influx. *Mol Biol Cell* 18, pp. 176–188.

Huebner, J.L., Johnson, K.A., Kraus, V.B. and Terkeltaub, R.A. 2009. Transglutaminase 2 is a marker of chondrocyte hypertrophy and osteoarthritis

severity in the Hartley guinea pig model of knee OA. *Osteoarthritis Cartilage* 17, pp. 1056–1064.

Humphreys, B.D. and Dubyak, G.R. 1996. Induction of the P2z/P2X7 nucleotide receptor and associated phospholipase D activity by lipopolysaccharide and IFN-gamma in the human THP-1 monocytic cell line. *J Immunol* 157, pp. 5627–5637.

Humphreys, B.D. and Dubyak, G.R. 1998. Modulation of P2X 7 nucleotide receptor expression by pro- and anti-inflammatory stimuli in THP-1 monocytes sion is of interest because activation of this recep- release of the pro-inflammatory cytokine interleu- THP-1 monocytic cell line . Induction was . 64(August), pp. 265–273.

Iismaa, S.E., Mearns, B.M., Lorand, L. and Graham, R.M. 2009. Transglutaminases and disease: lessons from genetically engineered mouse models and inherited disorders. *Physiol Rev* 89, pp. 991–1023.

Iversen, R., Di Niro, R., Stamnaes, J., Lundin, K.E. a, Wilson, P.C. and Sollid, L.M. 2013. Transglutaminase 2-specific autoantibodies in celiac disease target clustered, N-terminal epitopes not displayed on the surface of cells. *Journal of immunology (Baltimore, Md. : 1950)* 190(12), pp. 5981–91.

Jacobson, K. a, Jarvis, M.F. and Williams, M. 2002. Purine and pyrimidine (P2) receptors as drug targets. *Journal of medicinal chemistry* 45(19), pp. 4057–93.

Jandu, S.K., Webb, A.K., Pak, A., Sevinc, B., Nyhan, D., Belkin, A.M., Flavahan, N. a, Berkowitz, D.E. and Santhanam, L. 2013. Nitric oxide regulates tissue transglutaminase localization and function in the vasculature. *Amino acids* 44(1), pp. 261–9.

Jarvis, M.F. and Khakh, B.S. 2009. ATP-gated P2X cation-channels. *Neuropharmacology* 56(1), pp. 208–215.

Jiang, L.H., Baldwin, J.M., Roger, S. and Baldwin, S. a 2013. Insights into the Molecular Mechanisms Underlying Mammalian P2X7 Receptor Functions and Contributions in Diseases, Revealed by Structural Modeling and Single Nucleotide Polymorphisms. *Frontiers in pharmacology* 4(55), pp. 1–17.

Jiang, R., Taly, A. and Grutter, T. 2013. Moving through the gate in ATP-activated P2X receptors. *Trends in biochemical sciences* 38(1), pp. 20–9.

Jin, X., Stamnaes, J., Klöck, C., DiRaimondo, T.R., Sollid, L.M. and Khosla, C. 2011. Activation of extracellular transglutaminase 2 by thioredoxin. *J Biol Chem* 286, pp. 37866–37873.

John, S., Thiebach, L., Frie, C., Mokkapati, S., Bechtel, M., Nischt, R., Rosser-Davies, S., Paulsson, M. and Smyth, N. 2012. Epidermal transglutaminase (TGase 3) is required for proper hair development, but not the formation of the epidermal barrier. *PloS one* 7(4), p. e34252.

Johnson, K., Hashimoto, S., Lotz, M., Pritzker, K. and Terkeltaub, R. 2001. Interleukin-1 induces pro-mineralizing activity of cartilage tissue transglutaminase and factor XIIIa. *Am J Pathol* 159, pp. 149–163.

Johnson, K.A., van Etten, D., Nanda, N., Graham, R.M. and Terkeltaub, R.A. 2003. Distinct transglutaminase 2-independent and transglutaminase 2-dependent pathways mediate articular chondrocyte hypertrophy. *J Biol Chem* 278, pp. 18824–18832.

Johnson, K.A. and Terkeltaub, R.A. 2005. External GTP-bound transglutaminase 2 is a molecular switch for chondrocyte hypertrophic differentiation and calcification. *J Biol Chem* 280, pp. 15004–15012.

Jorgensen, N.R., Geist, S.T., Civitelli, R. and Steinberg, T.H. 1997. ATP- and gap junction-dependent intercellular calcium signaling in osteoblastic cells. *J Cell Biol* 139, pp. 497–506.

Kaczmarek-Hájek, K., Lörinczi, E., Hausmann, R. and Nicke, A. 2012. Molecular and functional properties of P2X receptors--recent progress and persisting challenges. *Purinergic Signal* 8(3), pp. 375–417.

Kawai, Y., Kaidoh, M. and Ohhashi, T. 2008. MDA-MB-231 produces ATP-mediated ICAM-1-dependent facilitation of the attachment of carcinoma cells to human lymphatic endothelial cells. *American journal of physiology. Cell physiology* 295(5), pp. C1123–32.

Kawate, T., Michel, J.C., Birdsong, W.T. and Gouaux, E. 2009. Crystal structure of the ATP-gated P2X(4) ion channel in the closed state. *Nature* 460(7255), pp. 592–8.

Kawate, T., Robertson, J.L., Li, M., Silberberg, S.D. and Swartz, K.J. 2011. Ion access pathway to the transmembrane pore in P2X receptor channels. *The Journal of general physiology* 137(6), pp. 579–90.

Keller, M., Regg, A., Werner, S. and Beer, H.D. 2008. Active caspase-1 is a regulator of unconventional protein secretion. *Cell* 132, pp. 818–831.

Khakh, B.S., Bao, X.R., Labarca, C. and Lester, H.A. 1999. Neuronal P2X transmitter-gated cation channels change their ion selectivity in seconds. *Nature neuroscience* 2(4), pp. 322–330.

Khakh, B.S. and North, R.A. 2006. P2X receptors as cell-surface ATP sensors in health and disease. *Nature* 442, pp. 527–532.

Khoury, G. a, Baliban, R.C. and Floudas, C. a 2011. Proteome-wide post-translational modification statistics: frequency analysis and curation of the swiss-prot database. *Scientific reports* 1, pp. 1–5.

Kim, S.Y. 2006. Transglutaminase 2 in inflammation. *Front Biosci* 11, pp. 3026–3035.

Király, R., Barta, E. and Fésüs, L. 2013. Polymorphism of transglutaminase 2: unusually low frequency of genomic variants with deficient functions. *Amino Acids* 44, pp. 215–225.

Király, R, Demény, M. and Fésüs, L. 2011. Protein transamidation by transglutaminase 2 in cells: a disputed Ca2+-dependent action of a multifunctional protein. *FEBS J* 278, pp. 4717–4739.

Király, Róbert, Demény, M. and Fésüs, L. 2011. Protein transamidation by transglutaminase 2 in cells: a disputed Ca2+-dependent action of a multifunctional protein. *The FEBS journal* 278(24), pp. 4717–39.

Klippel, J.H. 2007. Primer on the Rheumatic Diseases Stone, J. H., Crofford, L. J., and White, P. eds.

Knight, M.M., McGlashan, S.R., Garcia, M., Jensen, C.G. and Poole, C. a 2009. Articular chondrocytes express connexin 43 hemichannels and P2 receptors - a putative mechanoreceptor complex involving the primary cilium? *Journal of anatomy* 214(2), pp. 275–83.

Komáromi, I., Bagoly, Z. and Muszbek, L. 2011. Factor XIII: novel structural and functional aspects. *Journal of thrombosis and haemostasis : JTH* 9(1), pp. 9–20.

Kondo, N., Ishii, Y., Kwon, Y.-W., Tanito, M., Horita, H., Nishinaka, Y., Nakamura, H. and Yodoi, J. 2004. Redox-sensing release of human thioredoxin from T lymphocytes with negative feedback loops. *Journal of immunology (Baltimore, Md. : 1950)* 172(1), pp. 442–8.

Van der Kraan, P.M. 2012. Osteoarthritis year 2012 in review: biology. *Osteoarthritis and cartilage / OARS, Osteoarthritis Research Society* 20(12), pp. 1447–50.

Kumar, S. and Mehta, K. 2012. Tissue transglutaminase constitutively activates HIF-1α promoter and nuclear factor-κB via a non-canonical pathway. *PloS one* 7(11), p. e49321.

Kuncio, G.S., Tsyganskaya, M., Zhu, J., Liu, S., Nagy, L., Thomazy, V., Davies, P.J.A., Zern, M.A., Chou, C., Streets, A.J., Watson, P.F., Huang, L., Verderio, E.A.M., Johnson, T.S., Auld, G.C., Ritchie, H., Robbie, L.A., Booth, N.A. and Gerald, S. 1998. TNF- α modulates expression of the tissue transglutaminase gene in liver cells. *Am J Physiol* 242, pp. G240–G245.

Kurta, T., Korponay-szabo, I.R., Király, R., Csosz, E., Kurtán, T., Antus, S., Szigeti, K., Simon-Vecsei, Z., Korponay-Szabó, I.R., Keresztessy, Z. and Fésüs, L. 2009. Functional significance of five noncanonical Ca2+-binding sites of human transglutaminase 2 characterized by site-directed mutagenesis. *FEBS J* 276(23), pp. 7083–7096.

Kyostio-Moore, S., Nambiar, B., Hutto, E., Ewing, P.J., Piraino, S., Berthelette, P., Sookdeo, C., Matthews, G. and Armentano, D. 2011. STR/ort mice, a model for

spontaneous osteoarthritis, exhibit elevated levels of both local and systemic inflammatory markers. *Comp Med* 61(4), pp. 346–355.

Labasi, J.M., Petrushova, N., Donovan, C., McCurdy, S., Lira, P., Payette, M.M., Brissette, W., Wicks, J.R., Audoly, L. and Gabel, C. a 2002. Absence of the P2X7 receptor alters leukocyte function and attenuates an inflammatory response. *J Immunol* 168(12), pp. 6436–6445.

Lai, T.S., Hausladen, A., Slaughter, T.F., Eu, J.P., Stamler, J.S. and Greenberg, C.S. 2001. Calcium Regulates S-Nitrosylation, Denitrosylation, and Activity of Tissue Transglutaminase. *Biochemistry* 40, pp. 4904–4910.

De Lange-Brokaar, B.J.E., Ioan-Facsinay, A., van Osch, G.J.V.M., Zuurmond, a-M.M., Schoones, J., Toes, R.E.M., Huizinga, T.W.J. and Kloppenburg, M. 2012. Synovial inflammation, immune cells and their cytokines in osteoarthritis: a review. *Osteoarthritis Cartilage* 20(12), pp. 1484–1499.

De Laurenzi, V. and Melino, G. 2001. Gene Disruption of Tissue Transglutaminase. *Molecular and Cellular Biology* 21(1), pp. 148–155.

Lauzier, A., Charbonneau, M., Paquette, M., Harper, K. and Dubois, C.M. 2012. Transglutaminase 2 cross-linking activity is linked to invadopodia formation and cartilage breakdown in arthritis. *Arthritis research & therapy* 14(4), p. R159.

Leblanc, A., Gravel, C., Labelle, J. and Keillor, J.W. 2001. Kinetic studies of guinea pig liver transglutaminase reveal a general-base-catalyzed deacylation mechanism. *Biochemistry* 40, pp. 8335–8342.

Li, J., Liu, D., Ke, H.Z., Duncan, R.L. and Turner, C.H. 2005. The P2X7 nucleotide receptor mediates skeletal mechanotransduction. *The Journal of biological chemistry* 280(52), pp. 42952–9.

Liao, K.-C.C. and Mogridge, J. 2009. Expression of Nlrp1b inflammasome components in human fibroblasts confers susceptibility to anthrax lethal toxin. *Infect Immun* 77(10), pp. 4455–4462.

Liu, S., Cerione, R. a and Clardy, J. 2002. Structural basis for the guanine nucleotide-binding activity of tissue transglutaminase and its regulation of transamidation activity. *Proc Natl Acad Sci U S A* 99(5), pp. 2743–2747.

Loeser, R.F., Goldring, S.R., Scanzello, C.R. and Goldring, M.B. 2012. Osteoarthritis: A Disease of the Joint as an Organ. *Arthritis Rheum* 64(6), pp. 1697–1707.

Lopez-Castejon, G., Theaker, J., Pelegrin, P., Clifton, A.D., Braddock, M. and Surprenant, A. 2010. P2X(7) receptor-mediated release of cathepsins from macrophages is a cytokine-independent mechanism potentially involved in joint diseases. *J Immunol* 185(4), pp. 2611–9.

Lorand, L. and Graham, R.M. 2003. Transglutaminases: crosslinking enzymes with pleiotropic functions. *Nat Rev Mol Cell Biol* 4, pp. 140–156.

Lorand, L., Weissmann, L.B., Epel, D.L. and Bruner-Lorand, J. 1976. Role of the intrinsic transglutaminase in the Ca2+-mediated crosslinking of erythrocyte proteins. *Proceedings of the National Academy of Sciences of the United States of America* 73(12), pp. 4479–81.

Lortat-Jacob, H., Burhan, I., Scarpellini, A., Thomas, A., Imberty, A., Vivès, R.R., Johnson, T., Gutierrez, A. and Verderio, E. a M. 2012. Transglutaminase-2 interaction with heparin: identification of a heparin binding site that regulates cell adhesion to fibronectin-transglutaminase-2 matrix. *The Journal of biological chemistry* 287(22), pp. 18005–17.

Lu, B., Nakamura, T., Inouye, K., Li, J., Tang, Y., Lundbäck, P., Valdes-Ferrer, S.I., Olofsson, P.S., Kalb, T., Roth, J., Zou, Y., Erlandsson-Harris, H., Yang, H., Ting, J.P., Wang, H., Andersson, U., Antoine, D.J., Chavan, S.S., Hotamisligil, G.S. and Tracey, K.J. 2012. Novel role of PKR in inflammasome activation and HMGB1 release. *Nature* 488, pp. 670–674.

Mackenzie, A., North, R.A. and Surprenant, A. 2001. Novel secretory pathway for IL-1beta identified. *Biophysical Journal* 80, p. 1459.

MacKenzie, A., Wilson, H.L., Kiss-Toth, E., Dower, S.K., North, R.A. and Surprenant, A. 2001. Rapid secretion of interleukin-1 beta by microvesicle shedding. *Immunity* 15, pp. 825–835.

Mackenzie, A.B., Young, M.T., Adinolfi, E. and Surprenant, A. 2005. Pseudoapoptosis induced by brief activation of ATP-gated P2X7 receptors. *J Biol Chem* 280(40), pp. 33968–33976.

Marques-da-Silva, C., Chaves, M.M., Castro, N.G., Coutinho-Silva, R. and Guimaraes, M.Z.P. 2011. Colchicine inhibits cationic dye uptake induced by ATP in P2X2 and P2X7 receptor-expressing cells: implications for its therapeutic action. *British journal of pharmacology* 163(5), pp. 912–26.

Martinon, F., Burns, K. and Tschopp, J. 2002. The inflammasome: a molecular platform triggering activation of inflammatory caspases and processing of proIL-beta. *Mol Cell* 10, pp. 417–426.

Martinon, F., Mayor, A. and Tschopp, J. 2009. The Inflammasomes: Guardians of the Body. *Annual Review of Immunology* 27, pp. 229–265.

Mecham, R.P. 2011. *The extracellular matrix: an overview*. Mecham, R. P. ed.

Mehta, K. and Eckert, R. 2005. *Transglutaminases. Family of enzymes with diverse functions.* Mehta, K. and Eckert, R. eds. S. Karger AG, P.O. Box, CH–4009 Basel (Switzerland).

Mehta, K. and Han, A. 2011a. Tissue Transglutaminase (TG2)-Induced Inflammation in Initiation, Progression, and Pathogenesis of Pancreatic Cancer. *Cancers* 3(4), pp. 897–912.

Mehta, K. and Han, A. 2011b. Tissue Transglutaminase (TG2)-Induced Inflammation in Initiation, Progression, and Pathogenesis of Pancreatic Cancer. *Cancers* 3(4), pp. 897–912.

Mehta, K. and Lopez-Berestein, G. 1986. Expression of tissue transglutaminase in cultured monocytic leukemia (THP-1) cells during differentiation. *Cancer Res* 46, pp. 1388–1394.

Mehta, V.B., Hart, J. and Wewers, M.D. 2001. ATP-stimulated release of interleukin (IL)-1 beta and IL-18 requires priming by lipopolysaccharide and is independent of caspase-1 cleavage. *Journal of Biological Chemistry* 276, pp. 3820–3826.

Merz, D., Liu, R., Johnson, K. and Terkeltaub, R. 2003. IL-8/CXCL8 and growth-related oncogene alpha/CXCL1 induce chondrocyte hypertrophic differentiation. *Journal of immunology (Baltimore, Md. : 1950)* 171(8), pp. 4406–15.

Mhaouty-Kodja, S. 2004. Ghalpha/tissue transglutaminase 2: an emerging G protein in signal transduction. *Biol Cell* 96, pp. 363–367.

Mian, S., el Alaoui, S., Lawry, J., Gentile, V., Davies, P.J. and Griffin, M. 1995. The importance of the GTP-binding protein tissue transglutaminase in the regulation of cell cycle progression. *FEBS letters* 370(1-2), pp. 27–31.

Molberg, Ø. and Sollid, L.M. 2006. A gut feeling for joint inflammation - using coeliac disease to understand rheumatoid arthritis. *Trends Immunol* 27, pp. 188–194.

Morelli, A, Chiozzi, P., Chiesa, A., Ferrari, D., Sanz, J.M., Falzoni, S., Pinton, P., Rizzuto, R., Olson, M.F. and Di Virgilio, F. 2003. Extracellular ATP causes ROCK I-dependent bleb formation in P2X7-transfected HEK293 cells. *Mol Biol Cell* 14, pp. 2655–2664.

Morelli, Anna, Chiozzi, P., Chiesa, A., Ferrari, D., Sanz, J.M., Falzoni, S., Pinton, P., Rizzuto, R., Olson, M.F. and Virgilio, F. Di 2003. Extracellular ATP Causes ROCK I-dependent Bleb Formation in P2X7-transfected HEK293 Cells. 14(July), pp. 2655–2664.

Mosley, B., Urdal, D.L., Prickett, K.S., Larsen, A., Cosman, D., Conlon, P.J., Gillis, S. and Dower, S.K. 1987. The interleukin-1 receptor binds the human interleukin-1 alpha precursor but not the interleukin-1 beta precursor. *J Biol Chem* 262, pp. 2941–2944.

Murphy, G. 2008. The ADAMs: signaling scissors in the tumour microenvironment. *Nat Rev Cancer* 8, pp. 929–941.

Murtaugh, M.P., Arend, W.P. and Davies, P.J. 1984. Induction of tissue transglutaminase in human peripheral blood monocytes. *J Exp Med* 159, pp. 114–125.

Muszbek, L., Bereczky, Z., Bagoly, Z., Komáromi, I. and Katona, É. 2011. Factor XIII: a coagulation factor with multiple plasmatic and cellular functions. *Physiological reviews* 91(3), pp. 931–72.

Muszbek, L.A., Adany, R. and Mikkola, H. 1996. Novel aspects of blood coagulation ´ da factor XIII. I. Structure, distribution, activation and function. *Crit Rev Lab Sci* 33, pp. 357–421.

Nagy, L., Saydak, M., Shipley, N., Lu, S., Basilion, J.P., Yan, Z.H., Syka, P., Chandraratna, R.A.S., Stein, J.P. and Heyman, R.A. 1996. Identification and Characterization of a Versatile Retinoid Response Element (Retinoic Acid Receptor Response Element-Retinoid X Receptor Response Element) in the Mouse Tissue Transglutaminase Gene Promoter. *Journal of Biological Chemistry* 271(8), pp. 4355–4365.

Nakano, Y., Addison, W.N. and Kaartinen, M.T. 2007. ATP-mediated mineralization of MC3T3-E1 osteoblast cultures. *Bone* 41, pp. 549–561.

Nakaoka, H., Perez, D.M., Baek, K.J., Das, T., Husain, A., Misono, K., Im, M.J. and Graham, R.M. 1994. Gh: a GTP-binding protein with transglutaminase activity and receptor signaling function. *Science* 264, pp. 1593–1596.

Nanda, N., Iismaa, S.E., Owens, W. a, Husain, a, Mackay, F. and Graham, R.M. 2001. Targeted inactivation of Gh/tissue transglutaminase II. *J Biol Chem* 276(23), pp. 20673–20678.

Nemes, Z., Marekov, L.N., Fésüs, L. and Steinert, P.M. 1999. A novel function for transglutaminase 1: attachment of long-chain omega-hydroxyceramides to involucrin by ester bond formation. *Proceedings of the National Academy of Sciences of the United States of America* 96(15), pp. 8402–7.

Nicke, A., Kuan, Y.H., Masin, M., Rettinger, J., Marquez-Klaka, B., Bender, O., Górecki, D.C., Murrell-Lagnado, R.D. and Soto, F. 2009. A functional P2X7 splice variant with an alternative transmembrane domain 1 escapes gene inactivation in P2X7 knock-out mice. *J Biol Chem* 284, pp. 25813–25822.

Nickel, W. 2011. The unconventional secretory machinery of fibroblast growth factor 2. *Traffic* 12(7), pp. 799–805.

Nickel, W. and Rabouille, C. 2009. Mechanisms of regulated unconventional protein secretion. *Nature Reviews Molecular Cell Biology* 10, p. 234.

Nickel, W. and Seedorf, M. 2008. Unconventional mechanisms of protein transport to the cell surface of eukaryotic cells. *Annu Rev Cell Dev Biol* 24, pp. 287–308.

Nijenhuis, S., Zendman, A.J.W., Vossenaar, E.R., Pruijn, G.J.M. and vanVenrooij, W.J. 2004. Autoantibodies to citrullinated proteins in rheumatoid arthritis: clinical performance and biochemical aspects of an RA-specific marker. *Clinica chimica acta; international journal of clinical chemistry* 350(1-2), pp. 17–34.

Nishinaka, Y., Masutani, H., Nakamura, H. and Yodoi, J. 2001. Regulatory roles of thioredoxin in oxidative stress-induced cellular responses. *Redox Rep* 6, pp. 289–295.

North, R.A. 2002. Molecular physiology of P2X receptors. *Physiol Rev* 82, pp. 1013–1067.

Nurminskaya, M. and Kaartinen, M.T. 2006. Transglutaminases in mineralized tissues. *Front Biosci* 1(11), pp. 1591–606.

Nurminskaya, M. V and Belkin, A.M. 2012. Cellular functions of tissue transglutaminase. *Int Rev Cell Mol Biol* 294, pp. 1–97.

Nurminsky, D., Shanmugasundaram, S., Deaseym, S., Michaud, C., Allen, S., Hendig, D., Dastjerdi, A. and Francis-West, P Nurminskaya, M. 2011. Transglutaminase 2 regulates early chondrogenesis and glycosaminoglycan synthesis. *Mech Dev* 128(3-4), pp. 234–45.

Oh, Keunhee, Ko, E., Kim, H.S., Park, A.K., Moon, H.-G., Noh, D.-Y. and Lee, D.-S. 2011. Transglutaminase 2 facilitates the distant hematogenous metastasis of breast cancer by modulating interleukin-6 in cancer cells. *Breast cancer research : BCR* 13(5), p. R96.

Oh, K, Park, H., Byoun, O., Shin, D., Jeong, E., Kim, YW, Kim, YS, Melino, G., Kim, I. and Lee, D. 2011. Epithelial transglutaminase 2 is needed for T cell interleukin-17 production and subsequent pulmonary inflammation and fibrosis in bleomycin-treated mice. *J Exp Med* 208(8), pp. 1707–19.

Orlandi, A., Oliva, F., Taurisano, G., Candi, E., Di Lascio, A., Melino, G., Spagnoli, L.G. and Tarantino, U. 2009. Transglutaminase-2 differently regulates cartilage destruction and osteophyte formation in a surgical model of osteoarthritis. *Amino acids* 36(4), pp. 755–63.

Otto, G.P. and Nichols, B.J. 2011. The roles of flotillin microdomains--endocytosis and beyond. *Journal of cell science* 124(Pt 23), pp. 3933–40.

Parameswaran, K.N., Cheng, X.F., Chen, E.C., Velasco, P.T., Wilson, J.H. and Lorand, L. 1997. Hydrolysis of gamma:epsilon isopeptides by cytosolic transglutaminases and by coagulation factor XIIIa. *J Biol Chem* 272, pp. 10311–10317.

Pelegrín, P. 2011. Many ways to dilate the P2X7 receptor pore. *British journal of pharmacology* 163(5), pp. 908–11.

Pelegrin, P. and Surprenant, A. 2007. Pannexin-1 couples to maitotoxin- and nigericin-induced interleukin-1beta release through a dye uptake-independent pathway. *The Journal of biological chemistry* 282(4), pp. 2386–94.

Pelegrin, P. and Surprenant, A. 2006. Pannexin-1 mediates large pore formation and interleukin-1beta release by the ATP-gated P2X7 receptor. *The EMBO journal* 25(21), pp. 5071–82.

Peng, X., Zhang, Y., Zhang, H., Graner, S., Williams, J., Levitt, M. and Lokshin, A. 1999. Interaction of tissue transglutaminase with nuclear transport protein importin-alpha3. *FEBS letters* 446(1), pp. 35–9.

Penuela, S., Bhalla, R., Gong, X.-Q., Cowan, K.N., Celetti, S.J., Cowan, B.J., Bai, D., Shao, Q. and Laird, D.W. 2007. Pannexin 1 and pannexin 3 are glycoproteins that exhibit many distinct characteristics from the connexin family of gap junction proteins. *Journal of cell science* 120(Pt 21), pp. 3772–83.

Perregaux, D., Barberia, J., Lanzetti, A.J., Geoghegan, K.F., Carty, T.J. and Gabel, C.A. 1992. IL-1 beta maturation: evidence that mature cytokine formation can be induced specifically by nigericin. *J Immunol* 149, pp. 1294–1303.

Perregaux, D. and Gabel, C.A. 1994. Interleukin-1 beta maturation and release in response to ATP and nigericin. Evidence that potassium depletion mediated by these agents is a necessary and common feature of their activity. *J Biol Chem* 269, pp. 15195–15203.

Piccin, A., Murphy, W.G. and Smith, O.P. 2007. Circulating microparticles: pathophysiology and clinical implications. *Blood reviews* 21(3), pp. 157–71.

Pietroni, V., Di Giorgi, S., Paradisi, A., Ahvazi, B., Candi, E. and Melino, G. 2008. Inactive and highly active, proteolytically processed transglutaminase-5 in epithelial cells. *J Invest Dermatol* 128, pp. 2760–2766.

Pinkas, D.M., Strop, P., Brunger, A.T. and Khosla, C. 2007. Transglutaminase 2 undergoes a large conformational change upon activation. *PLoS Biol* 5, p. e327.

Pizzirani, C., Ferrari, D., Chiozzi, P., Adinolfi, E., Sandonà, D., Savaglio, E. and Di Virgilio, F. 2007. Stimulation of P2 receptors causes release of IL-1beta-loaded microvesicles from human dendritic cells. *Blood* 109(9), pp. 3856–64.

Pope, R.M. 2002. Apoptosis as a therapeutic tool in rheumatoid arthritis. *Nat Rev Immunol* 2, pp. 527–535.

Pratt, A.G., Isaacs, J.D. and Mattey, D.L. 2009. Current concepts in the pathogenesis of early rheumatoid arthritis. *Best practice & research. Clinical rheumatology* 23(1), pp. 37–48.

Qu, Y., Franchi, L., Nunez, G. and Dubyak, G.R. 2007. Nonclassical IL-1 beta secretion stimulated by P2X7 receptors is dependent on inflammasome activation and correlated with exosome release in murine macrophages. *Journal of Immunology* 179, pp. 1913–1925.

Qu, Y., Misaghi, S., Newton, K., Gilmour, L.L., Louie, S., Cupp, J.E., Dubyak, G.R., Hackos, D. and Dixit, V.M. 2011. Pannexin-1 is required for ATP release during apoptosis but not for inflammasome activation. *Journal of immunology (Baltimore, Md. : 1950)* 186(11), pp. 6553–61.

Rabouille, C., Malhotra, V. and Nickel, W. 2012. Diversity in unconventional protein secretion. *Journal of cell science* 125(Pt 22), pp. 5251–5.

Raghunath, M., Cankay, R., Kubitscheck, U., Fauteck, J.D., Mayne, R., Aeschlimann, D. and Schlötzer-Schrehardt, U. 1999. Transglutaminase activity in the

eye: cross-linking in epithelia and connective tissue structures. *Investigative ophthalmology & visual science* 40(12), pp. 2780–7.

Raghunath, M., Höpfner, B., Aeschlimann, D., Lüthi, U., Meuli, M., Altermatt, S., Gobet, R., Bruckner-Tuderman, L. and Steinmann, B. 1996. Cross-linking of the dermo-epidermal junction of skin regenerating from keratinocyte autografts. Anchoring fibrils are a target for tissue transglutaminase. *J Clin Invest* 98, pp. 1174–1184.

Rassendren, F., Buell, G.N., Virginio, C., Collo, G., North, R.A. and Surprenant, A. 1997. The permeabilizing ATP receptor, P2X7. Cloning and expression of a human cDNA. *J Biol Chem* 272, pp. 5482–5486.

Rathinam, V.A., Vanaja, S.K. and Fitzgerald, K.A. 2012. Regulation of inflammasome signaling. *Nat Immunol* 13, pp. 332–333.

Riccardi, D. and Kemp, P. 2012. The calcium-sensing receptor beyond extracellular calcium homeostasis: conception, development, adult physiology, and disease. *Annu Rev Physiol* 74, pp. 271–97.

Ritter, S.J. and Davies, P. 1998. Identification of a Transforming Growth Factor-beta 1/Bone Morphogenetic Protein 4 (TGF-beta 1/BMP4) Response Element within the Mouse Tissue Transglutaminase Gene Promoter. *Journal of Biological Chemistry* 273(21), pp. 12798–12806.

Roger, S., Gillet, L., Baroja-Mazo, A., Surprenant, A. and Pelegrin, P. 2010. C-terminal calmodulin-binding motif differentially controls human and rat P2X7 receptor current facilitation. *The Journal of biological chemistry* 285(23), pp. 17514–24.

Rousseau, J.C. and Delmas, P.D. 2007. Biological markers in osteoarthritis. *Nat Clin Pract Rheumatol* 3, pp. 346–356.

Rubartelli, a, Bajetto, a, Allavena, G., Wollman, E. and Sitia, R. 1992. Secretion of thioredoxin by normal and neoplastic cells through a leaderless secretory pathway. *The Journal of biological chemistry* 267(34), pp. 24161–4.

Rumney, R.M., Sunters, A., Reilly, G.C. and Gartland, A. 2012. Application of multiple forms of mechanical loading to human osteoblasts reveals increased ATP release in response to fluid flow in 3D cultures and differential regulation of immediate early genes. *J Biomech* 45, pp. 549–554.

La Sala, A., Ferrari, D., Corinti, S., Cavani, A., Di Virgilio, F. and Girolomoni, G. 2001. Extracellular ATP induces a distorted maturation of dendritic cells and inhibits their capacity to initiate Th1 responses. *J Immunol* 166, pp. 1611–1617.

La Sala, A., Ferrari, D., Di Virgilio, F., Idzko, M., Norgauer, J. and Girolomoni, G. 2003. Alerting and tuning the immune response by extracellular nucleotides. *J Leukoc Biol* 73, pp. 339–343.

Santhanam, L., Tuday, E.C., Webb, A.K., Dowzicky, P., Kim, J.H., Oh, Y.J., Sikka, G., Kuo, M., Halushka, M.K., Macgregor, A.M., Dunn, J., Gutbrod, S., Yin, D., Shoukas, A., Nyhan, D., Flavahan, N. a, Belkin, A.M. and Berkowitz, D.E. 2010. Decreased S-nitrosylation of tissue transglutaminase contributes to age-related increases in vascular stiffness. *Circulation research* 107(1), pp. 117–25.

Satpathy, M., Cao, L., Pincheira, R., Emerson, R., Bigsby, R., Nakshatri, H. and Matei, D. 2007. Enhanced peritoneal ovarian tumor dissemination by tissue transglutaminase. *Cancer research* 67(15), pp. 7194–202.

Scarpellini, A., Germack, R., Lortat-Jacob, H., Muramatsu, T., Billett, E., Johnson, T. and Verderio, E.A. 2009. Heparan sulfate proteoglycans are receptors for the cell-surface trafficking and biological activity of transglutaminase-2. *J Biol Chem* 284, pp. 18411–18423.

Schachter, J., Motta, A.P., de Souza Zamorano, A., da Silva-Souza, H.A., Guimarães, M.Z.P. and Persechini, P.M. 2008. ATP-induced P2X7-associated uptake of large molecules involves distinct mechanisms for cations and anions in macrophages. *Journal of cell science* 121(Pt 19), pp. 3261–70.

Schachter, J.B., Sromek, S.M., Nicholas, R.A. and Harden, T.K. 1997. HEK293 human embryonic kidney cells endogenously express the P2Y1 and P2Y2 receptors. *Neuropharmacology* 36, pp. 1181–1187.

Schaertl, S., Prime, M., Wityak, J., Dominguez, C., Munoz-Sanjuan, I., Pacifici, R.E., Courtney, S., Scheel, A. and Macdonald, D. 2010. A profiling platform for the characterization of transglutaminase 2 (TG2) inhibitors. *J Biomol Screen* 15, pp. 478–487.

Seelenmeyer, C., Wegehingel, S., Tews, I., Künzler, M., Aebi, M. and Nickel, W. 2005. Cell surface counter receptors are essential components of the unconventional export machinery of galectin-1. *The Journal of cell biology* 171(2), pp. 373–81.

Sidiropoulos, P.I., Goulielmos, G., Voloudakis, G.K., Petraki, E. and Boumpas, D.T. 2008. Inflammasomes and rheumatic diseases: evolving concepts. *Ann Rheum Dis* 67, pp. 1382–1389.

Siegel, M., Strnad, P., Watts, R.E., Choi, K., Jabri, B., Omary, M.B. and Khosla, C. 2008. Extracellular transglutaminase 2 is catalytically inactive, but is transiently activated upon tissue injury. *PLoS One* 3, p. e1861.

Singer, I.I., Scott, S., Hall, G.L., Limjuco, G., Chin, J. and Schmidt, J.A. 1988. Interleukin 1 beta is localized in the cytoplasmic ground substance but is largely absent from the Golgi apparatus and plasma membranes of stimulated human monocytes. *J Exp Med* 167, pp. 389–407.

Singh, U.S., Kunar, M.T., Kao, Y.L. and Baker, K.M. 2001. Role of transglutaminase II in retinoic acid-induced activation of RhoA-associated kinase-2. *The EMBO journal* 20(10), pp. 2413–23.

Smart, M.L., Panchal, R.G., Bowser, D.N., Williams, D.A. and Petrou, S. 2002. Pore formation is not associated with macroscopic redistribution of P2X7 receptors. *Am J Physiol Cell Physiol* 283(1), pp. C77–84.

Smolen, J.S., Aletaha, D., Grisar, J., Redlich, K., Steiner, G. and Wagner, O. 2008. The need for prognosticators in rheumatoid arthritis. Biological and clinical markers: where are we now? *Arthritis Res Ther* 10, p. 208.

Sokolove, J. and Lepus, C.M. 2013. Role of inflammation in the pathogenesis of osteoarthritis: latest findings and interpretations. *Therapeutic advances in musculoskeletal disease* 5(2), pp. 77–94.

Solle, M., Labasi, J., Perregaux, D.G., Stam, E., Petrushova, N., Koller, B.H., Griffiths, R.J. and Gabel, C.A. 2001. Altered cytokine production in mice lacking P2X(7) receptors. *J Biol Chem* 276, pp. 125–132.

Sollid, L.M. 2002. Coeliac disease: dissecting a complex inflammatory disorder. *Nature Reviews Immunology* 2, pp. 647–655.

Sollid, L.M. and Jabri, B. 2013. Triggers and drivers of autoimmunity: lessons from coeliac disease. *Nat Rev Immunol* 13, pp. 294–302.

Song, Y., Kirkpatrick, L.L., Schilling, A., Helseth, D., Chabot, N., Keillor, J., Johnson, G. and Brady, S. 2013. Transglutaminase and polyamination of tubulin: posttranslational modification for stabilizing axonal microtubules. *Neuron* 78(1), pp. 109–23.

Sorge, R.E., Trang, T., Dorfman, R., Smith, S.B., Beggs, S., Ritchie, J., Austin, J.-S.S., Zaykin, D. V, Vander Meulen, H., Costigan, M., Herbert, T.A., Yarkoni-Abitbul, M., Tichauer, D., Livneh, J., Gershon, E., Zheng, M., Tan, K., John, S.L., Slade, G.D., Jordan, J., Woolf, C.J., Peltz, G., Maixner, W., Diatchenko, L., Seltzer, Z., Salter, M.W. and Mogil, J.S. 2012. Genetically determined P2X7 receptor pore formation regulates variability in chronic pain sensitivity. *Nat Med* 18(4), pp. 595–599.

Stamnaes, J., Pinkas, D.M., Fleckenstein, B., Khosla, C. and Sollid, L.M. 2010. Redox regulation of transglutaminase 2 activity. *J Biol Chem* 285, pp. 25402–25409.

Steinert, P., Chung, S. and Kim, S. 1996. Inactive zymogen and highly active proteolytically processed membrane-bound forms of the transglutami- nase 1 enzyme in human epidermal keratinocyte. *Biochem Biophys Res Commun* 221, pp. 101–6.

Stephens, P., Grenard, P., Aeschlimann, P., Langley, M., Blain, E., Errington, R., Kipling, D., Thomas, D. and Aeschlimann, D. 2004. Crosslinking and G-protein functions of transglutaminase 2 contribute differentially to fibroblast wound healing responses. *J Cell Sci* 117(Pt 15), pp. 3389–3403.

Steringer, J.P., Bleicken, S., Andreas, H., Zacherl, S., Laussmann, M., Temmerman, K., Contreras, F.X., Bharat, T. a M., Lechner, J., Müller, H.-M., Briggs, J. a G., García-Sáez, A.J. and Nickel, W. 2012. Phosphatidylinositol 4,5-bisphosphate (PI(4,5)P2)-dependent oligomerization of fibroblast growth factor 2 (FGF2) triggers

the formation of a lipidic membrane pore implicated in unconventional secretion. *The Journal of biological chemistry* 287(33), pp. 27659–69.

Stevenson, F.T., Torrano, F., Locksley, R.M. and Lovett, D.H. 1992. Interleukin 1: the patterns of translation and intracellular distribution support alternative secretory mechanisms. *J Cell Physiol* 152, pp. 223–231.

Stokes, L., Jiang, L.H., Alcaraz, L., Bent, J., Bowers, K., Fagura, M., Furber, M., Mortimore, M., Lawson, M., Theaker, J., Laurent, C., Braddock, M. and Surprenant, A. 2006. Characterization of a selective and potent antagonist of human P2X(7) receptors, AZ11645373. *Br J Pharmacol* 149, pp. 880–887.

Suh, B.C., Kim, J.S., Namgung, U., Ha, H. and Kim, K.T. 2001. P2X7 nucleotide receptor mediation of membrane pore formation and superoxide generation in human promyelocytes and neutrophils. *Journal of immunology (Baltimore, Md. : 1950)* 166(11), pp. 6754–63.

Sun, C., Heid, M.E., Keyel, P. a and Salter, R.D. 2013. The Second Transmembrane Domain of P2X7 Contributes to Dilated Pore Formation. *PloS one* 8(4), p. e61886.

Surprenant, A. and North, R.A. 2009. Signaling at purinergic P2X receptors. *Annu Rev Physiol* 71, pp. 333–359.

Surprenant, A., Rassendren, F., Kawashima, E., North, R.A. and Buell, G. 1996. The cytolytic P2Z receptor for extracellular ATP identified as a P2X receptor (P2X7). *Science* 272, pp. 735–738.

Suto, N., Ikura, K. and Sasaki, R. 1993. Expression induced by interleukin-6 of tissue-type transglutaminase in human hepatoblastoma HepG2 cells. *J Biol Chem* 268, pp. 7469–7473.

Szodoray, P., Szabo, Z., Kapitny, A., Gyetvai, A., Lakos, G., Szynt, S., Szycs, G. and Szekanecz, Z. 2010. Anti-citrullinated protein/peptide autoantibodies in association with genetic and environmental factors as indicators of disease outcome in rheumatoid arthritis. *Autoimmun Rev* 9, pp. 140–143.

Tarantini, F., Micucci, I., Bellum, S., Landriscina, M., Garfinkel, S., Prudovsky, I. and Maciag, T. 2001. The precursor but not the mature form of IL1alpha blocks the release of FGF1 in response to heat shock. *The Journal of biological chemistry* 276(7), pp. 5147–51.

Tarantino, U., Ferlosio, A., Arcuri, G., Spagnoli, L.G. and Orlandi, A. 2011. Transglutaminase 2 as a biomarker of osteoarthritis: an update. *Amino Acids* 44(1), pp. 199–207.

Telci, D., Collighan, R.J., Basaga, H. and Griffin, M. 2009. Increased TG2 expression can result in induction of transforming growth factor beta1, causing increased synthesis and deposition of matrix proteins, which can be regulated by nitric oxide. *The Journal of biological chemistry* 284(43), pp. 29547–58.

Telci, D., Wang, Z., Li, X., Verderio, E.A.M., Humphries, M.J., Baccarini, M., Basaga, H. and Griffin, M. 2008. Fibronectin-tissue transglutaminase matrix rescues RGD-impaired cell adhesion through syndecan-4 and beta1 integrin co-signaling. *The Journal of biological chemistry* 283(30), pp. 20937–47.

Théry, C., Zitvogel, L. and Amigorena, S. 2002. Exosomes: composition, biogenesis and function. *Nature reviews. Immunology* 2(8), pp. 569–79.

Thomas, H., Beck, K., Adamczyk, M., Aeschlimann, P., Langley, M., Oita, R.C., Thiebach, L., Hils, M. and Aeschlimann, D. 2013. Transglutaminase 6: a protein associated with central nervous system development and motor function. *Amino Acids* 44(1), pp. 161–177.

Thomas, L.M. and Salter, R.D. 2010. Activation of macrophages by P2X7-induced microvesicles from myeloid cells is mediated by phospholipids and is partially dependent on TLR4. *Journal of immunology* 185(6), pp. 3740–9.

Thomázy, V. a and Davies, P.J. 1999. Expression of tissue transglutaminase in the developing chicken limb is associated both with apoptosis and endochondral ossification. *Cell death and differentiation* 6(2), pp. 146–54.

Thomazy, V. and Fesus, L. 1989. Differential expression of tissue transglutaminase in human cells. An immunohistochemical study. *Cell Tissue Res* 255(1), pp. 215–224.

Thornberry, N.A., Bull, H.G., Calaycay, J.R., Chapman, K.T., Howard, A.D., Kostura, M.J., Miller, D.K., Molineaux, S.M., Weidner, J.R. and Aunins, J. 1992. A novel heterodimeric cysteine protease is required for interleukin-1 beta processing in monocytes. *Nature* 356, pp. 768–774.

Torrado, L.C., Temmerman, K., Müller, H.-M., Mayer, M.P., Seelenmeyer, C., Backhaus, R. and Nickel, W. 2009. An intrinsic quality-control mechanism ensures unconventional secretion of fibroblast growth factor 2 in a folded conformation. *Journal of cell science* 122(Pt 18), pp. 3322–9.

Torres, G.E., Egan, T.M. and Voigt, M.M. 1999. Hetero-oligomeric assembly of P2X receptor subunits. Specificities exist with regard to possible partners. *J Biol Chem* 274, pp. 6653–6659.

Trajkovic, K., Hsu, C., Chiantia, S., Rajendran, L., Wenzel, D., Wieland, F., Schwille, P., Brügger, B. and Simons, M. 2008. Ceramide triggers budding of exosome vesicles into multivesicular endosomes. *Science (New York, N.Y.)* 319(5867), pp. 1244–7.

Trombetta, E.S. and Parodi, A.J. 2003. Quality control and protein folding in the secretory pathway. *Annu Rev Cell Dev Biol* 19, pp. 649–676.

Tsuchiya, S., Yamabe, M., Yamaguchi, Y., Kobayashi, Y., Konno, T. and Tada, K. 1980. Establishment and characterization of a human acute monocytic leukemia cell line (THP-1). *Int J Cancer* 26, pp. 171–176.

Upchurch, H.F., Conway, E., Patterson, M.K.J., Birckbichler, P.J. and Maxwell, M.D. 1987. Cellular transglutaminase has affinity for extracellular matrix. *In Vitro Cell Dev Biol* 23(11), pp. 795–800.

Di Venere, A., Rossi, A., De Matteis, F., Rosato, N., Agrò, A.F. and Mei, G. 2000. Opposite effects of Ca(2+) and GTP binding on tissue transglutaminase tertiary structure. *J Biol Chem* 275, pp. 3915–3921.

Van Venrooij, W.J., Zendman, A.J.W. and Pruijn, G.J.M. 2006. Autoantibodies to citrullinated antigens in (early) rheumatoid arthritis. *Autoimmunity reviews* 6(1), pp. 37–41.

Verderio, E. a M., Telci, D., Okoye, A., Melino, G. and Griffin, M. 2003. A novel RGD-independent cel adhesion pathway mediated by fibronectin-bound tissue transglutaminase rescues cells from anoikis. *The Journal of biological chemistry* 278(43), pp. 42604–14.

Verderio, E., Nicholas, B., Gross, S. and Griffin, M. 1998. Regulated expression of tissue transglutaminase in Swiss 3T3 fibroblasts: effects on the processing of fibronectin, cell attachment, and cell death. *Experimental cell research* 239(1), pp. 119–38.

Di Virgilio, F. 2007. Liaisons dangereuses: P2X(7) and the inflammasome. *Trends Pharmacol Sci* 28, pp. 465–472.

Di Virgilio, F. 2005. Purinergic mechanism in the immune system: A signal of danger for dendritic cells. *Purinergic Signal* 1, pp. 205–209.

Di Virgilio, F. 2012. Purines, purinergic receptors, and cancer. *Cancer research* 72(21), pp. 5441–7.

Di Virgilio, F. 1995. The P2Z purinoceptor: an intriguing role in immunity, inflammation and cell death. *Immunol Today* 16, pp. 524–528.

Di Virgilio, F, Boeynaems, J.M. and Robson, S.C. 2009. Extracellular nucleotides as negative modulators of immunity. *Curr Opin Pharmacol* 9, pp. 507–513.

Di Virgilio, F., Chiozzi, P., Ferrari, D., Falzoni, S., Sanz, J.M., Morelli, A., Torboli, M., Bolognesi, G. and Baricordi, O.R. 2001. Nucleotide receptors: an emerging family of regulatory molecules in blood cells. *Blood* 97, pp. 587–600.

Di Virgilio, Francesco, Ferrari, D. and Adinolfi, E. 2009. P2X(7): a growth-promoting receptor-implications for cancer. *Purinergic signaling* 5(2), pp. 251–6.

Virginio, C., Church, D., North, R.A. and Surprenant, A. 1997. Effects of divalent cations, protons and calmidazolium at the rat P2X7 receptor. *Neuropharmacology* 36, pp. 1285–1294.

Virginio, C., MacKenzie, A., North, R. a and Surprenant, A. 1999. Kinetics of cell lysis, dye uptake and permeability changes in cells expressing the rat P2X7 receptor. *J Physiol* 519 Pt 2, pp. 335–346.

Wang, Q., AL, R., CM, L., CR, S., JJ, S., DM, Larsen, JF, C., G, B., SY, R., TM, L., I, H., HH, W., L, P., A, E., M, S., SB, G., T, W.-C., SR, G., NK, B., JM, T., R, G., MK, C., VM, H., DM, Lee and WH., R. 2012. Identification of a central role for complement in osteoarthritis. 17(12), pp. 1674–1679.

Wang, X., Matteson, J., An, Y., Moyer, B., Yoo, J.S., Bannykh, S., Wilson, I.A., Riordan, J.R. and Balch, W.E. 2004. COPII-dependent export of cystic fibrosis transmembrane conductance regulator from the ER uses a di-acidic exit code. *J Cell Biol* 167, pp. 65–74.

Watanabe, K., Tsunoda, K., Itoh, M., Fukui, M., Mori, H. and Hitomi, K. 2013. Transglutaminase 2 and Factor XIII catalyze distinct substrates in differentiating osteoblastic cell line: utility of highly reactive substrate peptides. *Amino acids* 44(1), pp. 209–14.

Wewers, M.D., Dare, H.A., Winnard, A. V, Parker, J.M. and Miller, D.K. 1997. IL-1 beta-converting enzyme (ICE) is present and functional in human alveolar macrophages: Macrophage IL-1 beta release limitation is ICE independent. *Journal of Immunology* 159, pp. 5964–5972.

Wickert, L.E., Blanchette, J.B., Waldschmidt, N. V, Bertics, P.J., Denu, J.M., Denlinger, L.C. and Lenertz, L.Y. 2013. The C-Terminus of Human Nucleotide Receptor P2X7 Is Critical for Receptor Oligomerization and N-Linked Glycosylation. *PloS one* 8(5), p. e63789.

Wilson, H.L., Wilson, S.A., Surprenant, A. and North, R.A. 2002. Epithelial membrane proteins induce membrane blebbing and interact with the P2X7 receptor C terminus. *J Biol Chem* 277, pp. 34017–34023.

Xin, F. and Radivojac, P. 2012. Post-translational modifications induce significant yet not extreme changes to protein structure. *Bioinformatics (Oxford, England)* 28(22), pp. 2905–13.

Xu, L., Begum, S., Hearn, J.D. and Hynes, R. 2006. GPR56, an atypical G protein-coupled receptor, binds tissue transglutaminase, TG2, inhibits melanoma tumor growth and metastasis. *Proc Natl Acad Sci U S A* 103, pp. 9023–9028.

Xu, S., Sukumar, P., Zeng, F., Li, J., Jairaman, A., English, A., Naylor, J., Ciurtin, C., Majeed, Y., Milligan, C.J., Bahnasi, Y.M., Al-Shawaf, E., Porter, K.E., Jiang, L., Emery, P., Sivaprasadarao, A. and Beech, D.J. 2008. TRPC channel activation by extracellular thioredoxin. *Nature* 451(7174), pp. 69–72.

Yakubov, B., Chelladurai, B., Schmitt, J., Emerson, R., Turchi, J.J. and Matei, D. 2013. Extracellular Tissue Transglutaminase Activates Noncanonical NF- κ B Signaling and Promotes Metastasis. 15(6), pp. 609–619.

Yan, Z., Khadra, A., Sherman, A. and Stojilkovic, S.S. 2011. Calcium-dependent block of P2X7 receptor channel function is allosteric. *The Journal of general physiology* 138(4), pp. 437–52.

Yan, Z., Li, S., Liang, Z., Tomić, M. and Stojilkovic, S.S. 2008. The P2X7 receptor channel pore dilates under physiological ion conditions. *The Journal of general physiology* 132(5), pp. 563–73.

Yoo, H., Ahn, E., Kim, SJ, Lee, S., Oh, S. and Kim, SY 2013. Divergent results induced by different types of septic shock in transglutaminase 2 knockout mice. *Amino Acids* 44(1), pp. 189–97.

Young, M.T. 2010. P2X receptors: dawn of the post-structure era. *Trends in biochemical sciences* 35(2), pp. 83–90.

Zehe, C., Engling, A., Wegehingel, S., Schfer, T. and Nickel, W. 2006. Cell-surface heparan sulfate proteoglycans are essential components of the unconventional export machinery of FGF-2. *Proc Natl Acad Sci U S A* 103, pp. 15479–15484.

Zemskov, E. a, Loukinova, E., Mikhailenko, I., Coleman, R. a, Strickland, D.K. and Belkin, A.M. 2009. Regulation of platelet-derived growth factor receptor function by integrin-associated cell surface transglutaminase. *The Journal of biological chemistry* 284(24), pp. 16693–703.

Zemskov, E. a, Mikhailenko, I., Strickland, D.K. and Belkin, A.M. 2007. Cell-surface transglutaminase undergoes internalization and lysosomal degradation: an essential role for LRP1. *Journal of cell science* 120(Pt 18), pp. 3188–99.

Zemskov, E.A., Janiak, A., Hang, J., Waghray, A. and Belkin, A.M. 2006. The role of tissue transglutaminase in cell-matrix interactions. *Front Biosci* 11, pp. 1057–1076.

Zemskov, E.A., Mikhailenko, I., Hsia, R.C., Zaritskaya, L. and Belkin, A.M. 2011. Unconventional secretion of tissue transglutaminase involves phospholipid-dependent delivery into recycling endosomes. *PLoS One* 6, p. e19414.

Zhu, W.Q. and Ochieng, J. 2001. Rapid release of intracellular galectin-3 from breast carcinoma cells by fetuin. *Cancer Res* 61, pp. 1869–1873.

Zimmerman, H. 2000. Ectonucleotidases: some recent developments and a note on nomenclature. *Drug. Dev. Res.* 52, pp. 44–56.

Appendix 1

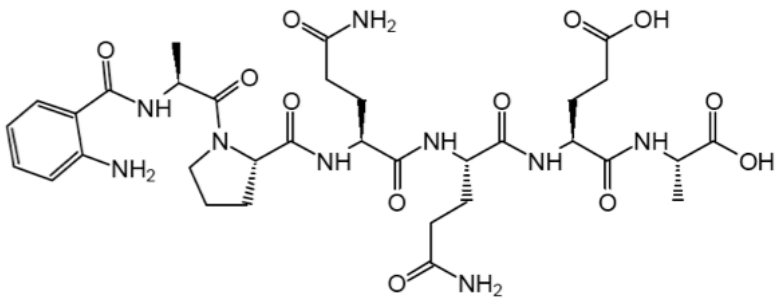

Supplementary Fig. 1 Chemical structure of the Abz-APQQEA peptide.

Appendix 2

Real-time fluorescence assay for monitoring transglutaminase activity

Magdalena Adamczyk, Andreas Heil and Daniel Aeschlimann
Matrix Biology & Tissue Repair Research Unit, School of Dentistry, Cardiff University, Heath Park, Cardiff, CF14 4XY, UK

Application Note 234, Rev. 04/2013

- Isopeptidase assay for kinetic analysis of transglutaminase activity
- Optimized protocols for FLUOstar OPTIMA and Omega allow for rapid implementation and standardization of measurements
- Assay is amenable to high throughput analysis of regulators/ inhibitors of catalysis

Introduction

Transglutaminases (TGs) form a family of enzymes that catalyze various posttranslational protein modifications such as crosslinking, esterification and deamidation in a Ca^{2+}-dependent manner.[1] Their main function is the formation of covalent N^{ε}-(γ-glutamyl)lysine bonds within or between polypeptides to stabilize protein assemblies. The activity of these enzymes is crucial for tissue homeostasis and function in a number of organ systems, and the lack of or the excessive crosslinking activity have been linked to human disease processes[1,2].

Here we perform kinetic measurements using recombinant TG2 and a fluorescent peptide model substrate on a FLUOstar OPTIMA and FLUOstar Omega in a format suitable for high-throughput analysis. This assay principle can be applied to kinetic studies on closely related enzymes including TG6[3] and can be optimised by modification of the backbone peptide sequence.

Assay Principle

A

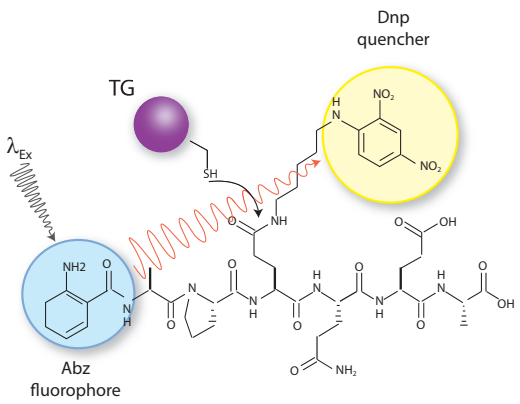

Fig 1A: *Structure of quenched substrate Abz-APE(γ-cad-Dnp)QEA whereby 2-aminobenzoyl (Abz) and 2,4-dinitrophenyl (Dnp) are fluorescent donor and quenching acceptor group, respectively.*

The TG enzymatic reaction is a two-step process. The thioester intermediate of the enzyme formed with the substrate in the first step subsequently reacts with a nucleophile to regenerate active enzyme and release a 'crosslinked' polypeptide. The second step is reversible and, in the presence of an excess of crosslinked substrate, TG catalyzes isopeptide bond hydrolysis[4]. We have exploited this latter activity for real-time monitoring of TG activity and characterize the effect of potential regulators on TG activity.

B

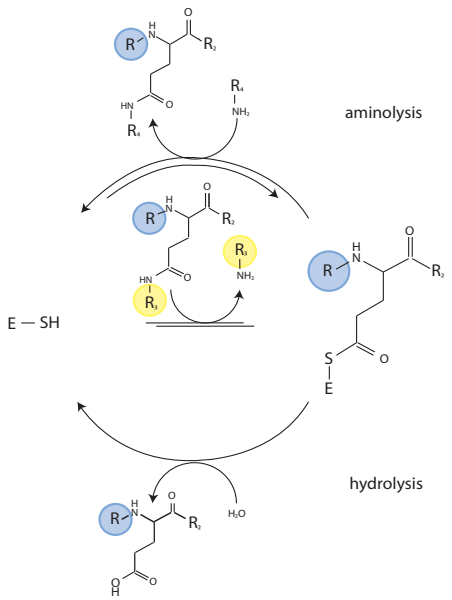

Fig. 1B: *Reaction scheme for TG catalyzed isopeptidase reaction with substrate Abz-APE(γ-cad-Dnp)QEA in the presence of an excess of unlabeled primary amine (R_4-NH_2, e.g. glycine methylester). R: Abz-AP; R_2: QEA; R_3: $(CH_2)_4$-NH-Dnp; E-SH (TG2 with active site thiol group).*

Abz-APE(γ-cad-Dnp)QEA is a quenched fluorescent probe derived from a known glutamine donor substrate[5] that mimics a crosslinked TG reaction product. In this peptide the fluorophore (2-aminobenzoyl (Abz)) is quenched by a 2,4-dinitrophenyl-cadaverine (cad-Dnp) substituent on the first Gln residue, essentially replacing the Lys side chain in N^{ε}-(γ-glutamyl)lysine linked peptides (Fig. 1A). TG2-catalysed hydrolysis of the isopeptide bond releases the cad-Dnp moiety (Fig. 1B) and consequently generates an increase in light emission at λ_{max}=418 nm from the Abz group. The thioester enzyme intermediate formed is subsequently deacylated through either aminolysis or hydrolysis. Specificity of the reaction is guided by the amino acid residues that surround the reactive Gln residue[3].

Materials and Methods

- ☐ FLUOstar OPTIMA or FLUOstar Omega (Fig. 3) microplate readers from BMG LABTECH
- ☐ Black optical bottom 96-well plates (165305, Nunc)
- ☐ Abz-APE(γ-cad-Dnp)QEA TG2 substrate (A102; Zedira, Darmstadt, Germany). 50 mM stock in DMSO
- ☐ Transglutaminase 2 [6], 1 mg/ml stock, cleared by centrifugation at 14,000 x g for 30 min at 4°C and concentration derived from OD_{280} using ε = 1352 cm^2/g; keep on ice and prevent repeated freeze-thawing (similar high quality product is available from Zedira: T002)

Assay buffer

The assay buffer consists of 62.5 mM Tris/HCl, pH 7.4, 125 mM NaCl. Add glycine methylester (or alternative amine donor substrate) and adjust pH immediately before use (at 37°C). Include DTT to prevent oxidative inactivation of TG.

Test protocol

Prime the FLUOstar injectors with 20 mM $CaCl_2$ for enzyme activation (inj. 1) and H_2O or 20 mM $MgCl_2$ for control reaction (inj. 2). Pre-warm assay buffer and plate to 37˚C and equilibrate instrument chamber at 37˚C. Dilute substrate Abz-APE(γ-cad-Dnp)QEA (1:800) in assay buffer and add 80 µl of mixture into wells of the 96-well plate. Add desired amount of enzyme, e.g. 1 µg of TG2, and make up volume with H_2O to 90 µl. Transfer plate immediately into the reader and start program.

Reaction mixture (final concentrations)

The final assay volume is 100 µl and consists of 1-100 µg/ml TG2, 50 µM Abz-APE(γ-cad-Dnp)QEA, 10-55 mM glycine methylester or alternative nucleophile, as well as 1-5 mM DTT. After injection there is 2 mM $CaCl_2$ present in samples. Detailed discussion can be found here:

http://www.cardiff.ac.uk/dentl/aeschlimann

Instrument settings

Mode:	Fluorescence Intensity, plate mode
Filters:	Ex320 for excitation and 440-10 for emission
Optics	top
No. of flashes:	20
Cycles:	90
Cycle time:	40 s (for 12 wells)
Injection cycle:	10
Injection volume:	10 µL
Shaking:	5 s after each cycle
Temperature:	37°C

Results and Discussion

After Ca^{2+} injection an increase in fluorescence can be observed dependent on the concentration of enzyme in sample (Fig. 2).

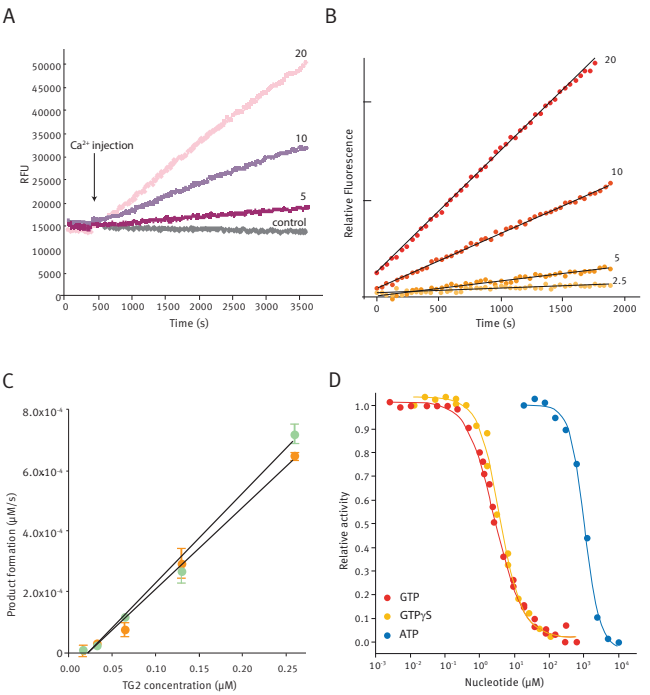

Fig. 2: *Raw data (A) and processed data (B) of substrate Abz-APE(γ-cad-Dnp) QEA conversion at different concentrations of TG2 (2.5 – 20 µg/ml) as measured with Optima instrument. Control given represents 20 µg/ml TG2 without Ca^{2+} injection. Data processing involved normalization for well-specific fluorescence and subtraction of control to account for fluorescence bleaching. C: Reaction rate is linearly correlated to enzyme concentration (orange, Optima data; green, Omega data). D: Allosteric regulation of TG2 by nucleotides. Isopeptidase activity of TG2 measured in the presence of different concentrations of nucleotides: GTP, red line; GTPγS, yellow line; and ATP, blue line.*

TG2-mediated substrate conversion is linear for ›30 min and initial reaction rates can be derived from linear regression of first 15-25 data points (Fig. 2A and B). Fluorescence emission of the standard peptide Abz-APQQEA was found to correlate linearly with concentration for 0.13-2.0 µM (gain 2450) on the FLUOstar OPTIMA and 0.016-0.5 µM (gain 2450) or 0.03-2.0 µM (gain 1883) on the FLUOstar Omega (Fig. 2C). Enzymatic conversion of Abz-APE(γ-cad-Dnp)QEA was measureable down to 1 µg/ml (~13 nM) for TG2 on the FLUOstar OPTIMA.

The plate format is ideal for investigating the effect of potential regulators or inhibitors on catalysis. GTP is a well characterized allosteric regulator of TG2[7]. Using the outlined reaction conditions and 20 µg/ml TG2 and different concentrations of nucleotides, we have determined IC_{50} concentrations of 2.9 µM, 3.6 µM, and ~1 mM for GTP, GTPγS and ATP, respectively, which is in good agreement with data in the literature (Fig. 2D).

Conclusion

Reported here are optimized experimental conditions for determination of TG2 isopeptidase activity with the fluorescent model substrate Abz-APE(γcad-Dnp)QEA using the FLUOstar OPTIMA/Omega plate readers to produce an assay that is rapid, direct and sensitive. Automated injection of Ca^{2+} for enzyme activation combined with the ability to continuously measure fluorescence intensity over a considerable time period with limited photobleaching facilitates the acquisition of kinetic data. Small sample size and plate format make the assay cost-effective and adaptable to high-throughput analysis.

Acknowledgements

This work was supported by grants from Coeliac UK and Arthritis Research UK (18461), and PhD studentships from Cardiff University/the President's Scholarship scheme to MA and AH.

References

1. Aeschlimann D, Thomazy, V. (2000). *Connect Tissue Res.* **41**:1-27.
2. Iismaa, S, et al., (2009). *Physiol. Rev.* **89**:991-1023.
3. Thomas H, et al., (2013). *Amino Acids.* **44**: 161-177.
4. Parameswaran, KN, et al., (1997). *J. Biol. Chem.* **272**:10311-10317.
5. Hohenadl C, et al., (1995). *J. Biol. Chem.* **270**: 23415-23420.
6. Hadjivassiliou M, et al., (2008). *Ann. Neurol.* **64**:332-343.
7. Lui S, et al., (2002). *Proc. Natl. Acad. Sci. USA.* **99**: 2743-2747.

Fig. 3: *BMG LABTECH's FLUOstar Omega multidetection microplate reader*

Germany:	**BMG LABTECH GmbH**	**Tel: +49 781 96968-0**
Australia:	BMG LABTECH Pty. Ltd.	Tel: +61 3 59734744
France:	BMG LABTECH SARL	Tel: +33 1 48 86 20 20
Japan:	BMG LABTECH JAPAN Ltd.	Tel: +81 48 647 7217
UK:	BMG LABTECH Ltd.	Tel: +44 1296 336650
USA:	BMG LABTECH Inc.	Tel: +1 877 264 5227
Internet:	**www.bmglabtech.com**	**applications@bmglabtech.com**

Appendix 3

Amino Acids (2013) 44:161–177
DOI 10.1007/s00726-011-1091-z

ORIGINAL ARTICLE

Transglutaminase 6: a protein associated with central nervous system development and motor function

Helen Thomas · Konrad Beck · Magdalena Adamczyk · Pascale Aeschlimann · Martin Langley · Radu C. Oita · Lars Thiebach · Martin Hils · Daniel Aeschlimann

Received: 28 June 2011 / Accepted: 16 September 2011 / Published online: 8 October 2011

Abstract Transglutaminases (TG) form a family of enzymes that catalyse various post-translational modifications of glutamine residues in proteins and peptides including intra- and intermolecular isopeptide bond formation, esterification and deamidation. We have characterized a novel member of the mammalian TG family, TG6, which is expressed in a human carcinoma cell line with neuronal characteristics and in mouse brain. Besides full-length protein, alternative splicing results in a short variant lacking the second β-barrel domain in man and a variant with truncated β-sandwich domain in mouse. Biochemical data show that TG6 is allosterically regulated by Ca^{2+} and guanine nucleotides. Molecular modelling indicates that TG6 could have Ca^{2+} and GDP-binding sites related to those of TG3 and TG2, respectively. Localization of mRNA and protein in the mouse identified abundant expression of TG6 in the central nervous system. Analysis of its temporal and spatial pattern of induction in mouse development indicates an association with neurogenesis. Neuronal expression of TG6 was confirmed by double-labelling of mouse forebrain cells with cell type-specific markers. Induction of differentiation in mouse Neuro 2a cells with NGF or dibutyryl cAMP is associated with an upregulation of TG6 expression. Familial ataxia has recently been linked to mutations in the TGM6 gene. Autoantibodies to TG6 were identified in immune-mediated ataxia in patients with gluten sensitivity. These findings suggest a critical role for TG6 in cortical and cerebellar neurons.

Keywords Transglutaminase 6 · Sequence · Structural model · Regulation · Central nervous system · Ataxia

Abbreviations

CNS	Central nervous system
DIG	Digoxigenin
GFAP	Glial fibrillary acidic protein
HD	Huntington's disease
PCR	Polymerase chain reaction
RT	Reverse transcription
SCA	Spinocerebellar ataxia
TG	Transglutaminase

Introduction

Transglutaminases (TG) are a family of structurally and functionally related enzymes that post-translationally modify proteins by catalysing a Ca^{2+}-dependent transferase reaction between the γ-carboxamide group of a

H. Thomas and K. Beck contributed equally to this work.

Electronic supplementary material The online version of this article (doi:10.1007/s00726-011-1091-z) contains supplementary material, which is available to authorized users.

H. Thomas · K. Beck · M. Adamczyk · P. Aeschlimann · M. Langley · R. C. Oita · D. Aeschlimann (✉)
Matrix Biology and Tissue Repair Research Unit, School of Dentistry, Cardiff University, Heath Park, Cardiff CF14 4XY, UK
e-mail: AeschlimannDP@Cardiff.ac.uk

M. Adamczyk · P. Aeschlimann
Arthritis Research UK Biomechanics and Bioengineering Centre, Cardiff University, 51 Park Place, CF10 3AT Cardiff, UK

L. Thiebach
Institute for Biochemistry, Medical Faculty, University of Cologne, Joseph-Stelzmann Str. 52, 50931 Cologne, Germany

M. Hils
ZEDIRA, Roesslerstr. 83, 64293 Darmstadt, Germany

peptide-bound glutamine residue and various primary amines. Most commonly, intra- or intermolecular γ-glutamyl-ε-lysine crosslinks are formed by reaction with the ε-amino group of a lysine residue (Folk and Chung 1973). The action of these enzymes consequently results in the formation of covalently crosslinked, often insoluble supramolecular structures and has a well-established role in tissue homeostasis in many biological systems (Aeschlimann and Thomazy 2000; Lorand and Graham 2003; Iismaa et al. 2009). Besides crosslinking, peptide-bound glutamine residues may be modified by TG through reaction of the acyl-enzyme intermediate with low-molecular-weight metabolites harbouring amino groups, or through hydrolysis or esterification. Conversion through hydrolysis is comparably slow and occurs preferentially at pH < 6.5. Nevertheless, the biological significance of enzymatic deamidation of glutamine has been illustrated by its role in T-cell activation in celiac disease (Molberg et al. 1998; Van de Wal et al. 1998). Transamidation has profound effects on the biological activity of many substrate proteins and it has become clear that some TGs preferentially form intermolecular crosslinks, whereas others catalyse primarily intramolecular reactions (Candi et al. 1995). Such protein modifications can be dynamic as conversion of the acyl-enzyme intermediate to the isopeptide bond is reversible (Parameswaran et al. 1997). TGs are evolutionarily related to papain-like cysteine proteases, both in terms of the structure of the core domain and the mechanism of catalysis, and more distantly to the peptide *N*-glycanases. Other enzymes have evolved in lower species that can catalyse the same transamidation reaction. These, however, bear no genetic relationship to the TG genes in man and the mechanism of catalysis is distinct, although it depends on a reactive thiol in the enzyme active site. These include *Streptomyces* microbial TG, bacterial toxins (including cytotoxic necrotizing factor from *E. coli* and dermonecrotic toxin from *Bordetella*), and thioredoxin/protein-disulfide isomerase-like enzymes from primitive eukaryotes (e.g. ERp60-like from nematodes and PDI from *Giardia*).

Nine different TG genes have been characterized in mammals (Aeschlimann and Paulsson 1994; Aeschlimann et al. 1998; Grenard et al. 2001). They exhibit a similar overall organization, with remarkable conservation of intron distribution and intron splice types. Detailed comparison of the structure of the individual genes shows that they may be divided into two subclasses, wherein the TGM2-7 and EBP42 genes contain 13 exons, and the F13A1 and TGM1 genes contain 15 exons (Grenard et al. 2001). Exon 9 of the former group is separated into two exons, 10 and 11, in the TGM1 and F13A1 genes, and the non-homologous *N*-terminal extensions of factor XIII a-subunit and TG1 that are absent in other TGs are comprised by an additional exon. Several TG gene products have been characterized in detail using a combination of mutagenesis and structural studies to elucidate the enzymatic mechanism and its regulation. The three-dimensional structures of three TGs have been solved, i.e. factor XIII a (Yee et al. 1994), TG2 (Liu et al. 2002) and TG3 (Ahvazi et al. 2002). All comprise of four domains that are similar in organization: an amino terminal β-sandwich domain which forms a functional unit with the core domain; the catalytic core domain that contains the conserved active site triad cysteine, histidine and aspartate residues; and two *C*-terminal β-barrel domains which are involved in the regulation of enzyme activity. Molecular modelling and docking studies on TG3 proposed that binding of two additional Ca^{2+} ions converts the enzyme to the active form on the approach of the first substrate (glutamine-containing polypeptide) (Ahvazi et al. 2004). A recent X-ray structure of a trapped transamidation intermediate of TG2 (Pinkas et al. 2007) explained for the first time how a crosslinked protein complex could be released from the enzyme after catalysis as well as the considerable increase in radius of gyration observed by small-angle X-ray scattering for activated TG2 in solution (Mariani et al. 2000). TG2 undergoes a large conformational change whereby the β-barrel domains are rotated almost 180° into the plane of the other two domains, thereby exposing the enzyme active site (Pinkas et al. 2007).

TGs have been implicated in the pathogenesis of several neurodegenerative diseases (polyglutamine expansion diseases, Alzheimer's, Parkinson's and supranuclear palsy), but despite extensive investigation over at least two decades ambiguity remains as to the physiological function of TGs in the central nervous system (CNS) as well as their role in pathogenesis (for review see Iismaa et al. 2009; Jeitner et al. 2009). It has been shown that pathological length CAG expansions are excellent substrates for TG2 and that TG2 activity is increased in the brains of patients with Huntington's disease (HD) and certain forms of spinocerebellar ataxia (SCA) (Lesort et al. 1999). In Alzheimer's disease TGs have been localised to plaques and tangles and these contain substrates of TG2 (Kim et al. 1999). Similarly, the presence of TG crosslinked α-synuclein in substantia nigra dopaminergic neurons of Parkinson's disease patients has been demonstrated (Andringa et al. 2004). The fact that increased levels of the γ-glutamyl-ε-lysine crosslink as well as *bis*-γ-glutamylpolyamine are found in the affected tissue and in the cerebrospinal fluid (Zainelli et al. 2003; Nemes et al. 2004; Jeitner et al. 2008) indicates that TG2 and possibly other TG isozymes extensively modify proteins and possibly also disease-specific protein aggregates. Mouse models have substantiated a direct role of TG2 in the pathogenesis of Huntington's and other neurodegenerative diseases albeit the mechanisms involved being somewhat unexpected. HD

mice (R6/1 and R6/2) lacking TG2 exhibit delayed mortality and behavioural deficits but have increased aggregate formation (Mastroberardino et al. 2002; Bailey and Johnson 2005). It is therefore possible that TG2 contributes to the pathogenesis by modulating the size of the aggregates formed, leading to the formation of smaller aggregates (Lai et al. 2004) that may be more neurotoxic. In an Alzheimer's disease model, fibrillar Aβ triggers dimerization of angiotensin II type 2 receptors (AT_2) which becomes a substrate for TG2 and is further oligomerized (AbdAlla et al. 2009). AT_2 oligomerization results in sequestration of $G\alpha_{q/11}$ G protein which impairs M1 muscarinic receptor function. Excitotoxic neuronal cell death is an important component of acute injury in the CNS and also chronic neurodegenerative diseases. Tissue-specific overexpression of TG2 in mice sensitizes hippocampal neurons to apoptosis upon glutamate receptor overstimulation (Tucholski et al. 2006) and ischemic injury induces rapid upregulation of TG2 expression (Ientile et al. 2004) consistent with its regulation by acute-phase injury cytokines. A recent study provides evidence that TG2 has a broad effect on gene transcription by regulating chromatin structure through *N*-terminal polyamination of histone H3 in a model of HD and that TG2 inhibition protects striatal neurons from NMDA-mediated toxicity (McConoughey et al. 2010). Inflammation is a component of neurodegenerative diseases including HD and mediators such as TNFα may play a critical role in upregulating TG2 expression locally. Cytokine-mediated TG2 induction in astrocytes has been shown for acute spinal cord injury (Monsonego et al. 1998) and MS lesions (van Strien et al. 2011). It has also become clear that there is significant complexity in the regulation of TG activity in the CNS. Two TG2 variants in addition to the full-length protein have been described in brain (Monsonego et al. 1998; Citron et al. 2002; Antonyak et al. 2006; Tee et al. 2010). These result from alternative splicing, giving rise to truncated proteins essentially lacking either β-barrel 2 or both β-barrel domains and having unique short *C*-terminal sequences. Expression of these variants causes distinct changes in regulation of cell differentiation and survival as a consequence of differences in GTP binding of the variant proteins (Antonyak et al. 2006; Tee et al. 2010). Although the major contribution to TG activity in the CNS, and cerebral cortex in particular, has been ascribed to TG2 (Bailey and Johnson 2004), γ-glutamyl-ε-lysine crosslinks are formed in TG2−/− brain (Mastroberardino et al. 2002). Abundant expression of at least two other TG isozymes, TG1 and TG3, in the CNS has been shown (Kim et al. 1999), but the functional importance of this remains to be investigated. Here we characterize the hitherto uncharacterized TGM6 gene product and discuss it in the wider context of CNS development.

Materials and methods

Detailed descriptions of experimental procedures are given in "Supplemental Material".

Cell culture

H69 cells (American Type Culture Collection) were maintained as floating cell aggregates at a density of 6–30 $\times$ 10^4 cells/ml in RPMI 1640 medium supplemented with 10% heat-inactivated foetal calf serum (FCS) containing 100 units/ml penicilin and 100 µg/ml streptomycin. HEK293-EBNA cells were grown in DMEM:Ham's F-12 medium (1:1) supplemented with 10% FCS, 250 µg/ml G418 (Invitrogen) and antibiotics. Neuro 2a cells (European Collection of Cell Cultures) were maintained in high-glucose DMEM supplemented with 10% FCS and antibiotics. For differentiation, cells were seeded at 5,000 cells/cm^2 in 24-well plates and stimulated for 3 days by reducing FCS to 0.5% and where indicated, adding 50 ng/ml NGF (Millipore), 1 mM dibutyryl cAMP (Sigma), or 10 µM retinoic acid (Sigma).

Cloning of human TG6

Overlapping fragments (corresponding to nucleotides 71–502, 409–876, 705–1,442, 1,369–1,720 and 1,666–2,292 in AF540969) of TG6 were amplified by RT-PCR from H69 poly(A)$^+$RNA. The 5′-end of the cDNA was isolated by 5′-RACE PCR as described (Grenard et al. 2001) and the transcription initiation site determined by primer extension. A full-length cDNA for TG6 was constructed by subcloning the overlapping fragments as described (Hadjivassiliou et al. 2008). The full-length cDNA encoding TG6-L or TG6-S was subcloned into the pCEP-4 vector for expression in HEK293 EBNA cells (Smyth et al. 2000). Cell strains stably expressing TG6 were generated by transfection with lipofectamine (10 µl for 2 µg plasmid DNA) and selection with puromycin, starting with 0.5 µg/ml puromycin after 48 h and gradually increasing to 10 µg/ml over a 10 day period.

Northern blotting

5 µg of H69 cell poly(A)$^+$RNA was separated in a 1.2% agarose gel, transferred to a nylon membrane and probed with a digoxigenin(DIG)-UTP-labelled single-stranded RNA probe corresponding to nucleotides 1,484–2,212 (AF540969) of TG6.

Analysis of TG expression in mouse brain and cloning of mouse TG6

For cloning of mouse TG6, we prepared cDNA from BALB/c brain and used a series of gene-specific

oligonucleotides modelled from the human TG6 sequence to isolate overlapping DNA fragments by PCR. The 5′-end of the sequence was determined using 5′-RACE PCR and yielded besides the full-length mTG6 sequence a transcript with an alternative exon 1 (AY177607). Real-time PCR to quantify TG6 mRNA expression was carried out on an ABI 7700 Sequence Detection System using the 5′ nuclease assay with primers 5′-CAGCAGTGGTAGGAGTGAC AG (300 nM) and 5′-CTCTTGGAAGGGGTTATGTTG (600 nM) and labelled (5′ 6-carboxyfluorescein and 3′ 6-carboxytetramethylrhodamine) probe 5′-CAAGGACAG CTAAGTATTGAGGTGCCCAG. Reaction conditions were as previously described except using 4 mM $MgCl_2$ (Stephens et al. 2004).

Molecular modelling

A three-dimensional model of human TG6 was generated using ProMod II (version 3.70 SP3; Arnold et al. 2006) with the X-ray derived coordinates of human TG3 in its activated form (Protein Data Bank code 1L9N, chain A; Ahvazi et al. 2002) and the GDP-bound form of TG2 (1KV3, chain C; Liu et al. 2002) as a template resulting in final total energies of −32,300 and −17,400 kJ/mol, respectively, after optimizing the alignment manually.

ELISA style transamidation assay

TG activity was determined by measurement of the incorporation of biotin-x-cadaverine (Molecular Probes) into *N,N*-dimethylcasein immobilized on the surface of protein binding 96-well plates essentially as described (Kleman et al. 1995).

Real-time fluorescence assay for determination of TG isopeptidase activity

The effect of nucleotides on TG activity [human TG6 (T021; Zedira) or TG2] was quantified by measuring changes in fluorescence intensity over time at 37°C as a result of cleavage of Abz-APE(γ-cad-Dnp)QEA (A102; Zedira) in the presence of different concentrations of GTP, GTPγS, GDP, GMP and ATP (Sigma). Fluorescence in the absence of enzyme activation (no Ca^{2+}) was subtracted and reaction rates derived by linear regression. To obtain steady-state kinetics for the replacement reaction, acyl donor substrate concentration was varied from 3.2 to 170 µM. Product concentration was derived from a concentration series of Abz-APQQEA. The kinetic parameters v_{max} and K_M were obtained through nonlinear regression $[v = (v_{max} \ S)/(K_M + S)]$ and k_{cat} calculated using $k_{cat} = v_{max}/E_0$. All experiments were performed at least twice independently.

In situ hybridization and immunolabelling of mouse tissue

Sagittal sections of adult BALB/c mouse brain or mouse embryos at different stages of gestation (E9–E16 and P0) were hybridized to DIG-labelled 325 bp sense and antisense RNA probes corresponding to the transcript region encoding the TG6 β-barrels. Binding of the probes was detected using alkaline phosphatase-conjugated anti-DIG antibodies and visualized with NBT/BCIP. Polyclonal antibodies to TG6 were raised in goat against a peptide comprising residues 482–492 of mouse TG6 conjugated to hemocyanin (Hadjivassiliou et al. 2008) and affinity purified over a thiol Sepharose column bearing disulphide-linked peptide CGWRDDLLEPVTKPS as described (Aeschlimann and Paulsson 1991). The sequence of this loop connecting the catalytic core and β-barrel 1 domain is shared among all TG6 splice variants but highly divergent between different TGs. The absence of cross-reactivity with other TG isozymes was established (Hadjivassiliou et al. 2008). Immunolabelling for TG6 (1 µg/ml) and β-tubulin III (Sigma T3952, 1:50 diluted) was performed as previously described using HRP-conjugated secondary antibodies and AEC (3-amino-9-ethyl carbazole) as a substrate (Aeschlimann et al. 1993).

Isolation and differentiation of cortical progenitor cells

Cerebral cortex of newborn Balb/c mice was dissected on ice in Hanks' balanced salt solution (HBSS) and digested for 20 min at 37°C in 0.1% trypsin, 0.05% DNAse I (Sigma) in HBSS. The tissue was washed and subsequently triturated in HBSS/DNAse I solution to dissociate cells. Cells were washed and subsequently maintained in DMEM/F12 containing 2% B27 supplement (Invitrogen). Number of vital cells was determined by trypan blue exclusion. For FACS analysis, cells were washed in 0.5% BSA in phosphate-buffered saline, pH 7.4 (PBS), filtered through 40 µm Falcon cell strainers (Becton–Dickinson) to remove remaining aggregates, fixed in 2% paraformaldehyde in PBS for 20 min on ice, permeabilized and stained with antibodies to TG6 (20 µg/ml) and cell lineage markers, glial fibrillary acidic protein (G-A-5, Sigma; 15 µg/ml), β-tubulin III (SDL.3D10, Sigma; 20 µg/ml) and RIP (Chemicon, 1:1,000 diluted). For culture (formation of neurospheres), medium was supplemented with 20 ng/ml FGF2 (R&D Systems), 20 ng/ml EGF (Sigma) and antibiotics and 1×10^6 cells seeded into 35 mm hydrophobic plastic dishes. For immunocytochemistry, cells were seeded at a density of 1×10^5 cells/well in a 12-well plate on laminin-111 coated [purified from EHS tumour (Aeschlimann and Paulsson 1991)] cover slips and grown for 5 days. Cells were fixed in 4% paraformaldehyde,

permeabilized and labelled with antibodies to TG6 and cell lineage markers.

Protein analysis

Protein concentrations were determined using the bicinchoninic acid reagent (Pierce) as described by the supplier with BSA as a standard. For immunoblotting, proteins were separated on 4–20% SDS–PAGE Tris–glycine gels under reducing conditions (1% 2-mercaptoethanol), transferred onto nitrocellulose membranes and stained with antibodies as described (Aeschlimann et al. 1993).

Results and discussion

TG6 cloning and primary structure

We have previously identified a cluster of TG genes in the human and mouse genome that contained a novel gene now termed TGM6 (Grenard et al. 2001). We used RT-PCR to screen different human cell lines for expression of the respective gene product. TG6 (previously called TG_Y) could not be detected in cells of a wide variety of origins including mesenchymal, epithelial and hematopoietic cells suggesting that it has a restricted expression pattern, but its expression could be verified in a lung small cell carcinoma cell line, H69, both by RT-PCR and Northern blotting (Fig. 1a).

A full-length cDNA sequence for TG6 was obtained by PCR using oligo(dT) primed cDNA from H69 cells and a series of sequence specific primers based on the presumed transcribed genomic sequence (Supplemental Fig. 1). 5′-RACE PCR was used to identify the position of exon 1 which contains essentially non-coding sequence and therefore shows no apparent similarity between different TG genes. Primer extension was used to identify the 5′-end of the cDNA and this located the major transcription initiation site 455 nt upstream of the translation start codon (Supplemental Fig. 2). The likely 3′-end of the TG6 transcript may be inferred from an EST sequence in GenBank™ (AA961594). Based on this, a polyadenylation signal (ATAAA) could be located 3,887 nt downstream of the termination codon. This is preceded by a CFI_m-binding site (TGTAA) and followed by a GT-rich sequence known to bind CstF and therefore conforms to the tripartite element required for efficient 3′ RNA processing (Venkataraman et al. 2005). The estimated size of the mRNA is therefore 6,480–6,490 nt which is in good agreement with the 6.3 kb transcript detected by Northern blotting (Fig. 1a). A prominent band at ~2.2 kb could indicate that a short transcript may also be abundant but the exact nature of that remains to be investigated. The obtained sequence for full-length human TG6 contained an open reading frame of 2,120 nt. The deduced protein consists of 706 amino acids and has a calculated molecular mass of 79,276 Da. This mass is in good agreement with the size of the single protein band detected by Western blotting of keratinocyte protein extract (natively expressed protein) or when overexpressed in HEK293 cells after transfection with a TG6 expression construct (Fig. 1d). Recombinant enzyme displayed Ca^{2+}-dependent transamidation activity (Fig. 1e).

A shorter transcript which apparently resulted from alternative splicing of the sequence encoded by exon 12 was also isolated from H69 cells (Fig. 1b). The absence of exon 12 results in a frame shift and thereby in premature termination within exon 13 (Supplemental Fig. 3). The sequence for the short form of TG6 (TG6-S) encoded a protein consisting of 625 amino acids (M_r 70,480, calculated). The TG6-S sequence terminates just after the first *C*-terminal β-barrel domain and has a unique 14 amino acid *C*-terminus (Fig. 1c). Overexpression in HEK293 cells gives rise to a stable protein of expected size (Fig. 1d) suggesting that this alternative splicing event may have biological significance. The β-barrel domains have been implicated in the regulation of enzyme-substrate interaction and may also be involved in intracellular signalling as a sequence within the second β-barrel domain of TG2 is required for binding of PLCδ1 (Hwang et al. 1995).

The H69 cell line displays neuronal characteristics including expression of neuron-specific enolase, brain isozyme of creatine kinase and L-dopa decarboxylase. We therefore reasoned that TG6 may be expressed in neurons. RT-PCR confirmed TG6 expression in mouse brain (see below). The cDNA sequence for mouse TG6 was isolated from brain, essentially using the same approach as for human (Supplemental Fig. 1). We have not determined the transcription initiation site. However, an EST sequence in GenBank™ (BY357397) derives from the genomic sequence upstream of the sequence we have isolated by RACE PCR indicating that transcription may be initiated at a position 389 nt upstream of the start codon, a position similar to that in the human gene in the aligned sequences. Two consecutive polyadenylation signals are present 1,096 nt downstream of the termination codon (Supplemental Fig. 1). Mouse and human TG6 have an 85% identity on the amino acid level.

Cloning identified two splice variants in mouse brain lacking either exon 3 or exon 3 together with exon 4 (Fig. 1c). Alternative splicing of exon 3 has been described by us and others for several TG genes including TG2, TG4, TG5 and band 4.2 protein and results in a TG with an altered *N*-terminal β-sandwich domain (Cohen et al. 1993; Aeschlimann et al. 1998; Candi et al. 2001; Cho et al. 2010; AK295775 in GenBank™). TG5 lacking exon 3 has

no transamidase activity (Candi et al. 2001). Omission of exon 3 and 4 results in a frame shift and premature termination before the sequence encoding the catalytic core domain, giving rise to a hypothetical 66 amino acid polypeptide without TG activity.

We could not detect alternative splicing of exon 12 in mouse brain or neuroblastoma cells. An identical sequence to H69 cell TG6-S was recently isolated from another cancer cell suggesting that this splice variant may be associated with oncogenic transformation. Four distinct *C*-terminally truncated versions of TG2 have been identified. Variants resulting from retention of intron 10 and 6, respectively, have been isolated from human disease states (Fraij et al. 1992; Citron et al. 2002). The former, TG2-S, results in a protein truncated within the sequence encoding β-barrel 1. Another TG2 short form resulting from splicing at an alternative 3′ site within exon 12 and 5′ acceptor site within exon 13 retains β-barrel 1 but has a distinct short *C*-terminal sequence (Monsonego et al. 1998; Citron et al. 2002). This variant was originally identified in rat astrocytes, but similar variants, TG2-V1 and TG2-V2, resulting from use of two alternative 5′ acceptor sites within exon 13 have subsequently been demonstrated in different human primary cells (Lai et al. 2007). However, in mouse brain no alternatively spliced variants of TG2 could be identified (Citron et al. 2005). Alternative splicing of exon 11 in human TG5 gives rise to a variant truncated within β-barrel 1 analogous to TG2-S (Candi et al. 2001). *C*-terminal truncation affects allosteric regulation of TG2 by GTP and has profound effects on cell differentiation and survival (Monsonego et al. 1998; Antonyak et al. 2006; Tee et al. 2010).

TG6 is a very low abundant transcript as indicated from directly analysing expression in specific cells and tissues as well as from whole genome expression profile studies. For mouse, the GenBank™ database contains a total of 21 independent ESTs. 18 of these are derived from skin and 1 each from retina and brain cortex. EST BB612839 is the splice variant lacking exon 3 and 4. For man, there is only a single EST from a lung small cell carcinoma. As a comparison, for TG2 the UniGene™ EST profile lists over 29,000 ESTs in normal human tissues alone.

TG6 origin in evolution

Alignment of TG sequences selected to represent major branches of animal evolution (Fig. 1f) indicates that the invertebrate and low chordata proteins are most closely related to the vertebrate isoforms TG4 and TG1. The factor XIII a-subunit derives from the same branch as TG1. The band 4.2 proteins show large divergence between species indicating low evolutionary pressure for conservation. In contrast to the mammalian and amphibian sequences, the three reported avian band 4.2 sequences do contain the catalytic triad residues indicating that these proteins may function as active enzyme. Within the vertebrate TGs, the enzymatically inactive band 4.2 protein and TG2 form separate branches. The TG5/TG7 and TG3/TG6 pairs, each encoded by genes located closely together on the same chromosomes, are most closely related. A closer inspection reveals that the frog sequences marked xTG5 and xTG6 in Fig. 1f have ambivalent characteristics, and depending on the settings of alignment parameters could be also regarded as xTG7 and xTG3, respectively. Similarly, two bird sequences are predicted, which share characteristics of the TG5 and TG7 families. These data suggest that TG5/TG7 and TG3/TG6 arose from tandem gene duplication. We have previously proposed that two genome duplications in

Fig. 1 Analysis of human TGM6 gene products. **a** Size of transcripts expressed in H69 cells. Northern blot containing 5 μg of poly(A^+) RNA from H69 cells that was probed with a 0.7 kb antisense RNA corresponding to the two *C*-terminal β-barrel domains of TG6. The migration position of RNA size markers is indicated on the right and the full-length TG6 transcript with an *arrow*. **b** RT-PCR analysis identified two transcripts in H69 cells. PCR products spanning the relevant region of the transcript (*left*) were separated in a 1% agarose gel calibrated with the 1-kb ladder (*right*). These were identified by sequencing to result from alternative splicing of exon 12 (Supplemental Fig. 3). **c** Schematic illustrating the relationship between gene organization and protein structure in the TG family. TG4 contains an additional exon, exon 1B, within intron 1 (Cho et al. 2010) that can differentially be spliced in and encodes 45 amino acids. The band 4.2L variant contains an extended exon 1 (*hatched box*) (Sung et al. 1992). Variability in the 5′ UTR has been reported in several TGM genes but does not alter the sequence of the protein encoded. Polyadenylated transcripts for TG6 isolated from H69 cells (hTG6) and mouse brain (mTG6) are shown underneath: *L* denotes full-length TG6, S TG6 lacking exon 12, d3 TG6 lacking exon 3 and d3,4 TG6 lacking exon 3 and 4. **d** Detection of TG6 in extracts of human keratinocytes (*lane 1*) or HEK293 cells transfected with hTG6-L (*lane 2*) or hTG6-S (*lane 3*) expression constructs by Western blotting. 10 μg extracted protein was separated by SDS–PAGE under reducing conditions, transferred to nitrocellulose membranes and labelled with antibodies to TG6. M_r standards are indicated on the left. Keratinocytes express TG6-L but not TG6-S indicating that alternative splicing is cell-type dependent. **e** Transamidation activity of recombinant hTG6-L. The time-course for the incorporation of biotin-x-cadaverine into *N,N*-dimethylcasein with different concentrations of TG6 or TG2 was determined. Activity was Ca^{2+}-dependent and maximal at $[Ca^{2+}] > 1$ mM (data for TG6 shown in insert). The data are shown as mean ± SD. **f** Protein sequence relationship of TGs. The dendrogram is based on a multiple sequence alignment of TGs including coagulation factor XIII a-subunit (F13A) and eryhtrocyte protein band 4.2 (EB42) from various species (*c* chicken, *h* human, *m* mouse, *x* frog, *Xenopus tropicalis*, *z* zebra fish, *Danio rerio*, *dr* fruit fly, *Drosophila melanogaster*, *hb* honey bee, *Apis mellifera*, *hc* horseshoe crab, *Tachypleus tridentatus*, *gh* grass hopper, *Schistocerca americana*, *hy* hydra, *Hydra magnipapillata*, *pw* pork worm, *Trichinella spiralis*, *py Physarum polycephalum*, *sa* sea anemonae, *Nematostella vectensis*, *sf* starfish, *Asterina pectinifera*, *ss* sea squirt, *Ciona intestinalis*). The TG6 branches adjacent to TG3 are highlighted by an *arrow*. All sequences except for the human, mouse and frog band 4.2 protein contain the Cys, His and Asp residues of the catalytic triad

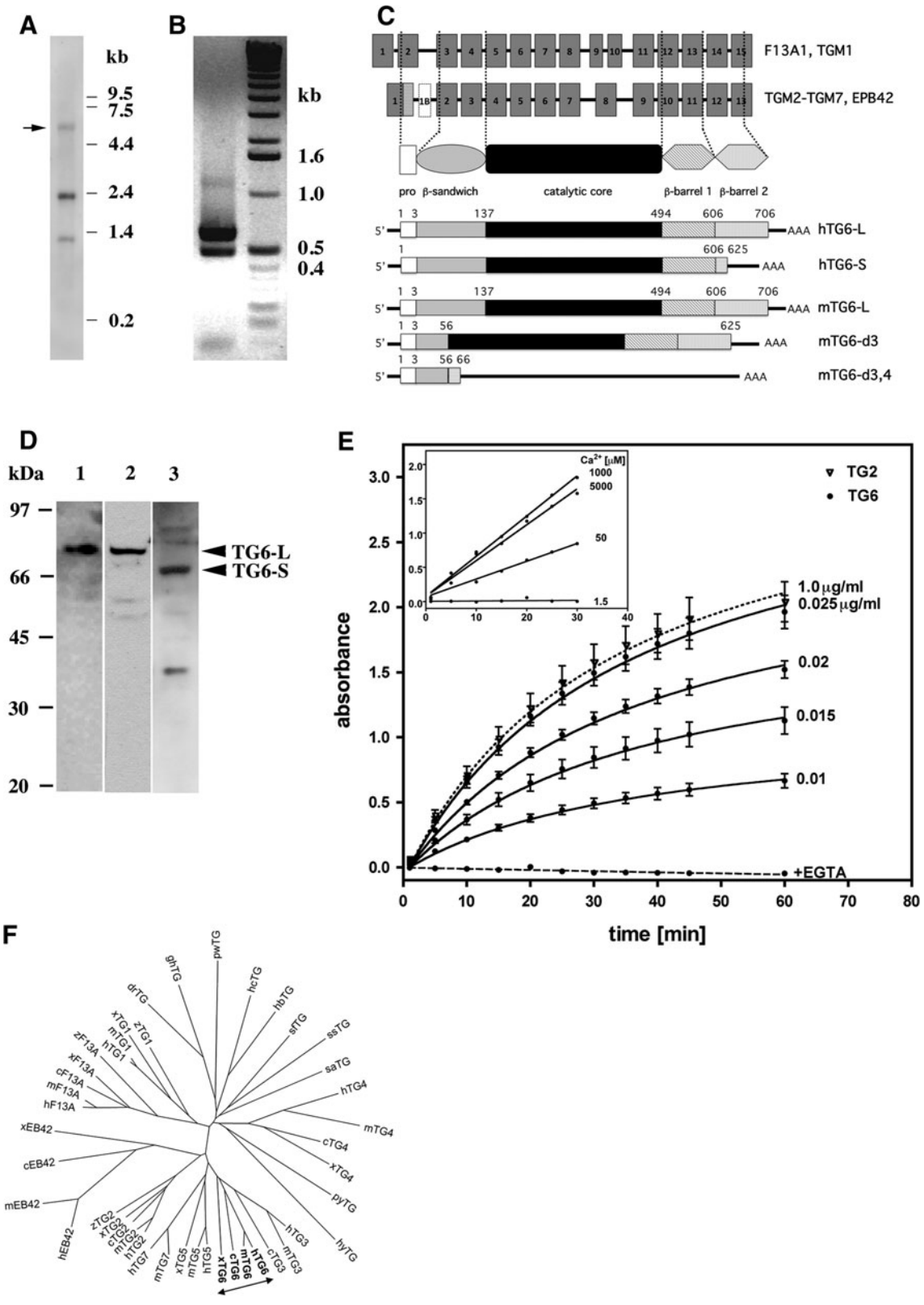

early vertebrates may have given rise to ancestral TGM1, F13A1, TGMn and TGM4 genes and the 'TGMn' branch subsequently further specified through tandem duplication to form the full complement of TG genes in mammals (TG2/3/5-7/EPB42; Grenard et al. 2001). The observation of four principle TG branches for the higher chordata is

consistent with the hypothesis of at least one whole genome duplication occurring after the urochordate ascidian *Ciona intestinalis*, as it has been proposed based on genome comparisons of ancestral vertebrates (Dehal and Boore 2005). More than one TG genes are also present in some protostome genomes. However, these appear to have arisen from gene duplication during prototsome speciation independent from evolution of the TGM genes found in vertebrates.

TG6 architecture predicted by molecular modelling

Based on the high sequence similarity between TG6 and TG3 (overall sequence identity: 50 with 59% within the catalytic core domain), we used the high-resolution X-ray derived human TG3 structure (activated form with three bound calcium ions) as a template for generating a model of human TG6-L (Fig. 2a). The flexible solvent exposed loop, which is not resolved in the X-ray structure connects the last α-helical region of the catalytic core to the first β-strand of the β-barrel 1 domain. The active site catalytic triad residues C274, H333 and D356 are at the base of a cavity, which is bound by the catalytic core and β-barrel 1 domains, and buried in a hydrophobic pocket, as in the case of TG3 (Fig. 2b). Consistent with biochemical data and the interpretation of the TG3 structure (Folk and Chung 1973; Ahvazi et al. 2002; Ahvazi and Steinert 2003), it can be assumed that the sulfhydryl group of C274 can form a thiolate-imidazolium ion pair with H333. The second nitrogen atom of the H333 ring is in hydrogen-bonding distance to the side chain oxygen atom of D356. The indole rings of the two tryptophan residues W238 and W330 are buried near the surface as in TG3 (W236, W327). It has been proposed that as a suitable glutamyl substrate approaches, an oxyanion intermediate forms with the former tryptophan, which results in break-down of the substrate to release NH_3 and forms a thiol-acyl intermediate with the enzyme. This intermediate is attacked by the ε-amine of a lysyl substrate to form another tetrahedral oxyanion intermediate with the latter tryptophan resulting in a cross-linked product (Pedersen et al. 1994). As in the TG3 structure, the corresponding hydroxyl oxygen of Y538 from the β-barrel 1 domain is within hydrogen-bonding distance of C274 and W238 and is located in the loop of the sequence motif I536–T539 that obstructs the entrance to the active site. The pair of serine residue S469↓S470 in TG3, which serve as cleavage site for proteolytic activation by cathepsin L (Cheng et al. 2006), is not found in TG6 though cleavage by another enzyme cannot be ruled out. However, TG6 has a high specific activity in the absence of proteolytic processing (Fig. 1d). A redox-sensitive Cys switch that is involved in oxidative inactivation of TG2 through formation of a vicinal disulfide bond (Cys370–Cys371) (Stamnaes et al. 2010a) is not replicated in TG6 in the same form as Cys230 is replaced by a serine residue. Nevertheless, TG6 is profoundly sensitive to oxidative inactivation.

Regulation of TG6 by co-factors

It is well established that transamidation activity of TGs requires binding of calcium ions (Folk and Chung 1973). As expected, activation of TG6 requires Ca^{2+}-binding and TG6 was found to display a similar concentration-dependence for activation as TG2 (Fig. 1e). In the case of factor XIII a, the activated enzyme contains a single calcium ion in a position near to the catalytic site (Fox et al. 1999) though its binding does not markedly alter the structure. For the zymogen form of TG3, a single tightly bound calcium ion has been found, but two further ions are bound upon proteolytic activation (Ahvazi et al. 2002). In our model of TG6, the highest affinity binding site 1 observed for TG3 is well conserved bringing the main chain carbonyl oxygen atoms of A223, N226, N228 and the side chain oxygens of N226, and D230 into coordinating distance of the TG3 inferred calcium ion position (Fig. 2c). A second calcium-binding site can be inferred to be formed by residues close to the *C*-terminal end of the catalytic core domain adjacent to the loop which joins the β-barrel 1 domain. The main chain oxygen atom of T417, and side-chain oxygens of N396, E445 and E450 are in a position to coordinate a calcium ion. In the case of TG3, calcium access to the related site in the zymogen form is hampered by the flexible loop (residues 462–471), which must be cleaved to allow entry. We do not yet know whether such a cleavage occurs in the case of TG6, though it could be speculated that the 11 residues longer loop might be more flexible to allow entry to this site, and this is supported by the high specific activity of the intact TG6 (Fig. 1e). A third calcium-binding site reported for activated TG3 is found adjacent to the catalytic triad histidine residue within a loop the position of which is shifted upon activation. The residues involved in calcium coordination are all conserved within the TG6 sequence and structural modelling suggests a corresponding orientation with the main chain carbonyl of S309 and side chain oxygen atoms of D303, D305, D327 and N307 as putative calcium acceptor sites.

It has been shown for TG2 (Achyuthan and Greenberg 1987; Im et al. 1990), TG3 (Boeshans et al. 2007) and TG5 (Candi et al. 2004) that enzymatic activity is inhibited by purine nucleotides. Ca^{2+}-binding and nucleotide binding occur at different sites and stabilize distinct conformations of TGs. The affinity of GTP is substantially reduced in the presence of extracellular Ca^{2+} concentrations allowing enzyme activation. In contrast to ATP, the affinity for GTP

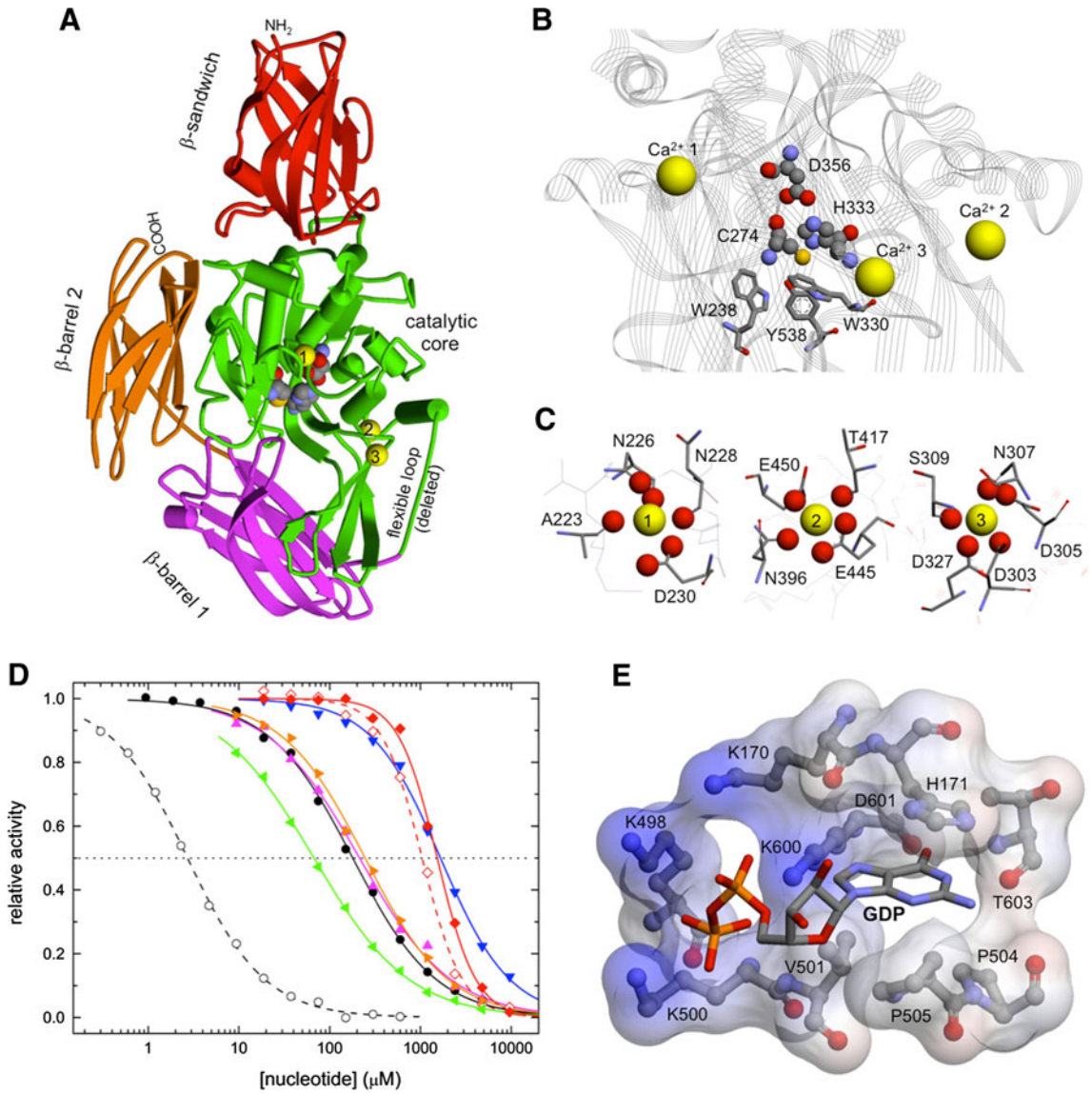

Fig. 2 Model of the structure of human TG6-L and its interaction with nucleotides. **a** The overall structure as modelled based on the calcium activated TG3 form is shown. *Cylinders* and *arrows* denote α-helical and *β*-strand conformations, respectively. The four domains (*β* sandwich, residues 3–136; catalytic core, res. 137–462; *β*-barrel 1, res. 494–605; *β*-barrel 2, res. 606–706) are depicted in different *colours*. The position of the three bound calcium ions of TG3 is shown by numbered *yellow spheres*. The residues of the catalytic triad are depicted in space-filling style. The flexible loop (res. 463–492) connecting the catalytic core with the *β*-barrel 1 domain has been deleted as the corresponding part is not resolved in the TG3 X-ray structure. **b** The residues of the catalytic triad and the adjacent tryptophan and tyrosine residues, the positions of which are proposed to be modulated by calcium (*yellow spheres*) binding, are shown as ball-and-stick and stick models, respectively. The side chain oxygen of Y538 is in hydrogen-bonding distance to the sulphur atom of C274. **c** Oxygen atoms of TG6 residues, which are within 3.5 Å distance of the calcium ion sites of the TG3 template, are shown as *red spheres*. Further calcium coordination could arise from water molecules not included in the modelling. **d** Transamidation activity (measured as isopeptide replacement activity) of TG6 (*closed symbols; solid lines*) and TG2 (*open symbols, dashed lines*) was measured in the presence of various concentrations of nucleotides, and half-maximum activity is indicated by a *dotted line*: GTP, *black*; GTP in the presence of 1 mM Mg^{2+}, *orange*; GTPγS, *green*; GDP, *magenta*; GMP, *blue*; and ATP, *red*. *Symbols* indicate representative values of duplicate independent measurements. **e** The putative nucleotide-binding pocket was inferred from the GDP-bound TG2 structure. A semitransparent surface showing the electrostatic potential (*blue* positive, *red* negative) is overlaid over the residues surrounding a GDP molecule

and Mg-GTP is high and therefore of biological significance. Besides inhibiting transamidation activity intracellularly, independent functions of GTP binding and hydrolysis in intracellular signalling have been proposed for TG2 (Im et al. 1990; Stephens et al. 2004; Iismaa et al. 2009).

We therefore determined the transamidation activity of TG6 in the presence of various nucleotides (Fig. 2d) using a quenched fluorescent substrate, Abz-APE(γ-cad-Dnp)QEA, for real-time monitoring as suggested by Lorand and co-workers (Parameswaran et al. 1997). Folk's work has shown that the reaction occurs in a two-step mechanism whereby the active site thiol is transiently acylated by the γ-carboxamide group of the peptide-bound glutamine to form a stable acyl-enzyme intermediate. The second step involves either hydrolysis to convert Q to E or aminolysis by reaction with a primary amine to form the isopeptide bond and this is rate-limiting (Folk and Chung 1973). This reaction is reversible and steady-state kinetics can be performed by coupling isopeptide hydrolysis to a second reaction driven by an excess amine donor substrate. Given that the reactive nucleophilic form of the substrate is the neutral amine, maximum substrate conversion is achieved with amines deprotonated at physiological pH such as glycinemethylester or ethylene diamine (pKa < 7) (Leblanc et al. 2001). The sequence of the fluorescent substrate is based on the amine acceptor site of osteonectin/BM-40/SPARC for TG2 (Hohenadl et al. 1995). Nevertheless, the kinetic parameters given in Table 1 show that this peptide is a better substrate for TG6 than for TG2. When compared with TG2, a $\sim$50-fold higher concentration of GTP (200 μM) is required for half-maximal inhibition of TG6, whereas for ATP ($\sim$1 mM) similarly high concentrations are needed. The non-hydrolyzable GTP analogue GTPγS is a more effective inhibitor than GTP as has been reported for TG2 (Achyuthan and Greenberg 1987). Activity of TG6 is inhibited to a similar degree by GTP and GDP both in the absence and presence of 1 mM Mg^{2+}, but the affinity for GMP is low. Taken together, these data suggest that TG6 has the potential to function as a guanine nucleotide exchange factor in receptor signalling similar to TG2.

Based on the GDP-bound form of human TG2 (PDB code 1KV3, chain C, Liu et al. 2002), we modelled a putative corresponding nucleotide-binding pocket between the catalytic and β-barrel 1 domains (Fig. 2e). Such a TG6 GDP-binding site would be delineated by residues K170 and H171 from the catalytic domain, and K498 to P505 as well as K600 to E605 from the β-barrel 1 domain. The ε-amino groups of lysine residues 170, 498, 500 and 600 envelop the phosphate groups of GDP, whereas V501–P505 and L604 surround the guanine group which is stacked by the imidazole ring of H171. In TG2, R478 and R580 form two ion pairs with the GDP α- and β-phosphates. These residues are replaced by K500 and K600 in TG6. S482 and Y583 of TG2, which form hydrogen bonds with the N1 and N2 atoms of the guanine base are replaced by P505 and T603, respectively, in TG6 of which the main chain oxygen of T603 hydrogen bonds to N1 and N2, and its oxygen to O6. Although the fold around a putative GDP molecule can be well adopted by TG6, the reduced number of interactions could be the cause for the observed decrease in nucleotide affinity (Fig. 2d).

Fig. 3 TG6 expression in mouse development. **a** Amplification of TGs from mouse whole brain cDNA. Products amplified with primers specific for TG1 (*lane 1*, 182 bp), TG2 (*2*, 177 bp), TG3 (*3*, 157 bp), TG5 (*5*, 135 bp), TG6 (*6*, 171 bp), and TG7 (*7*, 126 bp) could be detected but not TG4 (*lane 4*), factor XIII a-subunit (*lane 8*) and band 4.2 protein (*lane 9*). Products were analysed by electrophoresis in a 1% agarose gel calibrated with the 1-kb ladder. **b** TG6 expression in the developing and mature mouse brain. In situ hybrization was carried out with antisense (*b*) and sense (*c*) DIG-labelled TG6 RNA probes on serial sagittal sections of a newborn mouse or adult mouse brain (*dark brown* labelling with alkaline phosphatase and NBT/BCIP). A section stained with luxol fast *blue*/cresyl *violet a* shows the myelin and nuclei of nerve cells. *C* cortex, *Cer* cerebellum, *ChP* choroid plexus, *Hip* hippocampus, *Mid* mid brain, *St* striatum, *Tha* thalamus. Higher magnification images demonstrate labelling of cells in the cerebral cortex at P0 (*d*) and in mature brain (*e*) through layers II–VI, in Purkinje cells of the cerebellum (*g*) and keratinocytes in the epidermis and forming the hair shaft (*h*). Immunostaining of P0 serial section with antibodies recognizing the hinge region of TG6 confirms protein expression within the cell layers forming the motor cortex (*red brown* labelling with HRP and AEC) (*f*) and cells within grey matter of the spinal cord (FITC) (*i*). *WM* white matter, *GM* grey matter. **c** Sections of mouse embryo at the indicated developmental stages were hybrized with the antisense TG6 RNA probe. Images *a–c* depict a sagittal section through the developing head and images *d–f* a close-up of the telencephalon. A schematic illustrating the development of the cerebral cortex together with hematoxylin/eosin stained sections of the developing cerebral cortex at E11 and E16 is given in g. The cortical plate (*CP*) which will give rise to the multilayered neocortex (layers I–VI) develops between the marginal zone (*MZ*) and subplate (*SP*) which is derived from the preplate (*PP*). Pyramidal neurons within layer V/VI differentiate first and are positive for β-tubulin III by E16. Immunostaining for TG6 labels CP and layers V/VI of neocortex at E16 (*g*) whereas TG6 RNA expression is predominant in CP (*f*). *IZ* intermediate zone, *SVZ* subventricular zone, *VZ* ventricular zone

Substrate specificity

There is a large degree of overlap in glutamine donor substrates of TG6, TG3, and TG2. On the level of fine specificity, however, clear differences exist. In peptides, TG2 has a highly sequence-dependent targeting (Gorman and Folk 1984; Vader et al. 2002; Hitomi et al. 2009), whereas TG6 shows tolerance to a broader spectrum of sequence changes in the neighbouring amino acids (Stamnaes et al. 2010b). The most significant influence on substrate properties is exerted by proline residues. None of the enzymes can modify glutamine residues directly followed by proline (-QP-), whereas proline at position +2 (-QXP-) exerts a positive influence. Furthermore, while all three enzymes readily target -PQ- sequences, proline in position −2 (-PPQ-) has a detrimental effect on recognition by TG2, but not TG6 or TG3. An indication that different positions may have a greater impact on

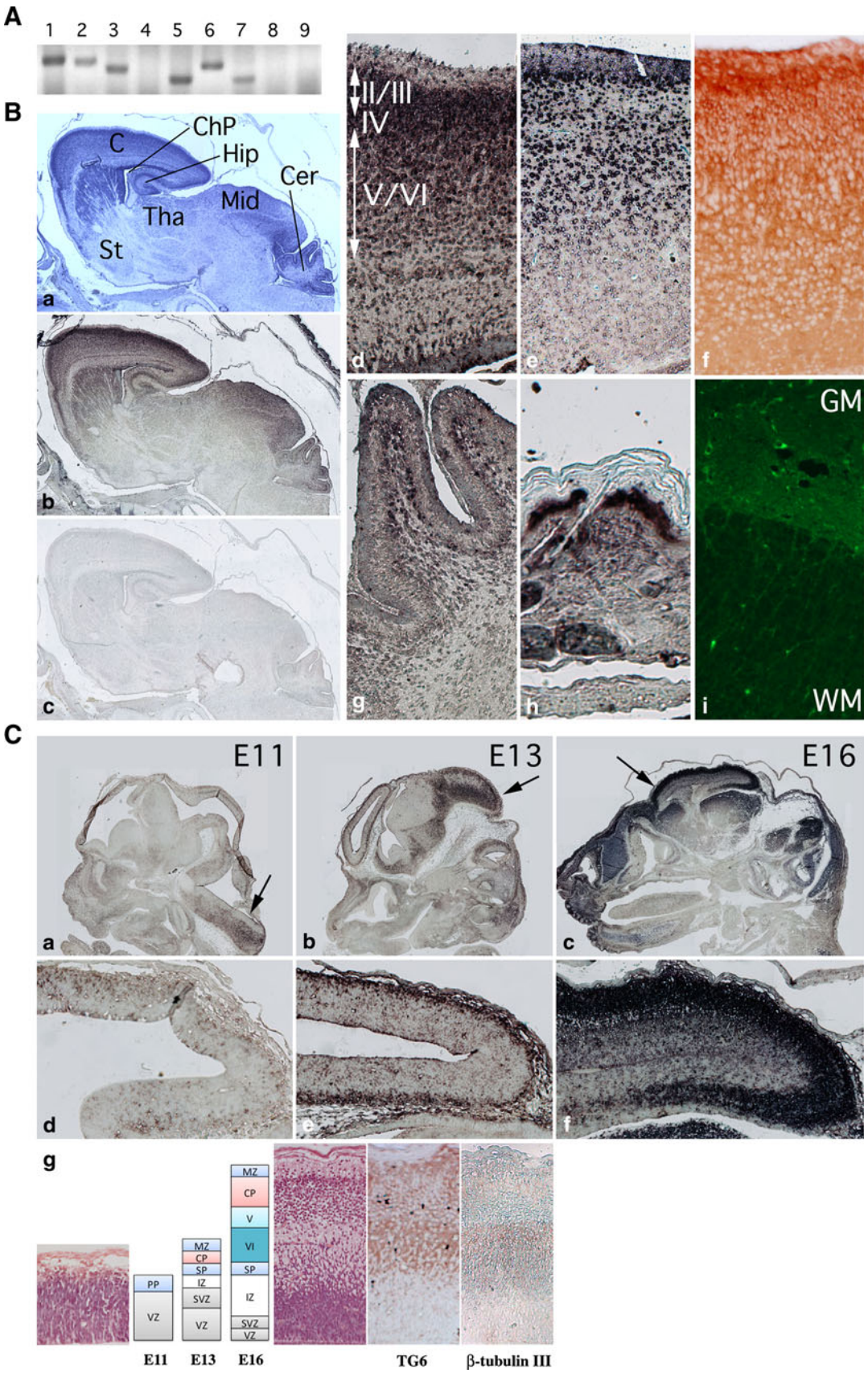
A
1 2 3 4 5 6 7 8 9
B
C
ChP
Hip
Cer
Mid
Tha
St
II/III
IV
V/VI
GM
WM
a
b
c
d
e
f
g
h
i
E11
E13
E16
MZ
CP
SP
IZ
SVZ
VZ
PP
V
VI
E11
E13
E16
TG6
β-tubulin III

Table 1 Kinetic parameters of TG2 and TG6 for the replacement reaction of Abz-APE(γ-cad-Dnp)QEA at 37°C, pH 7.4, in the presence of an excess glycinemethylester

	v_{max} (M/s)	k_{cat} (/s)	K_M (M)	k_{cat}/K_M (/M s)
TG2	$0.83 \pm 0.14 \times 10^{-9}$	$3.2 \pm 0.5 \times 10^{-3}$	$110 \pm 23 \times 10^{-6}$	$0.30 \pm 0.07 \times 10^{2}$
TG6	$2.6 \pm 0.4 \times 10^{-9}$	$10.1 \pm 1.6 \times 10^{-3}$	$49 \pm 12 \times 10^{-6}$	$2.1 \pm 0.6 \times 10^{2}$

Calculations were based on a molecular mass of 77 and 79 kDa for TG2 and TG6, respectively. The data are shown as mean ± SD

substrate recognition by the different enzymes comes from the observed differences in relation to altered peptide length *N*- or *C*-terminal to the reactive glutamine residue. TG6 and TG2 are profoundly sensitive to the *C*-terminal sequence, whereas reactivity of TG3 with peptide substrates is primarily influenced by the sequence *N*-terminal to the glutamine residue (Stamnaes et al. 2010b). TG6 can both deamidate (Stamnaes et al. 2010b) and transamidate (Fig. 1d) glutamine residues, but it has not been determined yet for TG6 whether the type of modification that occurs preferentially is influenced by the sequence context as has been demonstrated for TG2 (Boros et al. 2006).

TG6 is associated with neuronal differentiation in the central nervous system

RT-PCR from mouse brain cDNA using specific primers for TG6 and also the other members of the TG family revealed expression of TG1, TG2, TG3, TG5, TG6 and TG7 (Fig. 3a). These results are consistent with demonstration of expression of TG1, TG2, TG3, and TG5 in the brain (Kim et al. 1999; Bailey and Johnson 2004; Bailey et al. 2004) and together with cell biological studies points to a highly complex regulation of TG genes in the CNS. To obtain a clearer understanding of TG6 expression on the cellular level, in situ hybridisation was performed on sagittal newborn mouse sections. An antisense RNA fragment corresponding to the *C*-terminal end of TG6 was used as a probe as this area has the least similarity between the different TGs and a similar human probe gave no cross-hybridisation with other TG gene products in Northern blotting. In situ hybridisation revealed that TG6 expression is widespread in the brain (Fig. 3b), most prominently within the cell layers containing the neuronal cell bodies of the cerebral cortex (particularly layers II–IV containing granular neurons and pyramidal cells) (image d), olfactory lobe (data not shown; see Fig. 3c, image c) and the cerebellum (Purkinje cells) (image g). TG6 expression was detected in the spinal cord (image i) and in the retinal cells of the eye (data not shown). TG6 was expressed in tissues other than the CNS, most prominently in the skin (image h) and other stratified squamous epithelia. Interestingly, these cells derive embryologically from a common ectodermal progenitor. Immunolabelling with antibodies confirmed TG6 protein expression (image f).

Given the prominent expression of TG6 in the CNS in the developed organism, we were interested to identify whether the induction of TG6 expression correlated with any specific events in development. While the CNS is the first organ system to develop and to differentiate, it is also one of the last to be completed. The primary parts of the mouse brain can be identified soon after the neural groove, neural plate and head process stage at E7.5, and by day E14 has the typical anatomical layout of a mammalian brain. The neocortex is a highly organized six-layered structure that contains hundreds of different neuronal cell types and various subsets of glia. Progenitors residing in the ventricular zone produce the neurons of the different neocortical layers in a tightly controlled temporal order between about days E11 and E17.5 (Molyneaux et al. 2007). In situ hybridisation was therefore carried out on stage E11, E13 and E16 embryos (Fig. 3c). The walls of the primitive brain divide into an inner ependymal, an intermediate mantel, and outer marginal layer by E10, whereby the ependymal layer that ultimately forms the lining of the ventricles of the brain is the thickest layer. At E11, active proliferation of neuroblastic cells occurs in the walls of the entire CNS and these begin to occlude some of the neural cavities. Up to E11, the major neuroblastic activity is occurring behind the hindbrain where cranial ganglia V to IX develop. Little TG6 expression can be detected in the brain at E11 while labelling can be seen in the developing spinal cord (Fig. 3c, image a, arrow). By E13, TG6 expression is apparent in several parts of the brain and strong expression can now be detected in regions undergoing neuronal differentiation such as the mesencephalon (image b, arrow). From E13 to 16, the major neuroblastic activity occurs in the telencephalon where cells from the mantle layer migrate into the overlying marginal zone to form the neocortex which will become the outer grey matter of the cerebral hemispheres. At E13, TG6 expression is detected in a thin layer of the neocortex, presumably progenitor cells constituting the preplate (image e). By E16, TG6 is highly expressed in the outer layers of the neocortex (image f). TG6 mRNA expression is most prominent within the area of the cortical plate where neuronal differentiation occurs to form layers II–IV (image

f). TG6 protein is most prominent within layers V/VI where postmitotic neurons can be labelled for β-tubulin III at this stage (image g). Induction of TG6 expression appears to correlate both spatially and temporally with neurogenesis. In contrast, in situ hybridisation with a TG5 antisense RNA probe showed widespread expression throughout the CNS by E11 (data not shown).

Towards the latter stages of corticogenesis, astrocytes differentiate from radial glia. To clarify whether TG6 expression was associated with neurogenesis or astrocyte differentiation, progenitors were isolated from P0 stage mouse cortex and expanded in suspension culture as neurospheres (Murayama et al. 2002). To induce neuronal differentiation, progenitors were seeded on a laminin-111 substrate in the absence of mitogen for 5 days and subsequently labelled for TG6 and cell lineage markers. Cells of the neuronal lineage were identified using antibodies against β-tubulin III (Tuj-1), astrocytes with antibodies to glial fibrillary acidic protein (GFAP) and oligodendrocytes with RIP-antibodies (Sergent-Tanguy et al. 2003). Immunocytochemistry confirmed expression of TG6 in neuronal cells and its absence from the astroglial and oligodendroglial lineage (Fig. 4a). To exclude de novo expression of TG6 in neurons as a consequence of culture conditions, freshly isolated cells from the cerebral cortex of newborn mice were double-labelled with antibodies to TG6 and to the above cell lineage markers and analysed by FACS. 81% of cells were positive for TG6 and 58% for β-tubulin III, with 99% of β-tubulin III positive cells also positive for TG6. Physical parameters can be used to distinguish neurons, astrocytes and microglial cells as they differ in size and morphology (Sergent-Tanguy et al. 2003). Therefore, we plotted forward scatter (FSC), representing cell size, as a function of fluorescence intensity for TG6 labelling. Within the broad distribution of cells expressing TG6, two clusters of cells of different size were apparent and were gated (Supplemental Fig. 4, R1 and R2). Further analysis of gated cells for expression of cell lineage markers showed that both clusters were exclusively positive for β-tubulin III indicating that they are derived from the neuronal lineage and represent different neuronal populations (Supplemental Fig. 4).

Neuro2A is a mouse neural crest-derived cell line that has been extensively used to study neuronal differentiation, and specification into different neuronal lineages is possible (Tremblay et al. 2010). We initially confirmed that non-lineage-specific differentiation in low serum induced TG6 expression and subsequently used a number of differentiation factors to induce lineage-specific differentiation (Fig. 4b). Non-cholinergic differentiation with neurotrophin NGF was associated with strong upregulation of TG6. TG6 expression was also induced upon dopaminergic differentiation using dibutyryl cAMP, whereas TG6 was not upregulated in cells treated with retinoic acid, a known inhibitor of dopaminergic differentiation. Quantitative PCR indicated that TG6 expression was upregulated twofold upon serum starvation and fourfold by dibutyryl cAMP. Dopamine neurons are formed in the olfactory lobe and retina during embryonic development, two areas where strong TG6 expression was seen in in situ hybridization (Fig. 3). However, the highest level of TG6 expression in Neuro 2a cells was observed upon induction of cell death by metal ion chelation suggesting that the strong TG6 expression observed during cerebral cortex development may relate in parts to association with programmed cell death rather than neuronal differentiation.

Cerebellar ataxia as consequence of genetic defects in TGM6 gene or acquired autoimmunity to TG6

Celiac disease (CD) is a common T cell-mediated autoimmune disorder characterized by its linkage to specific human lymphocyte antigen alleles, HLA-DQ2 and -DQ8 (Jabri and Sollid 2009). In susceptible individuals, consumption of gluten triggers a $CD4^+$ T-cell response to gliadin as well as a B cell response to gliadin and self antigens. TG2 contributes to disease development in at least two ways: first, by deamidating gluten peptides, thereby increasing their reactivity with HLA-DQ2/DQ8, which potentiates the T-cell response (Molberg et al. 1998; Van de Wal et al. 1998). Second, TG2 is the major autoantigen targeted by the B cell response (Dietrich et al. 1997). Although the T-cell response in the mucosa of the small intestine is the key player in disease development, gluten sensitivity is a systemic disease and autoantibodies may play a role in extraintestinal pathogenesis (Caja et al. 2011). This is supported by the recent demonstration of circulation derived anti-TG3 autoantibodies inducing a dermatitis herpetiformis-like pathology in human skin-grafted SCID mice (Zone et al. 2011). Neurological disorders have also been recognised as a form of extraintestinal manifestation of gluten sensitivity, with cerebellar involvement (gluten ataxia) and peripheral nerve involvement (gluten neuropathy) being the most common presentations (Hadjivassiliou et al. 2010). We have shown that gluten ataxia patients develop autoantibodies that are specific to TG6 (Hadjivassiliou et al. 2008). Furthermore, antibodies isolated from celiac disease patients are frequently reactive with human and mouse neurons. However, this neuronal reactivity is specific for antibodies that are crossreactive between the closely related TG2, TG3 and TG6 enzymes and is not mediated by TG2 as it is preserved in a TG2−/− background (Boscolo et al. 2010). This is consistent with TG2 being primarily associated with the vasculature in non-disease brain (Aeschlimann and

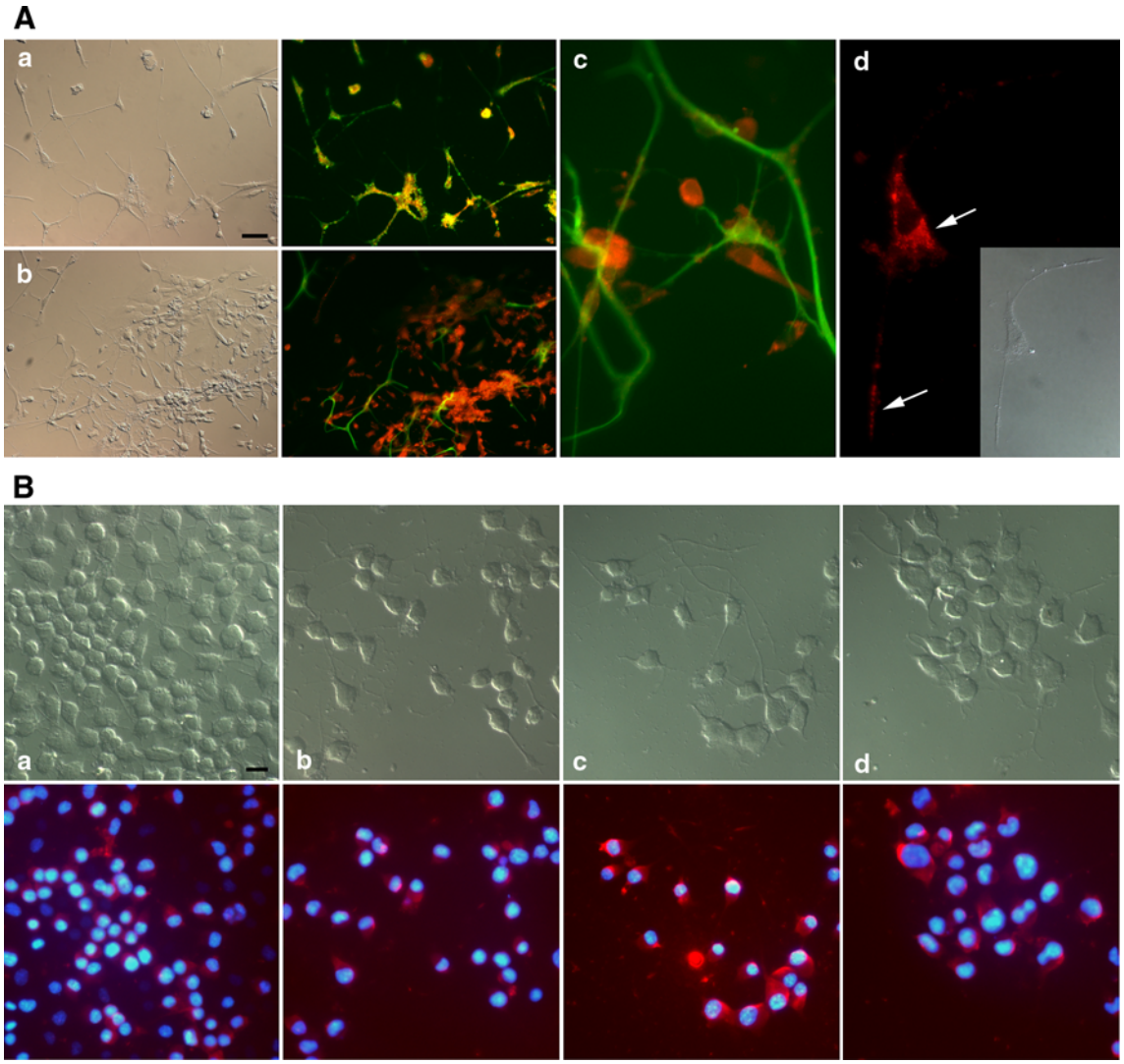

Fig. 4 **a** Confirmation of neurons as the primary source for TG6 expression in the mouse cerebral cortex. Progenitor cells from newborn mouse forebrain were grown as neurospheres and subsequently differentiated by culture in defined medium for 5 days on a laminin-111 substrate and double stained for TG6 (TRITC) and different cell markers (FITC): β-tubulin III isoform for neurons (*a*), GFAP for astrocytes (*b*, *c*). Co-expression of TG6 with β-tubulin III is highlighted by colour mixing (*yellow*, *a*). TG6 shows discrete subcellular distribution in large protein complexes or vesicles surrounding the nucleus and also in neurites (*d*, *arrows*). Left images in *a*, *b* and inset in *d* provide DIC images of the field of view shown under fluorescence illumination. *Size bar* 40 μm (*a*). **b** TG6 expression is upregulated concomitant with differentiation of Neuro 2a mouse neuroblastoma cells. Neuro 2a cells were grown with 10% FCS (*a*) or induced to differentiate by serum starvation (0.5% FCS) (*b*) or serum starvation in combination with NGF (50 ng/ml) (*c*) or dibutyryl cAMP (1 mM) (*d*) stimulation. After 3 days, cells were labelled with antibodies to TG6 (alexa fluor 568, *bottom panels*) and nuclei counterstained with Hoechst 34580. *Upper panels* provide DIC images of the field of view to illustrate changes in cell morphology. *Size bar* 10 μm (*a*)

Paulsson 1991; Hadjivassiliou et al. 2008; Boscolo et al. 2010) and suggests that TG6 may be the neuronal autoantigen recognised in these patients. To test whether patient-derived autoantibodies directly contribute to pathology we attempted passive disease transfer. Serum immunoglobulin from gluten ataxia patients, as well as clonal anti-TG immunoglobulins derived using phage display, caused deficits in motor coordination but not anxiety when injected intraventricularly in mice (Boscolo et al. 2010). The fact that isolated anti-TG immunoglobulins induce dramatic ataxia-like deficits in mice indicates selective neurotoxicity of anti-TG antibodies once exposed to the CNS and suggests that antibodies may play a role in disease transfer to the CNS. However, both scFv crossreactive between different TGs and TG2-specific scFv compromised motor coordination in mice.

Cerebellar ataxias are a complex and heterogeneous group of neurodegenerative diseases characterized by progressive imbalance and limb movement deficits. About 20% of cerebellar ataxias display a familial inheritance pattern. So far, 30 different genetic loci have been linked to different SCA subtypes and 19 causative genes identified. Among those are CAG repeat expansion diseases including SCA1–3, 6–8, 12, 17, 31 and DRPLA and non-repeat mutations such as SCA 5, 11, 13–16, 27 and 28. A recent paper identified mutations in TGM6 in two Chinese families with autosomal dominant ataxia using linkage analysis and exome sequencing (Wang et al. 2010). Taken together with our demonstration of neuronal expression of TG6 and the presence of autoantibodies to TG6 in immune-mediated ataxia, this suggests that TG6 may play an important role in neurons involved in motor control. The mutations identified in TGM6 are single nucleotide exchanges leading to alteration of amino acid residues that are strictly conserved in TG6 among different species (D327G, L517W). Structural modelling suggests that the former substitution could interfere with Ca^{2+} binding at site 3 (Fig. 2c) and may therefore compromise enzyme activation, whereas the deleterious effect of the latter substitution remains obscure. It is also not clear why mutation of a single allele should produce a dominant ataxia phenotype. Haploinsufficiency is possible but one might also speculate that the problem is unrelated to the catalytic function and could be caused by difficulties in folding of mutant proteins and this may ultimately be neurotoxic. It is also interesting to note that alternative splicing or mutations in TG2 that affect its regulation by GTP have been shown to have dramatic effects on neuronal differentiation and to be pro-apoptotic in different cell types (Antonyak et al. 2006; Tee et al. 2010).

In order to gain a better understanding of the TG6-related pathology further work needs to address the physiological function of TG6 in the CNS. Given that TG6 similar to TG2 is a protein that can be detected in the cell cytosol as well as at the cell surface it may have independent intra- and extracellular functions that may employ the enzyme's ability to bind GTP or act as a Ca^{2+}-dependent crosslinking enzyme, respectively. Recent progress in the development of more isozyme-specific inhibitors may facilitate the elucidation of the context within which TG6 is activated and plays a critical role.

Acknowledgments We are grateful to Dr V. Pekarik for advice regarding the culture of primary neuronal progenitor cells. This study was supported by a grant from Coeliac UK and Arthritis Research UK (18461) and PhD studentships from Cardiff University to HT and MA. The nucleotide sequences reported in this paper have been deposited in the GenBank™/EBI Data Bank with the accession numbers AF540969 (full length) and AF540970 (exon 12 splice variant) for human TG6 and AY159126 (full length), AY177606 (exon 3/4 splice variant) and AY177607 (alternative exon 1) for mouse TG6.

References

AbdAlla S, Lother H, el Missiry A, Langer A, Sergeev P, el Faramawy Y, Quitterer U (2009) Angiotensin II AT_2 receptor oligomers mediate G-protein dysfunction in an animal model of Alzheimer disease. J Biol Chem 284:6554–6565

Achyuthan KE, Greenberg CS (1987) Identification of a guanosine triphosphate-binding site on guinea pig liver transglutaminase. J Biol Chem 262:1901–1906

Aeschlimann D, Paulsson M (1991) Cross-linking of laminin-nidogen complexes by tissue transglutaminase. A novel mechanism for basement membrane stabilization. J Biol Chem 266:15308–15317

Aeschlimann D, Paulsson M (1994) Transglutaminases: protein crosslinking enzymes in tissues and body fluids. Thromb Haemost 71:402–415

Aeschlimann D, Thomazy V (2000) Protein crosslinking in assembly and remodelling of extracellular matrices: the role of transglutaminases. Connect Tissue Res 41:1–27

Aeschlimann D, Wetterwald A, Fleisch H, Paulsson M (1993) Expression of tissue transglutaminase in skeletal tissues correlates with events of terminal differentiation of chondrocytes. J Cell Biol 120:1461–1470

Aeschlimann D, Koeller MK, Allen-Hoffman BL, Mosher DF (1998) Isolation of a cDNA encoding a novel member of the transglutaminase gene family from human keratinocytes: detection and identification of transglutaminase gene products based on RT-PCR with degenerate primers. J Biol Chem 273:3452–3460

Ahvazi B, Steinert PM (2003) A model for the reaction mechanism of the transglutaminase 3 enzyme. Exp Mol Med 35:228–242

Ahvazi B, Kim HC, Kee SH, Nemes Z, Steinert PM (2002) Three-dimensional structure of the human transglutaminase 3 enzyme: binding of calcium ions changes structure for activation. EMBO J 21:2055–2067

Ahvazi B, Boeshans KM, Rastinejad F (2004) The emerging structural understanding of transglutaminase 3. J Struct Biol 147:200–207

Andringa G, Lam KY, Chegary M, Wang X, Chase TN, Bennett MC (2004) Tissue transglutaminase catalyzes the formation of alpha-synuclein crosslinks in Parkinson's disease. FASEB J 18:932–934

Antonyak MA, Jansen JM, Miller AM, Ly TK, Endo M, Cerione RA (2006) Two isoforms of tissue transglutaminase mediate opposing cellular fates. Proc Natl Acad Sci USA 103:18609–18614

Arnold K, Bordoli L, Kopp J, Schwede T (2006) The SWISS-MODEL Workspace: a web-based environment for protein structure homology modelling. Bioinformatics 22:195–201

Bailey CD, Johnson GV (2004) Developmental regulation of tissue transglutaminase in the mouse forebrain. J Neurochem 91:1369–1379

Bailey CD, Johnson GV (2005) Tissue transglutaminase contributes to disease progression in the R6/2 Huntington's disease mouse model via aggregate-independent mechanisms. J Neurochem 92:83–92

Bailey CD, Graham RM, Nanda N, Davies PJ, Johnson GV (2004) Validity of mouse models for the study of tissue

transglutaminase in neurodegenerative diseases. Mol Cell Neurosci 25:493–503

Boeshans KM, Mueser TC, Ahvazi B (2007) A three-dimensional model of the human transglutaminase-1: insights into the understanding of lamellar ichthyosis. J Mol Model 13:233–246

Boros S, Ahrman E, Wunderink L, Kamps B, de Jong WW, Boelens WC, Emanuelsson CS (2006) Site-specific transamidation and deamidation of the small heat-shock protein Hsp20 by tissue transglutaminase. Proteins 62:1044–1052

Boscolo S, Lorenzon A, Sblattero D, Florian F, Stebel M, Marzari R, Not T, Aeschlimann D, Ventura A, Hadjivassiliou M, Tongiorgi E (2010) Anti-transglutaminase antibodies cause ataxia in mice. PLOS ONE 5:e9698 (1–9)

Caja S, Mäki M, Kaukinen K, Lindfors K (2011) Antibodies in celiac disease: implications beyond diagnostics. Cell Mol Immunol 8:103–109

Candi EG, Melino G, Mei G, Tarcsa E, Chung SI, Marekov LN, Steinert PM (1995) Biochemical, structural, and transglutaminase substrate properties of human loricrin, the major epidermal cornified cell envelope protein. J Biol Chem 270:26382–26390

Candi E, Oddi S, Terrinoni A, Paradisi A, Ranalli M, Finazzi-Agró A, Melino G (2001) Transglutaminase 5 cross-links loricrin, involucrin, and small proline-rich proteins in vitro. J Biol Chem 276:35014–35023

Candi E, Paradisi A, Terrinoni A, Pietroni V, Oddi S, Cadot B, Jogini V, Meiyappan M, Clardy J, Finazzi-Agro A, Melino G (2004) Transglutaminase 5 is regulated by guanine-adenine nucleotides. Biochem J 381:313–319

Cheng T, Hitomi K, van Vlijmen-Willems IM, de Jongh GJ, Yamamoto K, Nishi K, Watts C, Reinheckel T, Schalkwijk J, Zeeuwen PL (2006) Cystatin M/E is a high affinity inhibitor of cathepsin V and cathepsin L by a reactive site that is distinct from the legumain-binding site. A novel clue for the role of cystatin M/E in epidermal cornification. J Biol Chem 281:15893–15899

Cho SY, Choi K, Jeon JH, Kim CW, Shin DM, Lee JB, Lee SE, Kim CS, Park JS, Jeong EM, Jang GY, Song KY, Kim IG (2010) Differential alternative splicing of human transglutaminase 4 in benign prostate hyperplasia and prostate cancer. Exp Mol Med 42:310–318

Citron BA, SantaCruz KS, Davies PJ, Festoff BW (2002) Intron-exon swapping of transglutaminase mRNA and neuronal Tau aggregation in Alzheimer's disease. J Biol Chem 276:3295–3301

Citron BA, Zoloty JE, Suo Z, Festoff BW (2005) Tissue transglutaminase during mouse central nervous system development: lack of alternative RNA processing and implications for its role(s) in murine models of neurotrauma and neurodegeneration. Brain Res Mol Brain Res 135:122–133

Cohen CM, Dotimas E, Korsgren C (1993) Human erythrocyte membrane protein 4.2 (pallidin). Semin Hematol 30:119–137

Dehal P, Boore J (2005) Two rounds of whole genome duplication in the ancestral vertebrate. PLOS Biol 3:e314

Dietrich W, Ehnis T, Bauer M, Donner P, Volta U, Riecken EO, Schuppan D (1997) Identification of tissue transglutaminase as the autoantigen of celiac disease. Nat Med 3:797–801

Folk JE, Chung SI (1973) Molecular and catalytic properties of transglutaminases. Adv Enzymol 38:109–191

Fox BA, Yee VC, Pedersen LC, Le Trong I, Bishop PD, Stenkamp RE, Teller DC (1999) Identification of the calcium binding site and a novel ytterbium site in blood coagulation factor XIII by x-ray crystallography. J Biol Chem 274:4917–4923

Fraij BM, Birckbichler PJ, Patterson MK Jr, Lee KN, Gonzales RA (1992) A retinoic acid-inducible mRNA from human erythroleukemia cells encodes a novel tissue transglutaminase homologue. J Biol Chem 267:22616–22623

Gorman JJ, Folk JE (1984) Structural features of glutamine substrate for transglutaminases. J Biol Chem 259:9007–9010

Grenard P, Bates MK, Aeschlimann D (2001) Evolution of transglutaminase genes: identification of a gene cluster on human chromosome 15q15. Structure of the genes encoding transglutaminase X and a novel gene family member, transglutaminase Z. J Biol Chem 276:33066–33078

Hadjivassiliou M, Aeschlimann P, Strigun A, Sanders D, Woodroofe N, Aeschlimann D (2008) Autoantibodies in gluten ataxia recognize a novel neuronal transglutaminase. Ann Neurol 64:332–343

Hadjivassiliou M, Sanders DS, Grünewald RA, Woodroofe N, Boscolo S, Aeschlimann D (2010) Gluten sensitivity: from gut to brain. Lancet Neurol 9:318–330

Hitomi K, Kitamura M, Sugimura Y (2009) Preferred substrate sequences for transglutaminase 2: screening using a phage-displayed peptide library. Amino Acids 36:619–624

Hohenadl C, Mann K, Mayer U, Timpl R, Paulsson M, Aeschlimann D (1995) Two adjacent N-terminal glutamines of BM-40 (osteonectin, SPARC) act as amine acceptor sites in transglutaminase C-catalyzed modification. J Biol Chem 270:23415–23420

Hwang KC, Gray CD, Sivasubramanian N, Im MJ (1995) Interaction site of GTP binding Gh (transglutaminase II) with phospholipase C. J Biol Chem 270:27058–27062

Ientile R, Caccamo D, Marciano MC, Currò M, Mannucci C, Campisi A, Calapai G (2004) Transglutaminase activity and transglutaminase mRNA transcripts in gerbil brain ischemia. Neurosci Lett 363:173–177

Iismaa SE, Mearns BM, Lorand L, Graham RM (2009) Transglutaminases and disease: lessons from genetically engineered mouse models and inherited disorders. Physiol Rev 89:991–1023

Im MJ, Riek RP, Graham RM (1990) A novel guanine nucleotide-binding protein coupled to the α1-adrenergic receptor. II. Purification, characterization, and reconstitution. J Biol Chem 265:18952–18960

Jabri B, Sollid LM (2009) Tissue-mediated control of immunopathology in coeliac disease. Nat Rev Immunol 9:858–870

Jeitner TM, Matson WR, Folk JE, Blass JP, Cooper AJ (2008) Increased levels of gamma-glutamylamines in Huntington disease CSF. J Neurochem 106:37–44

Jeitner TM, Muma NA, Battaile KP, Cooper AJ (2009) Transglutaminase activation in neurodegenerative diseases. Future Neurol 4:449–467

Kim SY, Grant P, Lee JH, Pant HC, Steinert PM (1999) Differential expression of multiple transglutaminases in human brain. Increased expression and cross-linking by transglutaminases 1 and 2 in Alzheimer's disease. J Biol Chem 274:30715–30721

Kleman JP, Aeschlimann D, Paulsson M, van der Rest M (1995) Transglutaminase-catalyzed cross-linking of fibrils of collagen V/XI in A204 rhabdomyosarcoma cells. Biochemistry 34:13768–13775

Lai TS, Tucker T, Burke JR, Strittmatter WJ, Greenberg CS (2004) Effect of tissue transglutaminase on the solubility of proteins containing expanded polyglutamine repeats. J Neurochem 88:1253–1260

Lai TS, Liu Y, Li W, Greenberg CS (2007) Identification of two GTP-independent alternatively spliced forms of tissue transglutaminase in human leukocytes, vascular smooth muscle, and endothelial cells. FASEB J 21:4131–4143

Leblanc A, Gravel C, Labelle J, Keillor JW (2001) Kinetic studies of guinea pig liver transglutaminase reveal a general-base-catalyzed deacylation mechanism. Biochemistry 40:8335–8342

Lesort M, Chun W, Johnson GV, Ferrante RJ (1999) Tissue transglutaminase is increased in Huntington's disease brain. J Neurochem 73:2018–2027

Liu S, Cerione RA, Clardy J (2002) Structural basis for the guanine nucleotide-binding activity of tissue transglutaminase and its regulation of transamidation activity. Proc Natl Acad Sci USA 99:2743–2747

Lorand L, Graham RM (2003) Transglutaminases: crosslinking enzymes with pleiotropic functions. Nat Rev Mol Cell Biol 4:140–156

Mariani P, Carsughi F, Spinozzi F, Romanzetti S, Meier G, Casadio R, Bergamini CM (2000) Ligand-induced conformational changes in tissue transglutaminase: Monte Carlo analysis of small-angle scattering data. Biophys J 78:3240–3251

Mastroberardino PG, Iannicola C, Nardacci R, Bernassola F, De Laurenzi V, Melino G, Moreno S, Pavone F, Oliverio S, Fesus L, Piacentini M (2002) 'Tissue' transglutaminase ablation reduces neuronal death and prolongs survival in a mouse model of Huntington's disease. Cell Death Differ 9:873–880

McConoughey SJ, Basso M, Niatsetskaya ZV, Sleiman SF, Smirnova NA, Langley BC, Mahishi L, Cooper AJ, Antonyak MA, Cerione RA, Li B, Starkov A, Chaturvedi RK, Beal MF, Coppola G, Geschwind DH, Ryu H, Xia L, Iismaa SE, Pallos J, Pasternack R, Hils M, Fan J, Raymond LA, Marsh JL, Thompson LM, Ratan RR (2010) Inhibition of transglutaminase 2 mitigates transcriptional dysregulation in models of Huntington disease. EMBO Mol Med 2:349–370

Molberg O, Mcadam SN, Körner R, Quarsten H, Kristiansen C, Madsen L, Fugger L, Scott H, Norén O, Roepstorff P, Lundin KE, Sjöström H, Sollid LM (1998) Tissue transglutaminase selectively modifies gliadin peptides that are recognized by gut-derived T cells in celiac disease. Nat Med 4:713–717

Molyneaux BJ, Arlotta P, Menezes JRL, Macklis JD (2007) Neuronal subtype specification in the cerebral cortex. Nat Rev Neurosci 8:427–437

Monsonego A, Friedmann I, Shani Y, Eisenstein M, Schwartz M (1998) GTP-dependent conformational changes associated with the functional switch between Galpha and cross-linking activities in brain-derived tissue transglutaminase. J Mol Biol 282:713–720

Murayama A, Matsuzaki Y, Kawaguchi A, Shimazaki T, Okano H (2002) Flow cytometric analysis of neural stem cells in the developing and adult mouse brain. J Neurosci Res 69:837–847

Nemes Z, Devreese B, Steinert PM, Van Beeumen J, Fésüs L (2004) Cross-linking of ubiquitin, HSP27, parkin, and alpha-synuclein by gamma-glutamyl-epsilon-lysine bonds in Alzheimer's neurofibrillary tangles. FASEB J 18:1135–1137

Parameswaran KN, Cheng XF, Chen EC, Velasco PT, Wilson JH, Lorand L (1997) Hydrolysis of gamma:epsilon isopeptides by cytosolic transglutaminases and by coagulation factor XIIIa. J Biol Chem 272:10311–10317

Pedersen LC, Yee VC, Bishop PD, Le Trong I, Teller DC, Stenkamp RE (1994) Transglutaminase factor XIII uses proteinases-like catalytic triad to crosslink macromolecules. Protein Sci 3:1131–1135

Pinkas DM, Strop P, Brunger AT, Khosla C (2007) Transglutaminase 2 undergoes a large conformational change upon activation. PLoS Biol 5:e327

Sergent-Tanguy S, Chagneau C, Neveu I, Naveilhan P (2003) Fluorescent activated cell sorting (FACS): a rapid and reliable method to estimate the number of neurons in a mixed population. J Neurosci Methods 129:73–79

Smyth N, Odenthal U, Merkl B, Paulsson M (2000) Eukaryotic expression and purification of recombinant extracellular matrix proteins carrying the Strep II tag. Methods Mol Biol 139:49–57

Stamnaes J, Pinkas DM, Fleckenstein B, Khosla C, Sollid LM (2010a) Redox regulation of transglutaminase 2 activity. J Biol Chem 285:25402–25409

Stamnaes J, Dorum S, Fleckenstein B, Aeschlimann D, Sollid LM (2010b) Gluten T-cell epitope targeting by TG3 and TG6; implications for dermatitis herpetiformis and gluten ataxia. Amino Acids 39:1183–1191

Stephens P, Grenard P, Aeschlimann P, Langley M, Blain E, Errington R, Kipling D, Thomas D, Aeschlimann D (2004) Crosslinking and G-protein functions of transglutaminase 2 contribute differentially to fibroblast wound healing responses. J Cell Sci 117:3389–3403

Sung LA, Chien S, Fan YS, Lin CC, Lambert K, Zhu L, Lam JS, Chang LS (1992) Erythrocyte protein 4.2: isoform expression, differential splicing, and chromosomal assignment. Blood 79:2763–2770

Tee AE, Marshall GM, Liu PY, Xu N, Haber M, Norris MD, Iismaa SE, Liu T (2010) Opposing effects of two tissue transglutaminase protein isoforms in neuroblastoma cell differentiation. J Biol Chem 285:3561–3567

Tremblay RG, Sikorska M, Sandhu JK, Lanthier P, Ribecco-Lutkiewicz M, Bani-Yaghoub M (2010) Differentiation of mouse Neuro 2A cells into dopamine neurons. J Neurosci Methods 186:60–67

Tucholski J, Roth KA, Johnson GV (2006) Tissue transglutaminase overexpression in the brain potentiates calcium-induced hippocampal damage. J Neurochem 97:582–594

Vader LW, de Ru A, van der Wal Y, Kooy YM, Benckhuijsen W, Mearin ML, Drijfhout JW, van Veelen P, Koning F (2002) Specificity of tissue transglutaminase explains cereal toxicity in celiac disease. J Exp Med 195:643–649

van de Wal Y, Kooy Y, van Veelen P, Peña S, Mearin L, Papadopoulos G, Koning F (1998) Selective deamidation by tissue transglutaminase strongly enhances gliadin-specific T cell reactivity. J Immunol 161:1585–1588

van Strien ME, Drukarch B, Bol JG, van der Valk P, van Horssen J, Gerritsen WH, Breve JJ, van Dam AM (2011) Appearance of tissue transglutaminase in astrocytes in multiple sclerosis lesions: a role in cell adhesion and migration? Brain Pathol 21:44–54

Venkataraman K, Brown KM, Gilmartin GM (2005) Analysis of a noncanonical poly(A) site reveals a tripartite mechanism for vertebrate poly(A) site recognition. Genes Dev 19:1315–1327

Wang JL, Yang X, Xia K, Hu ZM, Weng L, Jin X, JIang H, Zhang P, Shen L, Guo JF, Li N, Li YR, Lei LF, Zhou J, Du J, Zhou YF, Pan Q, Wang J, Wang J, Li RQ, Tang BS (2010) *TGM6* identified as a novel causative gene of spinocerebellar ataxias using exome sequencing. Brain 133:3510–3518

Yee VC, Pedersen LC, Le Trong I, Bishop PD, Stenkamp RE, Teller DC (1994) Three-dimensional structure of a transglutaminase: human blood coagulation factor XIII. Proc Natl Acad Sci USA 91:7296–7300

Zainelli GM, Ross CA, Troncoso JC, Muma NA (2003) Transglutaminase cross-links in intranuclear inclusions in Huntington disease. J Neuropathol Exp Neurol 62:14–24

Zone JJ, Schmidt LA, Taylor TB, Hull CM, Sotiriou MC, Jaskowski TD, Hill HR, Meyer LJ (2011) Dermatitis herpetiformis sera or goat anti-transglutaminase-3 transferred to human skin-grafted mice mimics dermatitis herpetiformis immunopathology. J Immunol 186:4474–4480

Appendix 4

Sequencing data P2X7Rstop clone 3

T7 forward result:

```
                          10        20        30        40        50
gi_33877741_  T-----MPACCSCSDVFQYETNKVTRIQSMNYGTIKWFFHVIIFSYVCFALVSDKLYQRK
              :     ::::::::::::::::::::::::::::::::::::::::::::::::::::
P2X7Rstop cl  TLGTFTMPACCSCSDVFQYETNKVTRIQSMNYGTIKWFFHVIIFSYVCFALVSDKLYQRK
                     10        20        30        40        50        60

                 60        70        80        90       100       110
gi_33877741_  EPVISSVHTKVKGIAEVKEEIVENGVKKLVHSVFDTADYTFPLQGNSFFVMTNFLKTEGQ
              ::::::::::::::::::::::::::::::::::::::::::::::::::::::::::::
P2X7Rstop cl  EPVISSVHTKVKGIAEVKEEIVENGVKKLVHSVFDTADYTFPLQGNSFFVMTNFLKTEGQ
                     70        80        90       100       110       120

                120       130       140       150       160       170
gi_33877741_  EQRLCPEYPTRRTLCSSDRGCKKGWMDPQSKGIQTGRCVVHEGNQKTCEVSAWCPIEAVE
              ::::::::::::::::::::::::::::::::::::::::::::::::::::::::::::
P2X7Rstop cl  EQRLCPEYPTRRTLCSSDRGCKKGWMDPQSKGIQTGRCVVHEGNQKTCEVSAWCPIEAVE
                    130       140       150       160       170       180

                180       190       200       210       220       230
gi_33877741_  EAPRPALLNSAENFTVLIKNNIDFPGHNYTTRNILPGLNITCTFHKTQNPQCPIFRLGDI
              ::::::::::::::::::::::::::::::::::::::::::::::::::::::::::::
P2X7Rstop cl  EAPRPALLNSAENFTVLIKNNIDFPGHNYTTRNILPGLNITCTFHKTQNPQCPIFRLGDI
                    190       200       210       220       230       240

                240       250       260       270       280       290
gi_33877741_  FRETGDNFSDVAIQGGIMGIEIYWDCNLDRWFHHCHPKYSFRRLDDKTTNVSLYPGYNFR
              ::::::::::::::::::::::::::::::::::::::::::::.       :
P2X7Rstop cl  FRETGDNFSDVAIQGGIMGIEIYWDCNLDRWFHHCHPKYSFRRLDDR-------P-----
                    250       260       270       280
```

P2X7R-for-3 results:

```
                                                 10        20        30
P2X7Rstop cl  --------------------------ENILPGLNITCTFHKTQNPQCPIFRLGDIFRETG
                                         .:::::::::::::::::::::::::::::::
gi_33877741_  ALLNSAENFTVLIKNNIDFPGHNYTTRNILPGLNITCTFHKTQNPQCPIFRLGDIFRETG
                     190       200       210       220       230       240

                  40        50        60        70        80        90
P2X7Rstop cl  DNFSDVAIQGGIMGIEIYWDCNLDRWFHHCHPKYSFRRLDDKTTNVSLYPGYNFRYAKYY
              ::::::::::::::::::::::::::::::::::::::::::::::::::::::::::::
gi_33877741_  DNFSDVAIQGGIMGIEIYWDCNLDRWFHHCHPKYSFRRLDDKTTNVSLYPGYNFRYAKYY
                     250       260       270       280       290       300

                100       110       120       130       140       150
P2X7Rstop cl  KENNVEKRTLIKVFGIRFDILVFGTGGKFDIIQLVVYIGSTLSYFGLAAVFIDFLIDTYS
              ::::::::::::::::::::::::::::::::::::::::::::::::::::::::::::
gi_33877741_  KENNVEKRTLIKVFGIRFDILVFGTGGKFDIIQLVVYIGSTLSYFGLAAVFIDFLIDTYS
                     310       320       330       340       350       360

                160       170       180       190       200       210
P2X7Rstop cl  SNCCRSHIYPWCKCCQPCVVNEYYYRKKCESIVEPKPTLKYVSFVDESHIRMVNQQLLGR
              ::::::::::::::::::::::::::::::::::::::::::::::::::::::::::::
gi_33877741_  SNCCRSHIYPWCKCCQPCVVNEYYYRKKCESIVEPKPTLKYVSFVDESHIRMVNQQLLGR
                     370       380       390       400       410       420

                220       230       240       250       260       270
P2X7Rstop cl  SLQDVKGQEVPRPAMDFTDLSRLPLALHDTPPIPGQPEEIQLLRKEATPRSRDSPVWCQC
              ::::::::::::::::::::::::::::::::::::::::::::::::::::::::::::
gi_33877741_  SLQDVKGQEVPRPAMDFTDLSRLPLALHDTPPIPGQPEEIQLLRKEATPRSRDSPVWCQC
                     430       440       450       460       470       480

                280       290       300
P2X7Rstop cl  GSCLPSQLPESHRCLEELCCRKKPGACITTSEL---------------------------
              ::::::::::::::::::::::::::::::
gi_33877741_  GSCLPSQLPESHRCLEELCCRKKPGACITTSELFRKLVLSRHVLQFLLLYQEPLLALDVD
```

pCR3.1-BGH reverse result:

```
P2X7Rstop cl  ------------------------------------------------------AKYY
                                                                     ::::
gi_33877741_  DNFSDVAIQGGIMGIEIYWDCNLDRWFHHCHPKYSFRRLDDKTTNVSLYPGYNFRYAKYY
                     250       260       270       280       290       300

                  10        20        30        40        50        60
P2X7Rstop cl  KENNVEKRTLIKVFGIRFDILVFGTGGKFDIIQLVVYIGSTLSYFGLAAVFIDFLIDTYS
              ::::::::::::::::::::::::::::::::::::::::::::::::::::::::::::
gi_33877741_  KENNVEKRTLIKVFGIRFDILVFGTGGKFDIIQLVVYIGSTLSYFGLAAVFIDFLIDTYS
                     310       320       330       340       350       360

                  70        80        90       100       110       120
P2X7Rstop cl  SNCCRSHIYPWCKCCQPCVVNEYYYRKKCESIVEPKPTLKYVSFVDESHIRMVNQQLLGR
              ::::::::::::::::::::::::::::::::::::::::::::::::::::::::::::
gi_33877741_  SNCCRSHIYPWCKCCQPCVVNEYYYRKKCESIVEPKPTLKYVSFVDESHIRMVNQQLLGR
                     370       380       390       400       410       420

                130       140       150       160       170       180
P2X7Rstop cl  SLQDVKGQEVPRPAMDFTDLSRLPLALHDTPPIPGQPEEIQLLRKEATPRSRDSPVWCQC
              ::::::::::::::::::::::::::::::::::::::::::::::::::::::::::::
gi_33877741_  SLQDVKGQEVPRPAMDFTDLSRLPLALHDTPPIPGQPEEIQLLRKEATPRSRDSPVWCQC
                     430       440       450       460       470       480

                190       200       210       220       230       240
P2X7Rstop cl  GSCLPSQLPESHRCLEELCCRKKPGACITTSELFRKLVLSRHVLQFLLLYQEPLLALDVD
              ::::::::::::::::::::::::::::::::::::::::::::::::::::::::::::
gi_33877741_  GSCLPSQLPESHRCLEELCCRKKPGACITTSELFRKLVLSRHVLQFLLLYQEPLLALDVD
                     490       500       510       520       530       540

                250       260       270       280       290       300
P2X7Rstop cl  STNSRLRHCAYRCYATWRFGSQDMADFAILPSCCRWRIRKEFPKSEGQYSGFKSPY*LESR
              ::::::::::::::::::::::::::::::::::::::::::::::::::::::
gi_33877741_  STNSRLRHCAYRCYATWRFGSQDMADFAILPSCCRWRIRKEFPKSEGQYSGFKSPY----
                     550       560       570       580       590

                310       320       330
P2X7Rstop cl  GPFEGKPIPNPLLGLDSTRTGHHHHHH

gi_33877741_  --------------------------
```

turquoise = V5-His tag

Sequencing data P2X7R-V5-His clone 3

T7 forward result:

```
                    10        20        30        40        50        60
P2X7R clone   LKLGTFTMPACCSCSDVFQYETNKVTRIQSMNYGTIKWFFHVIIFSYVCFALVSDKLYQR
              :::::::::::::::::::::::::::::::::::::::::::::::::::::::::::
gi_33877741_  ------TMPACCSCSDVFQYETNKVTRIQSMNYGTIKWFFHVIIFSYVCFALVSDKLYQR
                         10        20        30        40        50

                    70        80        90       100       110       120
P2X7R clone   KEPVISSVHTKVKGIAEVKEEIVENGVKKLVHSVFDTADYTFPLQGNSFFVMTNFLKTEG
              :::::::::::::::::::::::::::::::::::::::::::::::::::::::::::
gi_33877741_  KEPVISSVHTKVKGIAEVKEEIVENGVKKLVHSVFDTADYTFPLQGNSFFVMTNFLKTEG
                  60        70        80        90       100       110

                   130       140       150       160       170       180
P2X7R clone   QEQRLCPEYPTRRTLCSSDRGCKKGWMDPQSKGIQTGRCVVHEGNQKTCEVSAWCPIEAV
              :::::::::::::::::::::::::::::::::::::::::::::::::::::::::::
gi_33877741_  QEQRLCPEYPTRRTLCSSDRGCKKGWMDPQSKGIQTGRCVVHEGNQKTCEVSAWCPIEAV
                 120       130       140       150       160       170

                   190       200       210       220       230       240
P2X7R clone   EEAPRPALLNSAENFTVLIKNNIDFPGHNYTTRNILPGLNITCTFHKTQNPQCPIFRLGD
              :::::::::::::::::::::::::::::::::::::::::::::::::::::::::::
gi_33877741_  EEAPRPALLNSAENFTVLIKNNIDFPGHNYTTRNILPGLNITCTFHKTQNPQCPIFRLGD
                 180       190       200       210       220       230

                   250       260       270       280       290       300
P2X7R clone   IFRETGDNFSDVAIQGGIMGIEIYWDCNLDRWFHHCHPKYSFRRLDDKTTNVSLYPGYNF
              :::::::::::::::::::::::::::::::::::::::::::::::::::::::::::
gi_33877741_  IFRETGDNFSDVAIQGGIMGIEIYWDCNLDRWFHHCHPKYSFRRLDDKTTNVSLYPGYNF
                 240       250       260       270       280       290

                   310       320
P2X7R clone   RYAKYYKENNVEKRTLIKVFGIR-----------------------------------
              :::::::::::::::::::::::
gi_33877741_  RYAKYYKENNVEKRTLIKVFGIRFDILVFGTGGKFDIIQLVVYIGSTLSYFGLAAVFIDF
                 300       310       320       330       340       350
```

P2X7R-for-3 results:

```
P2X7R clone   ------------------------------------------------------------

gi_33877741_  TMPACCSCSDVFQYETNKVTRIQSMNYGTIKWFFHVIIFSYVCFALVSDKLYQRKEPVIS
                      10        20        30        40        50        60


P2X7R clone   ------------------------------------------------------------

gi_33877741_  SVHTKVKGIAEVKEEIVENGVKKLVHSVFDTADYTFPLQGNSFFVMTNFLKTEGQEQRLC
                      70        80        90       100       110       120


P2X7R clone   ------------------------------------------------------------

gi_33877741_  PEYPTRRTLCSSDRGCKKGWMDPQSKGIQTGRCVVHEGNQKTCEVSAWCPIEAVEEAPRP
                     130       140       150       160       170       180

                                           10        20        30
P2X7R clone   -------------------------ENILPGLNITCTFHKTQNPQCPIFRLGDIFRETG
                                        .:::::::::::::::::::::::::::::::
gi_33877741_  ALLNSAENFTVLIKNNIDFPGHNYTTRNILPGLNITCTFHKTQNPQCPIFRLGDIFRETG
                     190       200       210       220       230       240

                  40        50        60        70        80        90
P2X7R clone   DNFSDVAIQGGIMGIEIYWDCNLDRWFHHCHPKYSFRRLDDKTTNVSLYPGYNFRYAKYY
              ::::::::::::::::::::::::::::::::::::::::::::::::::::::::::::
gi_33877741_  DNFSDVAIQGGIMGIEIYWDCNLDRWFHHCHPKYSFRRLDDKTTNVSLYPGYNFRYAKYY
                     250       260       270       280       290       300

                100       110       120       130       140       150
P2X7R clone   KENNVEKRTLIKVFGIRFDILVFGTGGKFDIIQLVVYIGSTLSYFGLAAVFIDFLIDTYS
              ::::::::::::::::::::::::::::::::::::::::::::::::::::::::::::
gi_33877741_  KENNVEKRTLIKVFGIRFDILVFGTGGKFDIIQLVVYIGSTLSYFGLAAVFIDFLIDTYS
                     310       320       330       340       350       360

                160       170       180       190       200       210
P2X7R clone   SNCCRSHIYPWCKCCQPCVVNEYYYRKKCESIVEPKPTLKYVSFVDESHIRMVNQQLLGR
              ::::::::::::::::::::::::::::::::::::::::::::::::::::::::::::
gi_33877741_  SNCCRSHIYPWCKCCQPCVVNEYYYRKKCESIVEPKPTLKYVSFVDESHIRMVNQQLLGR
                     370       380       390       400       410       420

                220       230       240       250       260       270
P2X7R clone   SLQDVKGQEVPRPAMDFTDLSRLPLALHDTPPIPGQPEEIQLLRKEATPRSRDSPVWCQC
              ::::::::::::::::::::::::::::::::::::::::::::::::::::::::::::
gi_33877741_  SLQDVKGQEVPRPAMDFTDLSRLPLALHDTPPIPGQPEEIQLLRKEATPRSRDSPVWCQC
                     430       440       450       460       470       480

                280       290       300       310
P2X7R clone   GSCLPSQLPESHRCLEELCCRKKPGACITTSELFRK-----------------------
              ::::::::::::::::::::::::::::::::::
gi_33877741_  GSCLPSQLPESHRCLEELCCRKKPGACITTSELFRKLVLSRHVLQFLLLYQEPLLALDVD
                     490       500       510       520       530       540
```

pCR3.1-BGH reverse result:

```
                    10        20        30        40        50        60
P2X7R clone    KENNVEKRTLIKVFGIRFDILVFGTGGKFDIIQLVVYIGSTLSYFGLAAVFIDFLIDTYS
               ::::::::::::::::::::::::::::::::::::::::::::::::::::::::::::
gi_33877741_   KENNVEKRTLIKVFGIRFDILVFGTGGKFDIIQLVVYIGSTLSYFGLAAVFIDFLIDTYS
                      310       320       330       340       350       360

                    70        80        90       100       110       120
P2X7R clone    SNCCRSHIYPWCKCCQPCVVNEYYYRKKCESIVEPKPTLKYVSFVDESHIRMVNQQLLGR
               ::::::::::::::::::::::::::::::::::::::::::::::::::::::::::::
gi_33877741_   SNCCRSHIYPWCKCCQPCVVNEYYYRKKCESIVEPKPTLKYVSFVDESHIRMVNQQLLGR
                      370       380       390       400       410       420

                  130       140       150       160       170       180
P2X7R clone    SLQDVKGQEVPRPAMDFTDLSRLPLALHDTPPIPGQPEEIQLLRKEATPRSRDSPVWCQC
               ::::::::::::::::::::::::::::::::::::::::::::::::::::::::::::
gi_33877741_   SLQDVKGQEVPRPAMDFTDLSRLPLALHDTPPIPGQPEEIQLLRKEATPRSRDSPVWCQC
                      430       440       450       460       470       480

                  190       200       210       220       230       240
P2X7R clone    GSCLPSQLPESHRCLEELCCRKKPGACITTSELFRKLVLSRHVLQFLLLYQEPLLALDVD
               ::::::::::::::::::::::::::::::::::::::::::::::::::::::::::::
gi_33877741_   GSCLPSQLPESHRCLEELCCRKKPGACITTSELFRKLVLSRHVLQFLLLYQEPLLALDVD
                      490       500       510       520       530       540

                  250       260       270       280       290       300
P2X7R clone    STNSRLRHCAYRCYATWRFGSQDMADFAILPSCCRWRIRKEFPKSEGQYSGFKSPYLESR
               ::::::::::::::::::::::::::::::::::::::::::::::::::::::::::::
gi_33877741_   STNSRLRHCAYRCYATWRFGSQDMADFAILPSCCRWRIRKEFPKSEGQYSGFKSPY----
                      550       560       570       580       590

                  310       320       330
P2X7R clone    GPFEGKPIPNPLLGLDSTRTGHHHHHH

gi_33877741_   ---------------------------
```

turquoise = V5-His tag

Sequencing data P2X7Rstop clone 6

T7 forward result:

```
                    10        20        30        40        50        60
P2X7Rstop cl  LLKLGTFTMPACCSCSDVFQYETNKVTRIQSMNYGTIKWFFHVIIFSYVCFALVSDKLYQ
                     :::::::::::::::::::::::::::::::::::::::::::::::::::
gi_33877741_  --------MPACCSCSDVFQYETNKVTRIQSMNYGTIKWFFHVIIFSYVCFALVSDKLYQ
                            10        20        30        40        50

                     70        80        90       100       110       120
P2X7Rstop cl  RKEPVISSVHTKVKGIAEVKEEIVENGVKKLVHSVFDTADYTFPLQGNSFFVMTNFLKTE
              ::::::::::::::::::::::::::::::::::::::::::::::::::::::::::::
gi_33877741_  RKEPVISSVHTKVKGIAEVKEEIVENGVKKLVHSVFDTADYTFPLQGNSFFVMTNFLKTE
                    60        70        80        90       100       110

                    130       140       150       160       170       180
P2X7Rstop cl  GQEQRLCPEYPTRRTLCSSDRGCKKGWMDPQSKGIQTGRCVVHEGNQKTCEVSAWCPIEA
              ::::::::::::::::::::::::::::::::::::::::::::::::::::::::::::
gi_33877741_  GQEQRLCPEYPTRRTLCSSDRGCKKGWMDPQSKGIQTGRCVVHEGNQKTCEVSAWCPIEA
                   120       130       140       150       160       170

                    190       200       210       220       230       240
P2X7Rstop cl  VEEAPRPALLNSAENFTVLIKNNIDFPGHNYTTRNILPGLNITCTFHKTQNPQCPIFRLG
              ::::::::::::::::::::::::::::::::::::::::::::::::::::::::::::
gi_33877741_  VEEAPRPALLNSAENFTVLIKNNIDFPGHNYTTRNILPGLNITCTFHKTQNPQCPIFRLG
                   180       190       200       210       220       230

                    250       260       270       280       290       300
P2X7Rstop cl  DIFRETGDNFSDVAIQGGIMGIEIYWDCNLDRWFHHCHPKYSFRRLDDKTTNVSLYPGYN
              ::::::::::::::::::::::::::::::::::::::::::::::::::::::::::::
gi_33877741_  DIFRETGDNFSDVAIQGGIMGIEIYWDCNLDRWFHHCHPKYSFRRLDDKTTNVSLYPGYN
                   240       250       260       270       280       290

                    310
P2X7Rstop cl  FRYAKYYKENNVEKRTLIK----------------------------------------
              ::::::::::::::::::
gi_33877741_  FRYAKYYKENNVEKRTLIKVFGIRFDILVFGTGGKFDIIQLVVYIGSTLSYFGLAAVFID
                   300       310       320       330       340       350
```

P2X7R-for-3 results:

```
                                                  10        20        30
P2X7Rstop cl  ------------------------TRNILPGLNITCTFHKTQNPQCPIFRLGDIFRETGD
                                      ::::::::::::::::::::::::::::::::::
gi_33877741_  LLNSAENFTVLIKNNIDFPGHNYTTRNILPGLNITCTFHKTQNPQCPIFRLGDIFRETGD
                     190       200       210       220       230       240

                40        50        60        70        80        90
P2X7Rstop cl  NFSDVAIQGGIMGIEIYWDCNLDRWFHHCHPKYSFRRLDDKTTNVSLYPGYNFRYAKYYK
              ::::::::::::::::::::::::::::::::::::::::::::::::::::::::::::
gi_33877741_  NFSDVAIQGGIMGIEIYWDCNLDRWFHHCHPKYSFRRLDDKTTNVSLYPGYNFRYAKYYK
                     250       260       270       280       290       300

               100       110       120       130       140       150
P2X7Rstop cl  ENNVEKRTLIKVFGIRFDILVFGTGGKFDIIQLVVYIGSTLSYFGLAAVFIDFLIDTYSS
              ::::::::::::::::::::::::::::::::::::::::::::::::::::::::::::
gi_33877741_  ENNVEKRTLIKVFGIRFDILVFGTGGKFDIIQLVVYIGSTLSYFGLAAVFIDFLIDTYSS
                     310       320       330       340       350       360

               160       170       180       190       200       210
P2X7Rstop cl  NCCRSHIYPWCKCCQPCVVNEYYYRKKCESIVEPKPTLKYVSFVDESHIRMVNQQLLGRS
              ::::::::::::::::::::::::::::::::::::::::::::::::::::::::::::
gi_33877741_  NCCRSHIYPWCKCCQPCVVNEYYYRKKCESIVEPKPTLKYVSFVDESHIRMVNQQLLGRS
                     370       380       390       400       410       420

               220       230       240       250       260       270
P2X7Rstop cl  LQDVKGQEVPRPAMDFTDLSRLPLALHDTPPIPGQPEEIQLLRKEATPRSRDSPVWCQCG
              ::::::::::::::::::::::::::::::::::::::::::::::::::::::::::::
gi_33877741_  LQDVKGQEVPRPAMDFTDLSRLPLALHDTPPIPGQPEEIQLLRKEATPRSRDSPVWCQCG
                     430       440       450       460       470       480

               280       290       300       310
P2X7Rstop cl  SCLPSQLPESHRCLEELCCRKKPGACITTSELFRKLVLSRHVL-----------------
              ::::::::::::::::::::::::::::::::::::::::
gi_33877741_  SCLPSQLPESHRCLEELCCRKKPGACITTSELFRKLVLSRHVLQFLLLYQEPLLALDVDS
                     490       500       510       520       530       540
```

pCR3.1-BGH reverse result:

```
                                                  30        40        50
P2X7Rstop cl  -------------------------KIDIIQLVVYIGSTLSYFGLAAVFIDFLIDTYSS
                                       :.:::::::::::::::::::::::::::::::
gi_33877741_  ENNVEKRTLIKVFGIRFDILVFGTGGKFDIIQLVVYIGSTLSYFGLAAVFIDFLIDTYSS
                     310       320       330       340       350       360

                60        70        80        90       100       110
P2X7Rstop cl  NCCRSHIYPWCKCCQPCVVNEYYYRKKCESIVEPKPTLKYVSFVDESHIRMVNQQLLGRS
              ::::::::::::::::::::::::::::::::::::::::::::::::::::::::::::
gi_33877741_  NCCRSHIYPWCKCCQPCVVNEYYYRKKCESIVEPKPTLKYVSFVDESHIRMVNQQLLGRS
                     370       380       390       400       410       420

               120       130       140       150       160       170
P2X7Rstop cl  LQDVKGQEVPRPAMDFTDLSRLPLALHDTPPIPGQPEEIQLLRKEATPRSRDSPVWCQCG
              ::::::::::::::::::::::::::::::::::::::::::::::::::::::::::::
gi_33877741_  LQDVKGQEVPRPAMDFTDLSRLPLALHDTPPIPGQPEEIQLLRKEATPRSRDSPVWCQCG
                     430       440       450       460       470       480

               180       190       200       210       220       230
P2X7Rstop cl  SCLPSQLPESHRCLEELCCRKKPGACITTSELFRKLVLSRHVLQFLLLYQEPLLALDVDS
              ::::::::::::::::::::::::::::::::::::::::::::::::::::::::::::
gi_33877741_  SCLPSQLPESHRCLEELCCRKKPGACITTSELFRKLVLSRHVLQFLLLYQEPLLALDVDS
                     490       500       510       520       530       540

               240       250       260       270       280       290
P2X7Rstop cl  TNSRLRHCAYRCYATWRFGSQDMADFAILPSCCRWRIRKEFPKSEGQYSGFKSPY*LESRG
              ::::::::::::::::::::::::::::::::::::::::::::::::::::::::::
gi_33877741_  TNSRLRHCAYRCYATWRFGSQDMADFAILPSCCRWRIRKEFPKSEGQYSGFKSPY-----
                     550       560       570       580       590

300       310       320
P2X7Rstop cl  PFEGKPIPNPLLGLDSTRTGHHHH

gi_33877741_  -------------------------
```

turquoise = V5-His tag

Sequencing data P2X7R-V5-His clone 6

T7 forward result:

```
                    10        20        30        40        50        60
P2X7R clone   LKLGTFTMPACCSCSDVFQYETNKVTRIQSMNYGTIKWFFHVIIFSYVCFALVSDKLYQR
                    ::::::::::::::::::::::::::::::::::::::::::::::::::::::
gi_33877741_  -------MPACCSCSDVFQYETNKVTRIQSMNYGTIKWFFHVIIFSYVCFALVSDKLYQR
                           10        20        30        40        50

                    70        80        90       100       110       120
P2X7R clone   KEPVISSVHTKVKGIAEVKEEIVENGVKKLVHSVFDTADYTFPLQGNSFFVMTNFLKTEG
              ::::::::::::::::::::::::::::::::::::::::::::::::::::::::::::
gi_33877741_  KEPVISSVHTKVKGIAEVKEEIVENGVKKLVHSVFDTADYTFPLQGNSFFVMTNFLKTEG
                   60        70        80        90       100       110

                   130       140       150       160       170       180
P2X7R clone   QEQRLCPEYPTRRTLCSSDRGCKKGWMDPQSKGIQTGRCVVHEGNQKTCEVSAWCPIEAV
              ::::::::::::::::::::::::::::::::::::::::::::::::::::::::::::
gi_33877741_  QEQRLCPEYPTRRTLCSSDRGCKKGWMDPQSKGIQTGRCVVHEGNQKTCEVSAWCPIEAV
                  120       130       140       150       160       170

                   190       200       210       220       230       240
P2X7R clone   EEAPRPALLNSAENFTVLIKNNIDFPGHNYTTRNILPGLNITCTFHKTQNPQCPIFRLGD
              ::::::::::::::::::::::::::::::::::::::::::::::::::::::::::::
gi_33877741_  EEAPRPALLNSAENFTVLIKNNIDFPGHNYTTRNILPGLNITCTFHKTQNPQCPIFRLGD
                  180       190       200       210       220       230

                   250       260       270       280       290       300
P2X7R clone   IFRETGDNFSDVAIQGGIMGIEIYWDCNLDRWFHHCHPKYSFRRLDDKTTNVSLYPGYNF
              ::::::::::::::::::::::::::::::::::::::::::::::::::::::::::::
gi_33877741_  IFRETGDNFSDVAIQGGIMGIEIYWDCNLDRWFHHCHPKYSFRRLDDKTTNVSLYPGYNF
                  240       250       260       270       280       290

                   310
P2X7R clone   RYAKYYKENNVEKRTLIK------------------------------------------
              ::::::::::::::::::
gi_33877741_  RYAKYYKENNVEKRTLIKVFGIRFDILVFGTGGKFDIIQLVVYIGSTLSYFGLAAVFIDF
                  300       310       320       330       340       350
```

P2X7R-for-3 results:

```
                                                  10        20        30
P2X7R clone   ----------------------TTRNILPGLNITCTFHKTQNPQCPIFRLGDIFRETGD
                                    ::::::::::::::::::::::::::::::::::
gi_33877741_  LLNSAENFTVLIKNNIDFPGHNYTTRNILPGLNITCTFHKTQNPQCPIFRLGDIFRETGD
                     190       200       210       220       230       240

               40        50        60        70        80        90
P2X7R clone   NFSDVAIQGGIMGIEIYWDCNLDRWFHHCHPKYSFRRLDDKTTNVSLYPGYNFRYAKYYK
              ::::::::::::::::::::::::::::::::::::::::::::::::::::::::::::
gi_33877741_  NFSDVAIQGGIMGIEIYWDCNLDRWFHHCHPKYSFRRLDDKTTNVSLYPGYNFRYAKYYK
                     250       260       270       280       290       300

              100       110       120       130       140       150
P2X7R clone   ENNVEKRTLIKVFGIRFDILVFGTGGKFDIIQLVVYIGSTLSYFGLAAVFIDFLIDTYSS
              ::::::::::::::::::::::::::::::::::::::::::::::::::::::::::::
gi_33877741_  ENNVEKRTLIKVFGIRFDILVFGTGGKFDIIQLVVYIGSTLSYFGLAAVFIDFLIDTYSS
                     310       320       330       340       350       360

              160       170       180       190       200       210
P2X7R clone   NCCRSHIYPWCKCCQPCVVNEYYYRKKCESIVEPKPTLKYVSFVDESHIRMVNQQLLGRS
              ::::::::::::::::::::::::::::::::::::::::::::::::::::::::::::
gi_33877741_  NCCRSHIYPWCKCCQPCVVNEYYYRKKCESIVEPKPTLKYVSFVDESHIRMVNQQLLGRS
                     370       380       390       400       410       420

              220       230       240       250       260       270
P2X7R clone   LQDVKGQEVPRPAMDFTDLSRLPLALHDTPPIPGQPEEIQLLRKEATPRSRDSPVWCQCG
              ::::::::::::::::::::::::::::::::::::::::::::::::::::::::::::
gi_33877741_  LQDVKGQEVPRPAMDFTDLSRLPLALHDTPPIPGQPEEIQLLRKEATPRSRDSPVWCQCG
                     430       440       450       460       470       480

              280       290       300
P2X7R clone   SCLPSQLPESHRCLEELCCRKKPGACITTS-----------------------------
              ::::::::::::::::::::::::::::
gi_33877741_  SCLPSQLPESHRCLEELCCRKKPGACITTSELFRKLVLSRHVLQFLLLYQEPLLALDVDS
                     490       500       510       520       530       540
```

pCR3.1-BGH reverse result:

```
                                                    30        40        50
P2X7R clone   -------------------------GKFDIIQLVVYIGSTLSYFGLAAVFIDFLIDTYSS
                                       :::::::::::::::::::::::::::::::::
gi_33877741_  ENNVEKRTLIKVFGIRFDILVFGTGGKFDIIQLVVYIGSTLSYFGLAAVFIDFLIDTYSS
                     310       320       330       340       350       360

             60        70        80        90       100       110
P2X7R clone   NCCRSHIYPWCKCCQPCVVNEYYYRKKCESIVEPKPTLKYVSFVDESHIRMVNQQLLGRS
              ::::::::::::::::::::::::::::::::::::::::::::::::::::::::::::
gi_33877741_  NCCRSHIYPWCKCCQPCVVNEYYYRKKCESIVEPKPTLKYVSFVDESHIRMVNQQLLGRS
                     370       380       390       400       410       420

            120       130       140       150       160       170
P2X7R clone   LQDVKGQEVPRPAMDFTDLSRLPLALHDTPPIPGQPEEIQLLRKEATPRSRDSPVWCQCG
              ::::::::::::::::::::::::::::::::::::::::::::::::::::::::::::
gi_33877741_  LQDVKGQEVPRPAMDFTDLSRLPLALHDTPPIPGQPEEIQLLRKEATPRSRDSPVWCQCG
                     430       440       450       460       470       480

            180       190       200       210       220       230
P2X7R clone   SCLPSQLPESHRCLEELCCRKKPGACITTSELFRKLVLSRHVLQFLLLYQEPLLALDVDS
              ::::::::::::::::::::::::::::::::::::::::::::::::::::::::::::
gi_33877741_  SCLPSQLPESHRCLEELCCRKKPGACITTSELFRKLVLSRHVLQFLLLYQEPLLALDVDS
                     490       500       510       520       530       540

            240       250       260       270       280       290
P2X7R clone   TNSRLRHCAYRCYATWRFGSQDMADFAILPSCCRWRIRKEFPKSEGQYSGFKSPYLESRG
              ::::::::::::::::::::::::::::::::::::::::::::::::::::::::::::
gi_33877741_  TNSRLRHCAYRCYATWRFGSQDMADFAILPSCCRWRIRKEFPKSEGQYSGFKSPY-----
                     550       560       570       580       590

            300       310       320
P2X7R clone   PFEGKPIPNPLLGLDSTRTGHHHHHQ

gi_33877741_  -------------------------
```

turquoise: VS-His tag